

Systematic Reverse Genetic Screen to Identify
Novel Genes Required for Anterior Patterning
of the Red Flour Beetle
Tribolium castaneum

Dissertation

for the award of the degree

“Doctor rerum naturalium”

of the Georg-August-Universität Göttingen

submitted by

Jonas Schwirz

from Göttingen, Germany

Göttingen 2014

Thesis Committee

Prof. Dr. Ernst A. Wimmer (1st reviewer, advisor)

Johann-Friedrich-Blumenbach-Institute of Zoology and Anthropology, Dept. for Developmental Biology, Georg-August-University Göttingen

Prof. Dr. Andreas Wodarz (2nd reviewer)

Dept. of Anatomy and Cell Biology, Stem Cell Biology, University Medical Center Göttingen

PD Dr. Reinhard Schuh

Dept. of Molecular Developmental Biology, Max Planck Institute for Biophysical Chemistry

Members of the Examination Board

Referee: Prof. Dr. Ernst A. Wimmer, Johann-Friedrich-Blumenbach-Institute of Zoology and Anthropology, Dept. for Developmental Biology, Georg-August-University Göttingen

2nd Referee: Prof. Dr. Andreas Wodarz, Dept. of Anatomy and Cell Biology, Stem Cell Biology, University Medical Center Göttingen

Further members of the Examination Board

PD Dr. Reinhard Schuh, Dept. of Molecular Developmental Biology, Max Planck Institute for Biophysical Chemistry

Prof. Dr. Gregor Bucher, Johann-Friedrich-Blumenbach-Institute of Zoology and Anthropology, Department of Evolutionary Developmental Genetics, Georg-August-University Göttingen

Prof. Dr. Ralf Heinrich, Johann-Friedrich-Blumenbach-Institute of Zoology and Anthropology, Department of Cellular Neurobiology, Georg-August-University Göttingen

Dr. Roland Dosch, Department of Developmental Biochemistry, University Medical Center Göttingen

Date of oral examination: 29.04.2014

Herewith I declare, that I prepared the Dissertation
"Systematic Reverse Genetic Screen to Identify Novel Genes Required for Anterior Patterning of the Red Flour Beetle *Tribolium castaneum*"
on my own and with no other sources and aids than quoted.

Göttingen, 31.03.2014

Jonas Schwirz

Danksagung

Obgleich selbständig verfasst, wäre das Erstellen dieser Arbeit ohne die Hilfe vieler auf die eine oder andere Weise beteiligter Menschen nicht möglich gewesen. Ich möchte diese Stelle nutzen um diesen Personen herzlich zu danken und entschuldige mich im Vorraus schonmal dafür, falls ich jemanden vergessen haben sollte (es war bestimmt keine Absicht).

Mein außerordentlicher Dank geht an Prof. Dr. Ernst A. Wimmer für die Möglichkeit diese Arbeit anzufertigen. Vielen Dank für die fruchtvollen Diskussionen, die Freiheit dieses Projekt selbst zu gestalten, und die immer vorhandene Unterstützung wann immer sie nötig war. Die Erfahrungen am iBeetle Projekt teilzunehmen, auf wissenschaftliche Kongresse zu fahren, sowie mit anderen Arbeitsgruppen zu kooperieren, haben mich wissenschaftlich und persönlich weitergebracht.

Danken möchte ich auch Prof. Dr. Gregor Bucher für zahlreiche fachliche Diskussionen, sein Engagement für den iBeetle Screen und viele produktive Anmerkungen für dieses Projekt.

Vielen Dank an Prof. Dr. Andreas Wodarz und Prof. Reinhard Schuh für freundliche und konstruktive Anmerkungen zu dieser Arbeit im Rahmen der Thesis Committee Meetings.

Mein Dank geht an die Screener und Arbeitsgruppenleiter der Forschungsgruppe iBeetle, ohne die dieses Projekt nicht zustandegekommen wäre. Herausheben möchte ich hier Michael Schoppmeier für sehr konstruktive Anmerkungen und Hinweise für dieses Projekt und Christian Schmitt-Engel für die hervorragende Koordination des Screens während der ersten Screening Periode. Und natürlich für die stete Ansprechbarkeit und das Kreieren einer außerordentlichen Arbeitsatmosphäre, die es geschafft hat, auch stundenlanges Ovarpräparieren und schier unendliches Cuticulascreenen zu einer guten Zeit zu machen.

Mein besonderer Dank geht an Monique Weidner für ihren aufopferungsvollen Einsatz in diesem Projekt. Etliche Färbungen, Fixierungen und Präparationen wären ohne Hilfe in dem Zeitrahmen nicht möglich gewesen. Vielen herzlichen Dank auch an Daniela Grossmann für ihre Hilfsbereitschaft, ihr Engagement, das Füllen des Schokoladenfachs und viele, viele Hörbücher.

Danke an die Arbeitsgruppe des Instituts für Entwicklungsbiologie der Universität Köln für die Möglichkeit die Live Imaging Experimente zu machen und die außerordentlich nette Aufnahme in ihrem Labor. Im Speziellen danke ich Kristen Panfilio für die technische Betreuung und Prof. Dr. Siegfried Roth für angenehme und fachlich fruchtbare Diskussionen.

Ich danke der gesamten Abteilung Entwicklungsbiologie für die großartige Arbeitsatmosphäre, die das Anfertigen dieser Arbeit zu einer schönen Erfahrung gemacht hat. Danke an die technische Abteilung dafür, dass sie das Labor so gut am Laufen hält wie es ist. Dank an Peter Kitzmann für viele lustige Stunden bei Tennis und Fußball (auch der HSV wird irgendwann wieder gewinnen). Besonderer Dank gebührt Georg Oberhofer für seine Diskussionsfreude und für den Impuls die Videos reinzunehmen, was einen sehr positiven Einfluss auf diese Arbeit hatte. Danken möchte ich auch meinen ‚Mitbewohnern‘ Sara Khadjeh und Nata-scha Zhang für gute Zeiten innerhalb und außerhalb des Labors.

Ich danke Christian Schmitt-Engel und Bernhard Schmid für die kritische Durchsicht dieser Arbeit, sehr konstruktive Anmerkungen, und viele gute fachliche und fachfremde Diskussionen und Gespräche.

Vielen Dank noch mal an Sara und Chris sowie an Nikolaus Koniszewski und Dawid Lbik dafür dass sie mich immer ordentlich gesichert haben.

Dank an meine Freunde innerhalb und außerhalb des Labors für die stetige Unterstützung in allen Lebenslagen und ihre Anteilnahme an dieser Arbeit. Vielen Dank an meine Familie, allen voran meinen Brüdern, für ihr Verständnis, ihre Unterstützung, und ihre Geduld.

Table of contents

1	Summary	4
2	Introduction	5
2.1	Symmetry break and axis specification	5
2.2	Long germ and short germ mode of insect development.....	5
2.3	The anterior-posterior system in <i>Drosophila</i>	6
2.4	Segmentation and the anterior-posterior system in <i>Tribolium</i>	8
2.5	The dorsal-ventral system in <i>Drosophila</i>	12
2.6	The dorsal-ventral system in <i>Tribolium</i>	14
2.6.1	The BMP pathway	17
2.6.1.1	Smurf E3 ubiquitin ligases in the BMP pathway	18
2.6.1.2	MAD at the crossroads of signaling pathways	21
2.7	A genome wide RNAi screen in <i>Tribolium castaneum</i>	23
2.7.1	The iBeetle screening concept (design of the iBeetle screen).....	25
2.8	Aims of this study	27
3	Materials and Methods	28
3.1	<i>Tribolium castaneum</i> culture and strains	28
3.2	Molecular biology.....	28
3.3	Orthology and phylogeny analysis.....	30
3.4	Knock down of gene functions by RNA interference (RNAi).....	32
3.5	Histology.....	34
3.5.1	Fixation.....	34
3.5.2	Fuchsin stainings.....	34
3.5.3	Whole mount <i>in situ</i> hybridization	34
3.5.4	Immunohistochemistry.....	35
3.5.5	TUNEL assay	36
3.5.6	Cuticle preparations.....	36
3.6	The iBeetle screening procedure.....	37
3.6.1	Annotation of screening results	38
3.7	<i>In vivo</i> imaging.....	40
4	Results	41
4.1	Identification of anterior patterning phenotypes in the iBeetle screen.....	41
4.1.1	Phenotype identification and controls.....	41

Table of contents

4.1.2	Candidate selection strategy	46
4.1.3	Selection of primary candidates.....	47
4.2	Candidate selection, experimental phase	50
4.2.1	Primary candidates: re-screen	51
4.2.2	Selection of verified candidates	51
4.2.3	Reduction of candidates by expression pattern analysis and non-overlapping fragment injection	52
4.2.4	<i>Tc-wingless</i> expression in candidate RNAi embryos	56
4.3	Identification, isolation and characterization of <i>iB_02881</i> as <i>Tribolium smurf</i>	60
4.3.1	<i>Tribolium smurf</i> expression and RNAi phenotype.....	64
4.3.2	TUNEL stainings in <i>Tc-smurf</i> RNAi.....	73
4.3.3	Effect of <i>Tc-smurf</i> RNAi on the <i>dpp</i> pathway in <i>Tribolium</i>	75
4.3.4	Expression of marker genes in <i>Tc-smurf</i> RNAi.....	86
4.3.5	Live imaging of <i>Tc-smurf</i> RNAi embryos	90
4.4	Identification, isolation and characterization of <i>iB_03735</i> as <i>Tribolium TC004374</i>	97
4.4.1	Gene expression and cuticle phenotype of <i>TC004374</i>	101
4.4.2	Immunohistochemistry and expression of marker genes in <i>TC004374</i> RNAi during embryonic stages.....	105
4.4.3	TUNEL assay in <i>TC004374</i> RNAi embryos	110
4.4.4	Live Imaging of <i>TC004374</i> RNAi	112
4.5	Isolation and characterization of <i>Tribolium mothers against dpp</i>	117
5	Discussion	119
5.1	iBeetle screen and candidate gene selection	119
5.1.1	The iBeetle screen is an efficient approach to detect genes involved in head development and anterior patterning	119
5.1.2	New anterior patterning genes for <i>Tribolium</i> are identified through the iBeetle screen	122
5.1.3	Candidate selection from the database	123
5.1.4	From primary candidates to final candidates	123
5.2	<i>Tc-smurf</i>	125
5.2.1	<i>Tc-smurf</i> regulates phosphorylated MAD during <i>Tribolium</i> embryogenesis	125
5.2.2	Loss of <i>Tc-smurf</i> function can lead to pre-blastodermal lethality	126
5.2.3	<i>Tc-smurf</i> is involved in patterning the blastodermal fate map in <i>Tribolium</i>	127

5.2.4	A model for <i>Tc-smurf</i> function during germ band stages	131
5.2.4.1	Dpp displays a positive feedback loop during germ band stages in the <i>Tribolium</i> embryo	132
5.2.4.2	Tc-Dpp signaling inhibits <i>Tc-sog</i> expression	135
5.2.4.3	An anterior Tc-Dpp signaling center results in severe cell death	136
5.2.5	Outlook and conclusions for the function of <i>Tc-smurf</i> during embryogenesis	138
5.2.6	Smurf is more important for embryonic patterning in <i>Tribolium</i> than in <i>Drosophila</i>	139
5.2.7	Smurf proteins as ancestral regulators of TGF- β signaling.....	140
5.3	<i>TC004374</i>	141
5.3.1	<i>TC004374</i> encodes a molecule of unknown function	141
5.3.2	Potential function of <i>TC004374</i> in MAD regulation	142
5.3.3	<i>TC004374</i> is necessary for proper amnion development	146
5.4	General conclusions	148
6	References	149
7	Appendix	168
7.1	DVD content	168
7.2	Abbreviations.....	169
7.3	Primer list	170
7.4	Table for <i>DsRed</i> control movies	174
7.5	Table for <i>Tc-smurf</i> RNAi movies.....	176
7.6	Tables for <i>TC004374</i> RNAi movies	179

1 Summary

The formation of two main body axis is a crucial event during bilaterian development and has been in the focus of research for many years. The vinegar fly *Drosophila melanogaster* served as an excellent model organism for insect developmental biology. Body axis formation in the fly is today vastly understood. Nevertheless, comparative studies using the so-called 'candidate gene approach' in other species revealed that many aspects of *Drosophila* development seem to be evolutionarily derived. However, although very successful during the last decades, the candidate gene approach has its limitations and comprehensive and unbiased studies in species other than *Drosophila* are necessary in order to fill our gaps of knowledge about axis formation and early patterning in arthropods. The red flour beetle *Tribolium castaneum* offers a vast tool box for descriptive and functional analysis of the molecular processes during early development and has emerged to the second best arthropod model system after *Drosophila*. In this study the approach of a comprehensive RNA interference screen has been used to identify new factors required for anterior patterning in *Tribolium*. About 25 % of the *Tribolium* genome were screened during the first approximately 14 months of the iBeetle screen. Almost 10 % of all screened genes were annotated to result in head defects on the L1 larval cuticle after knock down. Out of this set of candidate genes a stepwise selection led to the identification of two genes for in depth analysis. The E3 ubiquitin ligase Tc-Smurf is necessary for patterning the blastodermal fate map in *Tribolium* and loss of Tc-Smurf function leads to loss of prospective head regions. Missing Tc-Smurf function during later stages can result in death of anterior body regions up to the entirety of embryonic cells. Tc-Smurf is necessary to control Decapentaplegic (Dpp) signaling during early and later stages of *Tribolium* embryogenesis and is especially important for restricting Dpp signaling in the anterior embryo. The second candidate gene *TC004374* probably plays an important role for the formation of the anterior amnion during differentiated blastoderm stages and for maintenance of amniotic tissue at the margin of the embryo during germ band stages. Loss of *TC004374* function also leads to ectopic domains of phosphorylated Mothers against Dpp (pMAD) protein in the embryonic headlobes. This indicates that both detected genes are involved in inhibition of Dpp signaling in the anterior embryonic region during *Tribolium* embryogenesis.

2 Introduction

2.1 Symmetry break and axis specification

Most animals on earth, including ourselves, belong to the bilateria which are characterized by two main body axes. One is the anterior-posterior axis (AP-axis), with a head in the anterior and a tail at the posterior. The other is the dorsal-ventral axis (DV-axis) which is formed perpendicular to the anterior-posterior axis and divides the animal in a back and a belly side (Gilbert, 2003). One major event is the task to establish these body axes early within the egg or later during embryonic development. Evolution has developed a fascinating tool box of different mechanisms to achieve this important break of symmetry. The ap-axis in chicken, for instance, is specified through gravity while in the nematode *Caenorhabditis elegans* the position of the sperm pronucleus is crucial (Gilbert, 2003).

Due to its importance for development it is not surprising that axis specification and the patterning along these axes during embryogenesis have been fields of intense research for many years and body axis formation in the vinegar fly *Drosophila melanogaster* is today one of the best understood events in early embryology. The description of early patterning processes in *Drosophila* laid the foundation for much what we know about the molecular processes during early embryonic development and was rewarded with the Nobel prize for Medicine in 1995 for Christiane Nüsslein-Volhard, Eric Wieschaus and Edward Lewis.

2.2 Long germ and short germ mode of insect development

In insects in general two modes of embryonic development are distinguished. During long germ development all body segments are established nearly simultaneously before gastrulation and almost the entire egg gives rise to the eventual embryo. The fraction of extraembryonic tissue in the blastoderm fate map is usually low. A prominent example for this mode of development is the fruit fly *Drosophila melanogaster*. In contrast, many insects show the short germ mode of insect embryogenesis. In short germ insects the embryonic germ rudiment forms in a posterior region of the egg and only a subset of anterior body segments is established during blastoderm stages. The rest of the segments is progressively formed after gastrulation in a posterior growth zone. The remaining (usually anterior and

dorsal) part of the egg gives rise to the extraembryonic serosa (reviewed in Davis and Patel, 2002). This way of development is also found in the beetle *Tribolium castaneum* which is the model system used in this study.

2.3 The anterior-posterior system in *Drosophila*

The understanding of anterior-posterior patterning processes in *Drosophila* was a breakthrough in our understanding of insect development and up to this day the vinegar fly serves as reference for all genetic processes studied in arthropod development.

Segmentation of the *Drosophila* embryo depends on a hierarchical gene cascade involving substantial input from maternally supplied factors which are deposited into the oocyte by nurse cells during oogenesis and specific signals from terminal follicle cells (Johnston and Nüsslein-Volhard, 1992; Riechmann and Ephrussi, 2001). One of the first events of axis specification is the determination of the posterior follicle cells through activation of the Epidermal growth factor receptor (EGFR) Torpedo by the Transforming growth factor (TGF)-like ligand Gurken (González-Reyes et al., 1995; Roth and Lynch, 2009). Those follicle cells induce a polarization of the microtubuli, resulting in anterior localization of the *bicoid* mRNA (Driever and Nüsslein-Volhard, 1988; Weil et al., 2006) while *Oskar* mRNA is localized to the other side of the egg where it leads to accumulation of mRNA for the posterior determinant Nanos (Ephrussi et al., 1991; Wang and Lehmann, 1991). These maternally localized mRNAs lead to diffusion gradients of Bicoid (BCD) and Nanos proteins along the anterior-posterior axis. By activation or repression of target gene transcription these protein gradients in turn lead to other protein gradients within the egg syncytium. BCD for instance represses *caudal* translation in the anterior of the egg while the Nanos protein together with its cofactor Pumilio inhibits protein translation from the ubiquitous *hunchback* mRNA, again resulting in two opposing protein gradients along the anterior-posterior axis (Barker et al., 1992; Dubnau and Struhl, 1996; Hülskamp et al., 1989; Irish et al., 1989a; Rivera-Pomar et al., 1996) (Figure 2-1). These early protein gradients coordinate the spatial expression of the first zygotically expressed genes, the so-called gap genes. Transcriptional activation and repression leads to local expression of *hunchback*, *knirps*, *giant* or *Krüppel*, which in turn regulate each other, leading to more and more spatially defined expression domains (Brönner and Jäckle, 1991; Driever

and Nüsslein-Volhard, 1989; Hülkamp et al., 1990; Kraut and Levine, 1991a; Kraut and Levine, 1991b; Schulz and Tautz, 1994; Schulz and Tautz, 1995; Simpson-Brose et al., 1994; Struhl et al., 1989; Tautz, 1988) (Figure 2-1). The genes *huckebein* and *tailless* are expressed at the poles of the egg and necessary for the development of the terminal regions of the embryo (Weigel et al., 1990). The expression of these genes depends on the activation of the receptor tyrosine kinase Torso through the product of the *torso-like* gene which is expressed in terminal follicle cells during oocyte maturation. Loss of function mutations for the terminal genes cause loss of the terminal structures (Casanova and Struhl, 1989; Furriols and Casanova, 2003; Klingler et al., 1988; Sprenger et al., 1989; Stevens et al., 1990).

The spatially restricted, partially overlapping gap gene domains regulate the next level of the gene cascade. By binding to specific enhancer elements, the gap genes control the expression of pair rule genes (Fujioka et al., 1999; Klingler and Gergen, 1993; Langeland et al., 1994; Pankratz and Jäckle, 1990; Reinitz and Sharp, 1995). These genes are expressed in partially overlapping stripe-like domains in every second segment anlage. Expression of the primary pair rule genes *hairy*, *runt* and *even-skipped* eventually regulates the expression of secondary pair rule genes (Carroll et al., 1988; Frasch et al., 1987; Gergen and Butler, 1988; Harding et al., 1986; Hartmann et al., 1994; Klingler and Gergen, 1993; Manoukian and Krause, 1992). In this manner the *Drosophila* embryo is more and more subdivided into segmental regions. Input from this pair rule gene network allows the precise regulation of segmentally expressed segment polarity genes (DiNardo and O'Farrell, 1987; Ingham et al., 1988; Lawrence et al., 1987). The genes *wingless* and *engrailed* are expressed in direct vicinity and control each others activity by interdependent regulation (Baker, 1988; DiNardo et al., 1985; Sanson, 2001). In this manner the *Drosophila* embryo is more and more subdivided into segmental regions. *wingless* and *engrailed* expressing cells define parasegment borders, the eventual segment borders form posterior to the *engrailed* expressing cells (Ingham et al., 1988; Lawrence and Struhl, 1996; Martinez-Arias and Lawrence, 1985). Interestingly this segment polarity gene regulation is specific for every procephalic head segment while it is identical in every segment posterior to the mandibular segment (Gallitano-Mendel and Finkelstein, 1997).

The identity of the different segments which are patterned through this regulatory cascade along the anterior-posterior axis of the embryo is mediated through activity of the highly conserved Hox genes (Garcia-Fernàndez, 2005; Lewis, 1978). The expression of these genes is mainly regulated through combinatorial regulation by gap and pair rule genes (Casares and Sanchez-Herrero, 1995; Harding and Levine, 1988; Irish et al., 1989b; Jack and McGinnis, 1990).

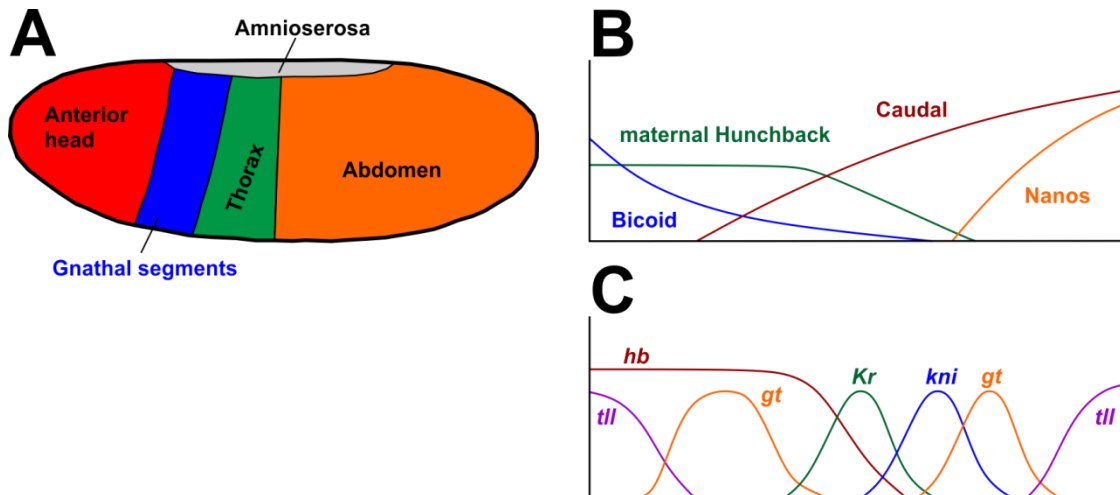


Figure 2-1 Fate map, early maternal gradients and Gap gene expression in *Drosophila*

(A) Fate map of a *Drosophila* blastoderm stage embryo. *Drosophila* is a long germ developing insect and all body segments are established during blastoderm stages. Anterior to the left and dorsal side up. (B) Protein gradients of maternal determinants. The transcripts for *hunchback* and *caudal* are ubiquitously present in the egg but their translation is regulated by the localized factors Bicoid and Nanos. Diffusion leads to protein gradients which, together with signals from the terminal system at the poles of the egg, regulate spatial expression of gap genes (C). The gap genes in turn interact by interdependent transcriptional regulation and further define their expression domains. The syncytial state of the egg allows the formation of protein gradients by simple diffusion. *hb*: *hunchback*, *tll*: *tailless*, *gt*: *giant*, *Kr*: *Krüppel*, *kni*: *knirps*. A after Hartenstein (1993), B and C after Peel et al. (2005). Anterior to the left in the schematic representations.

2.4 Segmentation and the anterior-posterior system in *Tribolium*

During the last twenty and more years, the red flour beetle *Tribolium castaneum* has become more and more popular as a model organism for insect developmental biology. The extensive knowledge gathered from *Drosophila* research has allowed to study and compare homologous genes in *Tribolium* and compare the molecular basis of segmentation between the long germ developing fly and this short germ insect (Brown and Denell, 1996; Denell, 2008; Schröder et al., 2008). Many similarities could be detected but also some striking differences were discovered. In summary it turned out that late processes during segmenta-

tion seem to be quite conserved. Parasegment boundaries are established by adjoining *Tc-wingless* and *Tc-engrailed* expression (Brown et al., 1994; Nagy and Carroll, 1994). Segment identity is controlled by Hox gene activity and overall expression and function of these Hox genes is very similar to *Drosophila* despite minor differences (Brown et al., 1999b; Curtis et al., 2001; Nie et al., 2001; Shippy et al., 1998; Shippy et al., 2000).

Bigger differences were detected by analysis of earlier patterning processes like pair rule and gap gene function. Some of these differences were not too surprising, since the short germ mode of development found in the beetle has different requirements during early embryonic processes. For example, most pair rule gene expression domains in *Tribolium* are generated during segment addition processes in the terminal growth zone (Brown and Denell, 1996) which is in strong contrast to *Drosophila* where all pair rule stripes are almost simultaneously formed as a readout of maternal determinants and gap gene input (Klingler and Tautz, 1999). Gap genes do play a role for *Tribolium* embryogenesis as well and there are some similarities in their expression compared to *Drosophila*. *Tc-knirps*, *Tc-giant*, and *Tc-hunchback* each form a gnathal and a more posterior domain in the embryo while *Tc-Krüppel* is expressed only in one domain. However, the expression domains usually do not directly correspond to the expression in *Drosophila* and most aspects of their regulation and interaction are still unknown. Additionally, due to the short germ mode of development, the posterior expression domains of *Tc-giant*, *Tc-knirps*, and the *Tc-Krüppel* domain become apparent at the posterior pole and are subsequently developing during germ band elongation. Posterior *Tc-hunchback* expression eventually develops during segment addition (Bucher and Klingler, 2004; Cerny et al., 2005; Cerny et al., 2008; Marques-Souza et al., 2008; Wolff et al., 1995). Gap gene function is also not directly comparable to *Drosophila*. Loss of function phenotypes of gap genes in *Tribolium* often show a disruption of posterior segmentation plus homeotic transformation of segments rather than a gap-like deletion of several segments which is typical for gap gene phenotypes in *Drosophila* (Bucher and Klingler, 2004; Cerny et al., 2005; Cerny et al., 2008; Marques-Souza et al., 2008; Rivera-Pomar and Jäckle, 1996). A fascinating finding was the identification of the gene *Tc-mille-pattes* (*Tc-mlpt*) which encodes for a polycistronic mRNA and has a gap-gene-like character. *Tc-mlpt* acts in a so far unknown manner and RNAi mediated knock down results in a breakdown of seg-

mentation and transformation of abdominal segments towards thoracic identity (Hashimoto et al., 2008; Savard et al., 2006).

Although some differences are present, *Tribolium* and *Drosophila* make use of similar processes to establish the different body segments. However, surprisingly little is known about early anterior-posterior axis formation in the beetle and how asymmetry is actually initiated. The anterior morphogen *bicoid* was shown to be specific for higher Diptera and is consequently not present in the beetle (Brown et al., 2001; Stauber et al., 1999). It has been suggested that Tc-Hunchback and Tc-Orthodenticle1 (*Otd1*) together substitute for Bicoid function since both mRNAs are maternally deposited and can be found ubiquitously in the early embryo. RNAi experiments, simultaneously targeting both genes, resulted in severe loss of anterior body structures, suggesting that both genes together initiate the formation of head, thorax and broad parts of the anterior abdomen (Li et al., 1996; Schinko et al., 2008; Schröder, 2003; Wolff et al., 1995). However, more recent work could show that neither Tc-Hunchback nor Tc-*Otd1* are key regulators for the initiation of early gnathal segments which means that they do not resemble the function of Bicoid (Kotkamp et al., 2010; Marques-Souza et al., 2008). Rather *Tc-otd1* fulfills the function of a head gap gene during later embryogenesis, as it is also described for *Drosophila* (Cohen and Jürgens, 1990; Schinko et al., 2008) and has an additional early function which is not yet entirely deciphered. Loss of early *Tc-otd1* function leads to a straightening of the germ-serosa boundary and an extension of the dorsal germ rudiment towards anterior, thereby reducing the extraembryonic tissue. It has been suggested that this is caused by a direct reduction of *Tc-sog* expression, an important ventral patterning gene, which would indicate a direct involvement of an anterior patterning system component in dorsal-ventral patterning. Another indication for a more tight connection between the anterior-posterior and the dorsal-ventral patterning system in *Tribolium* is caused by the observation that also RNAi against a maternally provided negative regulator of the canonical *wnt*-pathway, *Tc-axin*, causes at least a partial loss of the germ-serosa asymmetry in *Tribolium* (Fu et al., 2012). While the function of *Tc-axin* in this context is still completely unknown, the influence of *Tc-otd1* on setting the germ-serosa boundary is probably mediated by controlling the expression of the Hox-3 homolog *Tc-zen1*, an essential factor for development of the serosa (Falciani et al., 1996; Kotkamp et al., 2010; van der Zee et al., 2005). However, Tc-*Otd1* is not the only activator of

Tc-zen1 expression in the anterior of the embryo, input from the terminal system is also required. Double knock down of *Tc-otd1* with *Tc-torso* or *Tc-torso-like* indeed completely abolishes *Tc-zen1* expression (Kotkamp et al., 2010; Schoppmeier and Schröder, 2005). In *Drosophila*, the terminal system is necessary for proper formation of the head and the body regions posterior to the seventh abdominal segment (Klingler et al., 1988). In *Tribolium*, the posterior terminal system is of higher importance since loss of Tc-Torso-signaling leads to ablations of the first thoracic and all abdominal segments, ultimately resulting in loss of all growth zone-descended segments. This indicates that the ancestral function of the posterior terminal system might have been the determination of a growth zone (Schoppmeier and Schröder, 2005).

Since no clear organizer for anterior patterning could be identified to date, it has been suggested that input from the posterior factor Caudal might suffice to provide spatial information and to pattern the embryo along the anterior-posterior axis. This idea sounds plausible as the *Tribolium* embryo forms in the posterior half of the egg, near the posterior pole. *Tc-caudal* is a maternally supplied factor and initially ubiquitously expressed in the embryo. During development it is anteriorly repressed by the factors *Tc-zen2* and *Tc-mex3*, leading to a Caudal gradient which is low in the gnathal region of the blastoderm embryo and increases towards posterior, being highest at the posterior pole. During germ band elongation *Tc-caudal* is expressed in the posterior growth zone and is necessary for axis elongation. *Tc-caudal* RNAi indeed leads to loss of all body segments except for the anterior head (Copf et al., 2004; Schoppmeier et al., 2009; Schulz et al., 1998). However it is still unclear and arguable if this is due to a real early morphogen function (Figure 2-2).

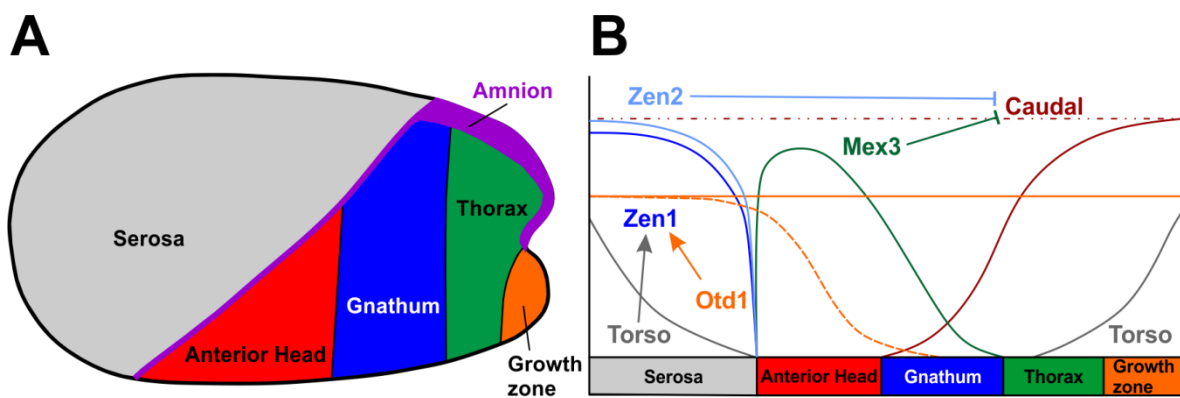


Figure 2-2 Fate map, expression domains and genetic interactions during the blastoderm stage of *Tribolium*

(A) Fate map of the differentiated blastoderm stage of *Tribolium castaneum*. Anterior to the left and dorsal side up. The anterior embryo gives rise to the extraembryonic serosa. Only the head and parts of the thorax are established in the blastoderm, the more posterior segments derive from a posterior growth zone. The anterior of the germ rudiment and the dorsalmost and dorsal posterior parts will form the amnion. (B) Schematic representation showing expression domains and interactions between early components in *Tribolium*. *Tc-caudal* is repressed in the anterior by *Tc-mex3* in the head region and *Tc-zen2* in the serosa. Without these genes it would be expressed ubiquitously (dashed red line). *Tc-otd1* is initially expressed ubiquitously (solid orange line) and later restricted to the anterior (dashed orange line). Otd1 and anterior Torso signal activate the serosa marker *Tc-zen1* in the anterior. A after Kotkamp et al. (2010), B integrates information from several publications (Kotkamp et al., 2010; Schoppmeier et al., 2009, van der Zee et al., 2005). Anterior to the left in the schematic representation.

2.5 The dorsal-ventral system in *Drosophila*

Also the establishment of the dorsal-ventral axis in *Drosophila* is initiated during maturation of the oocyte. DV-axis formation is dependent on action of Gurken-EGFR signaling during oogenesis. Gurken signaling along the prospective dorsal side of the oocyte leads to transcriptional inhibition of the ventralizing factor *pipe* in the dorsal half of the follicular epithelium. *pipe* expression in the ventral follicular epithelium stimulates a protease cascade that eventually activates the ligand for the Toll receptor, in turn leading to an intracellular degradation of Cactus, the inhibitor of Dorsal (reviewed by Moussian and Roth, 2005). Thus, expression of maternal factors leads to a concentration gradient of nuclear localized Dorsal transcription factor, along the DV-axis (Moussian and Roth, 2005; Stathopoulos and Levine, 2002). Different concentrations of nuclear Dorsal determine different fates along the ventral-dorsal axis, subdividing the embryo into three broad domains. Highest Dorsal levels on the ventral side determine mesodermal fate, marked for instance by expression of *twist* (Moussian and Roth, 2005). Intermediate levels of Dorsal define the neurogenic ectoderm and low levels or absence of the protein mark the non-neurogenic ectoderm and the amnioserosa (Moussian and Roth, 2005). Dorsal acts in *Drosophila* through activation and repression of a number of target genes. Wide-ranging genetic approaches using tiling arrays, whole-genome microarrays and ChIP-on-chip experiments have led to the identification of about 50 DORSAL target genes (Biemar et al., 2006; Stathopoulos et al., 2002; Zeitlinger et al., 2007) and make the system one of the best understood gene reg-

ulatory networks in embryonic development (Nunes da Fonseca et al., 2008; Stathopoulos and Levine, 2005).

Intermediate levels of Dorsal activate the transcription of *Dm-short-gastrulation* (*sog*) in two ventrolateral stripes in the neuroectodermal region of the embryo. *sog* encodes a secreted molecule which diffuses to the dorsal side (Francois et al., 1994; Srinivasan et al., 2002). The Sog protein is capable of binding the secreted signaling molecules Decapentaplegic (Dpp) and Screw (Scw) which belong to the BMP/Dpp-class of Transforming growth factor beta (TGF- β) signaling molecules. Dorsally, the Sog protein is cleaved by the metalloprotease Tolloid which allows Dpp and Scw to bind to their receptors. In this way Sog transports them dorsally and in turn inhibits Dpp-signaling in the prospective neuroectoderm (Eldar et al., 2002; Mizutani et al., 2005; Shimmi et al., 2005a; Wang and Ferguson, 2005) also reviewed in O'Connor et al., (2006). The *Drosophila* genome contains two closely related genes for this metalloprotease, *tolloid* and *tolkin*, which are not functionally redundant. The establishment of Dpp activity during embryonic development mainly depends on action of Tolloid (Marqués et al., 1997; Serpe et al., 2005). The process of Dpp/BMP modulation by extracellular regulators is very similar in vertebrates where the Dpp homolog BMP2/4 is bound by the Sog homolog Chordin, and Chordin cleavage again takes place through action of BMP1 (also called Xolloid) (reviewed in De Robertis and Kuroda, 2004)

The process of Dpp binding to Sog and subsequent Sog cleavage through Tolloid is quite well understood. However Dpp-signaling also depends on action of the extracellular CR domain protein Twisted-gastrulation (Tsg) which has a less well defined biochemical function (Little and Mullins, 2006). Three Tsg like proteins exist in *Drosophila* and all of them are positive regulators of Dpp. Tsg (Tsg1) and Shrew (Tsg3) are both necessary during embryonic development to generate high levels of Dpp on the dorsalmost side of the *Drosophila* embryo (Bonds et al., 2007; Nunes da Fonseca et al., 2010). The third paralogue, *crossveinless 1* (*cv1*, also called *tsg2*) is active during later developmental processes (O'Connor et al., 2006; Shimmi et al., 2005b; Vilmos et al., 2005). Interestingly, flies lacking function of both early active Tsg-proteins still show local Dpp activity (Nunes da Fonseca et al., 2010). Another mechanism used in the fly to restrict Dpp-signaling to the dorsal side is the direct transcriptional repression of *Dm-dpp* ventrally which results in the situation that patterning along the DV-axis takes place even if functional Sog is

absent (Jazwinska et al., 1999). Dorsal amplification of Dpp signaling also involves a positive feedback loop with the *zerknüllt* (*zen*) gene (Wang and Ferguson, 2005) whereas on the ventral side of the embryo *zen*, *tld* and *dpp* are repressed by Dorsal (Kirov et al., 1994; Shimell et al., 1991). *Drosophila* makes also use of the transcriptional repressor Brinker which negatively regulates Dpp target genes (Jazwinska et al., 1999; Liang et al., 2012). In addition to transcriptional and extra-cellular post-translational regulation of Dpp-signaling in *Drosophila*, several intra-cellular mechanisms have been described. One of them is characterized by the activity of the Smad ubiquitinylation regulatory factor (DSmurf). DSmurf is uniformly expressed and regulates Dpp signaling through degradation of the Dpp signaling effector Mothers against dpp (MAD) (Liang et al., 2003; Podos et al., 2001).

Using these complex mechanisms the fly generates a distinct Dpp signaling gradient along the dorsal-ventral axis, starting with a broad dorsal signaling domain which becomes quickly restricted to a narrow dorsal zone showing high signaling levels along the dorsal midline. Regions of highest Dpp activity are determined to form the amnioserosa, moderate Dpp signaling is found in the prospective dorsal epidermis and Dpp activity is low or absent in the regions of the neurogenic ectoderm and on the ventral side (Dorfman and Shilo, 2001; Ferguson and Anderson, 1992; Mizutani et al., 2006; Sutherland et al., 2003).

2.6 The dorsal-ventral system in *Tribolium*

Although our knowledge about DV-axis formation in *Tribolium* still lags far behind what is known in the fly, some clear differences but also similarities have become apparent during the last years. One big difference seems to be the impact of maternal versus zygotic input in DV-axis formation. While in *Drosophila* the factors for Toll signaling, like *cactus*, *dorsal*, and *toll* itself are supplied maternally, *Tc-toll* is expressed zygotically in the early *Tribolium* embryo. This expression is overlapping with the nuclear Tc-Dorsal gradient which led to the assumption, that Tc-Dorsal is necessary to activate *Tc-toll* (Chen et al., 2000; Maxton-Küchenmeister et al., 1999). Another difference affects the early Tc-Dorsal gradient. In *Drosophila* this gradient is stable until gastrulation and directly involved in establishing ventral cell fates. In *Tribolium* a gradient of Tc-Dorsal with peak levels on the ventral side is present as well, but this gradient is dynamic and Tc-Dorsal vanishes before gastrulation and the specification of ventral cells (Chen et al., 2000; Nunes da Fonse-

ca et al., 2008; Roth et al., 1989; Wheeler et al., 2005). Still Tc-Toll is necessary for all aspects of early DV-patterning in *Tribolium*. It is essential for the expression of *Tc-sog* and for most parts of *Tc-twist* expression (Nunes da Fonseca et al., 2008). However, it was shown that also without Tc-Toll a zygotic dorsal-ventral patterning process along the AP-axis involving Tc-Dpp remained active (Nunes da Fonseca et al., 2008). The Dpp system in *Tribolium* in general has a major impact on dorsal-ventral polarity and interfering with single components of this system causes severe phenotypes. *Tc-sog* RNAi embryos are completely dorsalized (double-dorsal phenotype) indicating that all ectodermal DV-patterning depends on the ventral expression of *Tc-sog*. *Tc-dpp* knock down in contrast leads to a complete loss of dorsal fates in favor of neurogenic ectoderm (van der Zee et al., 2006). The high relevance of Tc-Sog for patterning the ectoderm along the DV-axis seems to be an ancient feature at least in arthropods, since similar importance of Sog could be detected in the spider (Akiyama-Oda and Oda, 2006; Oda and Akiyama-Oda, 2008). In *Tc-sog* as well as in *Tc-dpp* RNAi phenotypes at least part of the extraembryonic serosa remains, showing that in contrast to *Drosophila* the formation of extraembryonic tissue does not entirely depend on dorsal-ventral patterning (van der Zee et al., 2006). The expression pattern of *Tc-dpp* is very dynamic during early embryogenesis and shows asymmetry along the DV- as well as along the AP-axis, indicating that Tc-Dpp signaling is not only coordinated along the DV-axis but also AP-wise (Nunes da Fonseca et al., 2010). During early blastoderm stages Tc-Dpp activity, as indicated by the distribution of phosphorylated MAD (pMAD), is restricted to a gradient in a dorsal anterior domain. It never forms a narrow dorsal stripe like in *Drosophila*. During differentiated blastoderm stages *Tc-dpp* expression is found in a narrow anterior domain at the border of serosal and embryonic tissue (germ serosa border) with higher expression levels in the ventral part. Dpp-signaling activity extends to the dorsal posterior part of the embryo where it eventually reaches peak levels which are necessary to build the dorsal amnion (Nunes da Fonseca et al., 2010; Sharma et al., 2013; van der Zee et al., 2005; van der Zee et al., 2006).

Regulation of Dpp signaling in *Tribolium* might be in some ways simpler, but without doubt it is different from *Drosophila*. One difference is that there is only one Dpp ligand (Tc-Dpp) in the beetle (van der Zee et al., 2006; Van der Zee et al., 2008). The *Tribolium brinker* homolog is not expressed in the early embryo,

hence it is not involved in early regulation of *Tc-dpp* target genes (van der Zee et al., 2006). Furthermore, *Tc-dpp* is not repressed by Tc-Dorsal which allows *Tc-dpp* expression also on the ventral most side of the embryo. *Tc-zen1* and *Tc-tolloid* are also not repressed by Tc-Dorsal which led to the assumption, that Tc-Dorsal completely lacks a repressor function (Chen et al., 2000; Nunes da Fonseca et al., 2008; Nunes da Fonseca et al., 2010). *Tc-zen1* is also not involved in formation of the Tc-Dpp gradient, since knock down embryos for *Tc-zen1* still show normal DV-polarity (van der Zee et al., 2005). Apart from *Tc-sog* two other extraembryonic Tc-Dpp regulators have been described which also have orthologs in *Drosophila*. *Tribolium* has one homolog of the metalloprotease Tolloid (Tc-Tld) which has an important function for dorsal-ventral patterning, since RNAi embryos for *Tc-tld* show almost complete loss of Tc-Dpp activity. Furthermore, knock down of the single *Tribolium* homolog for *twisted-gastrulation* (*Tc-tsg*) probably results in total loss of Tc-Dpp signaling as the phenotype resembles the *Tc-dpp* knock down phenotype (Nunes da Fonseca et al., 2010; van der Zee et al., 2006). *Tribolium* also shows expression of an ortholog to the pseudoreceptor Bambi (BMP and Activin Bound Inhibitor) which inhibits Dpp/BMP-signaling by building heterodimers with type I BMP receptors in vertebrates (Nunes da Fonseca et al., 2008; Onichtchouk et al., 1999; Van der Zee et al., 2008).

In summary, major differences between *Tribolium* and *Drosophila* dorsal-ventral patterning seem to lie in the degree of maternal and zygotic input into the system and the regulation of Dpp-signaling during development. It could be shown that negative and positive feedback loops are involved in patterning the *Tribolium* embryo along the DV-axis (Nunes da Fonseca et al., 2008, Figure 2-3), illustrating the extensive interactions of zygotic factors. Although many candidates known from *Drosophila* have been studied in *Tribolium* during the last years, many details of *Tribolium* DV-patterning remain unknown.

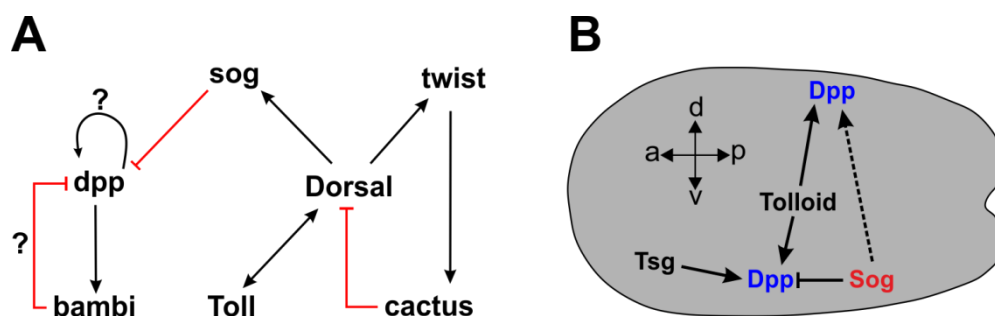


Figure 2-3 Dorsal-ventral patterning in *Tribolium*

(A) gene regulatory networks during dorsal-ventral patterning in *Tribolium*. Tc-Dorsal and Tc-Toll display a positive feedback loop. Tc-Dorsal inhibits *Tc-dpp* by activating *Tc-sog*, but it does not directly repress *Tc-dpp* expression. A self activation loop is suggested for *Tc-dpp* which at the same time might be regulated through a negative feedback loop via expression of the signaling inhibitor *Tc-bambi*. (B) Simplified model of extracellular Tc-Dpp signaling regulation in the *Tribolium* blastoderm. Tc-Sog is expressed on the ventralmost side and binds Tc-Dpp ligands. Dpp/Sog complexes diffuse to the dorsal side. Tc-Tolloid activates Tc-Dpp through cleaving of Tc-Sog molecules. This results in an indirect activation of Tc-Dpp dorsally through Tc-Sog-dependent transport of Tc-Dpp to the dorsal side. Tc-Twisted gastrulation (Tc-Tsg) is necessary for Tc-Dpp signaling. A based on (Nunes da Fonseca et al., 2008), B based on (Nunes da Fonseca et al., 2010; van der Zee et al., 2006).

2.6.1 The BMP pathway

Because of the great importance of the Transforming growth factor β (TGF- β)/bone morphogenetic protein (BMP) signaling pathway for DV-axis formation I will shortly focus on the diverse ways in which this pathway is regulated. TGF- β signaling has been in the focus of research for almost thirty years and its important function with respect to cell growth, differentiation and development has been intensively studied (Harland and Gerhart, 1997; Kingsley, 1994; Kitisin et al., 2007; Moses and Serra, 1996). The TGF- β superfamily consists of about a dozen gene families, however, all members can be grouped into two classes: the TGF- β -like class and the BMP-like class which also includes Decapentaplegic (Dpp) from *Drosophila* and *Tribolium* (Kingsley, 1994; Pang et al., 2011). Members of the second class are especially famous for their important functions during dorsal-ventral patterning in vertebrates and invertebrates (De Robertis and Kuroda, 2004; De Robertis and Sasai, 1996; Pang et al., 2011). Consistent with the important biological functions, TGF- β ligands and members of its associated signaling pathway have been identified in all metazoans studied so far. However no TGF- β receptor or ligand has been identified outside the metazoa (Huminiacki et al., 2009; Richards and Degnan, 2009). TGF- β -like ligands signal through a complex of type I and type II serine/threonine-kinase transmembrane receptors (T β R-I and T β R-II), which then activate the Smad signaling pathway by intracellular phosphorylation of receptor regulated Smads (R-Smads) through the type I kinase receptor. R-Smads are characterized by two protein domains, the Mad-homology domains 1 and 2 (MH1 and MH2) which are divided by a linker region. Receptors for TGF- β and activin signal through phosphorylation of Smad2 and Smad3 whereas receptors

for Decapentaplegic (Dpp)/BMP target MAD/Smads 1, 5 and 8 (Smad1/5/8) (Attisano and Tuen Lee-Hoeflich, 2001; Feng and Derynck, 2005; Massagué, 1998). These activated R-Smads bind to a common mediator Smad (co-Smad, Smad4/Medea) in the cytosol and this complex is then translocated into the nucleus where it regulates target gene transcription (reviewed in Derynck and Zhang, 2003).

The TGF- β -signaling pathway can be negatively regulated at several points, extracellularly, within the cytosol and in the nucleus. In the extracellular region diffusible factors like Chordin/Sog can prevent TGF- β -like proteins from receptor binding (reviewed in Balemans and Van Hul, 2002). As already mentioned Tolloid is capable of cleaving Chordin/Sog, thereby releasing BMP/Dpp and allowing it to activate target receptors (Marqués et al., 1997). Within the nucleus the corepressors of the Ski/SnoN protein family can directly associate with Smads and in this way inhibit TGF- β -signaling (Liu et al., 2001). In the cytosol there are several working points for signal regulation and modulation known. For instance the pseudoreceptor Bambi is able to prevent the TGF- β -receptors to build a functional complex (Onichtchouk et al., 1999). Furthermore TGF- β -signaling inhibition can be mediated via the activity of inhibitory Smads (I-Smads, Smad 6/7/Dad). These I-Smads display several different modes of operation. They form stable complexes with activated T β R-I and interfere in this way with R-Smad phosphorylation (Hayashi et al., 1997; Lönn et al., 2009). Smad 6 has been shown to bind to receptor-activated Smad1, in this way competing with Smad4 for R-Smad binding (Hata et al., 1998). Furthermore, I-Smads can recruit the Smad ubiquitin regulatory factor (Smurf) E3 ubiquitin ligases to type-I receptors which results in receptor polyubiquitination and subsequent degradation through the proteasomal pathway (Ebisawa et al., 2001; Itoh and ten Dijke, 2007; Xia et al., 2010; Yan et al., 2009). Finally, I-Smads can also act in the nucleus where they are able to interact with transcriptional repressors, or inhibit the formation of functional Smad/DNA complexes (Bai et al., 2000; Lin et al., 2003; Zhang et al., 2007).

2.6.1.1 Smurf E3 ubiquitin ligases in the BMP pathway

Smurf proteins belong to the Nedd4 family of E3 ubiquitin ligases which in turn are part of the HECT (homologous to E6AP C-terminus) type of E3 ligases

(Cao and Zhang, 2012; Rotin and Kumar, 2009). During ubiquitination one or more ubiquitin molecules are bound to a particular target. This multistep process involves activation of a ubiquitin via a ubiquitin activating enzyme (E1), its subsequent transfer to a ubiquitin conjugating enzyme (E2) and its eventual covalent conjugation to the target substrate via a ubiquitin ligase (E3) (reviewed in Pickart, 2001; Rotin and Kumar, 2009). Conjugation always takes place between the carboxyl group of the carboxy-terminal Glycine residue of ubiquitin and the ϵ -amino group of an internal Lysine in the substrate.

Polyubiquitination is the sequential transfer and subsequent conjugation of ubiquitins to one or more Lysine residues of the same substrate, resulting in chains of ubiquitin and involving ubiquitination of ubiquitin itself (reviewed in Hicke and Dunn, 2003; Rotin and Kumar, 2009). The substrate specificity during ubiquitination is mainly determined by the E3 ubiquitin ligases. For this reason genomes usually exhibit only few E1 activating enzymes (the human genome has 2 potential E1s), a small number of E2 conjugating enzymes (human: about 30) and many E3 ubiquitin ligases (the human genome encodes over 600 E3s) (Li et al., 2008; Rotin and Kumar, 2009).

The first described member of the Smurf family was XSmurf1 from *Xenopus laevis* which was reported for its role in the BMP pathway (Zhu et al., 1999). Shortly later a second Smurf protein (Smurf2) has been identified and a homolog was also described and functionally analyzed in *Drosophila* (Lin et al., 2000; Podos et al., 2001). All Smurf proteins consist of an N-terminal C2 domain, several WW domains and a C-terminal HECT domain. The N-terminal C2 domain is described to be capable of membrane binding and it is involved in the binding of certain substrates of human Smurf1 (Cao and Zhang, 2012; Tian et al., 2011; Yamaguchi et al., 2008). WW domains function in substrate interaction through binding to PY (PPxY) motifs and several interactions of Smurf proteins via these domains have been reported (Cao and Zhang, 2012; Macias et al., 2002). The binding efficiency may be improved through the phosphorylation of particular sites on certain substrates (Aragón et al., 2011). The HECT domain is the actual enzymatic domain of the Smurf proteins and necessary to bind the ubiquitin which is delivered by the E2 ubiquitin conjugating enzyme to the target protein. This happens through a conserved cysteine which forms thioester bonds with the ubiquitin molecule (Huang et

al., 1999; Rotin and Kumar, 2009). Figure 2-4 shows a schematic representation of the human Smurf1 protein.

Several functions of Smurf1 and Smurf2 during vertebrate development have been described. One of their main functions is probably the regulation of TGF- β signaling via interaction with Smad proteins but a high number of other interaction partners and substrates have been described since the first description of Smurf1 in 1999 (Cao and Zhang, 2012). In addition to targeting R-Smads for ubiquitination mediated degradation, Smurf proteins have been described to be recruited by adaptor proteins for the degradation of TGF- β and Dpp/BMP receptors (Ebisawa et al., 2001; Kavsak et al., 2000; Murakami et al., 2003; Xia et al., 2010). Despite the high conservation and the involvement in important signaling pathways the loss of function phenotypes for Smurfs are often surprisingly weak (Cao and Zhang, 2012). In vertebrates this might partially be due to functional redundancies between Smurf1 and Smurf2 as described for *Smurf* genes in the mouse (Narimatsu et al., 2009; Tang et al., 2011; Yamashita et al., 2005). Studies in *Xenopus* suggest that in the frog there are some overlapping functions of both *Smurf* genes but also distinct differences. During embryogenesis *Smurf1* is stronger expressed in the dorsal side of gastrula stage embryos and experiments using an antisense morpholino oligonucleotide and a dominant negative mutant resulted in neural defects (Alexandrova and Thomsen, 2006). *Xenopus Smurf2* is reported to be involved in both neural development and mesodermal patterning, hence both genes have important functions during *Xenopus* development (Das and Chang, 2012). Functional information about *Smurf* genes outside of the vertebrates is highly limited. A mutation in the *Drosophila* ortholog *DSmurf* caused defects in hindgut morphogenesis, loss of hindgut integrity, mild head defects and sometimes led to incomplete dorsal closure due to increased Dpp signaling and accumulated pMAD (Podos et al., 2001). It was found that DSmurf specifically targets MAD for proteasomal degradation and does not interact with Dad, Medea or DSmad2. Targeted expression of DSmurf abolished phosphorylated MAD and disrupted growth and patterning (Liang et al., 2003). However, it is also reported that DSmurf builds a complex with Fused, a serine/threonine kinase, to regulate the BMP receptor Thickveins in *Drosophila* cystoblasts (Xia et al., 2010). In addition to the function during development, several studies reported a function of DSmurf in

regulating Dpp signaling in the *Drosophila* germ line (Casanueva and Ferguson, 2004; Chang et al., 2013; Xia et al., 2010).



Figure 2-4 Domains of the human Smurf1 protein

Smurf proteins consist of four typical domains: an N-terminal C2 domain, several WW domains and a C-terminal, enzymatic HECT domain. The active center is formed by a cysteine (red). See text for further information. After (Cao and Zhang, 2012). Picture created with Geneious version 7 (Biomatters).

2.6.1.2 MAD at the crossroads of signaling pathways

Formation of the dorsal-ventral body axis via Dpp/BMP signaling is a conserved feature among animals and found in vertebrates and invertebrates (De Robertis, 2006; De Robertis, 2008; De Robertis and Sasai, 1996; Little and Mullins, 2006; O'Connor et al., 2006). The main anterior-posterior gradient for axis formation in *Xenopus* is provided by Wnt signals (Kiecker and Niehrs, 2001; Niehrs, 2004) and studies on the regeneration in planarians strongly support that canonical Wnt signaling specifies posterior fate (Gurley et al., 2008; Liu et al., 2013; Petersen and Reddien, 2008; Umesono et al., 2013). Regarding these conserved patterning pathways it is interesting that several studies during the last decade have detected a broad integrative potential for different signaling pathways on the level of the MAD/Smad1/5/8 protein (Eivers et al., 2008; Eivers et al., 2009b).

Dpp/BMP signaling leads to the C-terminal phosphorylation of MAD/Smad1/5/8 on two conserved serine residues by a serine/threonine receptor. Phosphorylated MAD/Smad can bind to the co-Smad Medea/Smad4 and enter the nucleus to control target gene expression (Feng and Derynck, 2005; Shi and Massagué, 2003). It was detected in human cell culture, that mitogen-activated protein kinase (MAPK) can also act on Smad1/5/8 via a canonical phosphorylation site (PXSP) in the linker region between the MH1 and MH2 domain of the protein. The serines in these sites are phosphorylated by MAPK following activation by EGFR signaling (Kretzschmar et al., 1997). The necessary phosphorylation sites can be found in all BMP-activated Smads (1/5/8), and are also present in *Drosophila* MAD (Eivers et al., 2008). Phosphorylation in this linker region leads to a termination of the Dpp/BMP signal via ubiquitination mediated degradation of the

MAD/Smad1/5/8 molecule (Fuentelba et al., 2007; Sapkota et al., 2007). The MAPK phosphorylation site is a few amino acids aminoterminal to the Smurf binding site. In the vicinity of the MAPK phosphorylation site there are several potential phosphorylation sites for Glycogen Synthase Kinase-3 (GSK3) (Eivers et al., 2008; Eivers et al., 2009b, Figure 2-5). A feature of GSK3 is that many of its substrates need to be pre-phosphorylated ('primed') by other protein kinases before they can be phosphorylated by GSK3. The priming takes place on a serine or threonine four amino acids carboxyterminal from a serine or threonine that can then in turn be phosphorylated by GSK3 (S/TXXXXS/T) (Cohen and Frame, 2001). GSK3 is part of the β -Catenin destruction complex which keeps β -Catenin levels low in the cytosol in the absence of Wnt signals (Logan and Nusse, 2004). Canonical Wnt signaling inhibits GSK3 by translocating it to LRP6-signalosome membrane vesicles (Bilic et al., 2007). In the case of MAD in *Drosophila* and Smad1/5/8 in vertebrates pre-phosphorylations for GSK3 can be delivered by MAPK. Indeed it has been shown that the double phosphorylation by MAPK and GSK3 resulted in Smad1 transport to the pericentrosomal region, proteosomal degradation and thus termination of the BMP signal (Fuentelba et al., 2007). In *Drosophila* MAD has a function for Wingless signaling during wing development and segmental patterning (Eivers et al., 2009a). Additionally, it was described that the Dpp and Wingless signaling pathways compete for unphosphorylated MAD. MAD can act in the Wingless pathway as long it is not phosphorylated by the Dpp receptor (Eivers et al., 2011). In summary at least three different pathways can regulate the activity of MAD/Smad1/5/8, allowing the integration of different pathways through different phosphorylation states of a single transcription factor.

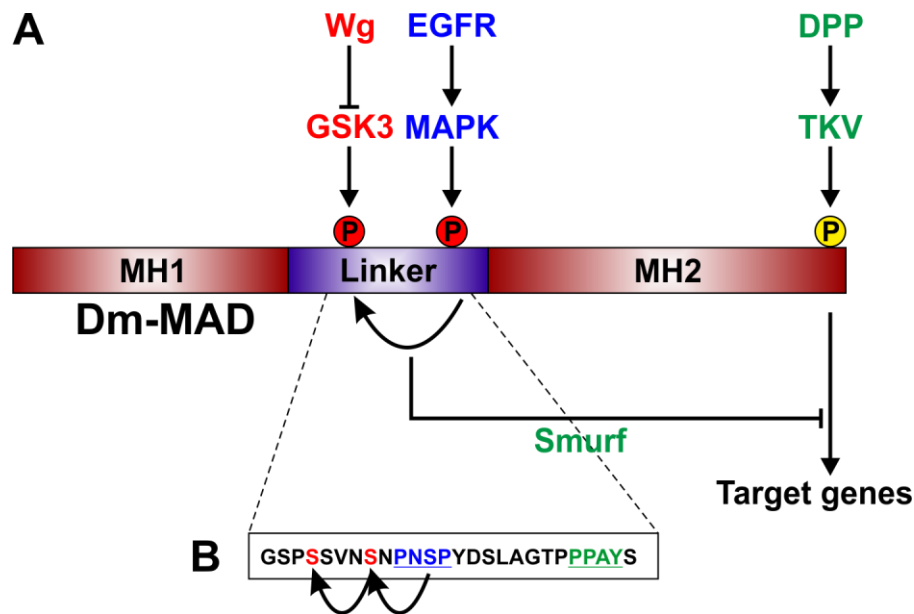


Figure 2-5 Different pathways converge on the phosphorylation state of the MAD protein

(A) Schematic drawing of the Mothers against Dpp protein (MAD) of *Drosophila melanogaster*. The Dpp pathway phosphorylates the protein at the C-terminus via the Thickveins (TKV) receptor, resulting in MAD binding to Medea, nuclear translocation and the regulation of target genes. MAP kinase (MAPK) can phosphorylate MAD in the linker region, which allows phosphorylation by GSK3 and proteasomal degradation through the Smurf E3 ubiquitin ligase. (B) Amino acid sequence of a part of the linker region from *Drosophila* MAD. Green (PPAY) is the Smurf binding site. Blue (PNSP) is the consensus sequence for MAPK phosphorylation. Phosphorylation takes place at the serine residue within the consensus sequence. Red marks the serines which can be phosphorylated by GSK3 after priming of the MAD molecule through MAPK. Slightly modified after (Eivers et al., 2008; Eivers et al., 2009b).

2.7 A genome wide RNAi screen in *Tribolium castaneum*

Due to easy culturing, short generation time, easily accessible embryos (Sokoloff, 1972), and the fact that the beetle is suited for a large set of experimental methods, *Tribolium castaneum* became a more and more popular model system for developmental biology and a number of other fields. The accessibility to standard techniques like immunohistochemistry and *in situ* hybridization (Patel et al., 1994; Sommer and Tautz, 1993) was a key requirement for the study of gene functions during development. The establishment of robust RNA interference (RNAi) techniques (Brown et al., 1999a; Bucher et al., 2002) and functional transformation systems (Berghammer et al., 1999b; Lorenzen et al., 2003; Pavlopoulos et al., 2004) allowed comprehensive functional analyses and even a large scale insertional mutagenesis screen (Trauner et al., 2009). One of the recent and most important mile stones in *Tribolium* research was the publication of the genome sequence (Richards et al., 2008). This comprehensive set of tools allowed the func-

tional analysis of genes which were described in *Drosophila* or vertebrates. Indeed, this ‘candidate gene approach’ served very successful for many years and a large number of genes have been analyzed in a number of processes, including segmentation (see 2.4), axis formation (see 2.4 and 2.6), or head patterning (Posnien et al., 2011; Schinko et al., 2008). However, this approach is restricted to inherent limitations and depends on the identification of candidates in other species. The different modes of development between *Drosophila* and *Tribolium* make it very likely that the beetle makes use of a number of different factors than the fly. And indeed the identification of the transcriptional repression of *Tc-caudal* through *Tc-mex3* as well as the identification of the unusual Gap-gene *Tc-mille-pattes* confirm this assumption (Savard et al., 2006; Schoppmeier et al., 2009). But also some key regulators for dorsal-ventral (2.5 and 2.6) and anterior-posterior (2.3 and 2.4) patterning are missing in *Tribolium* compared to *Drosophila* and the substitutes are not known in many cases. Filling the gaps in our knowledge on these developmental processes requires an extensive, unbiased screening approach.

The most reasonable way to meet this demand in *Tribolium* is a large scale RNAi screen. The powerful and easily applicable technique of parental RNAi allows the production of a high number of embryonic loss of function phenotypes with reasonable workload (Bucher et al., 2002). RNAi has a number of advantages over genetic screens in *Tribolium*. The lack of a comprehensive set of balancers for the ten chromosomes in *Tribolium* makes a mutagenesis screen in the beetle very laborious and costly (Berghammer et al., 1999a). Since a mutagenesis screen would require long term stockkeeping, a saturating screen in *Tribolium* is not suitable with the limited labs working on *Tribolium* worldwide (Trauner et al., 2009). A genome wide RNAi screen allows the annotation of the phenotype along with the identity of the targeted gene in a database, which allows permanent access to all necessary data for easy reproduction of the experiment without extensive stockkeeping (Schmitt-Engel, 2010; Schmitt-Engel et al., in preparation). As RNAi is a reverse genetics approach, no time consuming identification of the mutated gene is necessary. Furthermore, in a classical genetic screen only 25 % of the larvae are homozygous for a zygotic mutation (St Johnston, 2002). The strong RNAi response in *Tribolium* can reach up to 100 % efficiency for particular effects (Bucher et al., 2002). Finally, depending on a well annotated genome, it is a lot easier to estimate the saturation of an RNAi screen compared to a mutagenesis

screen where an unequal distribution of the mutations along the genome makes this task more complicated (Pollock and Larkin, 2004).

2.7.1 The iBeetle screening concept (design of the iBeetle screen)

Several German *Tribolium* research groups have joined under the guidance of Gregor Bucher (Göttingen) and Martin Klingler (Erlangen) to perform a genome wide RNAi screen in the red flour beetle to identify candidate genes involved in a set of different processes. By realizing this project, *Tribolium* is brought forward as a model organism for developmental biology. A detailed description of the screen, the participating research groups, and the core projects can be found in (Schmitt-Engel, 2010 and under <http://ibeetle.uni-goettingen.de/>). The design of the iBeetle screen has been a major topic in the PhD project of C. Schmitt-Engel. During this project, which contained a detailed pre-screen, it was successfully proven that the iBeetle screening concept is doable and leads to new phenotypes (Schmitt-Engel, 2010). In this paragraph the actual concept will be shortly mentioned, the detailed screening procedure for the pupal injection screen is explained in the materials and methods section (3.6).

The screening project is split into two major funding periods of three years each. The participating PhD students screen for about 12–14 month and work afterwards on a particular project to analyze candidate genes found during the screening process. The iBeetle screen is supposed to fulfill three major tasks:

- Identification of genes for processes which are not analyzable in *Drosophila* or very difficult to study in the fly. This is for instance true for larval leg musculature (the *Drosophila* larva does not have legs) or embryonic head development, since *Drosophila* undergoes head involution (Bucher and Wimmer, 2005).
- The identification of genes which are not present or have a different function in the fly.
- The establishment of *Tribolium* as a usable screening platform for genome wide studies and the acquisition of a comprehensive set of functional data for particular developmental processes. The latter will be available via an online database and open for the entire *Tribolium* community (iBeetle-Base, <http://ibeetle-base.uni-goettingen.de/search/phenotypeSearch.jsf>).

The *iBeetle* screen consists of two experimentally independent screening parts: the larval injection screen, mainly focusing on insect metamorphosis and development of the odoriferous glands (which are not present during larval stages), and the pupal injection screen, having the main focus on embryonic development including embryonic muscle formation. Transgenic lines driving tissue-specific GFP expression are used in both screening parts in order to make the screen more effective. The transformation marker is in both cases an *EGFP* gene under control of the 3xP3 promoter (Berghammer et al., 1999b; Horn and Wimmer, 2000). In the larval injection screen, dsRNA injection is performed with female *Tribolium* L5 and L6 larvae and the injected animals are analyzed in downstream screening steps. Injection takes place in larvae of the *mD17* strain which carry a not localized insertion of a *minos-3xP3-EGFP* construct, leading to EGFP expression in the metathoracic musculature which allows screening for muscle defects in this body part (Pavlopoulos et al., 2004). Since the larval injection screen had no impact on the project described in this thesis, I refer to (Schmitt-Engel, 2010; Schmitt-Engel et al., in preparation) for more information. In the pupal injection screen female pupae of the *Pig-19* strain (Lorenzen et al., 2003; Trauner et al., 2009) were injected, crossed to male beetles, and the offspring was analyzed for developmental defects (parental RNAi) (Bucher et al., 2002). During this screening part the main focus was on the offspring of the injected animals. The *Pig-19* strain expresses GFP in the larval body musculature, allowing the identification of defects during muscle development or mesoderm establishment in general. Defects affecting ectodermal structures were analyzed by doing cuticle preparations on the progeny of injected females.

The *iBeetle* screen is designed as a first pass screen, which means that every injection is done only once (although in several animals), without experimental replicates. In order to monitor and maintain the screening quality, continuous positive and negative controls are included in the screening process.

2.8 Aims of this study

The intention of this project was to discover and analyze new genes which are required for the formation of the anterior body region of *Tribolium* in order to fill some of the remaining gaps of knowledge in this field of research. The main interest laid in the identification and further analysis of factors which are not known to be involved in this patterning process in *Drosophila*. To achieve this aim the project was roughly divided into three different phases: First a screening phase of approximately fourteen months to identify potential candidate genes. During this phase I actively participated in the pupal injection screening procedure of the iBeetle project. All phenotypes detectable with the iBeelte system - including head and anterior patterning defects - were annotated by all screeners, (Schmitt-Engel, 2010; Schmitt-Engel et al., in preparation). Secondly, a candidate selection phase of about six months, which still had screening character but already involved other analytical methods like *in situ* hybridization stainings to confirm the gene specific effects and to get a deeper understanding of the observed phenotypes. The ambition of this phase was to pick the most exciting and promising candidates from the high number of potential patterning genes which showed head phenotypes after RNAi mediated knock down. Aim of the last phase was to decipher the genetic and mechanistic networks underlying the observed phenotypes and genes. This aim was mostly followed by analysis of molecular markers after candidate gene knock down.

3 Materials and Methods

3.1 *Tribolium castaneum* culture and strains

Tribolium castaneum beetles were reared under standard conditions (Brown et al., 2009). The wild type strain *San Bernardino* (*SB*) was used for RNAi experiments, *in situ* hybridization, and immunohistochemistry. The *Pig-19* strain (formerly also called *pBA19*) was used for injection of female pupae which were mated to adult males from the *Black* (Sokoloff et al., 1960) strain (dark adult cuticle) in the iBeetle screen, to allow easy discrimination between injected females and not injected males in the downstream screening analysis. The *Pig-19* strain was also used in later experiments for dsRNA injection, *in situ* hybridization, and immunohistochemistry. For live imaging experiments a transgenic line expressing nuclear localized GFP in all cells was used (*nGFP*-line) (Sarrazin et al., 2012).

3.2 Molecular biology

Unless mentioned otherwise, cloning techniques were carried out using standard methods (Sambrook and Russell, 2001).

Genes were cloned from complementary DNA (cDNA) using gene specific primers. cDNA was synthesized using the SMARTer® cDNA Synthesis Kit (Clontech, Mountain View, CA, USA). Messenger RNA (mRNA) was isolated from a 0–72 h embryo collection using TRIzol® Reagent (Life Technologies, Carlsbad, CA, USA). For rapid amplification of cDNA ends (RACE), first strand cDNA was synthesized using the SMARTer™ RACE cDNA Amplification Kit (Clontech, Mountain View, CA, USA). mRNA for RACE was isolated from a 0–72 h embryo collection using the MicroPoly(A)Purist™ Kit (Life Technologies, Carlsbad, CA, USA). Gene specific primers were designed based on the AUGUSTUS gene predictions (AUGUSTUS UTR and hints from cDNA) and available transcriptome data using the *Tribolium* gene browser (<http://bioinf.uni-greifswald.de/gb2/gbrowse/tribolium/>). Genes were either identified by using their iBeetle ID number (e.g. *iB_02881*) which is implemented in the gene browser, or by searching for *Tribolium* orthologs with *Drosophila* gene sequences at the National Center for Biotechnology Information (NCBI, <http://blast.ncbi.nlm.nih.gov/Blast.cgi>) using the Basic Local Alignment Search Tool (Altschul et al., 1990). Primer synthesis was carried out by

Eurofins MWG Operon (Ebersberg, Germany). A complete list of primers used in this work is attached in the appendix and on the DVD (DVD, folder 'primers'). Gene fragments were amplified using Advantage® 2 Polymerase (Clontech, Mountain View, CA, USA). Fragments were cloned into the pCR®II vector using the TA Cloning® Kit (Life Technologies, Carlsbad, CA, USA). Several clones were kindly provided by other people or laboratories (Table 3-1).

Cloned gene fragments were sequenced by Macrogen (Seoul, Korea and Amsterdam, Netherlands) usually using standard M13F (GTAAAACGACGGCCAGTG) or M13R (GGAAACAGCTATGACCAT) primers. For some genes additional sequencing primers were used:

For *Tc-smurf* the additional sequencing primer JSP182 (ATCGCCGACTTCGACGTCTGTTATTCC), for *TC008419* the additional sequencing primer JSP181 (ATCAACAACACCAACTCCGACCGG), and for *TC006853* the additional sequencing primer JSP183 (TCTGATCTCATTGTACCGCAGCGACAAG) has been used.

All gene sequences isolated during this project are included in the DVD (folder 'Genes_Sequences', subfolders for every gene).

Clone	Provided by	Location	Gene Accession number	Göttingen Tribolium Group Nr. (if available)
<i>Tc-pnr</i>	Michael Schoppmeier	Department of Biology, Developmental Biology, Erlangen	XM_967958	
<i>Tc-wg</i>	Johannes Schinko	Department for Developmental Biology, Göttingen	NM_001114350	104
<i>Tc-sog</i>	Fonseca/Roth	Bio Center Köln, Department for Developmental Biology	NM_001042571	161
<i>Tc-mlpt</i>	Schoppmeier/Savard	Department of Biology, Developmental Biology, Erlangen	NM_001134482	93
<i>Tc-zen1</i>	Martin Klingler	Department of Biology, Developmental Biology, Erlangen	NM_001043348	150
<i>Tc-six3</i>	Nico Posnien	Department for Developmental Biology, Göttingen	NM_001113467	39

Clone	Provided by	Location	Gene Accession number	Göttingen <i>Tribolium</i> Group Nr. (if available)
<i>Tc-twist</i>	Siegfried Roth	Bio Center Köln, Department for Developmental Biology	AJ829922	
<i>Tc-ash</i>	Nikolaus Koniszewski	Department for Developmental Biology, Göttingen	NM_001039448	134
<i>Tc-dpp</i>	Nico Posnien	Department for Developmental Biology, Göttingen	NM_001039451	56
<i>DsRed</i>	Hendrikje Hein	Department for Developmental Biology, Göttingen	---	99

Table 3-1 (Also previous page) Origin of used cDNA clones that were provided by other groups

Indicated is the name of the gene, the provider and the location, the gene accession number according to GenBank (<https://www.ncbi.nlm.nih.gov/genbank/>), and (if available) the clone number used by the Göttingen *Tribolium* Group (Department for Developmental Biology).

3.3 Orthology and phylogeny analysis

In order to identify the orthology of genes of interest, the nucleotide sequence information of candidates was used for BLAST analysis using the blastx algorithm on the NCBI database for non-redundant protein sequences of *Drosophila melanogaster* (Altschul et al., 1990). The obtained fly sequences were in turn used for a BLAST search in the *Tribolium* genome, to check if the expected orthology could be confirmed (reciprocal blast). More detailed phylogenetic analyses were not done for the preliminary selection of iBeetle candidates.

To identify other potential members of the *Smurf* family in *Tribolium* as well as closely related genes, the following approach was pursued. The isolated *Tribolium Smurf* coding sequence was used for a tblastx analysis on the *Tribolium* nucleotide collection. The first hit that was *not* identical to the initial sequence was used for blasting in the *Drosophila* database. This strategy led to the identification of the *Tribolium* and *Drosophila NEDD4* sequences. *Drosophila Smurf* and *NEDD4* sequences were used for blastx on the human nucleotide collection. Homologous sequences in other insects, vertebrates and other groups were identified by using the *Drosophila* and human sequences followed by a reciprocal BLAST to confirm homology. The obtained protein sequences were aligned using the MUSCLE

alignment algorithm implemented in the Geneious 7 software (Biomatters, Auckland, New Zealand) using default settings. Phylogenetic analysis was conducted using the Geneious Tree Builder with the Jukes-Cantor genetic distance model, neighbor-joining (Saitou and Nei, 1987) as tree-building method, and a number of 10.000 replicates for creation of the bootstrap consensus tree (Felsenstein, 1985). The alignments, all sequences used for the alignment, as well as a text file linking the ID used in the tree to the gene name can be found on the DVD (folder Smurf_Phylogeny).

A similar approach was carried out for *TC004374*. The gene belonging to the iBeetle number *iB_03735* was identified using the *Tribolium* gene browser and the *Drosophila* ortholog was found by blastx search in non-redundant protein sequences of *Drosophila melanogaster*. For phylogeny the translated AA sequence from clone *JS_M133* was used for successive protein blast (blastp) on non redundant protein sequences of a selection of species using the NCBI database. The first two to three non-identical hits were selected for the phylogenetic analysis. Members of the Nudix protein family from *Homo sapiens*, *Mus musculus* and *Xenopus sp.* were searched using the NCBI protein database for family members (e.g. NUDT1 *Homo sapiens*, NUDT2 *Homo sapiens*,..., NUDT 22 *Homo sapiens*). All NUDT proteins of these species that could be found were aligned to the other Nudix proteins using the MUSCLE alignment algorithm implemented in the Geneious 7 software (Biomatters, Auckland, New Zealand) with default settings, without trimming the obtained sequences. The tree was constructed using the FastTree option of Geneious with default settings. The alignment and all sequences as well as a text file linking the ID used in the tree to the original sequence name can be found on the DVD (folder: *TC004374_Phylogeny*). All species used for phylogeny as well as their common names, the Taxonomy ID and the corresponding phylum are depicted in Table 3-2.

Scientific name	Common name	Taxonomy ID (NCBI)	Phylum
<i>Apis mellifera</i>	Honey bee	7460	Arthropoda
<i>Bombus terrestris</i>	Buff-tailed bumblebee	30195	Arthropoda
<i>Caenorhabditis elegans</i>	Roundworm	6239	Nematoda
<i>Camponotus floridanus</i>	Florida carpenter ant	104421	Arthropoda
<i>Crassostrea gigas</i>	Pacific oyster	29159	Mollusca
<i>Crepidula fornicata</i>	Common slipper shell	176853	Mollusca
<i>Danio rerio</i>	Zebrafish	7955	Chordata
<i>Daphnia pulex</i>	Common water flea	6669	Arthropoda
<i>Drosophila melanogaster</i>	Common fruit fly	7227	Arthropoda
<i>Homo sapiens</i>	Human	9606	Chordata
<i>Ixodes scapularis</i>	black-legged tick	6945	Arthropoda
<i>Mnemiopsis leidyi</i>	Warty comb jelly or sea walnut	27923	Ctenophora
<i>Mus musculus</i>	House mouse	10090	Chordata
<i>Nasonia vitripennis</i>	Jewel wasp	7425	Arthropoda
<i>Nematostella vectensis</i>	starlet sea anemone	45351	Cnidaria
<i>Tribolium castaneum</i>	Red flour beetle	7070	Arthropoda
<i>Trichoplax adhaerens</i>	“flat animal”, placozoan	10228	Placozoa
<i>Xenopus (Silurana) tropicalis</i>	Western clawed frog	8364	Chordata
<i>Xenopus laevis</i>	African clawed frog	8355	Chordata

Table 3-2 Species used for phylogenetic analysis

Indicated is the scientific name, the common name, the Taxonomy ID according to NCBI and the phylum of every species.

3.4 Knock down of gene functions by RNA interference (RNAi)

RNAi in *Tribolium* was performed via double strand RNA (dsRNA) injection using established techniques (Posnien et al., 2009a). For pupal and adult injections a FemtoJet® express device (Eppendorf, Hamburg, Germany) was used with an applied injection pressure of 300–700 hPa for pupae and 500–1000 hPa for adult beetles.

Templates for *in vitro* transcription were amplified by PCR using primers with an attached T7 polymerase promoter sequence (see appendix or DVD). dsRNA was produced using the Ambion® MEGAscript® T7 kit (Life Technologies, Carlsbad, CA, USA). For the iBeetle screen dsRNA at a concentration of 1µg/µl was injected into female pupae, for follow up experiments the concentration ranged from 0,15–3µg/µl and some injections were done in adult beetles (Table 3-3). For previ-

ously unknown genes at least two non-overlapping fragments were used for RNAi to rule out potential off target effects. These imply the results of not-intended mRNA degradations induced by the injected dsRNA due to sequence homology to more than just one transcript. Moreover the cDNA sequences used as templates for dsRNA synthesis of *Tc-smurf*, *TC004374*, and *Tc-Cyclin J* were analyzed using E-RNAi on the website of the German Cancer Research Center (DKFZ) (<http://www.dkfz.de/signaling/e-rnai3/>) (Horn and Boutros, 2010). dsRNAs were designed to have a minimum number of off target sequences and no off target 21-mer. The number of potential off target sequences for siRNAs of different length is indicated in Table 3-4 for dsRNAs used after the iBeetle screen.

Gene	dsRNA concentration	Size [bp]	pRNAi	aRNAi
<i>Tc-sog</i>	1400ng/μl	866	X	
<i>Tc-smurf</i>	1000-3000ng/μl	407; 186; 205; 604; 611	X	X
<i>TC004374</i>	1000-3000ng/μl	488; 590; 360; 540; 479	X	X
<i>Tc-CyclinJ</i>	1000ng/μl	516	X	

Table 3-3 dsRNAs used after the iBeetle screening phase

The table depicts the gene, the used dsRNA concentrations, the fragment size, and the parental RNAi method (pRNAi: pupal RNAi, aRNAi: adult RNAi). In case more than one fragment was used for knock down analysis the sizes of all fragments are given. For *Tc-smurf* and *TC004374* the location of the different sequences with respect to the cDNA sequence is shown in the results chapter.

Gene	Fragment	Off target sequences		
		21 nt	19 nt	17 nt
<i>TC004374</i>	Exon 1+2 fragment	0	0	4
<i>TC004374</i>	Exon 3+4 fragment	0	0	1
<i>Tc-CyclinJ</i>	JS_M294	0	0	9
<i>Tc-smurf</i>	iB_02881_iBeelte_Fragment 1	0	0	0
<i>Tc-smurf</i>	JS_M115 Fragment	0	2	8
<i>Tc-smurf</i>	Exon 5+6 Fragment	0	0	3

Table 3-4 (previous page) dsRNA test for off target sequences using E-RNAi

The sequences used for the injected dsRNAs were tested with the E-RNAi tool from the German Cancer Research Center (DKFZ) for potential off target effects in the *Tribolium* genome. The table indicates the targeted gene, the name of the respective dsRNA fragment and the numbers of 21-, 19- and 17-mers that potentially affected a not intended transcript.

3.5 Histology

Unless mentioned otherwise standard buffers and solutions were used and prepared according to descriptions in (Sambrook and Russell, 2001).

3.5.1 Fixation

Standard protocols were used for embryo fixations (Schinko et al., 2009). Embryo collections used for *in situ* hybridization, antibody staining, and TUNEL assay ranged from 0–48 h. Usually 2 ml fix buffer (1.3 x PBS and 67 mM EGTA, pH = 8.0) and 300µl formaldehyde (37 %) were used. Only for large amounts of embryos the volume of fix buffer and formaldehyde has been increased to 3 ml and up to 400 µl, respectively.

3.5.2 Fuchsin stainings

Tribolium embryos of the desired age were dechorionated and fixed as described in 3.5.1 and (Schinko et al., 2009). They were washed three times for 10 minutes in 70 % Ethanol in H₂O, followed by one washing step in 35 % Ethanol and two washing steps in pure H₂O. Embryos were then treated with 2N HCl at 60°C for 10 minutes followed by two H₂O washing steps. Staining took place in fuchsin solution (0.5 g of pararosanilin in 400 ml of distilled water) for 30 minutes followed by destaining with 95 % Ethanol under continuous liquid replacement until the solution became clear. Embryos were dehydrated by washing two times 5 minutes with 100 % Ethanol before washing with 1:1 Ethanol:BBBA (benzyl benzoate:benzyl alcohol solution 4:1). Embryos were transferred to and mounted in BBBA.

3.5.3 Whole mount *in situ* hybridization

In situ hybridization (ISH) was done as previously described, using Nitro blue tetrazolium (NBT) and 5-Bromo-4-chloro-3-indolyl phosphate (BCIP) (Schinko et

al., 2009). For double *in situ* hybridization staining Vector® Red (Vector Laboratories, Burlingame, CA, USA) was used as reagent for the second color development. Embryonic nuclei were stained using 1 µg/µl Hoechst 33342 in 1X PBT for 20 minutes during the last washing steps of ISH, followed by at least two washing steps with 1X PBT.

For germ band stage embryos the yolk was usually removed for imaging by using an eyebrow glued to a toothpick. Embryos were embedded in 100 % glycerol. Blastoderm stages and germ band stages that did not require yolk removal were either embedded in 100% glycerol, using small spacers of plasticine in each corner of the cover slip to avoid squeezing of the embryos, or mounted in 80 % glycerol on a microscope slide with an indentation without using a cover slip. The second procedure allowed turning and manipulation of the embryos and prevented squeezing artifacts. Pictures were taken using a Zeiss Axioplan 2 microscope with DIC and Image-Pro® Plus software (Media Cybernetics, Bethesda, MD, USA). Fluorescence of Hoechst and Vector® Red staining was documented using a mercury vapor lamp and DAPI or Cy3 filter sets.

3.5.4 Immunohistochemistry

For antibody staining fixed embryos (3.5.1) were rehydrated using a methanol/PBT series of 20:80, 40:60, 60:40, 80:20 ratio of PBT to methanol, each time giving the embryos 6 minutes to adapt and settle. Rehydration was followed by four washing steps in PBT for 6, 6, 20, and again 6 minutes. Blocking was performed for 1 hour in blocking solution (PBT containing 5 % sheep serum or 5 % goat serum (Sigma-Aldrich, St. Louis, USA) and 0,1–0,2% bovine serum albumin (BSA). Incubation with primary antibodies (please see Table 3-1 for details on antibodies and applied concentrations) were done for at least 3 h in blocking solution, followed by washing six times for 10 minutes in PBT. One additional washing step was done at 4°C over night in 50 % blocking solution in PBT followed by washing again four times for at least 10 minutes in PBT. Blocking, secondary antibody incubation, and washing were performed analogous to the primary antibody incubation. In case fluorophore-labeled secondary antibodies were used, embryos were protected from light during all washings and incubations after adding the antibody. For alkaline phosphatase (AP)-conjugated antibodies the color reaction was performed as described for *in situ* hybridization using Nitro blue tetrazolium (NBT) and

5-Bromo-4-chloro-3-indolyl phosphate (BCIP) (Schinko et al., 2009). Hoechst 33342 staining, embryo mounting, and imaging for NBT/BCIP stained embryos was done as described under 3.5.3. Fluorophore-labeled embryos were imaged using a Zeiss LSM780 inverse confocal microscope system, using a 405 nm laser for excitation and 410–542 nm filter for emission detection of the Hoechst 33342 signal and a 561 nm laser for excitation and 563–654 nm filter for emission detection of the Alexa 568 signal.

Antibody	Complete Name	prim/sec	company	order Number	concentration
pMad	Phospho-Smad1/5 (Ser463/465) (41D10) Rabbit mAb	Prim	Cell Signaling	#9516	1:800
goat anti rabbit AP	Alkaline Phosphatase-AffiniPure Goat Anti-Rabbit IgG (H+L)	Sec	Jackson Immuno Research	111-055-144	1:800
goat anti rabbit Alexa 568	Alexa Fluor® 568 F(ab') ₂ Fragment of Goat Anti-Rabbit IgG (H+L)	Sec	life technologies	A-21069	1:500
pMAPK	Monoclonal Anti-MAP Kinase, Activated (Diphosphorylated ERK-1&2) antibody produced in mouse, clone MAPK-YT, ascites fluid	Prim	Sigma	M8159-.2ML	1:2500

Table 3-5 Antibodies used for immunohistochemistry

Indicated are company, order number, and applied concentration of the antibodies used in this study. Prim: primary antibody. Sec: secondary antibody.

3.5.5 TUNEL assay

Embryos were treated for rehydration, refixation, and proteinase K-digestion as described for *in situ* hybridization (3.5.3). TUNEL (Gavrieli et al., 1992) was done as formerly described for *Cupiennius salei* (Prpic and Damen, 2005). Embryos were treated, mounted and imaged as described for *in situ* hybridization (3.5.3).

3.5.6 Cuticle preparations

Embryos/first instar larvae were dechorionated in 50 % 'Klorix' bleach, embedded in a mixture of Hoyer's medium and lactic acid in a ration 1:1 and incubated at 65°C overnight as previously described (Bucher and Klingler, 2004). Larval cuticles were analyzed using a Zeiss Axioplan 2 microscope with dark field or fluorescence microscopy to detect cuticle autofluorescence. Images were taken using the FITC filter set and the ImageProPlus (Media Cybernetics, Rockville, USA) software. Z-projections of cuticle stacks were generated by recording 30–50

planes, deconvolving them using the “No Neighbour” method of ImageProPlus and using the Z-projection methods “Maximum Projection” or “Sum Slices” of ImageJ (Version 1.47, <http://rsbweb.nih.gov/ij/disclaimer.html>).

3.6 The iBeetle screening procedure

For the iBeelte screen certain parameters such as pupal age at injection, incubation times, and annotations needed to be comparable and standardized between the screeners. To this end a strict protocol was used by all screeners. Although some procedures were already described in former parts of the materials and methods chapter, I will give an overview of the detailed screening procedure for the pupal injection screen here.

All incubations were done at 31°C. Female pupae from the *Pig-19* strain were injected and mated to males from the *Black* strain to allow easy discrimination between injected females and non-injected males during later time points of the screening procedure. All observations, including important aspects of the experiments, were annotated in a common database (3.6.1) using a controlled vocabulary.

Injection was defined as **day 0** in the protocol. Pupae were considered old enough if at least the base of the mandibles was darkened, which indicates about 75 % of pupal development. On each injection day 22 *iBeetle* dsRNAs (synthesized by Eupheria Biotech GmbH, Dresden, Germany) and two buffer controls were injected in 10 females each. The entity of the injections of one injection day was called a ‘repetition’. After injection the pupae were transferred to petri dishes containing approximately 10 g of flour.

After three days (**day 3** of the protocol) the eclosure and lethality rate for each injection was documented and the now adult beetles were transferred to a 25-well block system. Male beetles from the *Black* strain were added. Since *Tribolium* beetles tend to cannibalize on pupae this was not done directly on the injection day.

On **day 9** the first egg collection was done and the eggs were placed in 300 µm meshes above vials containing safflower oil. As soon as the animals hatched, they crawled through the mesh into the oil, so the hatch rate could be estimated later. Differences in the amount of eggs in relation to the buffer controls were annotated in the database. Dead females were counted and documented.

A second egg collection was done on **day 11**. Again the amount of eggs in relation to the controls was checked and differences were annotated. The eggs were directly transferred to 180 µm meshes and put back to 31°C on a small amount of flour to allow hatching larvae to feed.

On **day 13** the first egg collection (from day 9) was processed for cuticle analysis (3.5.6). If many non-hatched animals were detectable after dechorionization two preparations were done on one microscope slide, one of them was gently squeezed to allow stretching of the larvae to ease analysis of weaker cuticle phenotypes, the other one was embedded without squeezing as comparison. On day 13 of screening analysis also ovary preparations were performed for females showing affected egg deposition. The ovaries of usually four females of one *iBeetle* injection were dissected in PBS using fine forceps (Dumont #5), shortly fixed in 3,5 % formaldehyde in PBS, and mounted in PBS on a cover slide. Dissected ovaries were subjected to a brief microscope analysis and all detectable phenotypes were annotated in the data base.

On **day 14** fresh preparations from the second egg collection were done by de-chorionizing the eggs in two steps for three minutes in 50 % bleach each. Eggs and larvae were carefully mounted in Voltalef oil and covered with a cover slip. The muscle pattern was analyzed under a Zeiss Axioplan 2 microscope using DIC and a mercury vapor lamp with FITC filter for detecting the GFP signal in the muscles. Any detectable phenotype was annotated in the database.

Cuticle analysis was done at protocol **day 15** or later. Since cuticle preparations are stable for several months this part of analysis was time wise more flexible and could be done later. Cuticles were analyzed and documented as described in 3.5.6. Only single plane images were taken (no Z-stacks).

3.6.1 Annotation of screening results

Important parameters during the screening as well as all observed phenotypes were annotated in a database using an online interface (ibeetle-base.uni-goettingen.de) and a controlled vocabulary. Free text fields allowed additional descriptions or comments. Pictures were uploaded for documentation. Part of every annotated phenotype was its penetrance. In case of ovary analysis, penetrance of phenotypes was annotated as the number of females showing an ovary phenotype compared to the total number (usually four) of dissected females. For muscle and

cuticle analysis the occurrence of the phenotype in relation to the total number of counted eggs or animals on the slide was annotated. As an estimation, a subset of the animals on the slide was counted. This was done by counting the cuticles once or twice crosswise along the microscope slide. The occurrence of the phenotype in relation to the total number of counted eggs or animals on the slide was annotated. In case only few cuticles were on the slide, all animals or eggs were counted. Penetrances were annotated as: <30 %, 30-50 %, 50-80 % and >80 %. All penetrances were referring to the total number of animals on the analysis slide. An exemplary screenshot of the iBeetle annotation database is shown below (Figure 3-1).

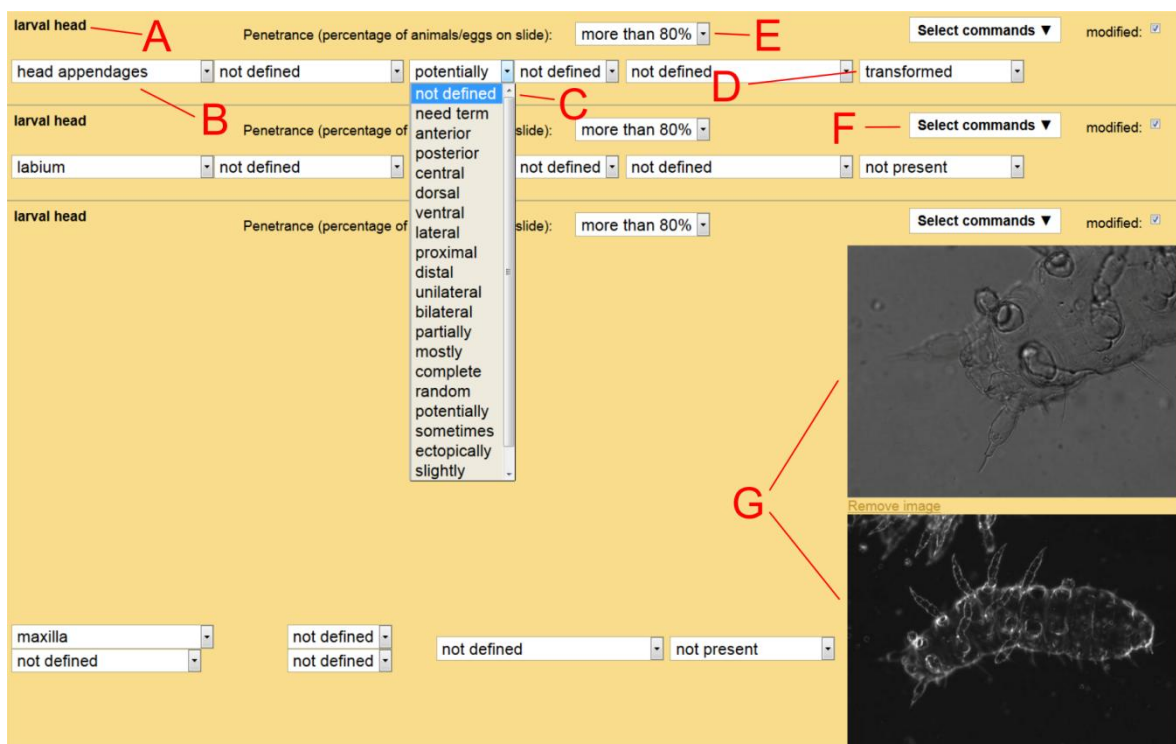


Figure 3-1 Database annotation

The picture shows an exemplary screenshot from the iBeetle annotation database. Depicted is the annotation of one of the positive controls on day 15 (cuticle analysis) of the pupal injection screen. Shown on the upper left is the affected animal tagma, in this case “larval head” (A). Directly below is the entity, the affected structure (B). There are several dropdown menus to describe the phenotype in more detail (one dropdown menu is active). These are called ‘qualifiers’ (C). The last dropdown menu in the line describes how the entity is actually altered in the annotated phenotype (modifier, D). The penetrance of the phenotype is also annotated (E) and additional comments can be entered (F). Every morphological phenotype is documented by taking and uploading pictures (G)

3.7 *In vivo* imaging

Female pupae or adult female beetles of the *nGFP* line (Sarrazin et al., 2012) were injected with dsRNA as described (Posnien et al., 2009a). Embryos of 4-8 h collections (development at 30°C) were de-chorionized in 100 % 'Klorix' bleach and thoroughly washed. For imaging the embryos were mounted in and properly covered with Halocarbon oil 700 (Sigma-Aldrich, St. Louis, USA) on a cover slip, using four bisected cover slips at each edge as spacers to avoid damaging of the embryos. Imaging was done at 30°C, using an inverse DeltaVision microscope with a programmable, movable stage, a mercury vapor lamp, and the FITC filter set for excitation and emission (Applied Precision, A GE Healthcare Company, Issaquah, Washington, USA). Z-stacks were taken in 13 slices, using an optical section spacing of 5 µm, resulting in a total Z-axis spacing of 65 µm, which is approximately the distance from the embryonic surface plane to the equator. Up to 55 embryos were imaged in one time lapse experiment with time intervals of 10 minutes between recordings. Imaging took place for 15–23 hours. Embryos treated with dsRNA against *DsRed* served as control. Exposure time for every image was 0,4 s.

4 Results

4.1 Identification of anterior patterning phenotypes in the iBeetle screen

To identify previously unknown genes involved in insect head development and anterior patterning I participated in a genome-wide RNA interference (RNAi) screen in the red flour beetle *Tribolium castaneum* (Schmitt-Engel et al., in preparation). Aims and concept of the screen are described in the introduction and the detailed procedure as well as the database annotation is described in the materials and methods section (3.6). All results for this project come from the pupal injection screen.

4.1.1 Phenotype identification and controls

During the ongoing screening procedure phenotypes for all screened parameters were identified in an unbiased manner (section 3.6 contains a detailed description of the screening procedure). An exemplary collection of phenotypes identified by myself during the different steps of the pupal injection screen is depicted in Figure 4-1 and will be explained in the following paragraph.

The pupal injection screen involved three major analysis steps. If the egg lay on day 11 of an experiment was reduced, the ovaries of usually four beetles per *iBeetle* dsRNA were dissected and analyzed. One example for an oogenesis phenotype is shown in Figure 4-1 C. Injection of *iB_01308* dsRNA (ortholog to *Drosophila* is the *Spase 22/23-subunit*) leads to an accumulation of different stages of oocytes within a single egg chamber (Figure 4-1 C) in contrast to the wild type (wt), where every egg chamber only contained one oocyte of a particular stage.

During the mesoderm screening part the progeny of dsRNA injected females was screened for defects in muscle and mesoderm development. This was done for all injected dsRNAs where eggs were available, hence excluding only cases where dsRNA injection resulted in sterility or lethality of the injected females. For the pupal injection screen the *Pig-19* strain was chosen which expresses GFP in the skeletal musculature of the *Tribolium* larva, resulting in a characteristic and reliably scoreable pattern (Figure 4-1 D+E). Every alteration of this pattern was annotated. Specific muscle phenotypes displayed for instance detachment or degeneration of muscle bundles as detected after RNAi with *iB_00174* dsRNA (ortholog

to *ALG-2 interacting protein X* in *Drosophila melanogaster*). Phenotypic larvae showed condensed or missing muscle bundles in the entire animal (Figure 4-1 F).

The most extensive analysis step was the inspection of the L1 larval cuticle in the ectoderm screening part. Again the progeny of all dsRNA injected females was analyzed for all cases where eggs were available. All phenotypes for my project were found during this analysis step. The *Tribolium* larva possesses all body parts of a typical insect including walking legs on the thoracic segments and easily identifiable head appendages, which makes it especially well suited for the study of insect head development (Bucher and Wimmer, 2005; Posnien et al., 2010), (Figure 4-1 G+G'). Apart from the prominent head appendages, the *Tribolium* larva displays a characteristic and described pattern of sensillae and setae (or bristles) which can serve as landmarks and are usable for the identification of certain head regions (Posnien and Bucher, 2010; Schinko et al., 2008). This allowed even the identification of very subtle phenotypes during the iBeetle screen. One example can again be given by RNAi with *iB_00174* dsRNA (the same dsRNA that caused the foresaid muscle phenotype). Cuticle preparations of L1 larvae deficient for *iB_00174* function looked phenotypically almost like wild type (Figure 4-1 H), but the larvae did not hatch. A large amount (50–80 %, data not shown) of these larvae lacked a specific head bristle, the posterior of the so-called 'gena triplet' (Figure 4-1 H'). Other phenotypes especially interesting for the project in this thesis were anterior patterning defects, as caused by knock down with *iB_02262* dsRNA (ortholog to *Drosophila Miff*) (Figure 4-1 J). I will come back to the characterization and selection of relevant cuticle phenotypes for my project in a later section of this chapter (4.1.3). The last example shows a very strong defect of larval morphology. Although these kind of cuticle phenotypes were often difficult to interpret they could be of high interest for specific questions. Heavily fragmented cuticles can be a feature of strong dorsal-ventral patterning defects (Siegfried Roth, personal communication). Strong defects were one feature of RNAi with *iB_05337* dsRNA (ortholog to *Drosophila CG42284*) (Figure 4-1 I).

In total 13,8 % of all dsRNAs injected during the screen led to embryonic lethality after cuticle secretion (i.e. leading to analyzable cuticle defects). From this fraction about 40 % did not show a morphological cuticle defect. In total 8,3 % of all dsRNAs injected resulted in a morphological defect of the L1 cuticle (Christian Schmitt-Engel, personal communication, Schmitt-Engel et al., in preparation).

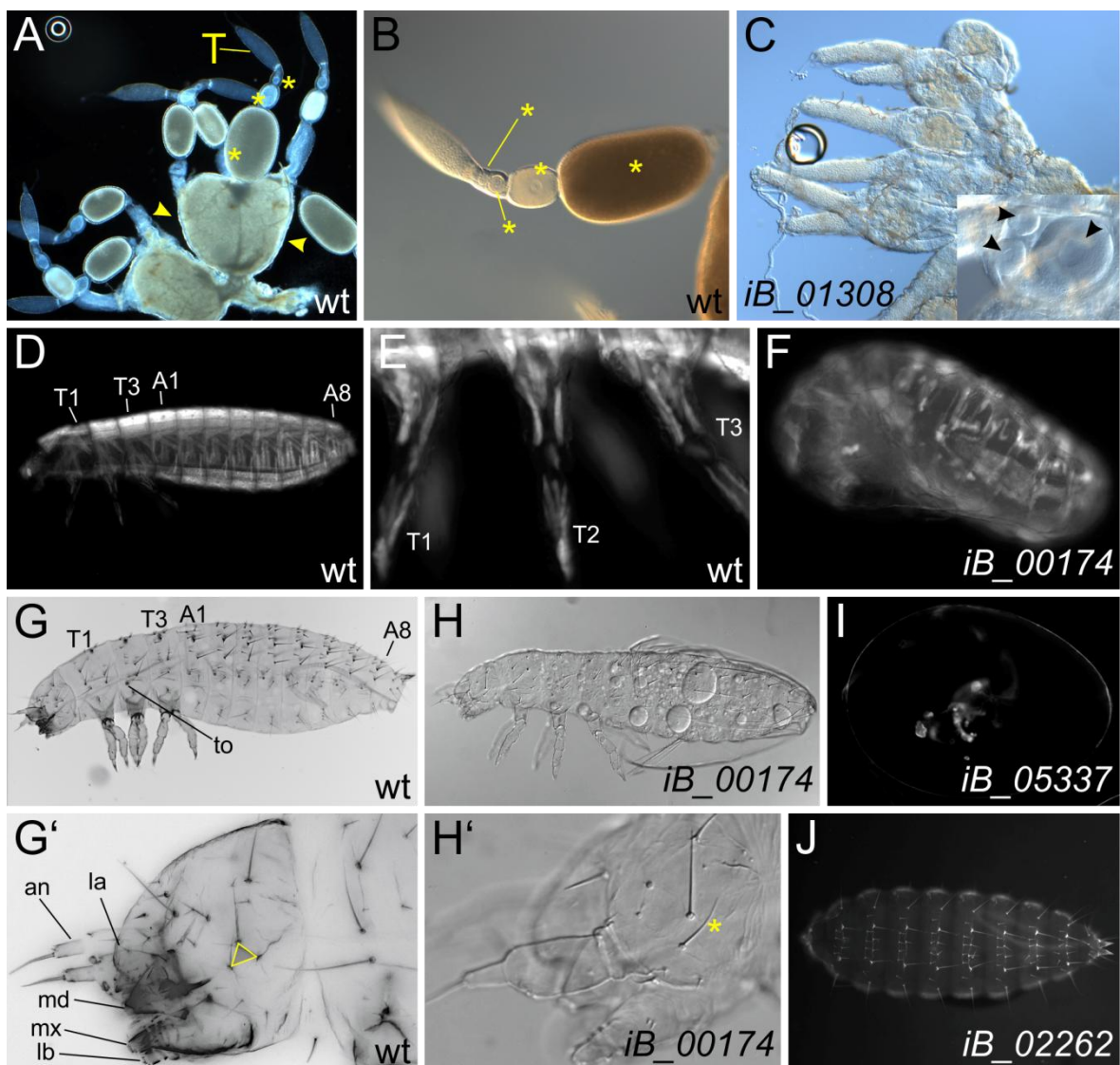


Figure 4-1 Exemplary phenotypes from the iBeetle screen

The pictures for iBeetle number genes were taken by myself during the iBeetle screen and deposited into the iBeetle annotation database. **D–H**: lateral views, anterior to the left, dorsal side up. **J**: anterior to the left, dorsal view. *Drosophila* orthologs to the iBeetle numbers are given in the text. T1, T2, T3: thoracic segment 1, 2 and 3; A1: abdominal segment 1; A8: abdominal segment 8; to: tracheal opening; an: antenna; md: mandible; mx: maxilla; lb: labium; la: labrum. **(A)** Wild type (wt) ovary with several ovarioles, consisting of the tropharium (T) and the vitellarium, which usually contains different stages of follicles (asterisks), with one oocyte per follicle. Arrowheads point to the lateral oviduct with at least two mature eggs (arrowheads). **(B)** Higher magnification of a wt ovariole (asterisks indicate follicles). **(C)** RNAi phenotype showing different stages of oocytes within a single follicle. Inset shows a higher magnification of the same phenotype, arrowheads point to the different nuclei. **(D)** The *Pig-19* strain expresses GFP in the skeletal musculature of the *Tribolium* larva. **(E)** Thoracic leg musculature in higher magnification. **(F)** Muscle phenotype displaying detached and missing muscle bundles. **(G)** Wt L1 cuticle, **(G')** shows a higher magnification of the head with the bristle pattern. The yellow triangle highlights the bristles of the so-called gena-triplet. **(H)** Subtle cuticle phenotype, displaying a missing bristle of the gena-triplet group. **H'** Shows a higher magnification of the larval head in **H** with the yellow asterisk indicating the position of the missing posterior gena triplet bristle (compare to the triangle in **G'**). **(I)** Strong phenotype during cuticle analysis, showing highly fragmented cuticle remnants. **(J)** Anterior patterning phenotype, head and thorax are completely missing.

In order to monitor and maintain screening quality, controls were included during the screening procedure. Buffer injections were done at the beginning and the end of every screening day as negative controls. dsRNAs against genes with known knock down phenotypes served as positive controls. Usually at least one positive control was injected per injection day. Although the screeners knew that they were injecting a positive control, they did not know which gene was targeted (Schmitt-Engel et al., in preparation). Due to the systematic approach of the iBeetle screen, also genes with known and often already published phenotypes were targeted by iBeetle dsRNAs (genes with known phenotypes). These genes served as internal positive controls for the screening procedure. The positions of these controls within the screen were unknown to the screeners and annotations for these genes with known phenotypes were collected and analyzed by Christian Schmitt-Engel after the first screening phase.

The results for the controls are summarized in Figure 4-2. Data collection for the controls has been done by all screeners of the first iBeetle phase (including me). Analysis and processing of the data was done by Christian Schmitt-Engel. Figure is courtesy of Gregor Bucher and Christian Schmitt-Engel (Schmitt-Engel et al., in preparation). In summary over 80% of the positive controls were correctly annotated. Adding also the partially recognized phenotypes (positive controls where most but not all aspects of the phenotype were identified) increases this number to over 90%. Some of the phenotypes were missed by the screeners (in total 16 for larval and pupal screen together), and some were lost because of technical reasons. In most cases this was due to lethality as a result of the injection procedure before the RNAi effect of the control dsRNA became apparent. Regarding just the pupal injection screen, the number of recognized and recognized plus partially recognized phenotypes reached almost 90 % and 95 %, respectively (Figure 4-2).

RNAi against genes with known phenotypes revealed in almost 80% of injections (51 of 65) the expected phenotype, correctly annotated by the screeners. For 3 genes out of 65 the experiment resulted in technical lethality or the phenotype was missed by the respective screener. RNAi against 11 genes (17%) resulted in a reproducibly different phenotypes which could be explained by the technical procedure differing from those in the respective publication. During the iBeetle screen larvae and pupae were injected at very specific points of development, for pupae

this was a late pupal stage. For some of the genes with known phenotypes the developmental stage at injection had an influence on the resulting RNAi phenotype (Schmitt Engel, personal communication and Schmitt-Engel et al., in preparation). In the pupal injection screen all genes with known phenotypes were at least partially recognized, for 6 of them the phenotype differed reproducibly from the published phenotype (Figure 4-2 B).

Finally, less than 2% (4 out of 251) of the negative controls (buffer injections) led to false positive annotations. Almost the same number (3 out of 251) resulted in technical lethality after injection (Figure 4-2 C).

In summary the controls show that a high percentage of the positive controls was correctly annotated and only a low fraction of the negative controls led to false positive results. This supports the expectation that the iBeetle screen provides a reliable dataset for candidate gene selection.

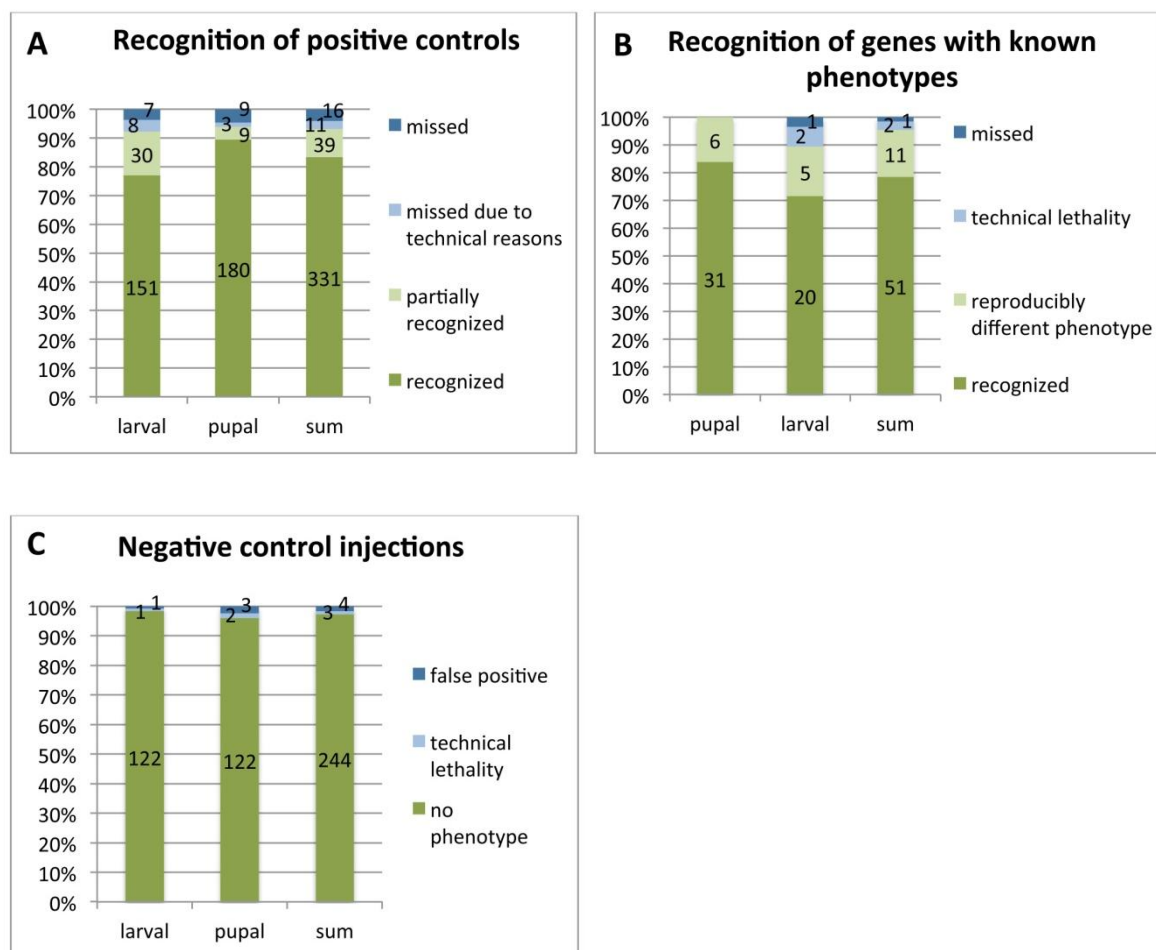


Figure 4-2 Results of the control injections

Different controls were done in order to maintain and monitor screening quality. This panel shows the results of all controls of the first screening phase, including my own results. (A) Positive control dsRNAs were injected

Results

regularly as part of the screening procedure. The screeners knew that they were injecting a positive control but they did not know the targeted gene. In summary over 90 % of all positive controls were at least partially recognized. **(B)** Due to the systematic approach of the iBeetle screen, also genes with published and/or known phenotypes were targeted. These served as additional controls. Analysis of 65 genes with known phenotypes showed that almost 80 % were identified with the published or known phenotype. Injection of 11 dsRNAs resulted in phenotypes reproducibly different from the published ones. 3 genes were missed during the screen. **(C)** in about 97% of the negative controls (buffer injections) no phenotype was annotated. This data was collected by all screeners of the first iBeetle screening phase and processed and combined by Christian Schmitt-Engel, panels courtesy of Gregor Bucher and C. Schmitt-Engel (Schmitt-Engel et al., in preparation).

4.1.2 Candidate selection strategy

As explained in the introduction (2.7 and 2.7.1) the iBeetle screen is designed as a six year project with two major screening phases. I took part in the first screening phase, and as a result the whole iBeetle data collection was not complete at the beginning of the analysis phase for this thesis. During the next sections I will describe how the final two candidates were selected for detailed analyses, starting from about 3500 datasets. One dataset is the complete, aggregated information related to the injection of one individual iBeetle dsRNA, containing experimental documentation and comments, phenotype descriptions, and pictures. In general, two phases could be distinguished: the first comprised the selection of a primary set of candidates, only depending on the information available from the database. The second was an experimental phase, consisting of a reproduction of the iBeetle experiment and successive small-scale screening experiments to further characterize the phenotypes (a workflow overview is shown in Figure 4-3). The single steps will be presented in detail in the next chapters.

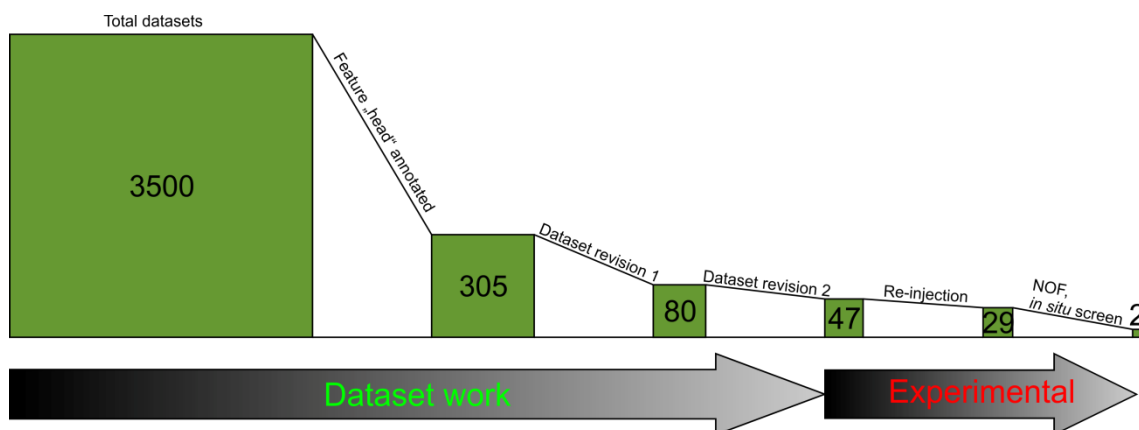


Figure 4-3 From annotated phenotype to candidate

Phenotypes were selected from a total of about **3500 individual datasets**. First database search yielded **305 annotations**. Careful by hand inspection of the annotations eventually led to a selection of **47 primary candidates** for re-injection (reproduction of the iBeetle experiment). After phenotype analysis **29 verified candidates** were chosen for injection of a non-overlapping dsRNA fragment (NOF) and subjected to *in situ* hybridization analyses to identify expression patterns and to better characterize the embryonic phenotypes. From this list **2 final candidates** were chosen for closer inspection and analyses.

4.1.3 Selection of primary candidates

By the conclusion of the first screening phase the database was searched for phenotypes that represented defects in head development during early embryogenesis. A preliminary search function in the iBeetle annotation database was used for this purpose because the final iBeetle database (<http://ibeetle-base.uni-goettingen.de/search/phenotypeSearch.jsf>) was not complete at that time point. The search term for candidate selection was “pupal day 15/larval head” without any other restraints. “pupal day 15” restricted the search to the cuticle analysis step of the pupal injection screen. The additional term “larval head” selected all datasets which contained at least one annotation for the targa head. No other filters were set in order to avoid losing potentially interesting phenotypes. The database search yielded 305 hits out of about 3500 datasets for the pupal injection screen (status January 2012). Note that this number is not comparable to the numbers given in 4.1.1 for the total number of cuticle phenotypes in the iBeetle screen, where more stringent criteria were used. C. Schmitt-Engel took the hatch rate before cuticle preparation and the number of analyzable animals on the cuticle preparation slide into account to define specific morphological defects of L1 larval cuticles. This was done in order to exclude potential background effects or phenotypes of very low penetrance (Schmitt-Engel et al.).

A step by step inspection of all datasets obtained by the search function was done to exclude cases of background and most likely not head specific phenotypes. Phenotypes were not further considered if the hatch rate on day 13 was high (annotated with “70-100 %”), the “number of animals on slide” on day 15 was low (annotated with <20 or <50) and the phenotype itself showed an incidence of less than 30 %. Additionally, the pictures could often give a good impression of the potential quality of a head defect. Other important criteria concerned the penetrance and the specificity of the annotated phenotypes. The screening database

allowed four steps of penetrance annotation (explained in 3.6.1). All annotations over 50 % were considered to be highly penetrant. The specificity was defined as the impression given by the annotation of a phenotype and the corresponding pictures in the respective dataset, meaning that head phenotypes coupled with a range of defects of different strength and in different body regions were only considered if the head phenotype was prevailing. Two exemplary annotations for highly penetrant phenotypes, one considered specific for head defects and one not considered specific, are given in Figure 4-4.

The dataset-based candidate selection resulted in a list of 80 iBeetle numbers which were plausibly annotated to cause a specific head defect after RNAi (DVD, Excel worksheet 'candidates', folder 'Candidates_List'). Any gene previously not reported to be involved in head development or anterior patterning was considered to be interesting. For this reason the phenotypes caused by the gene knock downs within this first list were very diverse. To get an impression about the modes of head defects detected during the screen and how they were represented among the detected cuticle phenotypes these 80 candidates were sorted into four categories:

- Head bristle defects: usually quite subtle cuticle defects only affecting the head bristle pattern.
- Head appendage altered/missing: the size, orientation, or shape of one or more pairs of head appendages was altered. Appendages could also be missing, but most head parts were present.
- General head defects: broader head regions were affected or missing.
- Anterior patterning: a phenotypic series was present on the cuticle analysis slide with different fractions of missing anterior body cuticle.

The results of this rough categorisation are given in Figure 4-5. 12 of the candidate genes were already on a primary analysis list of other members of the iBeetle consortium and were sorted out to avoid double analysis. 2 genes were already known (*Tc-pumilio* and *Tc-hunchback*; Schröder, 2003, Schmitt-Engel, 2010) and were consequently also not considered. Selecting for the most penetrant and specific of the remaining candidates allowed to sort out 19 more genes and resulted in 47 iB-numbers (DVD, Excel worksheet 'candidates', folder 'Candidates_List') which were chosen for re-injection.

iB_03735	
Total percentage of affected eggs/embryos/larvae:	50–80%
Strong defects (abdomen posterior partially remaining):	<30%
Head not present:	<30%
Head and thorax partially not present:	30–50%
Procephalic head not present:	30–50%
iB_00579	
Total percentage of affected eggs/embryos/larvae:	50%–80%
Empty eggs (egg without cuticle):	30%–50%
strong defects: cuticle remnants with some identifiable segments	<30%
Strong defects (appendages partially remaining):	<30%
Head, thorax and abdomen irregular:	<30%
Head appendages position irregular	<30%
Thorax segment partially not present:	<30%
Abdomen segment number decreased:	<30%
Head appendages partially not present:	<30%

Figure 4-4 Exemplary annotations for head defects from the iBeetle database

Given are the database annotations for two exemplary phenotypes. The annotations were slightly modified to enhance readability. The annotation for the upper candidate (*iB_03735*) is a good example for a gene potentially involved in anterior patterning processes. Strong phenotypes showed absence of the entire larval cuticle except for parts of the abdomen, weak phenotypes showed only deletion of anterior head parts. All aspects of the annotation made sense in terms of anterior patterning processes, the phenotype was therefore considered as specific. The overall (total) penetrance was high (50–80%). A comparative example is given with the annotation for *iB_00579*: although the total penetrance was 50–80% and therefore high, the annotation (together with the pictures) did not suggest a specific head patterning function, although the head or parts of the head were frequently affected.

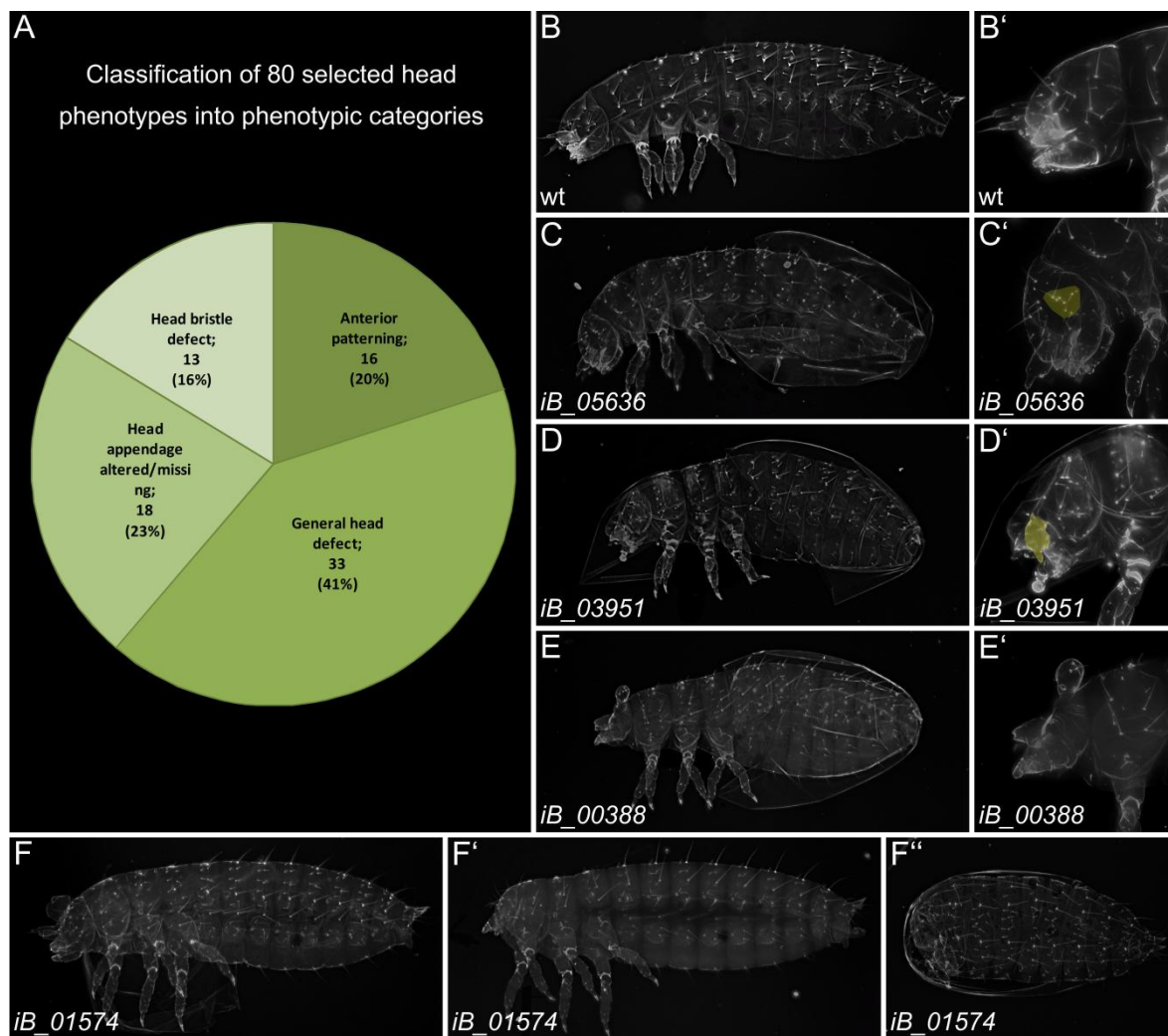


Figure 4-5 Head phenotypes of primary candidates and phenotype categorization

The figure shows four different categories of head defects which were detected during the iBeetle screen. All of them were considered relevant. Dorsal up and anterior to the left in all images. Images **B'**, **C'**, **D'** and **E'** show a higher magnification of the larval head in **B**, **C**, **D** and **E**, respectively. **A** displays the distribution of the phenotypes of the 80 preliminary candidates among the phenotypic categories. (**B**, **B'**) The *Tribolium* L1 larva bears all typical structures of an insect head, as well as an easily analyzable and consistent head bristle pattern (Posnien and Bucher, 2010; Posnien et al., 2010; Schinko et al., 2008). (**C**) Head bristle defects: cuticle phenotypes could be subtle, in this cuticle the number of head bristles in the gena region is increased (yellow region in **C'**, compare to same region in **B'**). (**D**) Head appendage altered/missing: these phenotypes were characterized by missing or altered head appendages, here represented by a shortened and bent antenna (yellow structure in **D'**). (**E**, **E'**) General head defects: this group was defined by loss or alteration of broader head regions. In this cuticle labrum, antennae, and parts of the head capsule are missing. There could also be a smooth transition to anterior patterning phenotypes. (**F**, **F'**, **F''**) Anterior patterning phenotypes: these phenotypes usually showed a phenotypic series with a variable degree of absent anterior structures.

4.2 Candidate selection, experimental phase

Mining the iBeetle database yielded a number of 47 potential head patterning genes. Since the iBeetle project was designed as a first pass screen the pheno-

types from the database were considered to be preliminary results. For this reason the first step in candidate gene selection was the confirmation of the iBeetle phenotypes in independent experiments for this group of 47 genes.

4.2.1 Primary candidates: re-screen

In order to get a better impression of the cuticle phenotypes and to confirm the screening results, the iBeetle dsRNAs were injected in the same strain used during the screen (*Pig-19*). The resulting F1 larval cuticles were analyzed. For 21 of the candidates the cuticle phenotype was confirmed. In 19 cases the resulting phenotype was mostly confirmed. This means that the phenotype was detected, but with noticeable different penetrance, or with other, originally not annotated phenotypic aspects. 7 dsRNAs did not result in the expected phenotype. Information about which iBeetle phenotypes could be reproduced can be found on the DVD (Excel worksheet 'candidates', folder 'Candidates_List').

4.2.2 Selection of verified candidates

After the re-injections a number of further candidate genes was sorted out. The selection of genes that were kept depended on the results of the cuticle phenotype analysis and the criteria (penetrance and specificity) remained the same as under 4.1.3. Only in one case a candidate was kept in spite of not being confirmed, due to an interesting phenotype annotated during the screen which affected specifically the antenna (*iB_05573*). 25 genes of the original 47 remained for the next analysis steps. 4 additional iBeetle numbers (*iB_04437*, *iB_04484*, *iB_04439*, *iB_04393*) were added to the final list from the ongoing screening process. The 29 candidates, together with information on the reproducibility of the iBeetle phenotype, are listed in Table 4-1 at the end of the next chapter (page 56). For the four candidates that were included from the ongoing screening process the original iBeetle experiment was not repeated and they were directly included in the downstream phenotype confirmation process. All chosen iBeetle candidates had an annotated penetrance of at least 30 % for the respective head phenotype and about 72 % (21 out of 29) showed a hatch rate of under 50 % which indicated embryonic lethality after gene knock down (Excel worksheet 'candidates', folder 'Candidates_List').

4.2.3 Reduction of candidates by expression pattern analysis and non-overlapping fragment injection

The group of 29 candidates was considered to serve as a pool for the selection of a small number of final candidates which were supposed to be analyzed in detail. For selecting the most reliable and at the same time interesting final genes, the candidates were simultaneously subjected to two small-scale screening experiments to get an impression of:

- The corresponding expression patterns
- Potential off target effects or strain specific effects

Gene expression in a localized domain can be an indication for a specific function in a certain region of the embryo during development. There are numerous examples for genes which are locally expressed in the head region during *Tribolium* development like for instance *Tc-orthodenticle1* (*Tc-otd1*), *Tc-six3* and *Tc-mex3* (Posnien et al., 2011; Schinko et al., 2008; Schoppmeier et al., 2009).

Parts of and/or the entire coding sequences suggested by the gene models of the *Tribolium* gene browser (<http://bioinf.uni-greifswald.de/gb2/gbrowse/tribolium/>) of the chosen genes were cloned using gene specific primers and an embryonic cDNA collection. In case of *iB_05636*, cloning of a gene fragment was not successful and the expression pattern for this candidate was consequently not analyzed.

In order to determine the expression patterns of the potential candidate genes, the cloned gene fragments (sequences on DVD, folder *Genes_Sequences*, primers on DVD and in appendix) were used to synthesize RNA probes for whole mount *in situ* hybridization experiments on wild type (wt) *Tribolium* embryos. For three candidates localized gene expression could be detected during at least a subset of developmental stages.

The only candidate gene for which a specific localized expression domain in the head region could be determined during embryonic development was the candidate *iB_02587*. During differentiated blastoderm stages it was expressed in serosa cells and in the posterior pit (Figure 4-6 A). A roundish expression domain in the midline region anterior to the mandibular segment anlagen arose *de novo* during early elongating germ band stages. Expression in the posterior germ band was also detected during these stages. Serosa expression clustered in a dorsal domain

(Figure 4-6 B, C). The head expression domain persisted until germ band retraction and disappeared slowly afterwards. Two lateral stripes of *iB_02587* expression were observed in fully retracted embryos (Figure 4-6 D). Using the putatively complete coding region of this gene (clone M93) for blastx analysis resulted in the *Serpin-27A* (*Spn27A*) gene as the closest ortholog in *Drosophila melanogaster*. The gene codes for a serine protease inhibitor. Serpin-27A plays an essential role in localizing Toll signaling in *Drosophila* by spatially restricting the activity of the Easter protease and is thereby involved in dorsal-ventral axis formation in the fly. *Drosophila* embryos deficient for Serpin-27A function show high levels of Toll signaling and fail to form a cuticle since all cells adopt the mesodermal fate (Hashimoto et al., 2003; Ligoxygakis et al., 2003). The function of the *Tribolium* ortholog appeared to be different, however, a specific head cuticle phenotype for this candidate could not be confirmed after injection of a NOF in the *SB* strain. Therefore *iB_02587* was eventually sorted out from further analysis (see below).

iB_04393 was initially expressed ubiquitously, during later germ band stages stronger expression could be detected in the embryonic midline, in the developing appendages and the segmental borders (Figure 4-6, E+F). The fly ortholog of this gene is *Drosophila melanogaster fat* (Dm\ft, FlyBase ID FBgn0001075) which is involved in cell adhesion and planar cell polarity (Ambegaonkar et al., 2012; Hynes and Zhao, 2000; Matakatsu and Blair, 2004). After revision of the cuticle phenotype for *iB_04393* RNAi the phenotype turned out not to be head and head appendage specific, so this candidate was consequently sorted out of further analysis.

The third iBeetle candidate that showed a localized expression during *in situ* hybridization was *iB_00388*. During late embryonic stages (Figure 4-6 G) expression of *iB_00388* was observed in the central nervous system (CNS). Referring to BLAST analysis this gene is the ortholog to *APP-like protein interacting protein 1* (*Aplip1*) from *Drosophila*. The late CNS expression was in accordance with data from *Drosophila*, where expression in neural tissue has also been reported (Taru et al., 2002). According to FlyBase (<http://flybase.org/>) *Aplip1* transcripts are highly abundant in embryos 12–18 hours after egg deposition, and low and absent in 6–12 hours and 0–6 hour old embryos, respectively. The head phenotype observed after injection of *iB_00388* dsRNA could not be confirmed by injection of a NOF in

the *SB* strain and the candidate was eventually not followed up any further (see below).

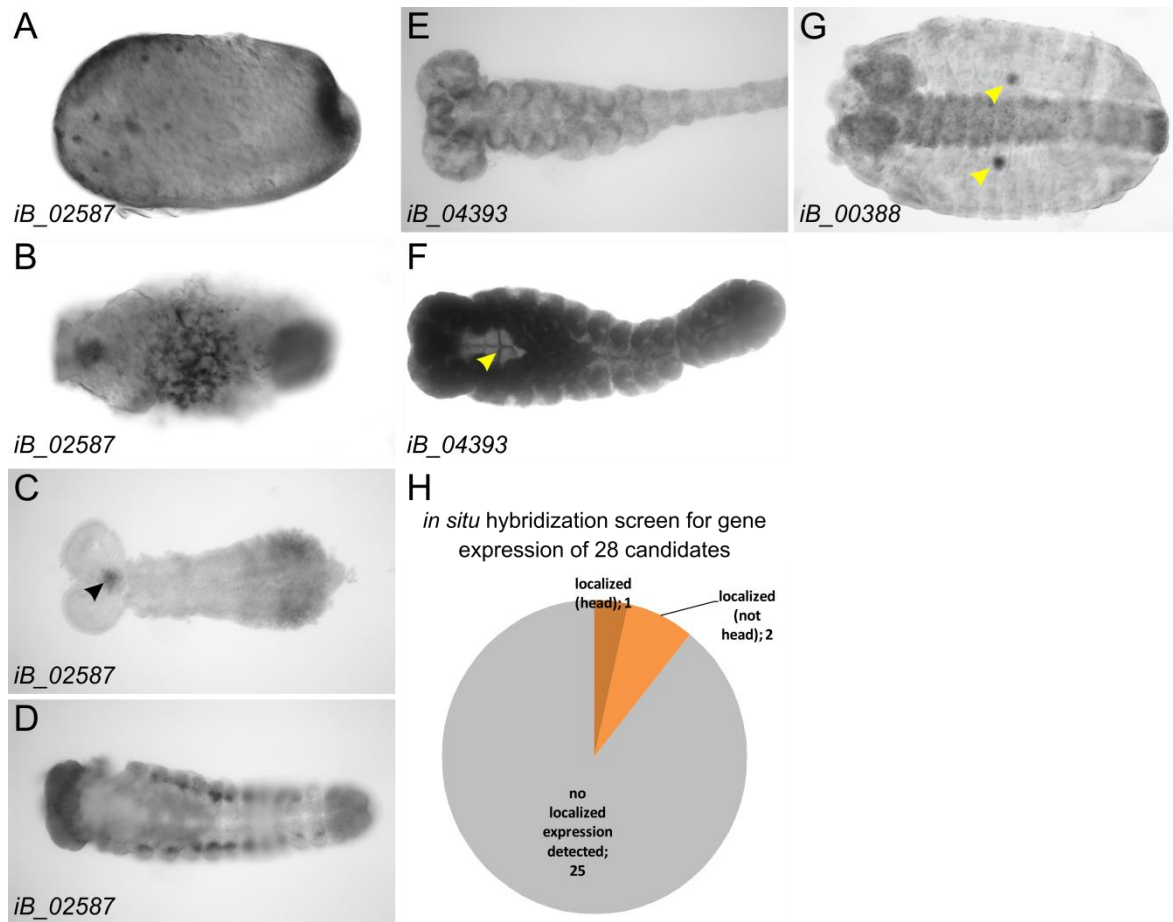


Figure 4-6 Expression patterns of verified candidates

Orientation: anterior to the left for all pictures, for A: dorsal side up, B: dorsal view. The expression patterns of 28 candidate genes were tested using RNA *in situ* hybridization probes. Three genes showed localized expression during at least a subset of embryonic stages. **(A+B)** *iB_02587* (*Tc-Spn27A*) was expressed in serosa cells and in the posterior pit during differentiated blastoderm stages. During germ band stages the *Tc-Spn27A* expressing cells in the serosa clustered at the dorsal side (B). **(B+C)** During early germ band stages expression was detectable in the posterior and in a circular domain in the posterior pregnathal head anlage (arrow-head in C). **(D)** Lateral stripes of expression could be detected during retracted germ band stages. **(E)** For *iB_04393* (*Tc-fat*) domains of stronger gene expression were found in the epithelia of developing appendages during later germ band stages. Initially, this gene was uniformly expressed. **(F)** In retracted germ band stages stronger expression could also be detected in the ventral midline and between segmental borders (arrow-head). **(G)** Localized expression for *iB_00388* (ortholog of *Dm-Aplip1*) was detectable in the CNS during late embryonic stages. Dark stained spots laterally to the CNS expression (arrowheads) are unspecific stainings of the pleuropodia. **(H)** The *in situ* hybridization screen detected three genes with localized expression at least during a subset of embryonic stages. For 25 genes no localized expression was detected.

In spite of being usually highly specific, RNAi can cause off target effects due to sequence similarity to other genes. To identify potential off target effects, dsRNAs targeting independent (non-overlapping) sequence parts of the gene of interest were designed. These dsRNAs are here referred to as non-overlapping fragments (NOF). Furthermore, mutant phenotypes in mouse and *Drosophila* can depend on the genetic background of different strains (Dworkin et al., 2009; Gibson and van Helden, 1997; Linder, 2006; Pickett and Meeks-Wagner, 1995; Threadgill et al., 1995), a phenomenon that we have also observed for the RNAi effect in *Tribolium* (Kitzmann et al., 2013). To rule out off target and strain specific effects for the chosen final candidate genes, NOFs for 26 of the candidates were injected into female pupae of the *Tribolium San Bernardino* (SB) strain, followed by mating to SB male beetles. One candidate (*iB_04393*) was taken out of analysis after revision of the phenotype annotation in the iBeetle database. For two genes the synthesis of the NOF was delayed and they were injected later into the *Pig-19* strain. One phenotype could be confirmed, the other one not. For a total of 13 genes the phenotype was confirmed after injection of the NOF. For a total of 15 candidates at least a specific head phenotype was not confirmed. The reason why a high number of phenotypes was not reproduced, and whether this was due to the different strain or the NOF, was not analyzed in detail. Reproducibility of iBeetle phenotypes and strain and fragment specific effects are a topic in the paper about the iBeetle screen and are discussed in more detail therein (Schmitt-Engel et al., in preparation).

Information which phenotypes were confirmed during this step of analysis is given in Table 4-1 (column 'Validated Candidates NOF in SB strain'). Comprehensive information on the candidates, also including the dsRNA sequences can be found on the DVD (Excel worksheet 'candidates', folder 'Candidates_List').

Results

dsRNA_ID	TC_Number	Re-screen: Confirmed?	Validated Candidates, NOF in SB strain: Confirmed?	Validated Candidates: Results <i>in situ</i> screen
iB_00009	TC000056	mostly	no	not localized
iB_00067	TC000311	yes	yes	not localized
iB_00388	TC002493	mostly	no	CNS expression during later germband stages
iB_00992	TC006094	yes	yes	not localized
iB_01098	TC006853	yes	yes	not localized
iB_01217	TC007548	yes	delayed delivery not confirmed in pBA19	not localized
iB_01556	TC009450	mostly	yes	not localized
iB_01702	TC010491	mostly	yes	not localized
iB_02262	TC014225	mostly	no	not localized
iB_02476	TC015430	mostly	delayed delivery, confirmed in pBA19	not localized
iB_02587	TC030076	yes	head no, rest yes	Serosa and head domain
iB_03735	TC004374	yes	no(fr.2)/yes(fr.3)>80%	not localized
iB_03951	TC005441	yes	no	not localized
iB_04050	TC005983	yes	no	not localized
iB_04130	TC006392	yes	no	not localized
iB_05324	TC012802	yes	no	not localized
iB_05326	TC012819	yes	yes	not localized
iB_05394	TC013165	yes	no (100% empty egg)	not localized
iB_05573	TC014156	no	no	not localized
iB_05636	TC014467	mostly	yes	not cloned
iB_01574	TC009549	yes	no	not localized
iB_02881	TC006704	yes	yes	not localized
iB_03525	TC003240	yes	yes	not localized
iB_06031	TC030580	mostly	no	not localized
iB_05754	TC015120	mostly	yes	not localized
iB_04437	TC008149	Gene added later to analysis	yes	not localized
iB_04484	TC008419	Gene added later to analysis	no	not localized
iB_04439	TC008169	Gene added later to analysis	no	not localized
iB_04393	TC007877	Gene added later to analysis	Sorted out due to not specific head phenotype	initially ubiquitous, during later germband stages stronger expression in midline and limb buds

Table 4-1 Group of 29 candidates: results of phenotype confirmation experiments and *in situ* hybridization screen

Given are the dsRNA IDs from the iBeetle screen (**dsRNA ID**), the corresponding gene identifiers according to BeetleBase (<http://beetlebase.org/cgi-bin/gbrowse/BeetleBase3.gff3/>) (**TC-number**), the reproducibility of the phenotype during the re-injection experiments (**Re-screen: Confirmed?**), the reproducibility of the phenotype after injection of a non-overlapping fragment (**Validated Candidates, NOF in SB strain: Confirmed?**) and the results of the screen for the gene expression patterns (**Validated Candidates: Results *in situ* screen**).

4.2.4 *Tc-wingless* expression in candidate RNAi embryos

The aim of this project was the identification of genes which are required for early anterior patterning processes. To this end RNAi embryos were analyzed to verify if knock down of the candidate genes resulted in specific anterior defects

during early embryonic stages or if the observed effects in larval cuticles were rather secondary due to general disruption of embryogenesis or later cuticle secretion. RNAi embryos were collected for all 26 injections from the non-overlapping fragment (NOF) injection in the *SB* strain experiment (4.2.3, Table 4-1). The embryo collections contained about 8–24 h old embryos which developed at 31°C and were collected over a period of about one week. To facilitate phenotype identification and interpretation the embryos were stained for expression of the segment polarity gene *Tc-wingless* (*Tc-wg*). *Tc-wg* is expressed in a segmental pattern in the *Tribolium* germ band (Nagy and Carroll, 1994). Germ band stage embryos were analyzed for phenotypic defects and *Tc-wg* misexpression. This experiment was done once for every candidate and some of the dsRNA injected females showed decreased egg deposition, resulting in limited RNAi embryos for phenotype analysis. For this reason the results must be seen as preliminary. For 15 dsRNA injections the observed phenotype was wild type, or the amount of obtained germ band stage embryos was not sufficient to draw a conclusion (not shown). Figure 4-7 depicts embryos from those 11 embryo collections where morphological or *Tc-wg*-expression defects could be detected in at least three germ band stage embryos. For some of the candidate genes a head specific knock down effect could not be confirmed by NOF injection into the *SB* strain (marked by a red box in the right column of Figure 4-7). For many of the not confirmed candidates a high number of strong phenotypes or empty eggs (no detectable cuticle in the egg after cuticle preparation) was found during cuticle analysis. This might be an indication for a rather broad and more general developmental defect. It might also be that the phenotype observed after injection into the *SB* strain was stronger than the phenotype obtained in the *Pig-19* strain. For other candidates the cuticle phenotype could be confirmed (green boxes) but the embryonic phenotype looked rather unspecific for head or anterior patterning defects (e.g. *iB_00992*, Figure 4-7 B–B”; *iB_01556* Figure 4-7 C–C”; *iB_03525*, Figure 4-7 F–F”). For these three candidates also high numbers of strong cuticle defects, not head specific defects, or empty eggs were documented for the cuticle analysis. Because the embryonic phenotypes indicated general developmental defects these candidates were no longer considered.

One interesting observation was the shift of the ocular *Tc-wg*-expression domain towards a more anterior central position seen for the candidate *iB_05754*

(Figure 4-7 K–K’). This effect was observed in several embryos. Although the cuticle preparation for this candidate showed a high number of empty eggs and strong defects and the head defects which were seen did not appear to be specific, the embryonic phenotype suggests specific RNAi-mediated defects in the head tissue. It might well be that this gene is involved in head patterning as well as in other developmental processes during embryogenesis. This might result in pleiotropic effects on level of the L1 epidermis which hampers the interpretation of the cuticle phenotype. Finally, for two of the tested candidates specific anterior defects were observed in the cuticle preparations as well as in *Tc-wg*-stained RNAi embryos. For this reason they were selected for a detailed analysis.

iB_02881 showed a high penetrance of headless or head-defective cuticles in the cuticle collection. These phenotypes will be explained in more detail in 4.3.1, pictures are given in Figure 4-10. Headless or head size reduced embryos were also found in the RNAi embryos stained for expression of *Tc-wg* by *in situ* hybridization. Additionally, anterior stripes for *Tc-wg* expression were often missing (Figure 4-7 E–E’).

Two NOF dsRNAs, covering the original iBeetle fragment, were injected for *iB_03735*. Injection of the first NOF dsRNA against *iB_03735* did not result in defects on the L1 cuticle, and also no developmental defects were found in the RNAi embryos stained for *Tc-wg* expression. However, injection of a second NOF resulted with high penetrance in the cuticle phenotype observed in the screen and the analysis of RNAi embryos also confirmed specific anterior defects (Figure 4-7 G–G’). Cuticle phenotypes for *iB_03735* RNAi displayed head defects and missing anterior body regions (shown in Figure 4-27). The different phenotypes obtained after injection of different dsRNAs for this candidate suggested a transcript- or splice variant-specific knock down effect for this gene. The gene model and the dsRNA fragments which resulted in head and anterior patterning phenotypes for *iB_03735* will be shown later (4.4).

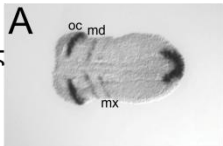
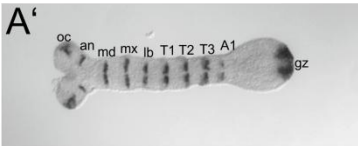
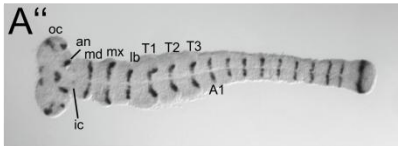
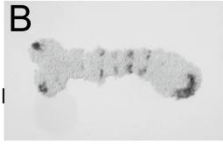
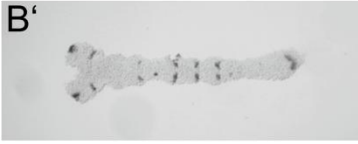
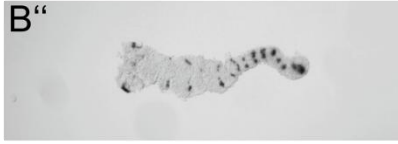

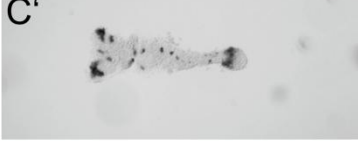
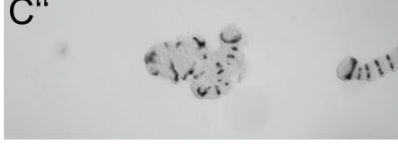


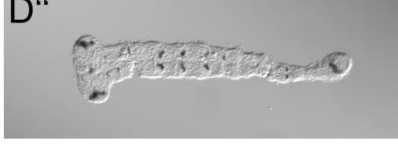



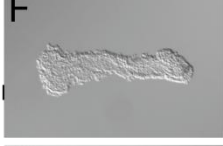

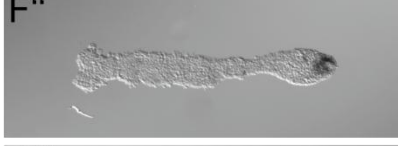


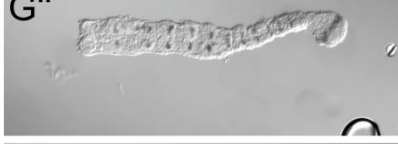
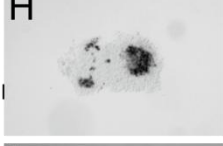











				Results for cuticle analysis NOF in SB strain
wild type				
iB_00992				iB phenotype: confirmed Many strong phenotypes and EE
iB_01556				iB phenotype: confirmed with very low penetrance diverse defects many EE (>50%)
iB_01574				iB phenotype: not confirmed many EE (30-50%) maybe stronger than in screen
iB_02881				iB phenotype: confirmed high penetrance, identical to iBeetle phenotype iB phenotype: confirmed
iB_03525				iBeetle phenotype: confirmed few embryos many EE
iB_03735				iB phenotype: not confirmed (for 1 st NOF) confirmed (for 2 nd NOF) high penetrance
iB_04050				iB phenotype: not confirmed different phenotype than in screen many EE (30-50%)
iB_06031				iB phenotype: not confirmed
iB_03951				iB phenotype: not confirmed many EE and strong defects head defects do not look specific
iB_05754				iB phenotype: low penetrance but confirmed many EE and strong defects

Figure 4-7 *Tc-wg* *in situ* hybridization screen in candidate RNAi embryos

Germ band stage embryos of different age were stained for the expression of the segment polarity gene *Tc-wg*. The column to the right gives a brief summary for the results of the corresponding cuticle analysis for NOF

Results

injections in SB females. Green boxes: iBeetle phenotype confirmed, red boxes: iBeetle phenotype not confirmed. Anterior to the left for all embryos. Embryos in one row are successively older from left to right. Not all embryos in one column are the same age. **(A–A’)** In wild type embryos *Tc-wg* is expressed in every segment and in the posterior segment addition zone or growth zone (gz). Abbreviations for the segments are given next to the corresponding *Tc-wg*-stripe. oc: ocular, ic: intercalary. Abbreviations for the other segments are the same as in Figure 4-1 and can also be found in the abbreviation list. **(B–B’)** Embryos after RNAi against *iB_00992* showed missing or irregular *Tc-wg* stripes and sometimes abnormal morphology. **(C–C’)** The RNAi phenotype of *iB_01556* looked similar but stronger. **(D+D’)** *iB_01574* RNAi could cause loss of almost all *Tc-wg* stripes, however morphological defects were not as severe as in B’–C’. **(E–E’)** Knock down of *iB_02881* resulted in smaller headlobes or deletions of entire anterior body regions. **(F, F’)** *iB_03525* RNAi could result in complete absence of *Tc-wg*-stripes associated with smaller headlobes. However, also relatively intact embryos with missing posterior *Tc-wg* stripes were observed in the embryo collection **(F’)**. **(G–G’)** Knock down of *iB_03735* led to headless embryos **(G’)** or reduced heads. Note the point-like ocular *Tc-wg* expression domains in G and G’ (arrowheads). **(H)** Early stage embryo of RNAi against *iB_04050* which showed severe morphological defects and impaired *Tc-wg* expression. In later stage embryos, a thinner germ band with missing posterior *Tc-wg* stripes was observed **(H’)**. In some embryos the germ band was shortened **(H’)**. **(I)** Young germ band stage embryo after *iB_06031* RNAi, morphologically similar to the phenotype seen in G. Also the ocular *Tc-wg* expression stripe was changed to a point like expression domain (arrowhead). **(I’ and I’)** *Tc-wg* pattern of this embryo was only mildly affected, however, the embryo in I’ showed strong defects in *Tc-wg* pattern and general morphology. **(J–J’)** *Tc-wg* expression was lost in some segments of *iB_03951* RNAi embryos. **(K–K’)** Random loss of segmental *Tc-wg*-expression was detected in *iB_05754* RNAi embryos. Note the anterior shift of the ocular (oc) *Tc-wg* expression in K’ and K’ (compare to A’ and A’). Lack of anterior tissue could potentially also be seen in the young embryo in K (black arrowhead).

4.3 Identification, isolation and characterization of *iB_02881* as *Tribolium smurf*

BLAST analysis using the translated nucleotide sequence of the *iB_02881* iBeetle fragment against non-redundant protein sequences of *Drosophila melanogaster* (blastx) using the online BLAST algorithm (<http://blast.ncbi.nlm.nih.gov/Blast.cgi>; National Center for Biotechnology Information, NCBI) resulted in the gene *lethal with a checkpoint kinase* (FlyBase symbol *DmeNack*) as closest fly homolog. The FlyBase ID is *FBgn0029006*. Other names for the gene product according to FlyBase are DSmurf, dSmurf, Smurf, D-smurf and dSmurf1 (the abbreviation Smurf is for **Smad ubiquitination regulatory factor**, Zhu et al., 1999). Reciprocal BLAST in *Tribolium* confirmed the orthology and identified a hypothetical protein. The iBeetle dsRNA *iB_02881* targets a gene with the number *TC_006704*. I will refer to the *Drosophila* ortholog under the name *DSmurf*, since this is the name used in the first publication studying the function of this gene (Podos et al., 2001). *Smurf1* and *Smurf2* are the vertebrate orthologs

(Lin et al., 2000; Zhu et al., 1999). Consequently I will refer to the *Tribolium* gene as *Tc-smurf*. Using the *Tribolium* genome browser and the AUGUSTUS prediction 'UTR and hints from cDNA', gene specific primers (JSP143 and JSP145) were generated to isolate the presumably entire coding sequence (CDS) of *Tc-smurf* from an embryonic cDNA collection. The isolated sequences resembled the predicted gene model in general, showing only slight differences (Figure 4-8 A, sequences and alignments on DVD, folder *Genes_Sequences/iB_02881_TcSmurf*, file *Alignment_Figure4_8*). Two CDS transcripts (JS_M111 and JS_M109) of 2736 bp and 2748 bp were isolated. The 12 nucleotides that caused the difference between the two isolated transcripts were located at the 5' region of exon 5. The transcripts encoded gene products of 910 AA and 914 AA respectively.

Tc-smurf encodes a HECT-type E3 ubiquitin ligase of the Nedd4 family. E3 ligases catalyze the last step in the ubiquitination process by accepting the ubiquitin from a ubiquitin conjugating protein and catalyzing its transfer to the target protein. In HECT-type E3s the C-terminal HECT domain is necessary for enzymatic activity through a conserved cysteine, which forms thioester bonds with the ubiquitin molecule (Huang et al., 1999; Rotin and Kumar, 2009). For *Tc-Smurf*, protein domains and the catalytic cysteine were identified using PROSITE (Swiss Institute of Bioinformatics). The cysteine was found to be localized at AA position 878 and 882 for the translated nucleotide sequences of clone M111 and M109, respectively. Additionally to the enzymatic HECT domain *Tc-Smurf* contains an N-terminal C2 domain and three WW domains (Figure 4-8 A+B). See introduction (2.6.1.1) for information on the different protein domains.

BLAST search using blastx in the *Tribolium* genome with JS_M111 as template did not yield a second *smurf* paralog in the beetle. This is consistent with data from other protostomes as, according to my BLAST approach (3.3, Orthology and phylogeny analysis) all analyzed protostome taxa contained only one *smurf* gene. The two closest hits after the *Tc-smurf* sequence (*TC006704*, Score 1647, Identity 99 %) were the *Tribolium* orthologs to the HECT type E3 ubiquitin ligases *Nedd4* (*TC008896*, Score 379, Identity 49 %) and *suppressor of deltex* (*TC014416*, Score 376, Identity 48 %). Phylogenetic analysis using the neighbor joining method, the *C. elegans* Protein WWP-1 as outgroup and based on alignments of either the entire protein sequence or only the HECT domain confirmed the BLAST results and grouped *Tc-Smurf* to the *Smurf* protein group with high

Results

similarity to DSmurf. The identified Tc-Nedd4 groups to the Nedd4 clade, confirming the assumption that only one true *Smurf* paralog exists in *Tribolium* (Figure 4-9, alignments on DVD, folder *Smurf_Phylogeny/Alignments*).

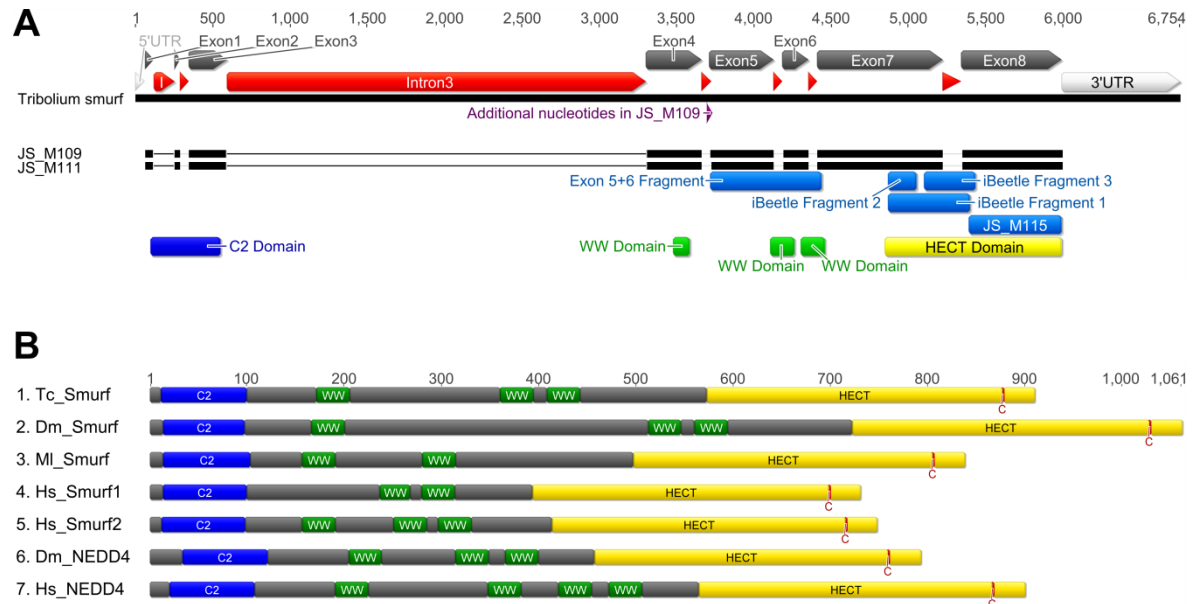


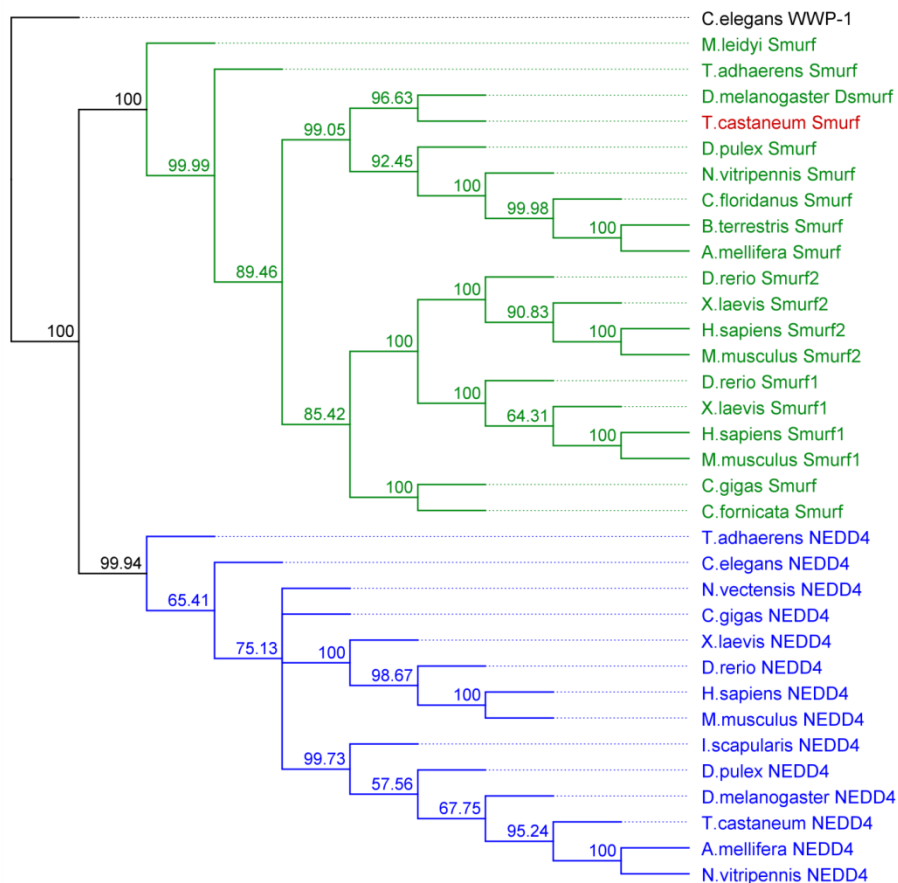
Figure 4-8 Gene model and molecular characterization of *Tribolium* Smurf

(A) Gene model of *Tc-smurf*. Shown are the positions of the untranslated regions (white), exons (grey), and introns (red). The light blue annotations below the depicted transcripts (JS_M109 and JS_M111) show the location of different dsRNA sequences used in this study with respect to the *Tc-smurf* cDNA sequence. Dark blue, green, and yellow annotations show the positions of the encoded, conserved protein domains. The purple annotation indicates the position of the 12 nucleotides which are present in JS_M109 and absent in JS_M111. (B) Depicted is the 910 AA version of Tc-Smurf. The protein contains a C-terminal catalytic HECT domain (active cysteine depicted as a red C), three substrate-binding WW domains and an N-terminal C2 domain. The C2 domain might be involved in membrane binding and in binding to certain substrates. For comparison other members of the NEDD4 family are shown. One of the major differences between different Smurf proteins applies to the number of WW domains. Protein domains were identified using PROSITE (Swiss Institute of Bioinformatics). Tc: *Tribolium castaneum* (red flour beetle), Dm: *Drosophila melanogaster* (common fruit fly), Hs: *Homo sapiens* (human), Ml: *Mnemiopsis leidy* (sea walnut, comb jelly). Numbers on top indicate AA position, images created with Geneious version 7.0 (Biomatters).

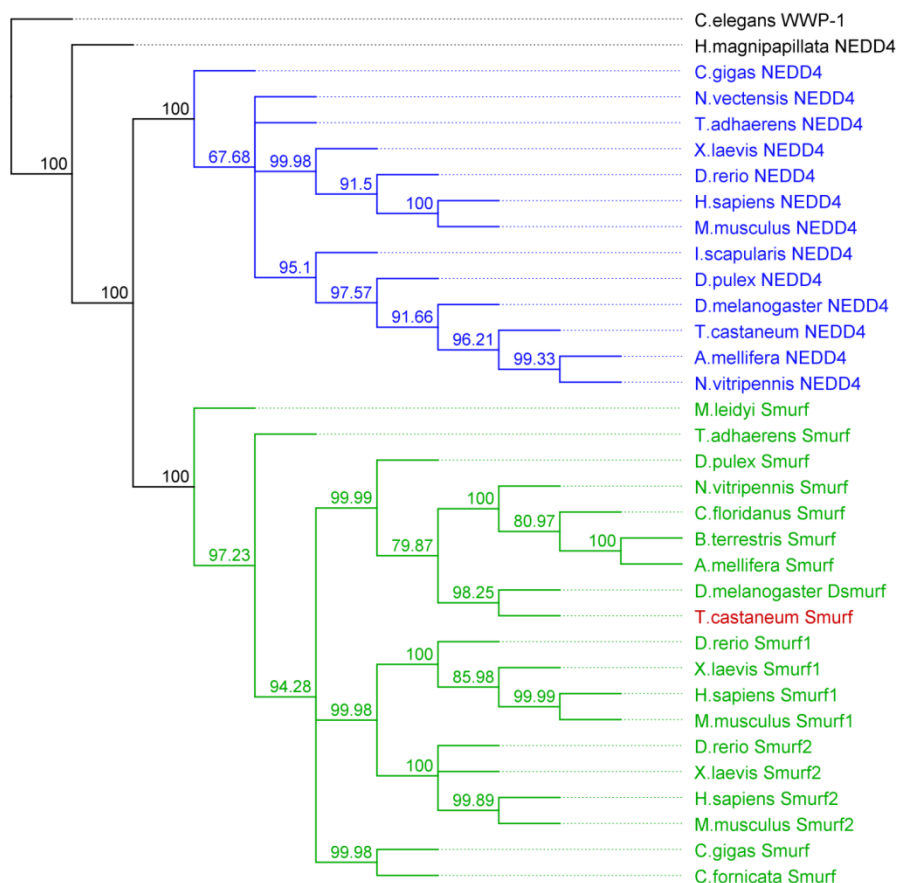
Figure 4-9 (next page) Phylogenetic analysis of *Tribolium* Smurf

Phylogenetic trees were constructed by using a MUSCLE alignment based on the entire amino acid sequence (A) or on the HECT domain only (B) with the neighbour joining method. *T.castaneum* Smurf groups with high bootstrap value in the Smurf clade (green), with high similarity to *Drosophila* DSmurf. Tree and image created with Geneious version 7.0 (Biomatters). The complete species names, as well as their common names, phylum and Taxonomy ID are given in Table 3-2 (materials and methods section 3.3).

A



B



4.3.1 *Tribolium smurf* expression and RNAi phenotype

To analyze the expression pattern of *Tc-smurf*, DIG-labeled RNA antisense probes were synthesized based on either the entire coding sequence (JS_M111) of the *Tc-smurf* gene or on a 3'-part (JS_M115, Figure 4-8 A). These probes were used for *in situ* hybridization on embryos aged 0-48 hours, development at 31°C. Sense probes served as negative controls. No locally restricted expression of *Tc-smurf* could be detected at any stages analyzed, suggesting uniform expression of this gene. This is in accordance with data for *Drosophila DSmurf*, which is also reported to be expressed uniformly (Podos et al., 2001).

Tc-smurf was identified because of the highly penetrant anterior patterning phenotype detected during the iBeetle screen (exemplary phenotypes Figure 4-10 C and D). To rule out possible off target effects, two non-overlapping dsRNAs (*iBeetle fragment 2* and *iBeetle fragment 3*, Figure 4-8 A), covering the original iBeetle fragment, had been injected during the 'verified candidate' phase (4.2.3). Applying parental RNAi, both fragments resulted in the same phenotype as observed in the iBeetle screen with a high incidence of cuticles with anterior defects (Figure 4-10 C). These cuticle phenotypes were characterized by missing anterior body parts, mainly defective heads, but also by deletions of the entire anterior larval region, including thoracic segments, while dorsal-ventral identity of the remaining cuticle was concurrently retained. Using dsRNA based on a more 3' part of the mRNA (*JS_M115 fragment*, Figure 4-8 A) resulted also in anterior patterning defects, but the observed phenotypes were more severe and many cuticles displayed only some remaining abdominal segments (Figure 4-10 D). Also a high number of "empty eggs" (EE) occurred, indicating that these animals died before they were able to secrete a cuticle, or that they did not develop at all. To check whether these stronger phenotypes were unspecific off-target effects or, in contrast, represented a more efficient knock down of the *Tc-smurf* transcript, a third cDNA fragment was created as a dsRNA template. This fragment was based on the sequence of mainly exon 5 and 6 of the *Tc-smurf* gene (*Exon 5+6 fragment*, Figure 4-8 A). All dsRNA fragments were also tested for potential off-target effects using E-RNAi (German Cancer Research Center, <http://www.dkfz.de/signaling/e-rnai3/>, see also 3.4). To compare the different effects of these fragments, adult females of the *Pig-19* strain were injected with dsRNA against the non-overlapping *iBeetle fragment 1*, *JS_M115 fragment* and *Exon 5+6 fragment* (based on

JS_M111). Injection of dsRNA targeting *DsRed* served as a negative control. Since *Drosophila* DSmurf is reported to regulate Dpp signaling in the fly (introduction, see also Liang et al., 2003; Podos et al., 2001) and Tc-Sog is also a published antagonist to Tc-Dpp during early *Tribolium* development (van der Zee et al., 2006, see introduction), RNAi against *Tc-short-gastrulation* (*Tc-sog*) was included as a positive control and for phenotype comparison.

Animals that hatched and crawled through the 300 μ m mesh into glycerol were scored as wild type (wt), since *Tc-sog* and *Tc-smurf* RNAi phenotypes were lethal and did not hatch. Together with cuticles with wild type morphology during cuticle preparation they represented the group “wild type”. Anterior patterning defects were sorted into three categories, depending on how many tagmata were affected (Figure 4-10 E): ‘only head affected’, ‘head and thorax affected’ or ‘head and thorax completely absent’. In addition, cuticles were scored as completely dorsalized if they showed a tube-like phenotype without detectable ventral structures (example in Figure 4-10 B) especially in cases when ventral structures were replaced by duplication of dorsal structures. The group “empty egg and very strong” described empty vitelline membranes that showed only small cuticle remnants or did not contain an identifiable cuticle at all. These remnants were in case of *Tc-smurf* RNAi embryos usually hindgut cuticle and/or urogomphi. The group “other” represented phenotypes which could not be reliably grouped into one of the previous categories. These were for instance cuticle fragments or balls without detectable dorsal-ventral (DV) or anterior-posterior (AP) polarity but also other kind of cuticle phenotypes that occur occasionally in wild type egg collections.

Over 90 % of the offspring of *DsRed* dsRNA injected animals hatched and showed a wild type phenotype while 3 out of 208 analyzed animals showed head defects. *Tc-sog* RNAi caused a complete dorsalization (“double dorsal” phenotype) in over 80 % of the analyzed cuticles, characterized by a tube-like cuticle which displays only the typical long dorsal bristles, some of them having a basal scale. Another typical feature of the *Tc-sog*-RNAi phenotype was a second pair of posterior urogomphi, a dorsal body structure. This indicated a complete dorsalization of the body cuticle along the anterior-posterior axis. The head cuticle was always missing in these phenotypes (see also van der Zee et al., 2006) (Figure 4-10 B and E). Head defects without dorsalization of the remaining body cuticle was found in 3 out of 313 analyzed *Tc-sog* RNAi cuticles.

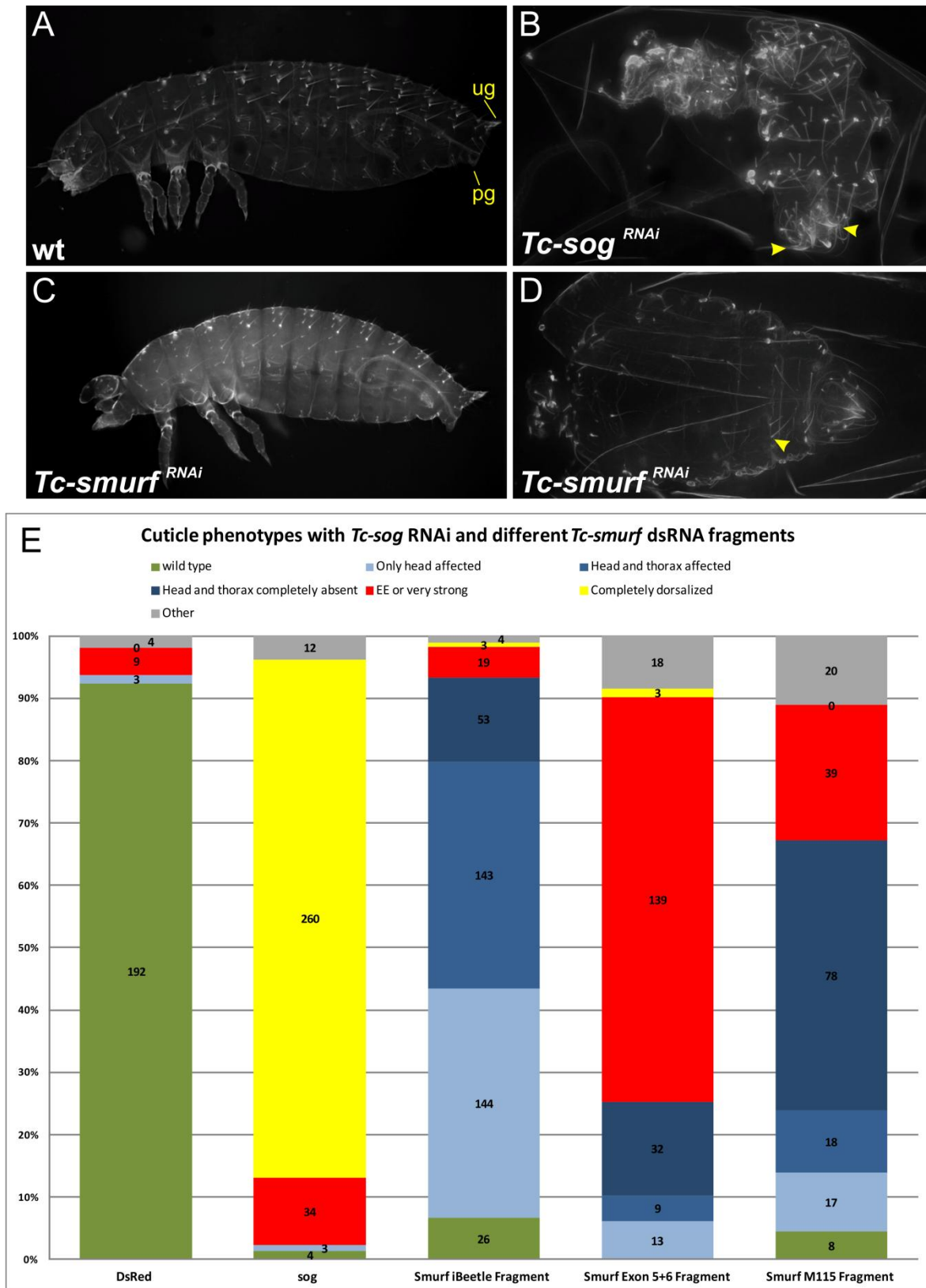


Figure 4-10 Cuticle phenotypes of *Tc-Smurf* RNAi using various dsRNA template fragments
 Loss of *Tc-smurf* function resulted in anterior patterning defects and potentially strong phenotypes. Anterior to the left for cuticles. **(A)** and **(C)** lateral views, **(B)** unknown, **(D)** ventral view. **(A)** Wild type L1 cuticle. Note the differences between the dorsal and ventral bristle pattern. ug: urogomphi, pg: pygopodia. **(B)** *Tc-sog* RNAi cuticle.

The head is absent and cuticle is completely dorsalized. Arrowheads point to duplicated urogomphi. (C) Weak *Tc-smurf* phenotype, only parts of the head cuticle are affected by the knock down. (D) Stronger *Tc-smurf* knock down phenotype in ventral view. Only about 6 abdominal fragments are remaining, but dorsal-ventral integrity does not seem to be affected. Arrowhead points to typical ventral bristles. (E) Result of a comparative RNAi experiment using dsRNAs against *DsRed* (negative control) *Tc-sog* and different dsRNAs against *Tc-smurf*.

All three different *Tc-smurf* dsRNA fragments caused anterior defects after injection, but with different penetrance and strength. RNAi using dsRNA against *iBeetle Fragment 1* caused defects of only the head or the head and the thorax in over 70 % of the animals. In contrast, RNAi using the *JS_M115 fragment* led to a high number of cuticles with only varying portions of the abdomen remaining and a higher amount of ‘empty egg and very strong’ phenotypes. RNAi using the *Exon 5+6 fragment* led to an even higher amount of ‘empty egg and very strong’ phenotypes and a smaller number of cuticles that showed a clear anterior patterning phenotype (about 25 %). All cuticles that were grouped into the anterior patterning categories retained some DV-polarity, which could be identified by characteristic ventral bristles or the pygopodia, although anterior structures of these cuticle remnants were occasionally dorsalized. In no case a double urogomphi phenotype could be detected in any cuticle resulting from *Tc-smurf* knock down. Deletion of body parts was found in all cases at the anterior of the animals, with the posterior being less prone to the loss of *Tc-smurf* function. The amount of missing anterior tissue could be very different between cuticles within one injection, but especially between cuticles that arose from the injection of different dsRNA fragments (Figure 4-10 E). In summary all *Tc-smurf* dsRNA fragments caused an anterior patterning defect with a very low number of phenotypically wild type animals (6,6 %, 4,4 % and 0 % for *iBeelte fragment 1*, *JS_M115 fragment* and *Exon 5+6 fragment*, respectively).

We have recently reported that RNAi effects in *Tribolium* can be strain specific (Kitzmann et al., 2013). To finally exclude this possibility for *Tc-smurf*, the different dsRNA fragments were injected in different beetle strains (*Pig-19* and *SB*). RNAi against *DsRed* and buffer injections served as negative controls. After adult injection, two-day egg-collections of eight living females for each condition were gathered on day 13 and day 19 after injection (dai), respectively. Cuticle preparations were done four days later. The phenotypes of the hatched animals were analyzed, counted and grouped into four categories similar to the approach in Figure

4-10 E. Hatched larvae and phenotypically wild type animals on the cuticle preparation slide were scored as “wild type”. All head defects and anterior deletions were collectively sorted as “anterior defect”. The category “other defect” combined all phenotypes that could not be clearly counted as wild type or anterior patterning phenotypes. In the case of *Tc-smurf* RNAi cuticle preparations, this group consisted almost entirely of empty eggs, heavily fragmented cuticles, or very small cuticle remnants.

The rate of “other defects” was higher for the *SB* strain in all experimental conditions and represented about 20–25 % of all examined animals for the buffer injections and the *DsRed* RNAi control, whereas the rate of these unspecific phenotypes was under 10 % for the *Pig-19* strain. Anterior defects occurred only in some individual cases in both strains. The numbers between the two independent egg collections were mostly similar.

RNAi with the *Tc-smurf iBeetle fragment 1* dsRNA resulted in anterior defects in over 65 % and over 80 % of all analyzed animals in the *SB* and *Pig-19* strain, respectively. Phenotypically wild type animals were more frequent for the injection in the *Pig-19* strain than for the injection in *SB*, suggesting a stronger sensitivity of the *SB* strain for the *Tc-smurf* knock down. The fraction of “other defects” was higher for *SB* (about 30 %) than for *Pig-19* (about 5 %). The numbers between the two egg collections were mostly similar.

RNAi with the *Tc-smurf JS_M115 fragment* dsRNA resulted in anterior defects in 37–42 % and 44–62 % of all analyzed animals in the *SB* and *Pig-19* strain, respectively. Phenotypically wild type animals were not detected. The fraction of “other defects” was slightly higher for *SB* (about 60 %) than for *Pig-19* (38–56 %). The numbers for *SB* were similar between the egg collections. For the injection into the *Pig-19* strain a decrease of ‘other defects’ (56 % to 38 %) in favour of ‘anterior defects’ (44 % to 62 %) could be observed between day 13 and 19 after injection.

RNAi with the *Tc-smurf Exon 5+6 fragment* resulted in a low number of clear anterior defects in both the *SB* and the *Pig-19* strain (about 1–7 % for *SB* and 4–19 % for *Pig-19*). The amount of ‘other defects’ was very high compared to all other conditions, especially in *SB* (about 90–99 %) but also in *Pig-19* (62–72 %). Obvious differences between the two strains affected mainly the amount of animals scored as phenotypically wild type. After injection into the *SB* strain almost

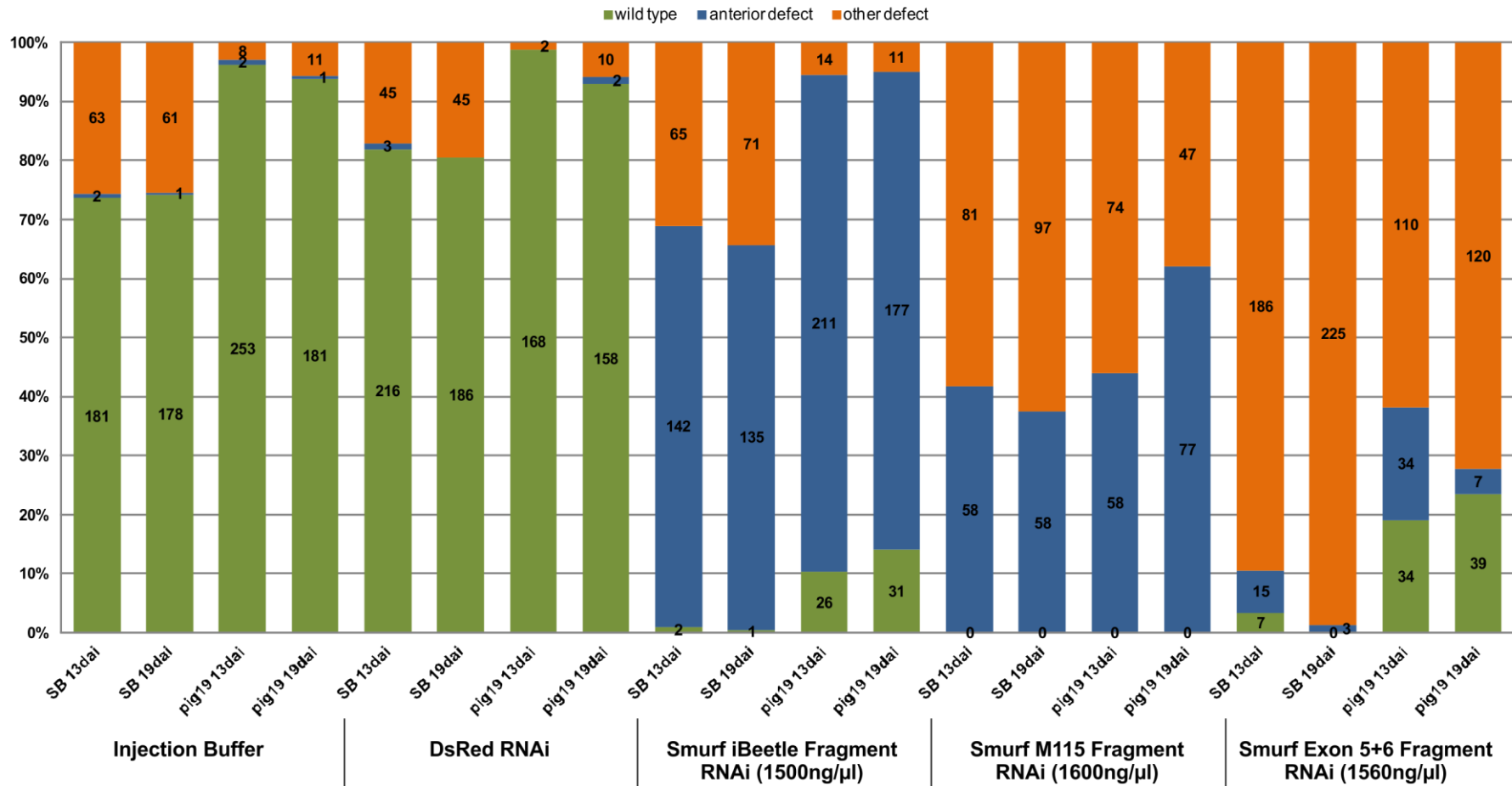
none (0–3 %) were scored as wt while in the *Pig-19* strain about 19–24 % were sorted into this category. Similar to RNAi with the *Tc-smurf iBeetle fragment 1* the *SB* strain appeared more sensitive to *Tc-smurf* knock down.

In summary, the phenotypes for the different *Tc-smurf* RNAi approaches were consistent between the different strains. Differences seen between the different fragments in the *Pig-19* strain could also be observed in the *SB* strain. Although phenotypes in the *SB* strain in general appeared to be slightly stronger, real strain specific effects for *Tc-smurf* RNAi were not apparent. The differences in the amount of ‘anterior defects’ and ‘other defects’ between the different *Tc-smurf* RNAi approaches raised the question whether the ‘other defects’ were qualitatively different phenotypes or just the result of a more efficient knock down. There were several reasons to consider the second assumption. The group of ‘other defects’ consisted almost entirely of empty eggs, heavily fragmented cuticles or very small cuticle remnants in case of *Tc-smurf* RNAi phenotypes. This could be seen in the experiment depicted in Figure 4-10, where EE and strong defects were separately counted from all other defects. A smaller number of clear anterior patterning phenotypes coincided with a higher number of EE and very strong defects if the results for the different *Tc-smurf* RNAi approaches were compared. These empty eggs could result from embryonic lethality before cuticle secretion. Another indication was the decline in ‘other defects’ in favour of ‘anterior defects’ between 13 dai and 19 dai after injection of the *Tc-smurf JS_M115 fragment* dsRNA into the *Pig-19* strain (Figure 4-11). Although the RNAi effect was in most cases stable for the 19 days of the experiment this observation was potentially the result of a decline of the knock down effect during the phase of the experiment.

Figure 4-11 (next page) *Tc-smurf* cuticle phenotypes in different strains using various dsRNA template fragments

Two day egg collections of eight injected adult females were gathered at 13 and 19 days after injection (dai) and aged for four days at 31°C. All progeny were scored and sorted in different phenotypic categories. wild type: animals hatched or no defect of the L1 epidermis detectable. Anterior defect: head defects or anterior deletions. Still remaining dorsal-ventral polarity. Other defect: all other kind of defects. Usually empty eggs or fragmented cuticles that could not be reliably analyzed. Buffer injections and RNAi against *DsRed* served as negative controls. The different strains did not result in qualitatively different phenotypes, but in some cases the *SB* strain appeared to be stronger affected by the RNAi effect than the *Pig-19* strain. All *Tc-smurf* dsRNA fragments resulted in anterior defects after injection. The amount of other defects (not analyzable due to missing or heavily affected cuticle) differed strongly between injections of different *Tc-smurf* dsRNA fragments. See text for more details.

Tc-Smurf cuticle phenotypes, different fragments, different strains



To address the question whether many of the *Tc-smurf* RNAi embryos died prior to cuticle secretion but succeeded to a certain point of development, fuchsin stainings were done on embryos resulting from the different RNAi experiments depicted in Figure 4-10 E. dsRNA injections took place in the *Pig-19* strain. Fuchsin staining allowed to discriminate between embryonic tissue with a high density of red stained nuclei and the surrounding extraembryonic tissue and yolk with less densely packed nuclei. Embryos that developed 24-48 h at 31°C were chosen for staining, since in a wild type embryo collection all animals in this clutch would have reached the fully developed germ band stage. This was confirmed in the *DsRed* RNAi control collection, since over 97 % of the scored embryos showed a proper embryonic germ band (Figure 4-12 A and B). *Tc-sog* RNAi embryos showed a developed germ band in over 80 % of the analyzed embryos. However, the germ band was usually less broad and the head tissue was missing in all germ bands analyzed more thoroughly, although this was not analyzed in detail (Figure 4-12 A and C) (see also van der Zee et al., 2006). *Tc-sog* RNAi also led to a larger fraction of embryos without any detectable embryonic tissue (about 15 %). Over 94 % of embryos subjected to knock down of *Tc-smurf* using the *iBeetle fragment 1* showed a germ band, usually with missing or potentially dispersing anterior tissue. Similar effects could be observed for knock down of *Tc-smurf* using the *JS_M115 fragment*. Identifiable germ bands were found in more than 85 % of the embryos analyzed. However, the germ bands looked often shorter than those resulting from the knock down using the *Tc-smurf iBeetle fragment 1*. The fraction of embryos that did not show any detectable embryonic tissue at all was largest for the RNAi approach using the *Tc-smurf Exon 5+6 fragment* (about 46 %). Still, about 44 % of the embryos in this sample showed a proper germ band, often with great portions of anterior tissue missing or potentially dispersing, as also observed for the other *Tc-smurf* RNAi approaches (Figure 4-12 A, D and E). Comparing these results to the numbers of anterior patterning phenotypes detected in L1 cuticle preparations (Figure 4-10 E), indicated that especially after RNAi using the *JS_M115 fragment* and *Tc-smurf Exon 5+6 fragment* a large fraction of embryos developed a germ band but never secreted a cuticle. However, it could not yet be clarified whether some embryos did not develop at all after *Tc-smurf* knock down.

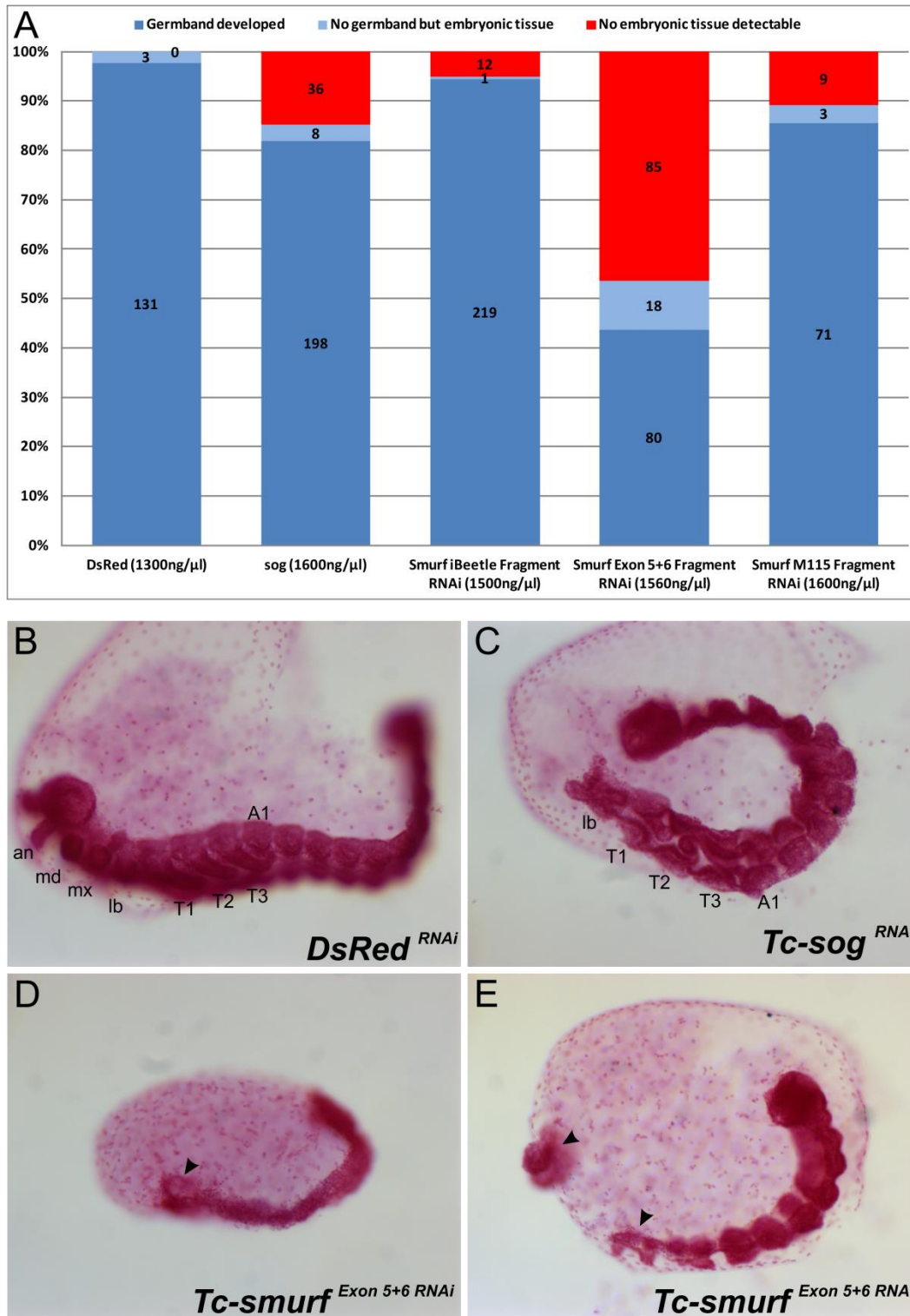


Figure 4-12 Embryonic phenotype caused by *Tc-smurf* knock down

(A) Quantitative analysis of the fuchsin staining. See text for more details. (B–E) Fuchsin stainings on RNAi embryos. Anterior to the left and dorsal side up in B–E. In the germ band in C the anterior ventral side faces to the viewer. (B) Retracting germ band stage *DsRed* RNAi embryo serving as negative control. All head parts are present. (C) *Tc-sog* RNAi embryo. The germ band is less broad and all embryonic structures anterior to the labial segment are missing. (D) *Tc-smurf* RNAi embryo. Note that the embryo is minimum 24 h of age. wild type embryos of this stage are fully elongated and would be displaying limb buds. The embryonic nuclei in the

anterior look less densely packed and more scattered than after *DsRed* and *Tc-sog* RNAi. Arrowhead points to a very weak and thin headlobe. (E) Embryo taken from the same knock down experiment as (D) but proceeded further in development. Some abdominal segments look morphologically wild type, but anterior tissue including the thoracic segments and the limbs is missing or decreased. The left arrowhead points to remnants of embryonic tissue. A gap is visible between this anterior tissue and the anterior of the remaining germ band, which like the embryo in (D) shows less densely packed and more scattered nuclei (right arrowhead).

In summary RNAi mediated knock down of *Tc-smurf* resulted in anterior defects with all different dsRNA fragments used for injection. These anterior defects represented the highest consistency between the knock down phenotypes. Defects in L1 cuticles as well as in embryonic tissue primarily affected the anterior region of the animals. One big difference between the phenotypes seen in L1 cuticles after *Tc-smurf* knock down affected the amount of remaining cuticle. This could differ strongly between the different dsRNA fragments used for RNAi but also between different cuticles resulting from one particular egg collection. All *Tc-smurf* RNAi embryos used for downstream analysis in the following chapters resulted from injection with the *Tc-smurf JS_M115 fragment*.

4.3.2 TUNEL stainings in *Tc-smurf* RNAi

RNAi against *Tc-smurf* led to head defects and anterior deletions in cuticle preparations as well as embryos. Cuticle phenotypes often only displayed a few remaining abdominal segments, i.e. all remaining segments of these phenotypes were derived from the growth zone. In *Tc-smurf* RNAi embryos stained for expression of the segmental marker *Tc-wingless* (*Tc-wg*) (Nagy and Carroll, 1994) anterior *Tc-wg* stripes were frequently missing (Figure 4-7 E and E'). Moreover, *Tc-smurf* RNAi embryos analyzed morphologically using fuchsine stainings usually showed missing anterior tissue and often less densely packed nuclei in the anterior of the remaining embryo. For this reason a TUNEL assay was performed to check for cell death in wild type, *Tc-sog*, and *Tc-smurf* RNAi embryos.

Usually no apoptosis was detected in wt embryos during blastoderm stages. This was also true for *Tc-sog* or *Tc-smurf* knock down embryos (not shown). Many elongating germ band stage embryos showed high levels of apoptosis in the anterior of the embryo after RNAi against *Tc-sog* or *Tc-smurf*, which could never be seen to such an extent in the wild type (Figure 4-13 A and B). Early germ band stages of *Tc-sog* RNAi embryos showed apoptosis in the very anterior of the embryo (Figure 4-13 C). In fully elongated and retracting germ band stage embryos

increased cell death could be detected in the embryonic midline and to some extent in the anterior (Figure 4-13 C and D). No increase in TUNEL-stained cells compared to the wt was detected for very early *Tc-smurf* RNAi germ rudiments or germ band stage embryos (Figure 4-13 E, due to the small headlobes it is clearly identifiable, that the embryo shown was affected by the knock down of *Tc-smurf*). During germ band elongation, high levels of cell death were detected in the anterior region of *Tc-smurf* RNAi embryos (Figure 4-13 F and F'). The embryo depicted in Figure 4-13 F shows only excessive cell death in the very anterior, more posterior parts of the animal are free of apoptotic cells and also look morphologically wild type. Many embryos, like the one shown in F', showed high levels of apoptosis in a more prolonged area of the germ band, especially in the midline. The results of the TUNEL assay show that loss of *Tc-smurf* function caused severe cell death in the anterior of the embryo during germ band stages.

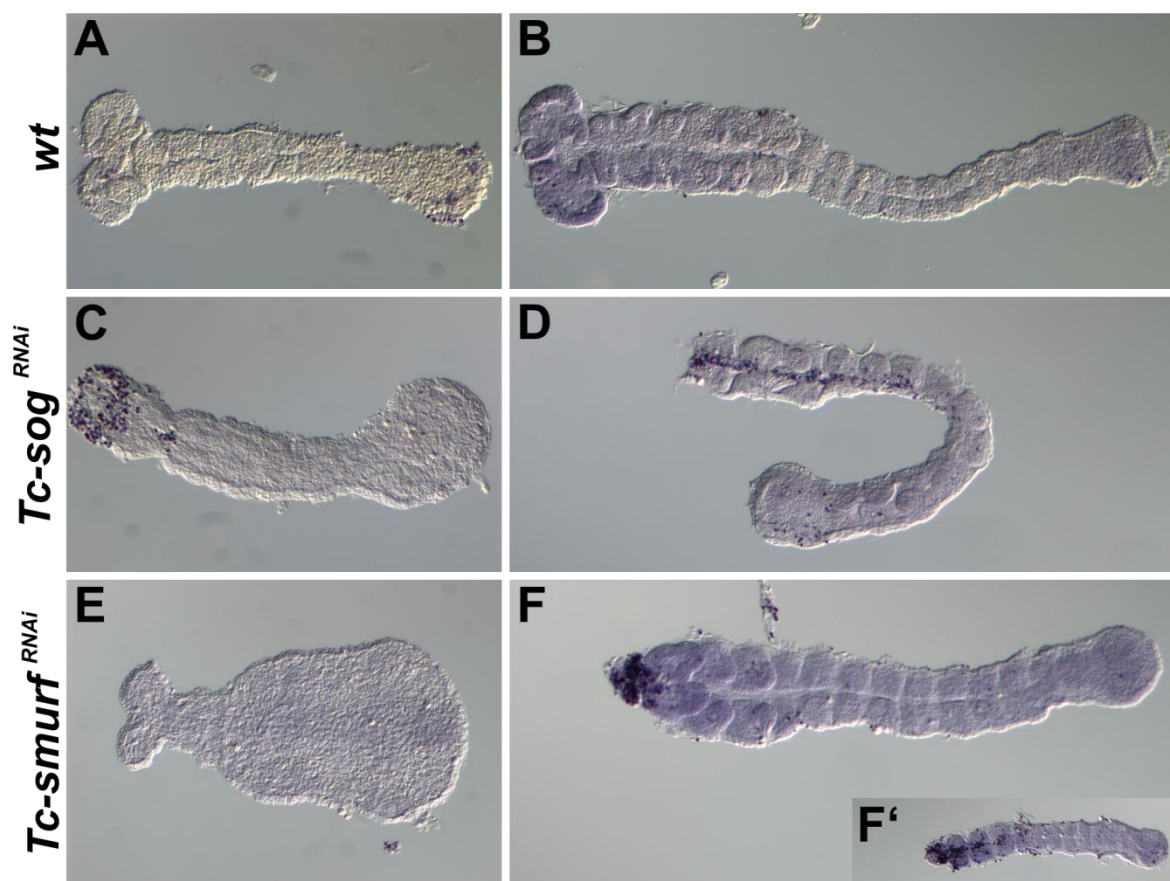


Figure 4-13 *Tc-smurf* RNAi causes severe cell death in the anterior of the embryo at germ band extension stages

TUNEL stainings were done in order to analyze the fate of embryonic cells during embryonic development. Anterior to the left in all pictures, in D the upper left end is anterior. (A and B) In the wild type (wt) no excessive cell death was detected during any stages analyzed. (C) *Tc-sog* RNAi embryos showed high levels of

apoptosis in the very anterior during early germ band stages (dark spots mark apoptotic cells) and in the anterior and midline during germ band elongation and retraction (D). (E) Excessive cell death was not observed before germ band elongation in *Tc-smurf* RNAi embryos. (F, F') During germ band stages, loss of *Tc-smurf* function led to severe cell death in the anterior of the embryos. (F') Shows an embryo in which apoptosis could be detected in a more extensive region of the embryo).

4.3.3 Effect of *Tc-smurf* RNAi on the *dpp* pathway in *Tribolium*

Smurf E3 ubiquitin ligases were reported to be negative regulators of the *dpp* pathway in *Drosophila* as well as in vertebrates. One major way how they act in this context is targeting of receptor activated Smads (R-Smads, in *Drosophila* Mothers against Dpp, MAD) for proteosomal degradation (Liang et al., 2003; Lin et al., 2000; Podos et al., 2001; Zhang et al., 2001; Zhu et al., 1999, see also introduction). To investigate whether the observed phenotype caused by *Tc-smurf* RNAi was due to impaired Tc-Dpp signaling, the distribution of phosphorylated (activated) Mothers against Dpp protein (pMAD) was analyzed in wild type, *Tc-sog* RNAi, and *Tc-smurf* RNAi embryos using a cross-reactive monoclonal antibody. Phosphorylated MAD/Smad is only present in cells with activated Dpp/BMP receptors (Dorfman and Shilo, 2001; Persson et al., 1998; Tanimoto et al., 2000; van der Zee et al., 2006). I also checked the expression patterns of *Tc-decapentaplegic* (*Tc-dpp*) and the *Tc-dpp* downstream gene *Tc-pannier* (*Tc-pnr*) (van der Zee et al., 2006). In the experiments shown here and also in upcoming chapters that deal with the function of *Tc-smurf*, *Tc-sog* was included as a positive control but also as a source for phenotype comparison. Since Smurf E3 ubiquitin ligases were published regulators of Dpp signaling, one upcoming question was, whether and how *Tc-smurf* was involved in this process in *Tribolium*. This was done by comparing the observed phenotype to the wild type but also to already published data on Dpp signaling processes in *Tribolium* (van der Zee et al., 2006), which I, for the matter of comparability, partially reproduced in my own experiments.

Expression of *Tc-dpp* is very dynamic during blastoderm stages and no alteration of *Tc-dpp* expression could be reliably detected for *Tc-smurf* knock down embryos during these stages. However, *Tc-dpp* expression and late blastoderm stages are very dynamic, hence subtle effects of *Tc-smurf* RNAi on *Tc-dpp* expression could not be excluded. The *Tc-dpp* expression pattern detected for wild type and *Tc-sog* RNAi was according to the published pattern (Sharma et al.,

2013; van der Zee et al., 2006). At differentiated blastoderm stages, which is the time point when serosa and embryonic tissue can firstly be discriminated due to the size and spacing of the nuclei, pMAD was unevenly distributed within the wild type embryo. Highest concentrations were detected at the posterior dorsal site, the prospective amnion. At the anterior dorsal site, pMAD concentration was higher than ventrally. An asymmetry was also present morphologically, since serosa and embryonic cells build an oblique border with less embryonic tissue at the dorsal than at the ventral site of the embryo (e.g. van der Zee et al., 2006) and (Figure 4-14 A–A’). Asymmetries were lost in *Tc-sog* RNAi embryos. pMAD was evenly distributed along the serosa cells and peak levels in the posterior dorsal part of the embryo were never reached compared to the wild type. The germ-serosa boundary was shifted to the posterior and became straight (Figure 4-14 B-B’ see also van der Zee et al., 2006). In *Tc-smurf* RNAi embryos the most obvious difference in stainings for pMAD during blastoderm stages was a non-quantified increase in staining activity which was also seen in germ band stages. This difference was observed in several independent experiments. Color development was always more than three times quicker in *Tc-smurf* RNAi embryos than in other conditions like in wild type or *Tc-sog* RNAi embryos. An indication for this difference is given by comparing the lower amount of unspecific pinkish staining in the yolk between C and A+B in Figure 4-14. This suggested a much higher cellular pMAD concentration in *Tc-smurf* RNAi embryos than in the wild type. However, unlike the situation in *Tc-sog* RNAi embryos the distribution of pMAD still showed anterior-posterior (AP) and dorsal-ventral (DV) polarity, with higher levels of pMAD at the dorsal site of the embryo and peak levels in the posterior dorsal region, sometimes even reaching the posterior ventral site of the embryo (Figure 4-14 C’). Morphologically, blastoderm stage *Tc-smurf* RNAi embryos showed different phenotypic aspects. In many embryos a distinguishable oblique germ-serosa boundary was detected (Figure 4-14 F’), indicating that dorsal-ventral fate was not or at least not completely impaired during this time point of development as it was the case for *Tc-sog* knock down embryos. Nevertheless, I could detect some individual cases, where the germ-serosa boundary was shifted to the posterior and straightened, similar to the situation in *Tc-sog* RNAi embryos. This could indicate that some ventral cells lost embryonic in favor of serosal fate. It was also observed that the

boundary appeared to be less exact and more fuzzy (compare germ-serosa boundary between C'' and A''+B'' in Figure 4-14).

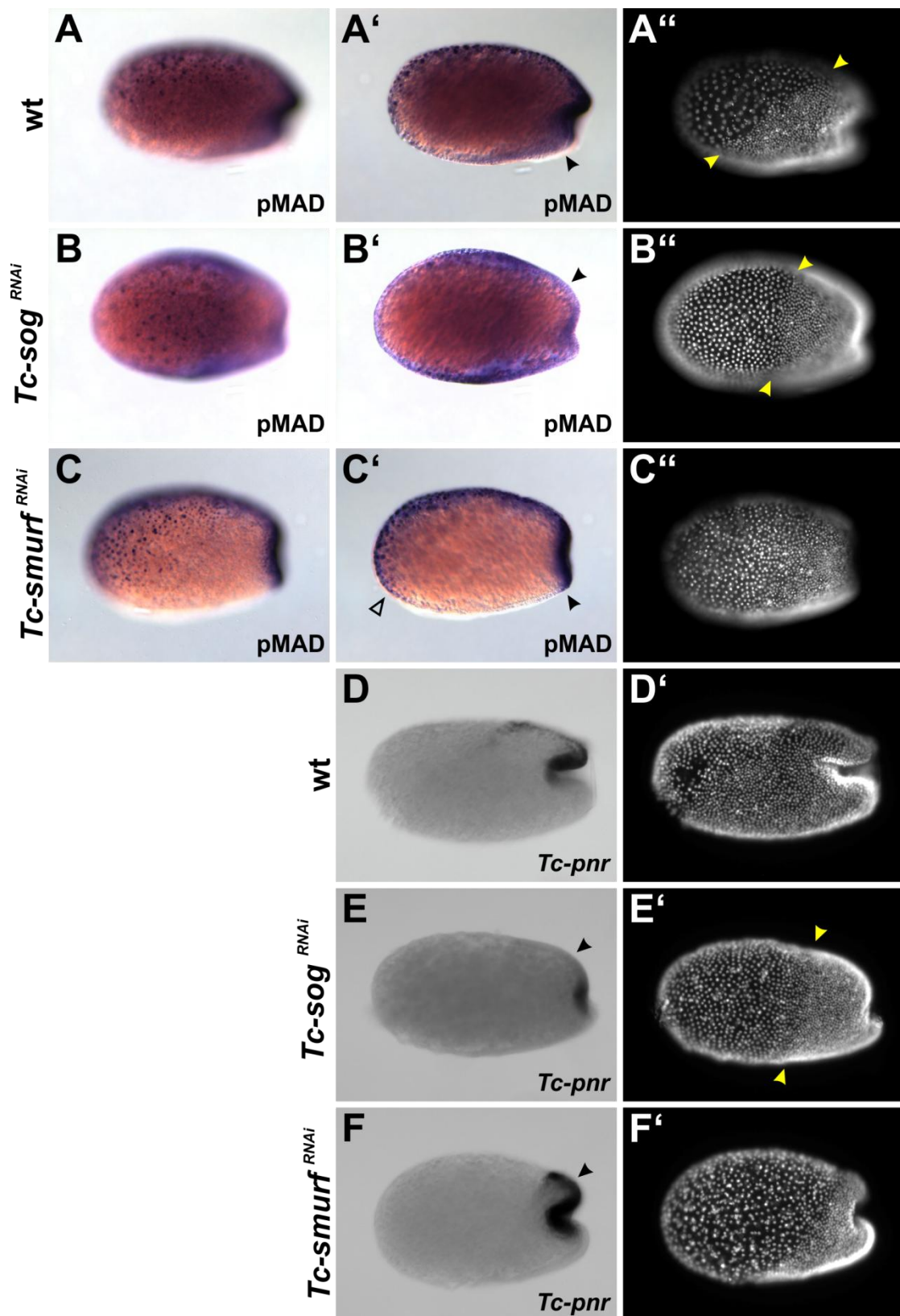


Figure 4-14 *pMAD and Tc-pnr* expression in wild type, *Tc-smurf* and *Tc-sog* RNAi blastoderm stages

Pictures in every row show the same embryo, **A-F** are surface views, **A',B'**, and **C'** are optical cross-sections. The right column shows surface views of embryos stained for nuclei with Hoechst 33342. Anterior to the left, dorsal side up for all pictures. (**A** and **A'**) During the differentiated blastoderm stage *pMAD* is distributed asymmetrically in the embryo. *pMAD* could be detected all along the dorsal side with highest concentrations in the dorsal and posterior embryonic tissue. At this time point prospective embryonic and serosal tissue form an oblique border, arrowheads in **A''** point to the dorsal and ventral edges, the polyploid serosa nuclei are larger and more widely spaced than the embryonic nuclei. (**B**, **B'**) In *Tc-sog* RNAi embryos *pMAD* is evenly distributed along the dorsal-ventral axis, no polarity could be detected within the serosa tissue. *pMAD* concentration in the embryonic cells was lower than in the wild type and peak concentrations in the dorsal posterior embryo was not reached (arrowhead points to weak staining in posterior dorsal embryo). (**B''**) The embryos lost dorsal-ventral polarity as indicated by straightening of the germ-serosa boundary, which was shifted to the posterior on the ventral side of the embryo. The yellow arrowheads mark the anterior border of the embryonic tissue. (**C**, **C'**) *pMAD* concentration appeared to be higher in *Tc-smurf* RNAi embryos as indicated by a much quicker color development in NBT/BCIP stainings (see text). The distribution is asymmetrical and similar to the wild type situation, although *pMAD* coverage ranged a bit further to the ventral side of the blastoderm (open arrowhead in **C'**), which could also be seen on the posterior ventral edge of the primitive pit (black arrowhead, compare to black arrowhead in **A'**). The germ serosa boundary was often not as defined in *Tc-smurf* RNAi embryos as it was in the wild type or in *Tc-sog* RNAi embryos (compare embryo in **C''** with embryos in **A''** and **B''**). (**D**) *Tc-pannier* was expressed in the prospective amnion in the wild type embryo, where *pMAD* concentration was highest (compare to **A'**). (**E**) In *Tc-sog* RNAi embryos *Tc-pnr* expression was reduced and anterior expression was often hardly detectable. Peak levels at the posterior dorsal position were not detectable (arrowhead). Arrowheads in **E'** mark the anterior borders of the embryonic tissue. (**F**) expression of *Tc-pnr* in *Tc-smurf* RNAi embryos was similar to the wild type expression pattern although it appeared to be a little bit stronger and might have reached a bit further ventrally in the posterior. *Tc-pnr* expression was very strong in the dorsal amnion (arrowhead).

Expression of *Tc-pnr*, which marks the prospective amnion in *Tribolium* differentiated blastoderm stage embryos (van der Zee et al., 2005, Figure 4-14 D), was lowered in *Tc-sog* RNAi embryos compared to the wild type situation, and the anterior dorsal expression was almost undetectable (Figure 4-14 E and van der Zee et al., 2006). *Tc-pnr* expression after *Tc-smurf* knock down did not differ strongly from the wild type situation, although it appeared to be stronger (Figure 4-14 F). However, this statement could not be undoubtedly made using *in situ* hybridization.

In wild type germ rudiment stage embryos, *Tc-dpp* expression was detected in the posterior of the germ rudiment and in the amnion. An intense expression was also found in the anterior amnion, but not in the embryonic tissue within the headlobes (Figure 4-15 A). During elongating germ band stages, *Tc-dpp* was expressed in the amnion, the dorsal ectodermal borders of the embryo, and in two stripes in the growth zone (see also van der Zee et al., 2006) (Figure 4-16 A).

These two stripes disappeared in fully elongated germ band stages and *Tc-dpp* was expressed *de novo* in the developing limb buds (Figure 4-16 D). In *Tc-sog* RNAi embryos two stripes of ectopic *Tc-dpp* expression along the ventral midline were detected in early germ rudiments (Figure 4-15 B). These ectopic stripes were also found during later germ band stages where they were continuous with the growth zone expression. Additionally, *Tc-sog* RNAi embryos showed a weakening and sometimes even disappearance of the dorsal margin expression (see also van der Zee et al., 2006) (Figure 4-16 B+E). *Tc-smurf* knock down also resulted in ectopic rows of *Tc-dpp* expression in the midline of germ rudiments and elongating germ band stage embryos (Figure 4-15 C+D, Figure 4-16 C+F). Especially in germ rudiments and early germ band stage embryos, a strong expression domain in the head lobes was present (Figure 4-15 C+D). Additionally, the anterior of germ rudiments and early germ band stage *Tc-smurf* RNAi embryos was often not covered by amnion (Figure 4-15 C). During later stages the ectopic stripes often did not seem to be as intense and continuous as those observed for *Tc-sog* RNAi. In older embryos the posterior of the germ band midline was frequently free of *Tc-dpp* expression (Figure 4-16 F).

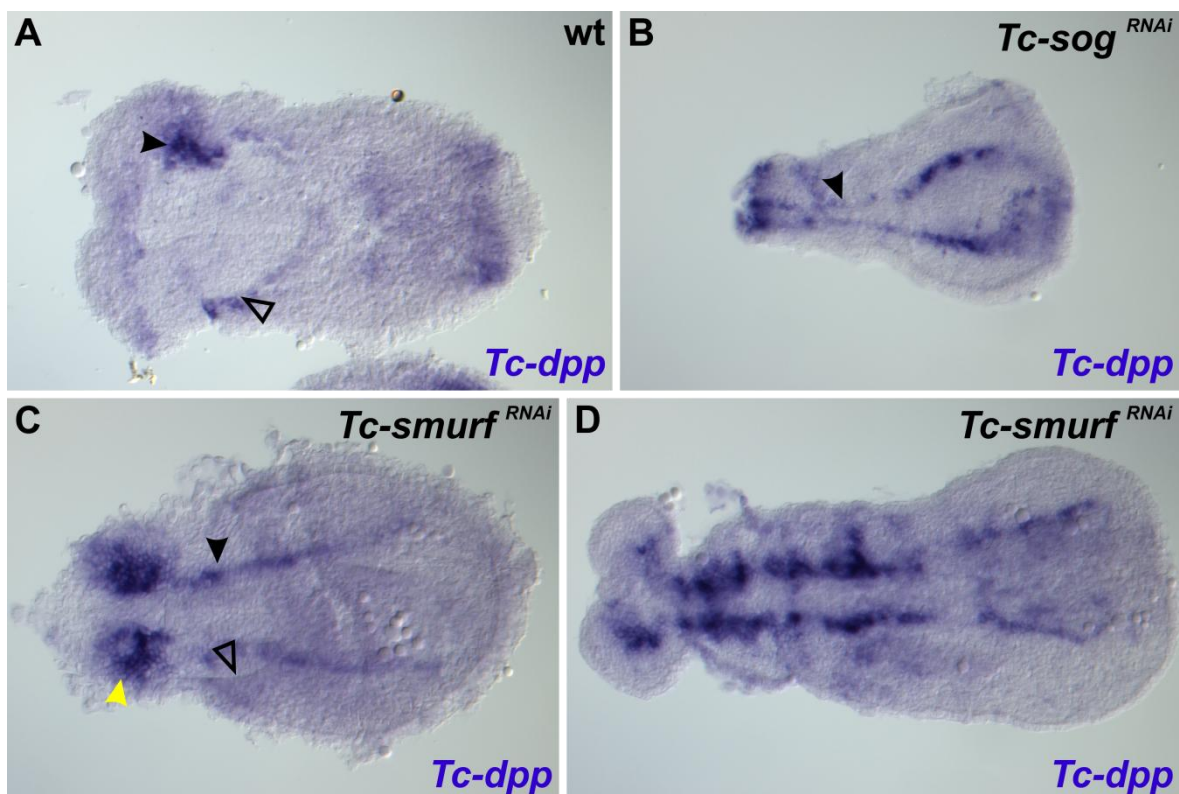


Figure 4-15 *Tc-dpp* expression in germ rudiment stages in wild type, *Tc-sog* and *Tc-smurf* RNAi embryos

Anterior to the left in all pictures. (A) During germ band stages, *Tc-dpp* is detected in the posterior of the embryo and in the amnion. A region of intense *Tc-dpp* expression is located in the anterior amnion (black arrowhead). In the depicted embryo the left anterior amnion was removed to show that *Tc-dpp* expression is not present in the embryo proper (open arrowhead points to the border of the amnion). (B) In *Tc-sog* RNAi embryos, *Tc-dpp* expression forms two ectopic stripes of *Tc-dpp* expression in the germ tissue (arrowhead). (C) In *Tc-smurf* RNAi embryos, a strong ectopic expression domain of *Tc-dpp* is present in the headlobes (yellow arrowhead), and two stripes of *Tc-dpp* expression are detected in the posterior region of the embryo (black arrowhead). The anterior of the germ rudiment stage embryo is not covered by amnion (open arrowhead points to amnion border). (D) The ectopic expression of *Tc-dpp* persists during onset of germ band elongation.

In wild type germ rudiments and early germ band stage embryos, pMAD was intensely detected in the amnion and in a very thin stripe at the dorsal margin, laterally in the embryo. During later germ band stages, pMAD localization in general resembled the expression of *Tc-dpp* (Figure 4-16 G+J). The amniotic localization of pMAD was also confirmed using confocal microscopy (Figure 4-17 A, B). In the embryonic germ band, pMAD was restricted to the dorsal margin (Figure 4-16 G, Figure 4-17 A, B). *Tc-sog* RNAi embryos also showed high levels of pMAD in the amnion directly after gastrulation. During germ band elongation, pMAD was present in two strong ectopic stripes along the ventral midline and also at the dorsal margin and in the amnion. However, pMAD was detectable at lower levels in the entire germ band tissue (Figure 4-16 H+K Figure 4-17 C+D). During early germ band stages, *Tc-smurf* RNAi embryos showed pMAD in the amnion and in high concentrations ectopically in the anterior (Figure 4-16 I). During later stages, pMAD domains in the dorsal margin, the amnion, and the developing limb buds could also be detected in *Tc-smurf* RNAi embryos. In the posterior of *Tc-smurf* RNAi embryos, pMAD was often restricted to the dorsal margin, although the borders of these domains looked frequently less clear and defined compared to the wild type situation. Most germ band stage embryos showed ectopic pMAD in the anterior (Figure 4-16 I+L, Figure 4-17 E+F). Some elongated germ band stage embryos showed absent heads but otherwise normal morphology, and a wild type pMAD pattern in the remaining tissue (not shown). In the pictures shown in Figure 4-16 H and Figure 4-17 E and F the embryos are headless. However, also many weaker or earlier phenotypes like the one in Figure 4-16 C with present, although reduced headlobes were observed which showed ectopic pMAD within the embryonic tissue of the headlobes.

In wild type embryos, the *Tc-dpp*-downstream gene *Tc-pannier* is expressed in the dorsal margin of the embryo and in the amnion (van der Zee et al., 2006) (Figure 4-16 M). In *Tc-sog* RNAi embryos, ectopic expression of *Tc-pnr* could be observed in two stripes in the midline, similar to the ectopic stripes seen for *Tc-dpp* and pMAD (van der Zee et al., 2006) (Figure 4-16 N). The expression pattern of *Tc-pnr* in *Tc-smurf* RNAi embryos also resembled the localization seen for pMAD in *Tc-smurf* RNAi embryos. In the posterior germ band, *Tc-pnr* was usually restricted to the dorsal margin, while it was detected ectopically almost in the entire embryonic tissue in the anterior (Figure 4-16 O). In summary, *Tc-smurf* knock down led to a stabilization of pMAD in blastoderm and germ band stage embryos. While the pMAD domains were only slightly altered during blastoderm stages, intense ectopic domains for pMAD as well as for *Tc-dpp* and *Tc-pnr* expression were found during germ band stages.

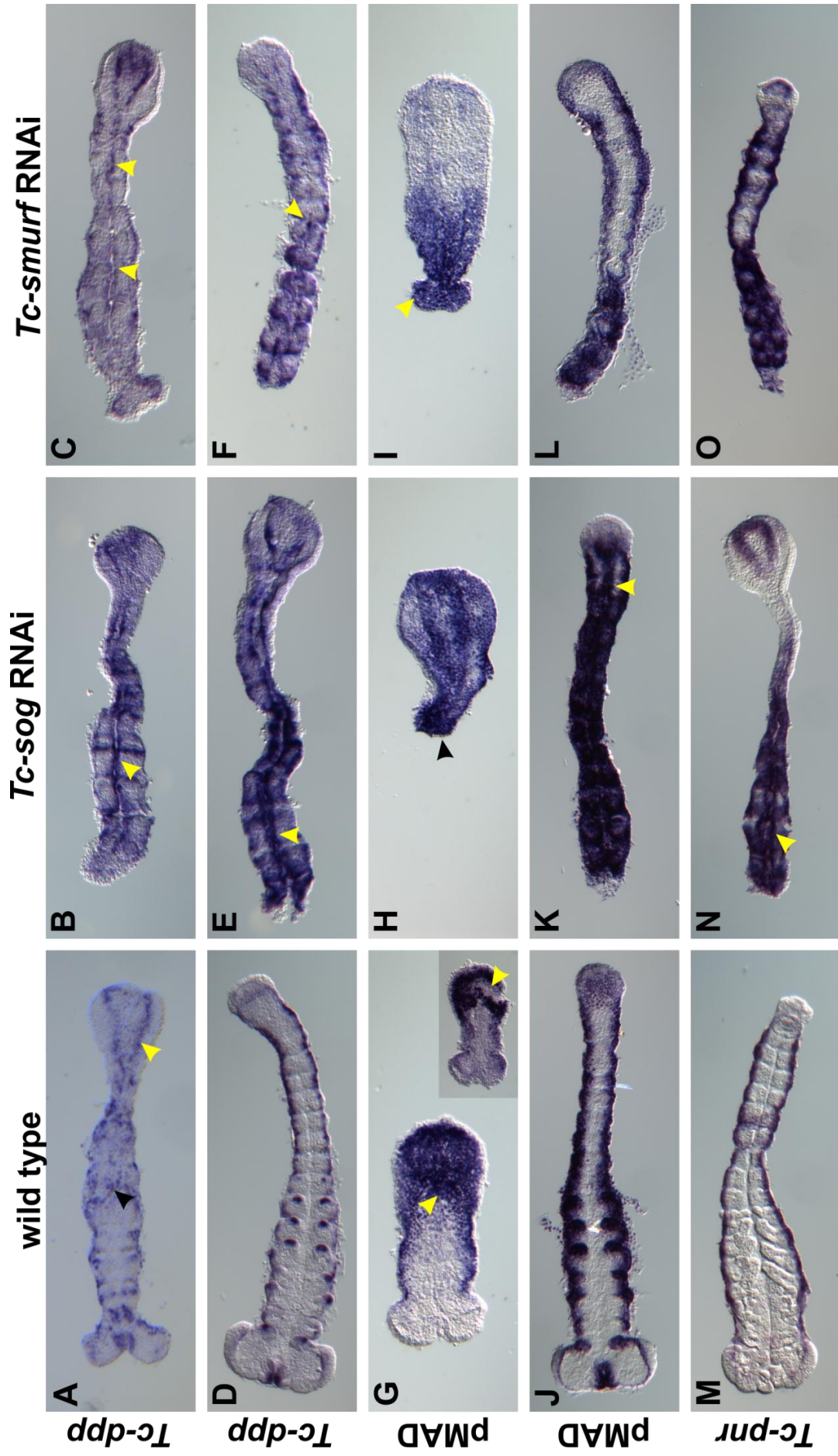


Figure 4-16 Dpp signaling components in wild type, *Tc-sog* and *Tc-smurf* RNAi embryos during germ band stages

Anterior to the left in all pictures. **(A)** In the wild type, *Tc-dpp* expression was found along the dorsal border, in two stripes in the growth zone (yellow arrowhead), and in amniotic cells during germ band elongation (black arrowhead). **(B)** *Tc-dpp* expression was detected in two ectopic rows in the midline after *Tc-sog* RNAi, as published previously (van der Zee et al., 2006) (yellow arrowhead in **B**). **(C)** In *Tc-smurf* RNAi embryos, *Tc-dpp* expression was found along the embryonic midline, continuous with the growth zone expression stripes. At the dorsal margin of these embryos, *Tc-dpp* expression was slightly reduced. **(D)** In wild type fully elongated germ band stage embryos, *Tc-dpp* was expressed along the dorsal ectoderm border and in the developing appendages including the labrum. Note that the amnion was for the most part removed in most of the embryos shown in this panel. **(E)** Ectopic expression of *Tc-dpp* in the midline persisted in *Tc-sog* RNAi embryos. **(F)** Spotty expression of *Tc-dpp* could be detected along the midline (yellow arrowhead) of *Tc-smurf* RNAi embryos. **(G)** In wild type early germ band stage embryos, pMAD was present in the posterior amnion (arrowhead) and in thin lateral stripes. The embryonic tissue below the stained amnion was free of pMAD as seen if the amnion is partially removed (inset). **(H)** *Tc-sog* RNAi embryos never developed a head (arrowhead). pMAD was present in the amnion. **(I)** High levels of pMAD were observed in the anterior of *Tc-smurf* RNAi embryos. In the embryo shown here, the amnion was probably entirely removed due to preparation. Amniotic localization of pMAD was usually detected after *Tc-smurf* RNAi (Figure 4-17 E). **(J)** pMAD localization in elongated germ band stage embryos in general correlated to *Tc-dpp* expression in the wild type, although the pMAD domains appeared broader and less constrained. **(K)** *Tc-sog* RNAi resulted in ectopic pMAD in two columns along the ventral midline (arrowhead). **(L)** the lateral dorsal margin localization of pMAD appeared a bit more fuzzy and wider in the posterior of *Tc-smurf* RNAi embryos, although the rest of the posterior abdomen looked morphologically wild type. pMAD was found ectopically all over the anterior tissue of the embryo. The germ band was narrowed in this region. The two ectopic stripes of midline pMAD localization as detected in *Tc-sog* RNAi (**K**, yellow arrowhead) were not detected. **(M)** *Tc-pannier* (*Tc-pnr*) expression in the dorsal ectodermal margin of a wild type retracting germ band stage embryo. **(N)** *Tc-pnr* was expressed in two ectopic stripes along the midline in *Tc-sog* RNAi embryos (yellow arrowhead) and at the dorsal margin. **(O)** *Tc-pnr* expression in *Tc-smurf* RNAi embryos correlated to the distribution of pMAD seen in **(L)**. The dorsal border of expression was less defined in the posterior, when compared to the wild type, and in the anterior of the embryo, *Tc-pnr* was found in ectopic domains.

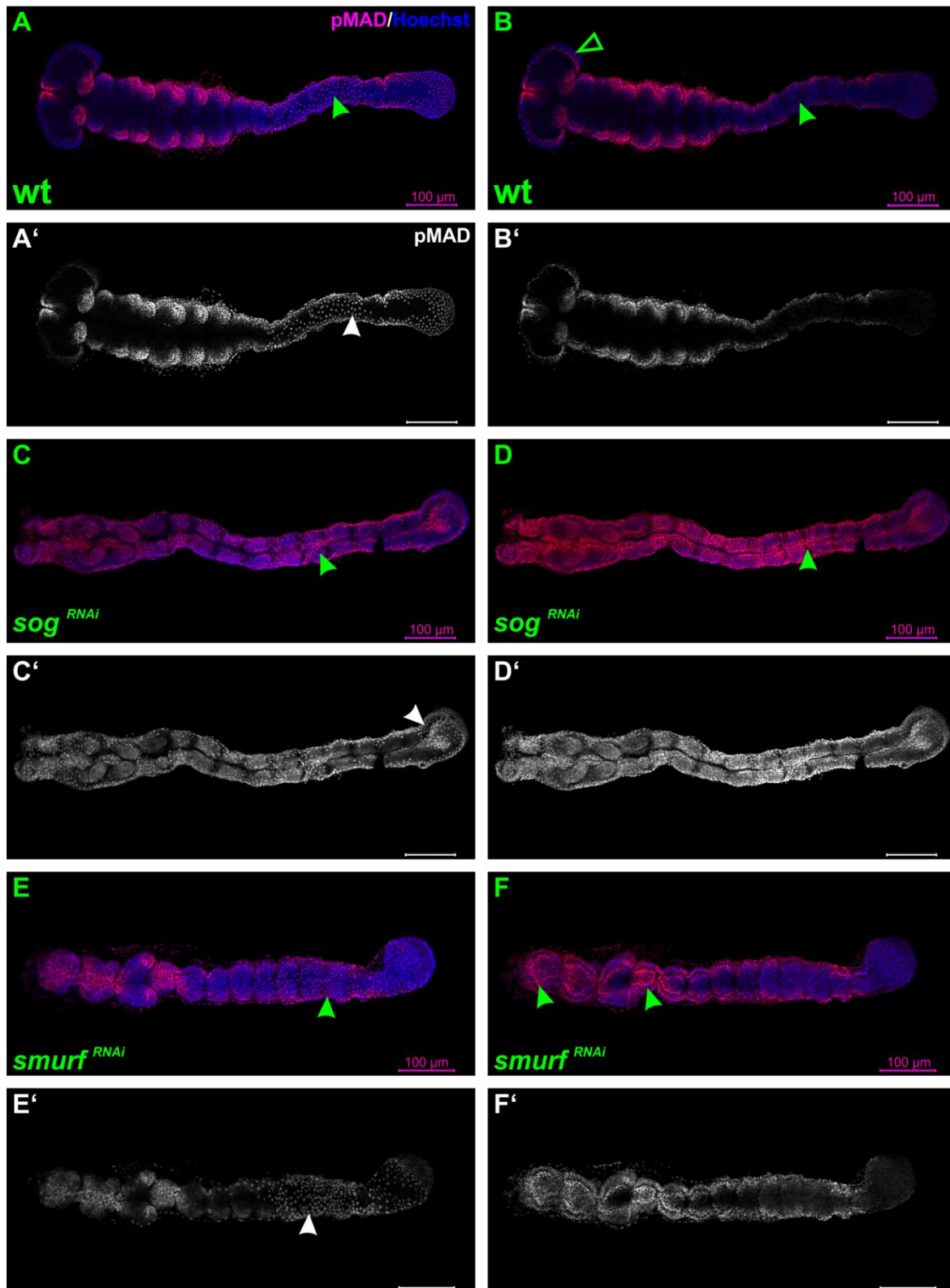


Figure 4-17 pMAD in wild type, *Tc-sog* and *Tc-smurf* RNAi, germ band stages

Immunohistochemical stainings of pMAD, every row shows the same embryo, left column more ventral focal plane than right column. Anterior to the left in all pictures. Black and white pictures show the pMAD staining from the picture atop without Hoechst 33342 counterstaining. (A+A') pMAD was detected at the dorsal margin of the embryo, the developing appendages and the amion (arrowheads points to pMAD positive amniotic nu-

clei). (**B+B'**) A very narrow stripe of cells stained for pMAD was present along the rim of the headlobes (open arrowhead). The inner tissue of the germ band was free of pMAD (arrowhead). (**C+C'**, **D+D'**) In *Tc-sog* RNAi embryos, pMAD was found in the amnion (arrowhead), but was also strongly present in the ventral midline (arrowhead in **D**). Lower levels of pMAD were observed all over the germ band. (**E+E'**) pMAD was also present in amniotic nuclei of *Tc-smurf* RNAi embryos (arrowhead). (**F+F'**) The posterior midline of the embryos was free of pMAD, but the dorsal margin domain appeared less constrained than in the wt (compare to **B**). In the anterior of the embryo, pMAD was detected ectopically in high levels all over the embryonic tissue (arrowheads in **F**).

Wild type and *Tc-smurf* RNAi embryos were stained for the expression of *Tc-sog*, to analyze whether some of the effects seen in *Tc-smurf* knock down embryos could be explained through loss of *Tc-sog* function. *Tc-sog* expression has been described before (van der Zee et al., 2006). During blastoderm stages, *Tc-sog* was expressed in a broad ventral domain highly overlapping with the presumptive mesoderm (not shown, see also van der Zee et al., 2006). After gastrulation, *Tc-sog* expression is present in two longitudinal stripes along the anterior-posterior axis in the ventral ectoderm, leaving the segmental mesoderm free of *Tc-sog* expression. *Tc-sog* expression was also detected in a circular domain in every headlobe and broadly in the growth zone, where it could also be detected in the mesoderm (Figure 4-18 A, see also van der Zee et al., 2006). In *Tc-smurf* RNAi embryos, growth zone expression of *Tc-sog* was still intensely detected. Expression in the germ band was located in the midline and faded towards anterior. Expression in the head was usually not detectable (Figure 4-18 B). This indicated, that loss of *Tc-smurf* function led to an inhibition of *Tc-sog* in the anterior of the animal but not in the posterior germ band and the growth zone.

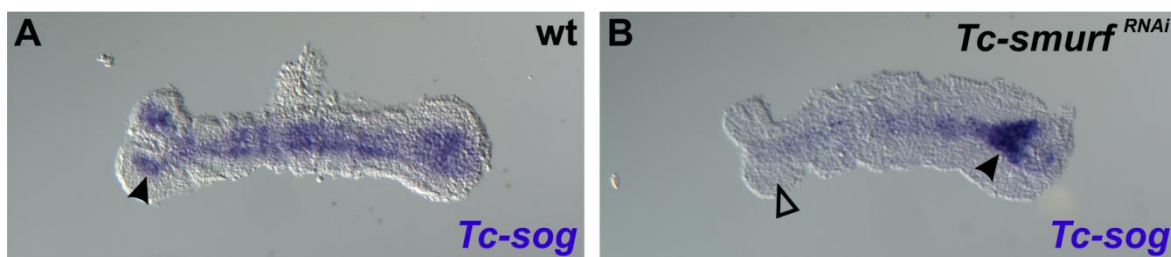


Figure 4-18 *Tc-sog* expression in wild type and *Tc-smurf* RNAi embryos

Anterior to the left. (**A**) In wt germ band stage embryos, *Tc-sog* was expressed in two longitudinal anterior-posterior stripes, a broad domain in the growth zone, and in a circular domain in every headlobe (arrowhead). (**B**) Expression in the growth zone appeared unaffected in *Tc-smurf* RNAi embryos (black arrowhead). Towards anterior, *Tc-sog* expression faded and was eventually completely gone (open arrowhead).

4.3.4 Expression of marker genes in *Tc-smurf* RNAi

To better understand to what extent cell fate and early pattern formation was altered in *Tc-smurf* RNAi embryos, *in situ* hybridization staining for early expressed genes was done in embryos of different stage of development. Differentiated blastoderm stage embryos were stained for expression of the genes *Tc-millepattes* (*Tc-mlpt*), *Tc-wingless* (*Tc-wg*) and *Tc-zerknüllt1* (*Tc-zen1*) (Falciani et al., 1996; Nagy and Carroll, 1994; Savard et al., 2006; van der Zee et al., 2005). *Tc-mlpt* is expressed in two domains during early development. A posterior domain marking the primitive pit, and a more anterior, wedge-shaped domain in the area of the developing head lobes (Savard et al., 2006) (Figure 4-19). A double staining in blastoderm stage embryos was done for the expression of the serosa marker *Tc-zen1* and for *Tc-wg*. Both genes are expressed in spatially different regions and can therefore be used simultaneously in an NBT/BCIP staining. *Tc-zen1* is expressed anteriorly and exclusively in the serosa, allowing easy identification of the germ serosa boundary (Falciani et al., 1996; van der Zee et al., 2005) (Figure 4-19 D, E, F). *Tc-wg* is expressed in two domains during differentiated blastoderm stages: In the primitive pit and in an anterior domain marking the ocular region of the developing head (Nagy and Carroll, 1994) (Figure 4-19 D).

In the completely dorsalized embryos caused by knock down of *Tc-sog*, the anterior *Tc-mlpt* domain formed a thin, almost radial symmetrical circle, and expression was detected up to the dorsal most regions of the embryo (Figure 4-19 B). Expression of *Tc-zen1* in *Tc-sog* RNAi embryos protruded posteriorly at the ventral side of the embryo compared to the wild type situation, resulting in loss of dorsal-ventral expression asymmetry. The anterior (ocular) *Tc-wg* domain was lost whereas the posterior expression could still be detected (Figure 4-19 E; van der Zee et al., 2006).

The effect of *Tc-smurf* knock down differed from the *Tc-sog* phenotype. The anterior *Tc-mlpt* expression was still wedge-shaped and restricted from the dorsal most cells of the embryo, but it was reduced in the anterior region of the germ rudiment, indicating missing prospective head tissue (Figure 4-19 C) which was also supported by analysis of concomitant nuclei staining (Figure 4-19 C'). Double staining for *Tc-zen1* and *Tc-wg* supported this observation. The anterior *Tc-wg* domain was lost, although the posterior domain was clearly detectable, which indicated that *Tc-smurf* was not in general necessary for *Tc-wg* expression during

blastoderm stages. The oblique border of *Tc-zen1* expression seen in lateral views in wild type embryos at the differentiated blastoderm stage was usually also observed in *Tc-smurf* RNAi embryos, albeit slight differences in the angle of this border could not be excluded (Figure 4-19 F). One regular observation was a bend at the posterior border of the *Tc-zen1* expression in *Tc-smurf* RNAi embryos (marked by arrowheads in Figure 4-19 F and F') which was never detected to such an extent in the wild type. This indicated potentially missing embryonic tissue in favour of serosa cells. Missing prospective head tissue was also indicated by the loss of the anterior *Tc-wg* expression domain observed in *Tc-smurf* RNAi embryos.

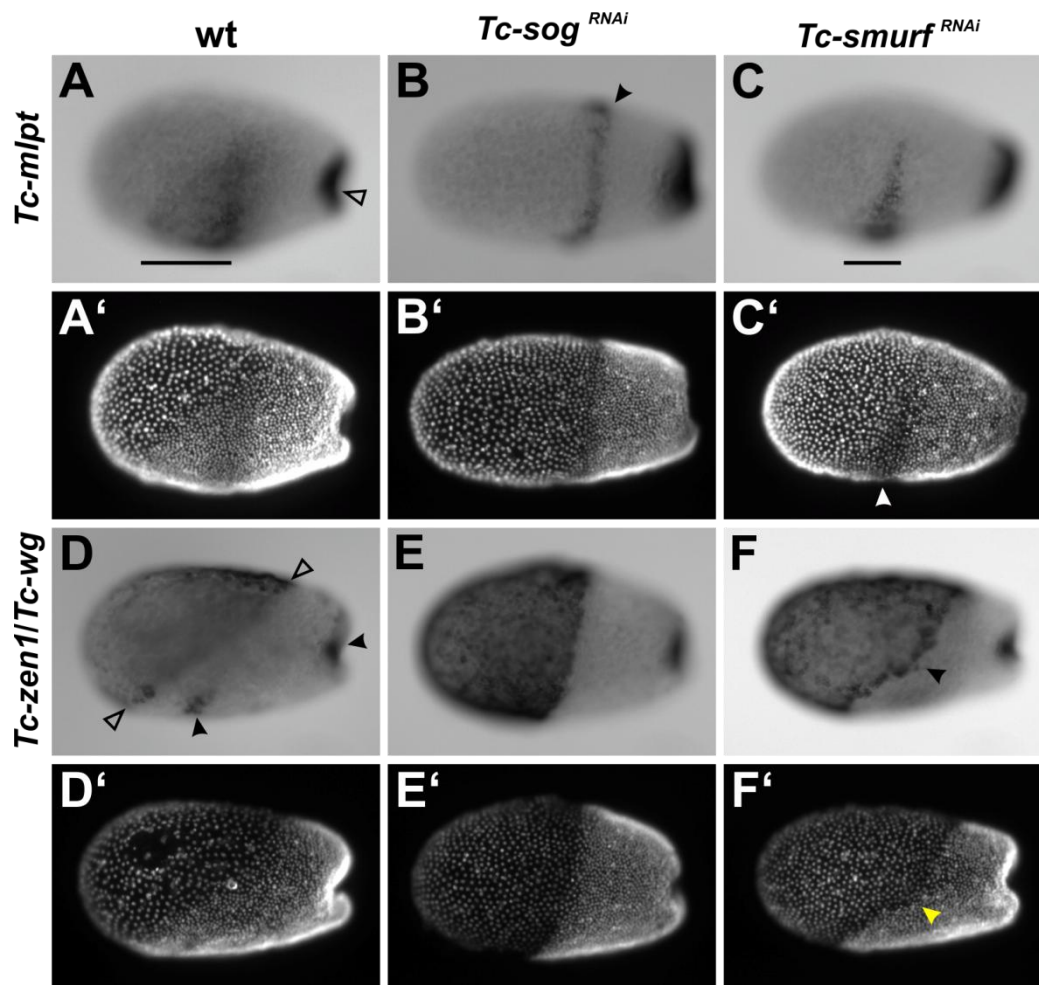


Figure 4-19 Expression of *Tc-mlpt*, *Tc-zen1*, and *Tc-wg* during differentiated blastoderm stages in wild type, *Tc-sog* RNAi, and *Tc-smurf* RNAi embryos

Anterior to the left and dorsal side up for all pictures. A'–F' show embryos in A–F stained for nuclei with Hoechst 33342. (A) *Tc-mlpt* expression was detected in a posterior (open arrowhead) and an anterior domain marking the prospective head (horizontal stripe marks the length of the domain on the ventral side). (B) Anterior domain of *Tc-mlpt* was thinner and ranged to the dorsal most part of the embryo in *Tc-sog* RNAi embryos. (C) The anterior *Tc-mlpt* domain was shortened anteriorly in *Tc-smurf* RNAi embryos (indicated by black bar). Loss of embryonic tissue could also be observed in Hoechst stainings (white arrow in C' points to germ serosa boundary, compare to A'). (D) *Tc-zen1* was restricted to the serosa and reached dorsally more posterior than

Results

ventrally, forming an oblique border of expression (open arrowheads point to the posterior *Tc-zen1* expression border). *Tc-wg* expression was detected in the primitive pit and in an anterior domain marking the ocular segment (black arrowheads). (E) In *Tc-sog* RNAi embryos the posterior *Tc-zen1* border was straightened and the anterior *Tc-wg* domain was lost. (F) In *Tc-smurf* RNAi embryos the anterior *Tc-wg* domain was lost, but the oblique border of the *Tc-zen1* expression was still present. A bend in this border could be detected in several embryos analyzed (black arrowhead in F and yellow arrowhead in F').

Germ band stage embryos were analyzed for changes in neuroectodermal and mesodermal fate by staining for the expression of the proneural gene *Tc-achaete-scute* (*Tc-ash*) (Wheeler et al., 2003) and the mesodermal marker *Tc-twist* (Chen et al., 2000; Handel et al., 2005; Sommer and Tautz, 1994). To facilitate staging and segment identification, the embryos were at the same time stained for the expression of the segment polarity gene *Tc-wg* (Nagy and Carroll, 1994). *Tc-ash* is expressed in the central nervous system (CNS) neural precursors and in an ectodermal stripe outside the nervous system in the anterior of every segment (Wheeler et al., 2003) (Figure 4-20 A). *Tc-twist* is expressed ventrally during blastoderm stages (not shown) and in mesodermal patches along the anterior-posterior axis during germ band stages (Sommer and Tautz, 1994) (Figure 4-20 G).

In *Tc-sog* RNAi embryos, CNS expression of *Tc-ash* during germ band stages was lost and only the transverse stripe in the anterior of the segments remained (Figure 4-20 C). *Tc-twist* expression was still detected in segmental patches along the midline of the embryo, indicating that mesoderm formation during germ band elongation was not fundamentally affected (see also van der Zee et al., 2006) (Figure 4-20 I). Segmental expression of *Tc-wg* was often partially missing in *Tc-sog* RNAi embryos (Figure 4-20 D, J).

In the posterior region of germ band-stage *Tc-smurf* RNAi embryos, the CNS as well as the anterior ectodermal stripe expression of *Tc-ash* was still present. In the anterior of the embryos the pattern continuity was often disrupted and CNS, but often also ectodermal stripe expression was lost (Figure 4-20, E). Additionally, *Tc-wg* expression was often absent from some of the anterior segments (Figure 4-20, F, L). Expression of *Tc-twist* was not noticeably affected in *Tc-smurf* RNAi embryos (Figure 4-20 K).

These results indicated that *Tc-smurf* is not or very weakly involved in specification of neurogenic or mesodermal fate in the posterior of the *Tribolium* embryo during germ band elongation. However, *Tc-smurf* seems to be essential for ante-

rior patterning during blastoderm stages and for the retention of anterior segments during germ band elongation.

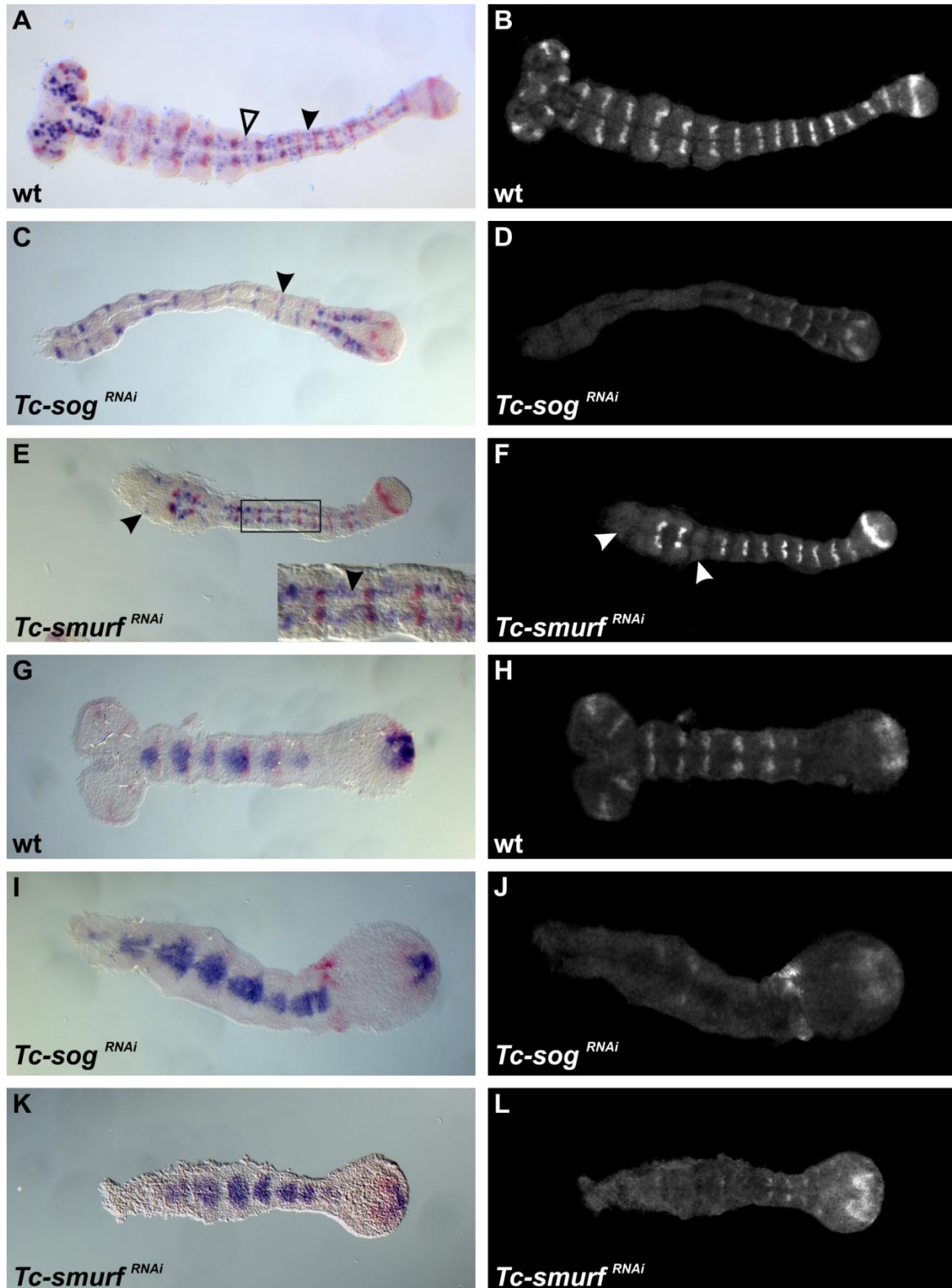


Figure 4-20 Expression of *Tc-ash* and *Tc-twist* in wild type, *Tc-sog* and *Tc-smurf* RNAi embryos during germ band stages

Anterior to the left in all images. A, C, and E show *Tc-ash* *in situ* hybridization staining with NBT/BCIP in blue, G, I, K show *Tc-twist* *in situ* hybridization staining with NBT/BCIP in blue. *Tc-wg* expression stained with Vec-

tor® Red in left column in red, in right column visualized by fluorescence. (A) *Tc-ash* was detected in the neural precursors (open arrowhead) and in an ectodermal stripe outside the nervous system in the anterior of every segment (black arrowhead). (B) *Tc-wg* was expressed in a segmental pattern. (C) CNS expression of *Tc-ash* was lost in *Tc-sog* RNAi embryos, only the segmental ectodermal stripe could be detected (arrowhead), anterior *Tc-wg*-stripes were often missing (D, also seen in J). (E) Posterior *Tc-ash* expression was not altered in *Tc-smurf* RNAi embryos as indicated by CNS expression (arrowhead in inset). Anterior *Tc-ash* expression was often lost, except for a few remaining *Tc-ash* expressing cells (arrowhead). (F+L) *Tc-wg* expression was often lost in anterior segments of *Tc-smurf* RNAi embryos (arrowheads). (G) *Tc-twist* (in blue) was expressed in mesodermal patches along the anterior-posterior axis of the embryo. (H) Segmental expression of *Tc-wg* in the embryo shown in G. (I, K) *Tc-twist* expression was not severely affected, neither by *Tc-sog* RNAi (I) nor by *Tc-smurf* RNAi (K).

4.3.5 Live imaging of *Tc-smurf* RNAi embryos

In situ hybridisation stainings for marker gene expression, immunohistochemistry, and the TUNEL assay provided a good insight about the *Tc-smurf* RNAi phenotype and the function of *Tc-smurf* during development. Nevertheless, *Tc-smurf* phenotypes appeared to be quite manifold. In addition, differentiated blastoderm stages of *Tribolium* embryos were very dynamic, with a high level of cell movements which continuously changed the shape of the embryo and made absolutely exact stage-matching challenging. To get a better impression about what exactly happened during embryogenesis, the development of *Tc-smurf* RNAi embryos was monitored over a period of time by doing live imaging experiments. The experiments were done using a transgenic line that expresses nuclear localized GFP in all embryonic cells (Sarrazin et al., 2012). The experimental setup allowed simultaneous imaging of several (up to 60) embryos. Not all embryos could be scored for every phenotype, for instance due to an unsuitable orientation or lethality before a phenotypic aspect became apparent. I will therefore always specify the amount of embryos showing a specific aspect in relation to all embryos that were scorable for the respective aspect. Injection of dsRNA against *DsRed* served as negative control, RNAi against *Tc-sog* served as positive control.

Figure 4-21 shows exemplary frames for the development of a control embryo (the complete movie can be found on the DVD, folder *Movies/Control*, file *wt_131204a02_07_R3D.dv.tif*). The reference time point used in all movies started with the flattening of the posterior pole, which happens directly before differentiated blastoderm formation (Kristen Panfilio, Köln, personal communication). The posterior flattening is followed by amniotic fold formation and concomitant gastru-

lation, the enveloping of the embryo by extraembryonic membranes and subsequent germ band formation. Posterior flattening served therefore as a developmental landmark for the live imaging analyses. Many aspects of *Tribolium* embryogenesis have previously been described using scanning electron microscopy and live imaging approaches (Benton and Pavlopoulos, 2014; Benton et al., 2013; Handel et al., 2000; Kittelmann, 2012). I will therefore stick to differences that could be detected between the development of *Tc-smurf* RNAi embryos, control embryos, and *Tc-sog* RNAi embryos.

During live imaging experiments a high number of *Tc-smurf* RNAi embryos (43 out of 83 imaged embryos) died before building a proper and organized blastoderm. At the beginning of the experiment these embryos usually showed a fluorescent cluster within the yolk, representing nuclei. Later during development nuclei were also found on the surface. Although this indicated that the nuclei underwent division cycles and also moved, these embryos never developed to a proper blastoderm stage and never formed a condensed germ rudiment (Figure 4-22, the movie can be found on the DVD, folder *Movies/smurfRNAi*, file *smurf_early_lethal_131204a02_23_R3D.dv.tif*). In the negative control only 2 out of 66 embryos showed this kind of early defect during development. This phenotype was clearly distinguishable from technical lethality for instance due to desiccation.

Figure 4-23 shows exemplary frames from a movie of a *Tc-smurf* RNAi embryo which developed to the germ band stage (the movie can be found on the DVD, folder *Movies/smurfRNAi*, file *smurf_301113a04_11_R3D.dv.tif*). The *Tc-smurf* RNAi embryo did not develop a clear germ-serosa border and the entire blastoderm looked less properly organized compared to the control (see frames for 40–120 minutes in Figure 4-21 and Figure 4-23). Formation of the amniotic fold happened at a comparable time point in the *Tc-smurf* RNAi and negative control embryo (about 160 minutes after posterior flattening in Figure 4-21 and Figure 4-23). In the control the amniotic fold moved anteriorly covering the embryo and taking the serosa with it (control Figure 4-21, 240–360 minutes), resulting in an embryo covered by two extraembryonic membranes. The movement of the amniotic fold and coverage of the germ rudiment was a quick process (240–280 minutes after posterior flattening in the control). Coverage of the embryo with the extraembryonic membranes was followed by a forward movement of the head

which happened quite suddenly (compare frames 280 and 360 minutes in Figure 4-21). In the *Tc-smurf* RNAi embryo the amniotic fold did not succeed in forward movement. 360 minutes after posterior flattening the fold itself could still be seen. Hence *Tc-smurf* RNAi embryos showed a delay in this process. Defects in embryo enveloping and gastrulation were detected in 16 out of 23 *Tc-smurf* RNAi embryos which could be analyzed for this phenotype (DsRed RNAi: 4 out of 41). Morphologically identifiable headlobes were first observed 160–200 minutes after posterior flattening in the control embryo. In the *Tc-smurf* RNAi embryo, headlobes could be observed about 240–280 minutes after posterior flattening. The headlobes of *Tc-smurf* RNAi embryos were strongly reduced in size compared to the control (Figure 4-23, 240–360 min frames), indicating that a smaller amount of cells was involved in forming the head. This kind of small head phenotype was detected in 15 out of 19 *Tc-smurf* RNAi embryos that could be scored for this phenotype (DsRed RNAi: 1 out of 49). Furthermore the head in the *Tc-smurf* RNAi embryo never moved forward (240–360 minutes frames in Figure 4-23). Instead, the anterior tissue of the *Tc-smurf* RNAi embryo started decaying, indicated by a loss of fluorescence (starting about 720 minutes after posterior flattening). The region of this cell death is indicated by a yellow bar in the frames 760–940 minutes (Figure 4-23). This anterior cell death was detected in 15 out of 20 analyzable embryos and was never seen in the control (n=46). The observed cell death in *Tc-smurf* RNAi embryos was in accordance with the observations for the TUNEL assay (4.3.2).

Figure 4-24 shows exemplary frames for the development of a *Tc-sog* RNAi embryo (the movie can be found on the DVD, folder *Movies/sogRNAi*, file *sog_031213a02_51.tif*). *Tc-sog* RNAi embryos formed a properly organized differentiated blastoderm with a clear germ serosa border (Figure 4-24, 80 minutes frame). In contrast to the *Tc-smurf* knock down embryos, *Tc-sog* RNAi embryos never formed a head (Figure 4-24, frames 160–280 minutes). The amount of tissue in the anterior of *Tc-sog* RNAi embryos which seemed to be dying during later germ band stages was small if detectable at all (indicated by a yellow arrowhead in the frames 960 and 1080 minutes after posterior flattening in Figure 4-24). The *Tc-sog* phenotype is comprehensively explained in van der Zee et al. (2006).

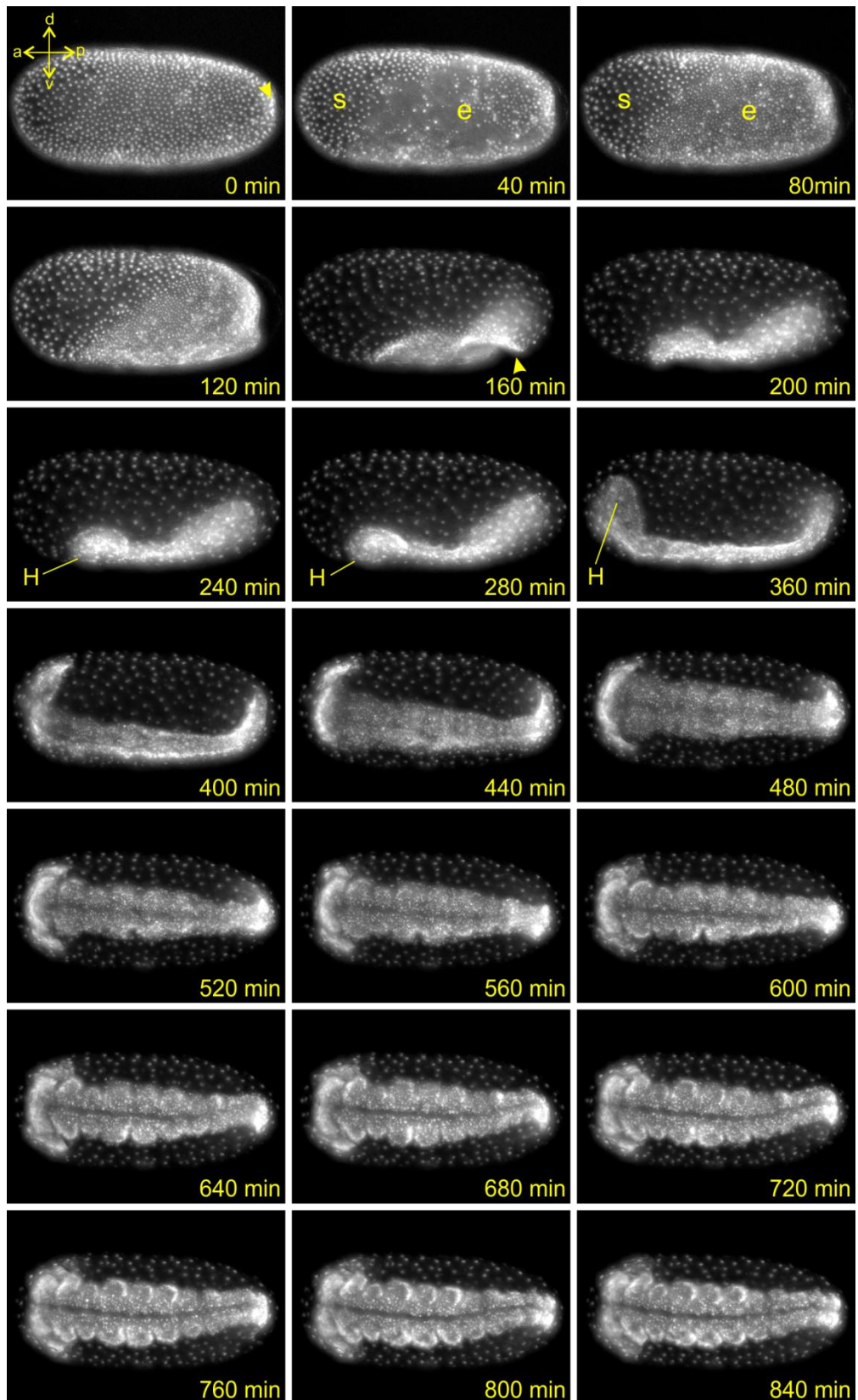


Figure 4-21 *In vivo* imaging of *Tc-DsRed* RNAi embryo (negative control)

Pictures are timed with respect to the time after flattening of the posterior pole (location of the prospective primitive pit) became firstly visible (arrowhead in upper left picture). Anterior to the left and dorsal side up. After rotation of the embryo the pictures give a ventral view. Embryonic and serosa nuclei could be distin-

Results

guished about 40 minutes after posterior flattening. The amniotic fold formed after about 160 minutes (arrowhead) and quickly pulled over the entire embryonic tissue, enveloping the embryo with two extraembryonic membranes. The serosa window closure could not be clearly identified in these movies due to lack of optical resolution. Another landmark of *Tribolium* development is forward movement of the head (H), which took place between 280 and 360 minutes after posterior flattening. Germ band elongation progressed and the embryo underwent a 90° rotation (280–480 min). Limb buds became visible about 560 minutes after posterior flattening.

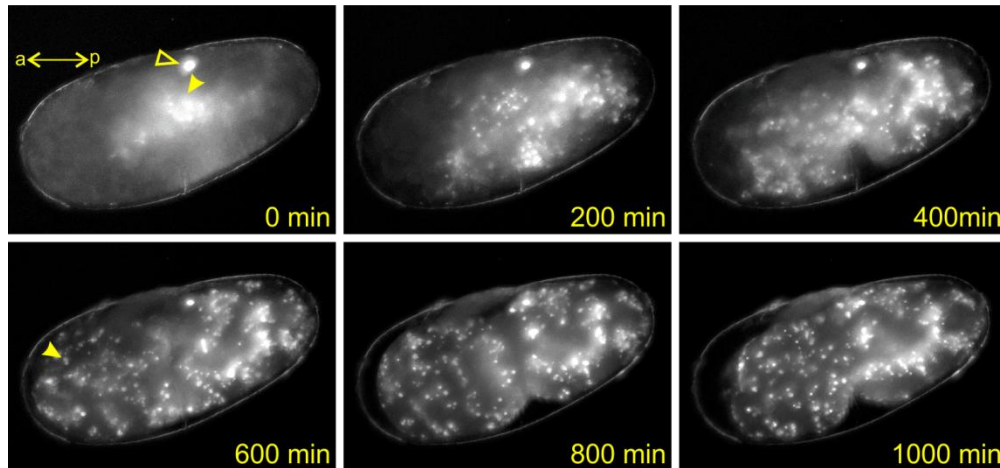


Figure 4-22 Live imaging of early embryonic death of *Tc-smurf* RNAi embryo

The embryo shown was about 8-10 h of age at the timepoint of the 0 min frame. The first frame could not be precisely timed due to the lack of morphological landmarks, and timing is hence not analogous to the timing used in Figure 4-21. The open arrowhead in the 0 min frame points to a highly fluorescent artifact probably on the surface of the embryo. This artifact is also visible in the other frames. At the beginning of imaging, a cluster of fluorescence could be detected deep within the yolk (arrowhead). 200 minutes later the nuclei have scattered further within the yolk and were eventually distributed among the egg. Some nuclei also reached the surface (600 minutes, arrowhead points to a surface nucleus). The nuclei were moving continuously within the egg, but a proper blastoderm or germ rudiment never formed (600–1000 minutes).

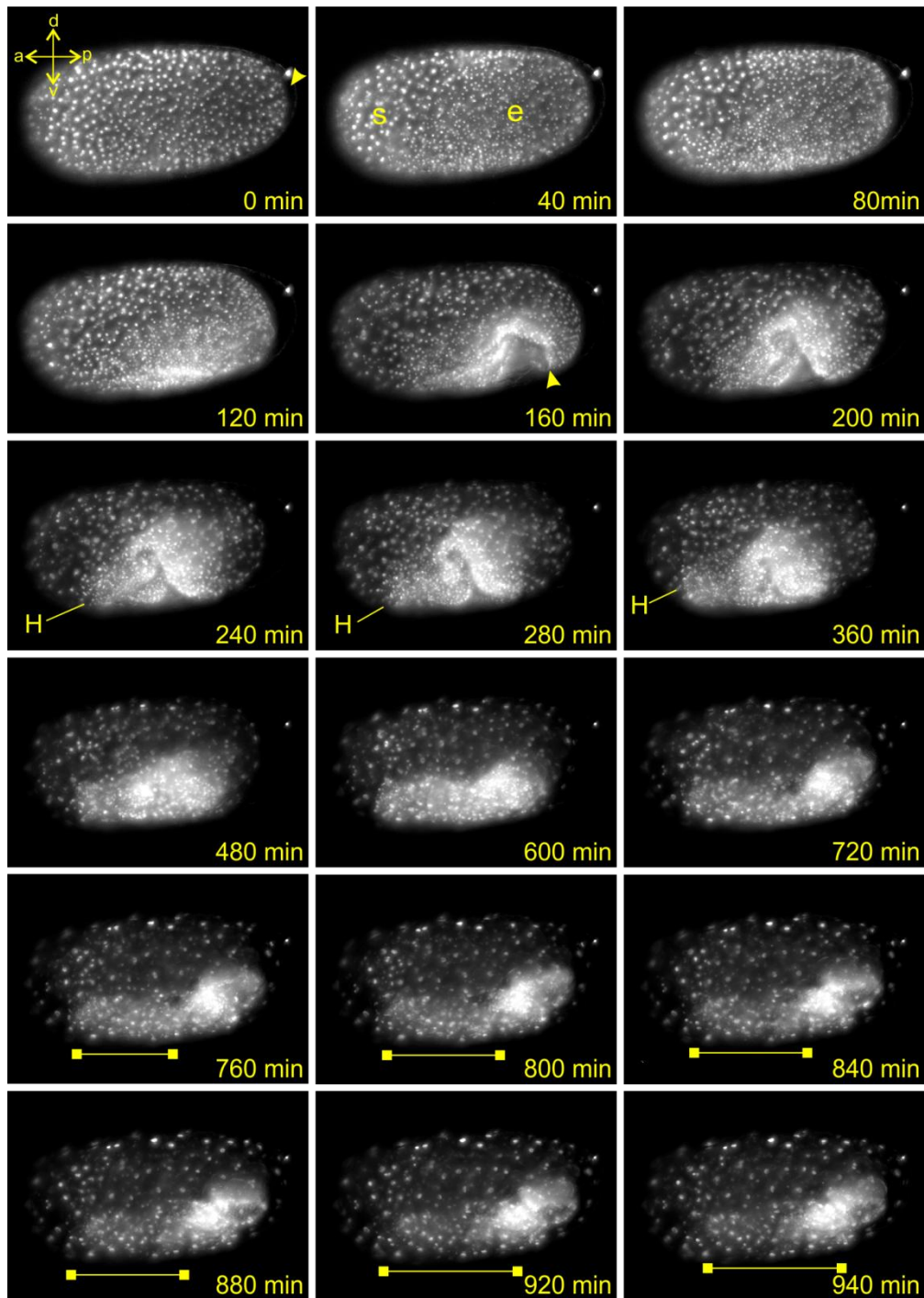


Figure 4-23 *In vivo* imaging of *Tc-smurf* RNAi embryo

Pictures are timed with respect to the time after flattening of the posterior pole (location of the prospective primitive pit) became firstly visible (arrowhead in upper left picture). During the next cell division cycle, serosa (s) and embryonic (e) cells became distinguishable due to the different size and spacing of the nuclei (40 min). This border was more indistinct compared to the control (compare pictures 80 and 120 minutes to Figure 4-21). The very broad amniotic fold (arrowhead in 160 min) persisted for an extended time period and did not succeed to cover the embryo (160–480 minutes). The headlobes (H) were strongly reduced in size. After about 720 minutes, the anterior embryonic tissue started to die, indicated by loss of fluorescence within the germ band (yellow bar in frames 760–940 min).

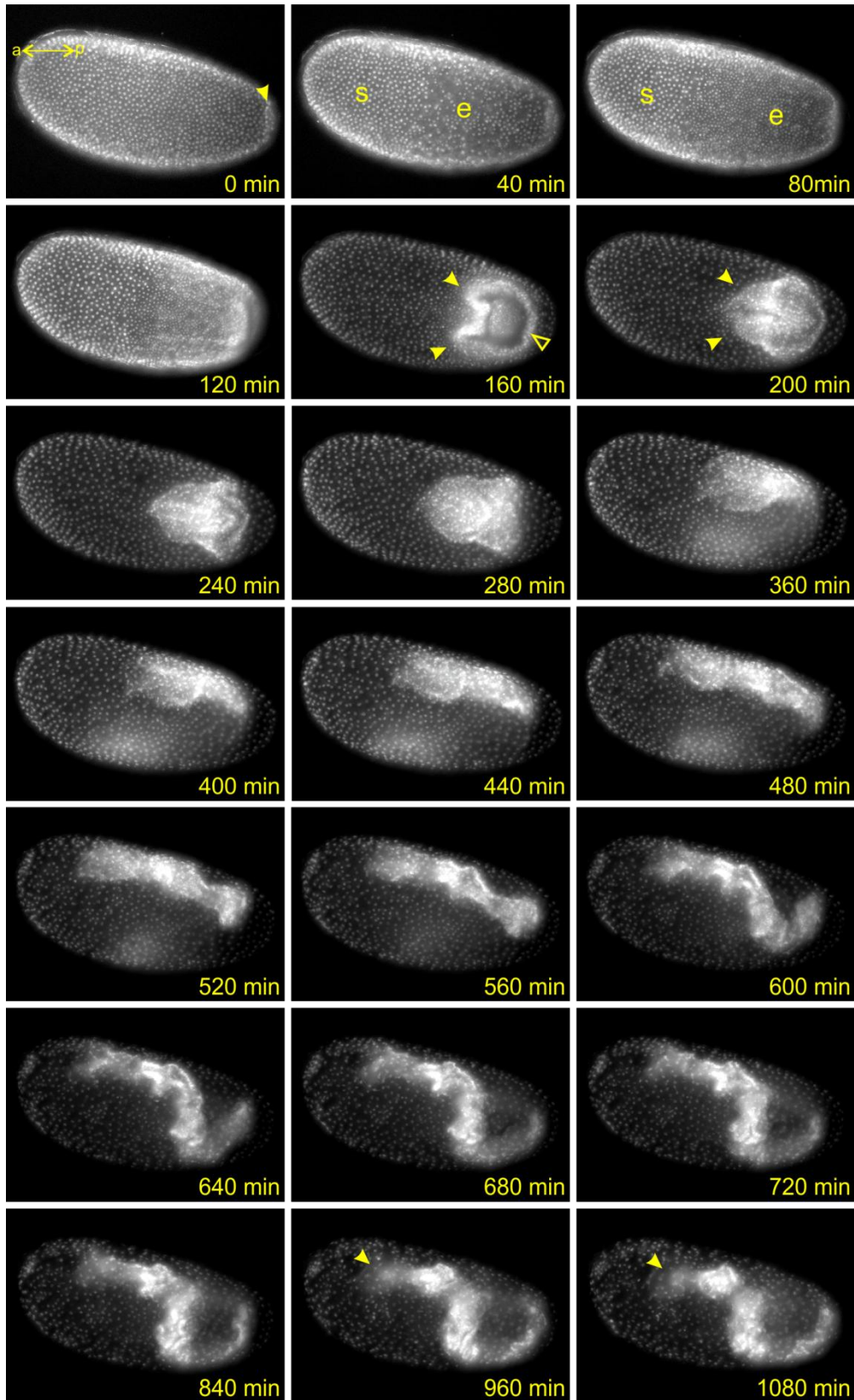


Figure 4-24 *In vivo* imaging of *Tc-sog* RNAi embryo

Pictures are timed with respect to the time after flattening of the posterior pole (location of the prospective primitive pit) became firstly visible (arrowhead in upper left picture). Pictures are ventral view, anterior to the left. Embryonic (e) and serosal (s) tissue could be distinguished after about 40 minutes. No headlobes were

formed (arrowheads in frames 160 and 200 min, compare to control, Figure 4-21). The amniotic fold formed properly (160 min, open arrowhead), and quickly covered the embryo (200–240 min), which then detached from the serosa and started rotating (280–360 min). The posterior of the embryo elongated into the yolk, forming a tube-like structure (440–1080 min). The anterior of this embryo never reached the anterior pole of the egg. The germ band was narrower than in the control (compare to Figure 4-21). A small area with disappearing cells could be seen in the anterior (arrowhead in frames 960 and 1080 min) indicating cell death.

4.4 Identification, isolation and characterization of *iB_03735* as *Tribolium TC004374*

BLAST analysis with the translated nucleotide sequence of the *iB_03735* iBeetle fragment against non-redundant protein sequences of *Drosophila melanogaster* (blastx) using the online BLAST function of the National Center for Biotechnology information (NCBI) (available at <http://blast.ncbi.nlm.nih.gov/Blast.cgi>) identified a predicted protein coding gene with the name *similar to 7,8-dihydro-8-oxoguanine-triphosphatase, putative isoform 1*, also called *TC004374*. The closest fly homolog was *CG10898*, FlyBase ID: *FBgn0037911*. BLAST search with the amino acid (AA) sequence of *CG10898* against non-redundant protein sequences of *Tribolium castaneum* (blastp) confirmed the homology. The two closest hits after *TC004374* (Score 382; Identity 54 %) were the hypothetical *Tribolium* proteins *TC006500* (Score 51,6; Identity 40 %) and *TC005943* (Score 33,9; Identity 30 %). Backblast with the putatively full AA sequence of *TC004374* (based on the AUGUSTUS gene model *g488.t1*) against non-redundant protein sequences of *Drosophila melanogaster* again identified *CG10898* (Score 382; Identity 54 %) as closest fly homolog, followed by *CG8128* (Score 45,8; Identity 32 %) and decapping protein 2 (*CG6169*, Score 40,8 %, Identity 34 %).

The gene was cloned using gene specific primers (JSP148 and JSP149) and the putatively full coding sequence (CDS) was isolated. The CDS of *TC004374* has a length of 1014 bp consisting of 4 exons and encoding a 337 AA protein. The AUGUSTUS gene model identified three potential transcripts of different length (*g488.t1*, *g488.t2* and *g488.t3*) for this gene. The four protein coding exons are separated by three introns, two of them short with a length of 45 and 48 bp, respectively. The intron in the middle position has a length of 2238 bp and contains another gene (*g489.t1*) on the complementary strand identified as being homologous to *Cyclin J* in *Drosophila*. Protein domain analysis using PROSITE (SIB,

Swiss Institute of Bioinformatics) identified a NUDIX hydrolase domain at AA positions 57–185 including a so-called NUDIX box motif at AA positions 92–113 (Figure 4-25). Supported by sequence homology and the NUDIX domain this gene belongs to the Nudix (**n**ucleoside **d**iphosphate linked to another moiety, **X**) superfamily of proteins, which is common in eukaryotes, bacteria, archaea and viruses and consists mainly of pyrophosphohydrolases. The substrates of these hydrolases can be quite diverse and the number of Nudix genes encoded by the genome differs highly between species (Bessman et al., 1996; McLennan, 2005). According to a blastx search against non-redundant protein sequences of human and mouse, the gene product of *TC004374* showed highest similarity to the mammalian NUDT18 protein (name of human ortholog is 8-oxo-dGDP phosphatase, accession number NP_079091). Backblast using blastp with the AA sequence of human NUDT18 confirmed this result and identified *TC004374* as first hit (Score 150; Identity 36 %), followed by *TC006500* (Score 46,6; Identity 38 %) and *TC005943* (Score 38,9; Identity 43 %). An analogous approach for *Drosophila* identified *CG10898* as closest homolog (Score 161; Identity 41 %), followed by *CG8128* (Score 50,1; Identity 40 %) and *CG4098* (Score 32; Identity 39 %).

Homology of *TC004374* to *Drosophila* *CG10898* and vertebrate NUDT18 was also supported by a phylogenetic analysis using a high number of Nudix proteins from diverse species (see 3.3 for details on tree construction and Figure 4-26). Referring to FlyBase no functional data for the fly ortholog of *TC004374*, *CG10898*, is available to date.

5'RACE PCR was performed to isolate the short g488.t3 transcript using a gene specific primer designed to bind to the 3' end of Exon 2 of the g488.t3 transcript. Several short PCR fragments were isolated and sequenced, however, none of them represented the g488.t3 annotation since all sequences contained nucleotide reads from Exon2 of the g488.t1 annotation. This leaves it unclear, whether this transcript was present during embryonic stages. In the following the name *TC004374* always refers to the large transcript g488.t1 if not mentioned otherwise.

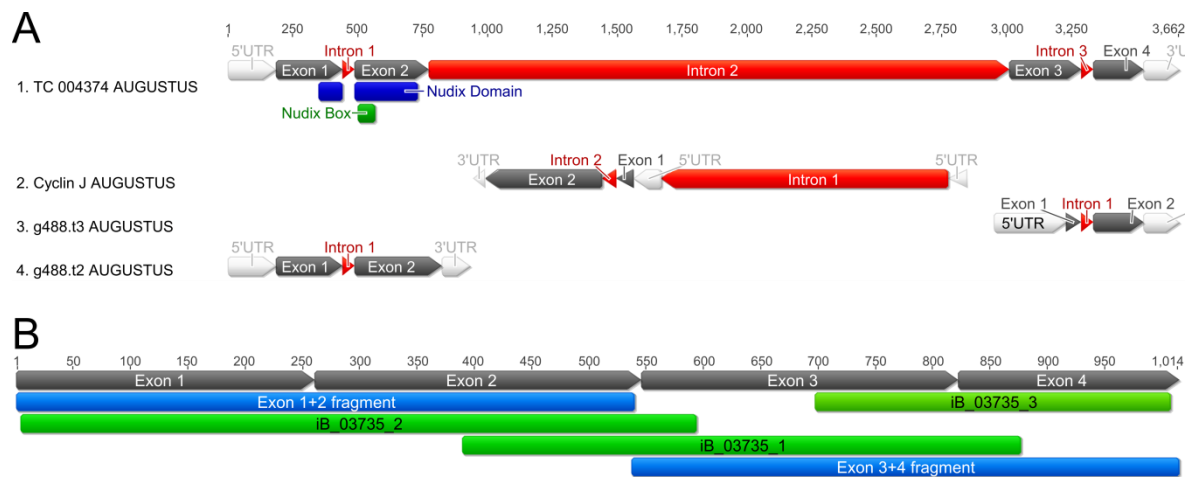


Figure 4-25 Gene locus of *TC004374* and sequence location of dsRNA templates used in this study
 Numbers on top indicate nucleic acid position. **(A)** Given are the exon/intron structure of *TC004374* and the regions of the open reading frame that encode the Nudix domain (blue) and Nudix box (green) (identified using PROSITE). Three transcripts are annotated in the *Tribolium* gene browser, the upper most transcript is g488.t1. The gene *Tc-CyclinJ* is located on the complementary strand of the second intron of the longest transcript of *TC004374*. **(B)** Location of dsRNA sequences used in this study in relation to the coding sequence of *TC004374*. Image created with Geneious version 7.0 (Biomatters).

Results

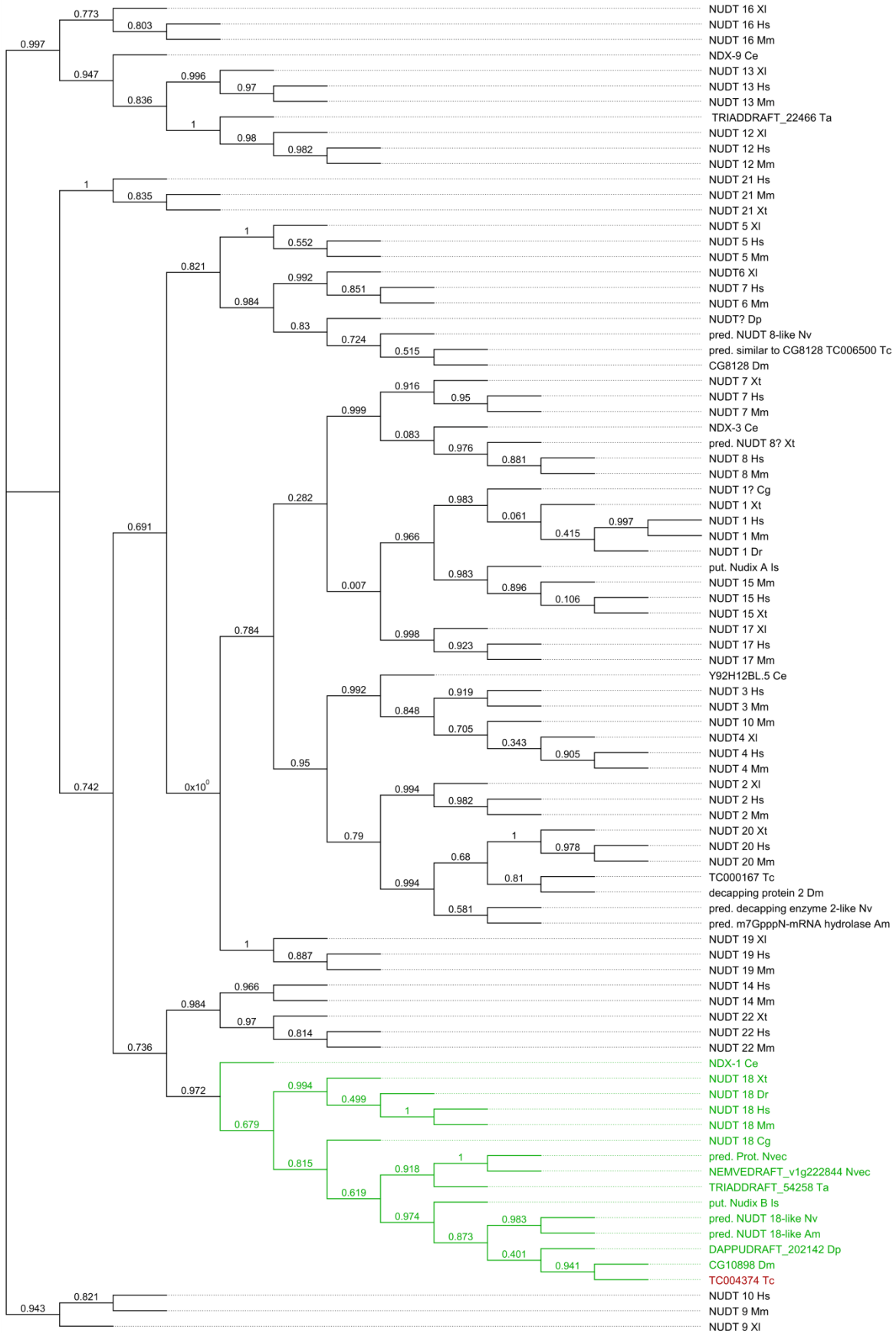


Figure 4-26 Phylogeny of TC004374

The tree shows the phylogeny of TC004374 in relation to other members of the Nudix protein family, especially to representatives from vertebrates. For some branches the FastTree support values are quite low, but orthology of TC004374 into the NUDT18 clade (green) and orthology to *Drosophila* CG10898 is highly supported. Xi: *Xenopus laevis*, Xt: *Xenopus tropicalis*, Hs: *Homo sapiens*, Mm: *Mus musculus*, Ce: *Caenorhabditis elegans*, Ta: *Trichoplax adhaerens*, Dp: *Daphnia pulex*, Tc: *Tribolium castaneum*, Is: *Ixodes scapularis*, Dm: *Drosophila melanogaster*, Nv: *Nasonia vitripennis*, Nvec: *Nematostella vectensis*, Cg: *Crassostrea gigas*, Am: *Apis mellifera*, Dr: *Danio rerio*. Common names, phylum and Taxonomy ID are given in Table 3-2 (materials and methods section 3.3). Image created with Geneious version 7.0 (Biomatters).

4.4.1 Gene expression and cuticle phenotype of TC004374

TC004374 was chosen as a potential interesting candidate after the screening steps due to a penetrant head phenotype detected during cuticle analysis and a small or absent head phenotype detected in the *Tc-wingless* (*Tc-wg*) *in situ* hybridization screen in RNAi embryos (Figure 4-7 G-G’’).

To analyze the expression pattern of *TC004374*, RNA antisense probes were synthesized based either on the entire coding sequence (JS_M133) of the *TC004374* gene or on a 3’-part, spanning 490 bp of exons 3+4 (JS_M255, sequences on DVD, folder *Genes_Sequences/iB_03735_TC004374/M133_M264_M255*). These probes were used for *in situ* hybridization on embryos of age 0-48 hours, development at 31°C. Sense probes served as negative controls. No localized expression for *TC004374* could be detected in any stages analyzed, suggesting uniform expression of this gene (not shown).

To ensure that the RNAi phenotype observed after injection of *TC004374* dsRNA was not due to degradation of *Tc-Cyclin J* transcripts, *Tc-Cyclin J* cDNA was isolated from an embryonic cDNA collection using gene specific primers (JSP198 and JSP199). After parental RNAi against *Tc-Cyclin J* all progeny showed an empty egg (EE) phenotype in cuticle analysis and brief light microscope analysis of these embryos supported the assumption that the embryos did not develop at all. This result confirmed that the anterior patterning phenotype observed for *TC004374* RNAi was not due to loss of *Cyclin J* function.

The cuticle phenotype resulting from *TC004374* RNAi was characterized by anterior deletions of body cuticle, similar to the cuticle phenotypes seen after *Tc-smurf* RNAi. *TC004374* RNAi phenotypes displayed head defects or broad deletions of anterior body cuticle (Figure 4-27, B+C). Two independent iBeetle dsRNA fragments (*iB_03735_2*, *iB_03735_3*), both partially overlapping with the original

iBeetle fragment (*iB_03735_1*) were injected for *TC004374* (green annotations in Figure 4-25 B). Injection of the *iB_03735_1* fragment resulted in the anterior patterning phenotype observed during the iBeetle screen. During injection of the two new non-overlapping fragments, only injection of the *iB_03735_3* dsRNA fragment resulted in the anterior patterning phenotype. After injection of dsRNA against *iB_03735_2* no cuticle defects were observed and almost all progeny of dsRNA injected females hatched. This gave rise to the assumption, that the anterior patterning phenotype depended on the 3' region of the *TC004374* gene. To further clarify this result dsRNAs based on two different sequence parts of the *TC004374* cDNA were synthesized. One targeting exons 1 and 2 (*Exon 1+2 fragment*), and one targeting Exons 3 and 4 (*Exon 3+4 fragment*). These dsRNAs were used for a parental RNAi experiment in different *Tribolium* beetle strains to verify the fragment specific phenotype and to test for strain specific effects at the same time (Figure 4-25 B for fragments and Figure 4-28 for results of the injections). Injections were done in the *SB*, *Pig-19*, and *Black* strains. Cuticle preparations on egg collections were done at three different time points to analyze a wearing off of the knock down effect (13, 20, and 27 days after injection, abbreviated dai). Buffer injections and RNAi against *DsRed* served as negative controls. Progeny of the injected females were counted and scored as described for the similar experiment for *Tc-smurf* (4.3.1).

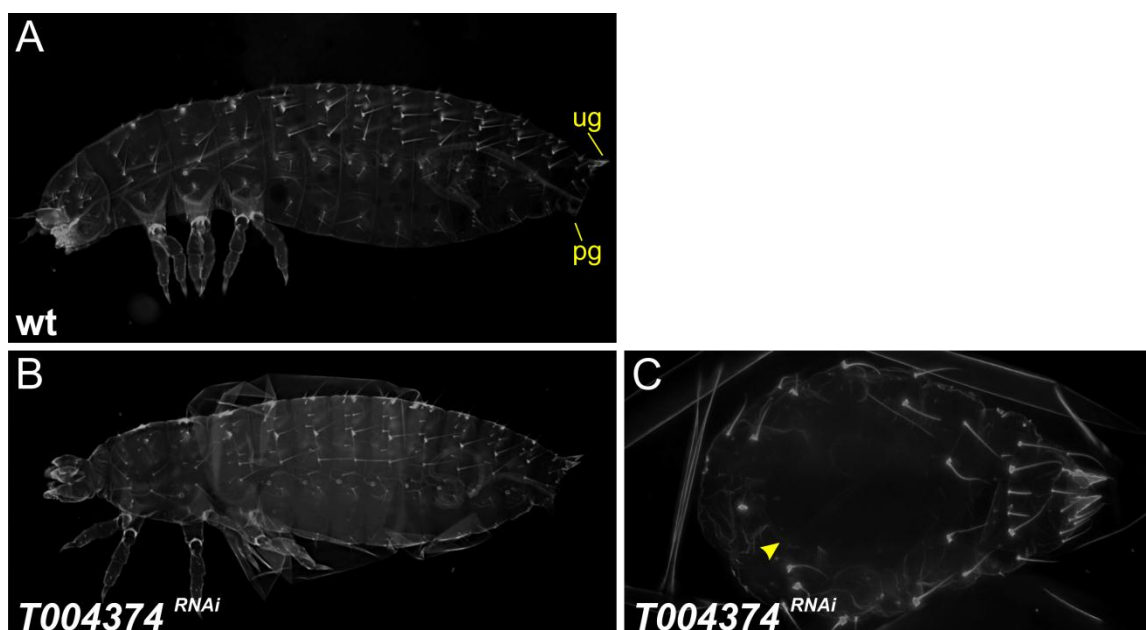


Figure 4-27 **Cuticle phenotype of *TC004374***

Anterior to the left for cuticles. **A** and **B** lateral views, **C** dorsal view. **(A)** Wild type L1 cuticle. ug: urogomphi, pg: pygopodia. **(B)** Mild *TC004374* RNAi phenotype, broad regions of the anterior head are missing. **(C)** Stronger *TC004374* RNAi cuticle phenotype. The entire head and thorax and part of the abdomen are missing. This cuticle also shows a dorsal hole (arrowhead).

Similar to the observations seen for the RNAi experiments for *Tc-smurf*, the *SB* strain showed a relatively high number of unspecific background phenotypes observable in all different conditions tested (grey bars in in Figure 4-28). The fraction of these background phenotypes ranged between 15 % and 30 % in the controls. Background phenotype levels in the *Black* and in the *Pig-19* strains never exceeded 10 %. Anterior defects were observed in 0–3 % of all analyzed progeny in the controls. Injection of the *TC004374 Exon 1+2* dsRNA fragment resulted in 0–1,7 % anterior defects, confirming that dsRNAs targeting the first two exons of *TC004374* did not lead to anterior patterning defects in any of the strains analyzed. Injection of the *TC004374 Exon 3+4* dsRNA fragment resulted in anterior patterning defects. The fraction of animals that showed defects or deletions of anterior body parts ranged, depending on the strain, from 26,6 % to 56,5 % 13 dai and wore off during the following two weeks of the experiment. 27 dai the fraction of anterior defects observed among all progeny ranged between 2,6 % and 4,7 % and was thereby comparable or almost comparable to the controls. If at all, the amount of other defects was only slightly increased in *TC004374 Exon 3+4* RNAi cuticles. The *Pig-19* strain appeared to react stronger to knock down of *TC004374* and the RNAi effect in this strain was also more stable over the time of the experiment. The fraction of anterior defects after injection in *Pig-19* was perceptibly higher than in the other strains 13 and 20 dai. Additionally, after injection in the *Black* and the *SB* strain, a strong decline in the fraction of anterior defects was already observed between 13 and 20 dai. After injection in the *Pig-19* strain this fraction was almost consistent between these two time points, although a small increase in wild type progeny could be observed. Almost no anterior defects were observed 27 dai. The different strains showed a different susceptibility to *TC004374* RNAi resulting in a different penetrance of the knock down effect. Qualitatively, anterior defects could be observed in all strains after *TC004374* RNAi. Strain specific effects could therefore be excluded. Due to the observed higher penetrance, *Pig-19* was used in all following experiments.

Results

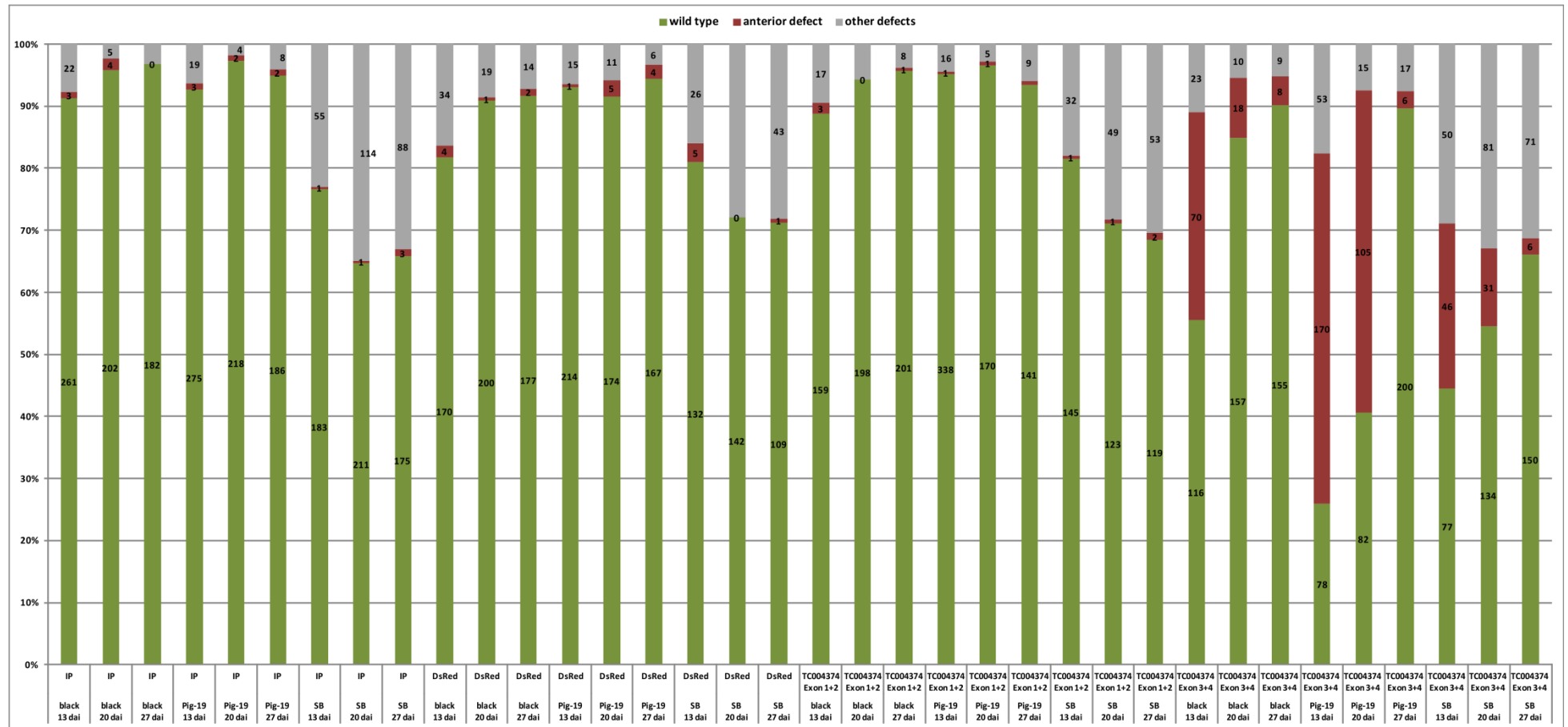


Figure 4-28 Fragment specific knock down phenotype of *TC004374*

Different strains showed a different ratio of background defects (grey bars). IP: Buffer injections. Only dsRNAs covering the region of Exon3+4 of the *TC004374* gene led to high proportions of anterior defects (red bars). The anterior defect phenotypes were detectable in all strains analyzed. A decline in these phenotypes was observed two to three weeks after injection. See text for more details.

4.4.2 Immunohistochemistry and expression of marker genes in *TC004374* RNAi during embryonic stages

To understand how *TC004374* acts during embryonic development in *Tribolium*, *in situ* hybridization stainings for the expression of selected marker genes and antibody stainings for the activated, dual-phosphorylated form of MAP kinase (pMAPK) and the activated, phosphorylated mothers against dpp (pMAD) protein were done. All RNAi embryos shown resulted from injection of the *TC004374* exon 3+4 fragment dsRNA into the *Pig-19* strain.

Due to the overall similarity between *TC004374* and *Tc-smurf* RNAi phenotypes, a gene expression analysis similar to the approach pursued for *Tc-smurf* was done for *TC004374*. Blastoderm stage *TC004374* RNAi embryos were stained for expression of *Tc-mille-pattes* (*Tc-mlpt*) (Savard et al., 2006) and double-stained for expression of *Tc-wingless* (*Tc-wg*) and *Tc-zen1* (Falciani et al., 1996; Nagy and Carroll, 1994; van der Zee et al., 2005) using *in situ* hybridization. The wild type expression domains of these genes are explained in 4.3.4. Both expression domains for *Tc-mlpt* were detected in *TC004374* RNAi embryos. The anterior wedge-shaped domain was not noticeably affected with respect to its anterior-posterior prolongation. The only alteration detected was a subtle shift of the dorsal-most part of the anterior *Tc-mlpt* expression to the ventral side (Figure 4-29 arrowhead in B, compared to A). Both *Tc-wg* domains were present in *TC004374* RNAi embryos (Figure 4-29, C and D). The most obvious morphological phenotype in *TC004374* RNAi embryos during differentiated blastoderm stages was a conspicuous bend in the germ rudiment (white arrowheads in Figure 4-29 B' and D'). The germ-serosa border was, depending on the exact stage, also not always absolutely oblique in the wild type. However, the strong angle observed in *TC004374* RNAi embryos (particularly visible in D and D') was never detected in wild type embryos.

Stainings for the expression of *Tc-wingless* (*Tc-wg*) (Nagy and Carroll, 1994) in *TC004374* RNAi embryos (*iB_03735* in the figure) during germ band stages are shown in (Figure 4-7, G-G''). Compared to the wild type the originally triangular ocular *Tc-wg* domain appeared dot-like and the antennal stripe was missing. In the stronger phenotype shown in G'' the headlobes were almost completely absent. In the wild type, the ocular *Tc-wg* domain reached the outer margin of the embryonic

tissue (Figure 4-7 A'). In contrast, in the embryos seen in Figure 4-7 G and G' the dots of *Tc-wg* expressing cells were surrounded by tissue without *Tc-wg* expression. No difference for the segmental *Tc-wg* expression in the germ band was observed compared to the wild type. The weak staining seen for all *Tc-wg* stripes in the *TC004374* RNAi embryos in Figure 4-7 was due to a weak staining efficiency during the experiment and was also present in the control.

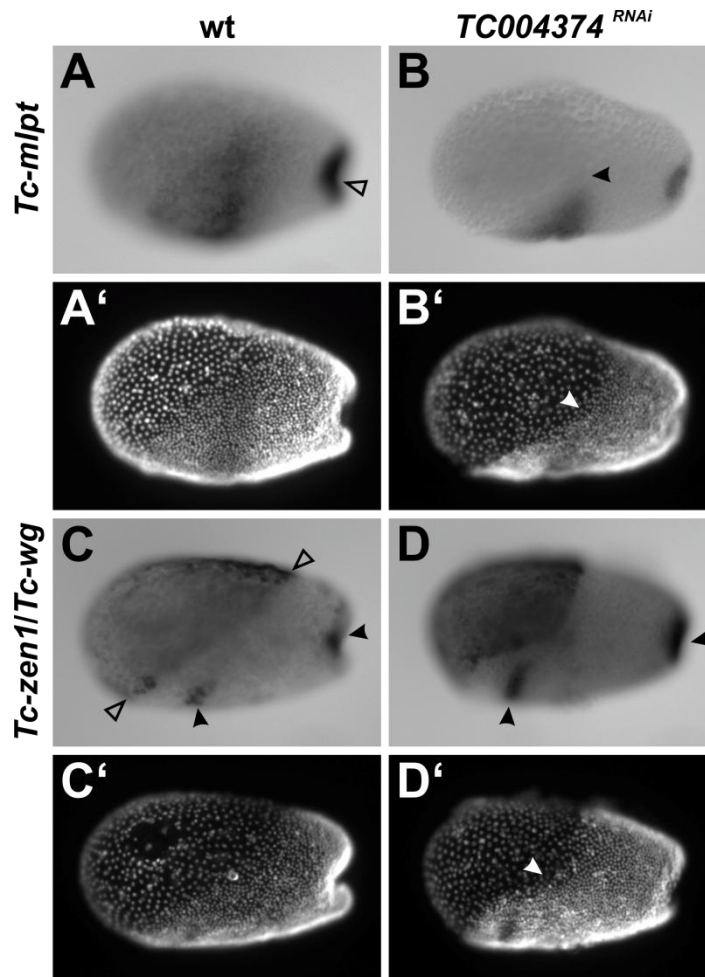


Figure 4-29 Expression of *Tc-mlpt*, *Tc-zen1* and *Tc-wg* during blastoderm stages in wild type and *TC004374* RNAi embryos

Anterior to the left and dorsal side up for all pictures. **A'–D'** show embryos in **A–D** stained for nuclei with Hoechst 33342. **(A)** *Tc-mlpt* was expressed in an anterior domain and in the primitive pit (open arrowhead in A). **(B)** In *TC004374* RNAi embryos the anterior *Tc-mlpt* domain was reduced in the dorsal part of the embryo (arrowhead points to dorsal edge of the expression). **(C)** *Tc-wg* expression was detected in two domains during differentiated blastoderm stages (black arrowheads): an ocular stripe and at the posterior pole. Open arrowheads point to the germ-serosa border. **(D)** Both *Tc-wg* domains were present in *TC004374* RNAi embryos (black arrowheads), but an obvious bend was observed in the germ serosa border (arrowhead in D', weaker but also present in B').

During germ band stages, ectopic pMAD was detected in the anterior and in the head in *Tc-smurf* RNAi embryos. To check if an accumulation of pMAD could also be observed in *TC004374* RNAi embryos, immunohistochemistry for pMAD was done on a collection of embryos aged 0–48 h at 31°C. pMAD localization in wild type embryos is described in 4.3.3. No effect of *TC004374* knock down on pMAD localization during blastoderm stages was observed. *TC004374* RNAi embryos displayed much smaller heads than wild type embryos of comparable age. Similar to the wild type, pMAD was detected in the amnion and in the dorsal margin of the germ band. However, in contrast to the wild type, strong ectopic domains of pMAD were detected in the headlobes (Figure 4-30, C and D). In the germ band, pMAD was restricted to the dorsal ectodermal borders of the embryos. In some embryos these pMAD domains appeared stronger and more broad in comparison to the wild type (Figure 4-30, D).

The heads of *TC004374* RNAi embryos were severely reduced in size (Figure 4-7 G–G’). To ascertain the effect of *TC004374* knock down on the most terminal anterior structures, RNAi embryos were stained for the expression of *Tc-six3* and the distribution of activated MAP kinase (pMAPK). *Tc-six3* expression during embryonic development has been described previously in detail (Kittelman, 2012; Posnien et al., 2009b; Posnien et al., 2011). In early germ rudiments, *Tc-six3* is expressed in one wide domain at the anterior rim. The expression domains separate in three single domains during germ band elongation, the central domain marking clypeus, labrum, stomodeum, and the outer domains marking neurogenic precursors (Kittelman, 2012; Posnien et al., 2011 and Figure 4-30 E and F). Later in development, expression domains occur *de novo* in the ocular region. The dynamics of *Tc-six3* expression during *Tribolium* germ band stages have been described in detail by Kittelman (2012). Data for *Tc-six3* expression during blastoderm stages in *TC004374* RNAi embryos was too limited to draw a final conclusion. During early germ band stages the anterior lateral domains of *Tc-six3* expression were absent, only a central, circular domain remained (Figure 4-30, G). In some early germ band stage embryos *Tc-six3* expression was not detectable at all. The ocular expression domains that arised *de novo* during later germ band elongation could at least partially be detected in the *TC004374* RNAi embryo depicted in Figure 4-30 H. The central, almost circular *Tc-six3* expression domain was still detectable, but shifted far posteriorly compared to the

central expression domain in wild type embryos. The posterior border of this circular domain almost touched the anterior border of the mandibular segment (Figure 4-30 H).

Distribution of active MAP kinase (pMAPK) during *Tribolium* embryogenesis has been described previously (Schoppmeier and Schröder, 2005; Wheeler et al., 2005). pMAPK was reported to be localized in two terminal domains during the uniform blastoderm stage and could be found in two narrow stripes on either side of the midline before gastrulation. During the differentiated blastoderm stage it was also localized at the border between embryo and serosa (Schoppmeier and Schröder, 2005; Wheeler et al., 2005). It was therefore interesting to determine whether *TC004374* RNAi had an effect on the distribution of pMAPK during embryogenesis. Early developmental stages were so far not analyzed far enough to make a clear conclusion whether knock down of *TC004734* affected the localization of pMAPK during differentiated blastoderm stages. The terminal domains of pMAPK were not affected in *TC004374* RNAi embryos. After gastrulation in wild type embryos the pMAPK marked stripes widened and the protein was found in a large fraction of neuroectodermal cells which became restricted to single columns of cells adjacent to the ventral epidermal midline. In the head, the stripes of pMAPK marked cells formed a Y-shaped pattern and marked a large number of cells within the headlobes (Figure 4-30 I) (see also Wheeler et al., 2005). During later germ band stages, pMAPK was detected *de novo* in the periphery of the ocular region. In *TC004374* RNAi embryos, the germ band localization for pMAPK was present and no clear aberration was detected. However, in the reduced headlobes of phenotypic *TC004374* RNAi embryos, pMAPK was absent (Figure 4-30 J).

In summary, knock down of *TC004374* caused a bend in the germ serosa boundary during differentiated blastoderm stages. This bend was potentially due to a loss of embryonic tissue on the anterior dorsal side, which was replaced by serosa. During germ band stages, knock down of *TC004374* resulted in a reduced head size. The loss of the outer (neurogenic) *Tc-six3* expression domains indicated that prospective neurogenic head tissue was most prone to loss of *TC004374* function. This assumption was supported by the loss of pMAPK in the headlobes of *TC004374* RNAi embryos, since MAPK signaling was suggested to indirectly pattern neural precursors in *Tribolium* (Wheeler et al., 2005).

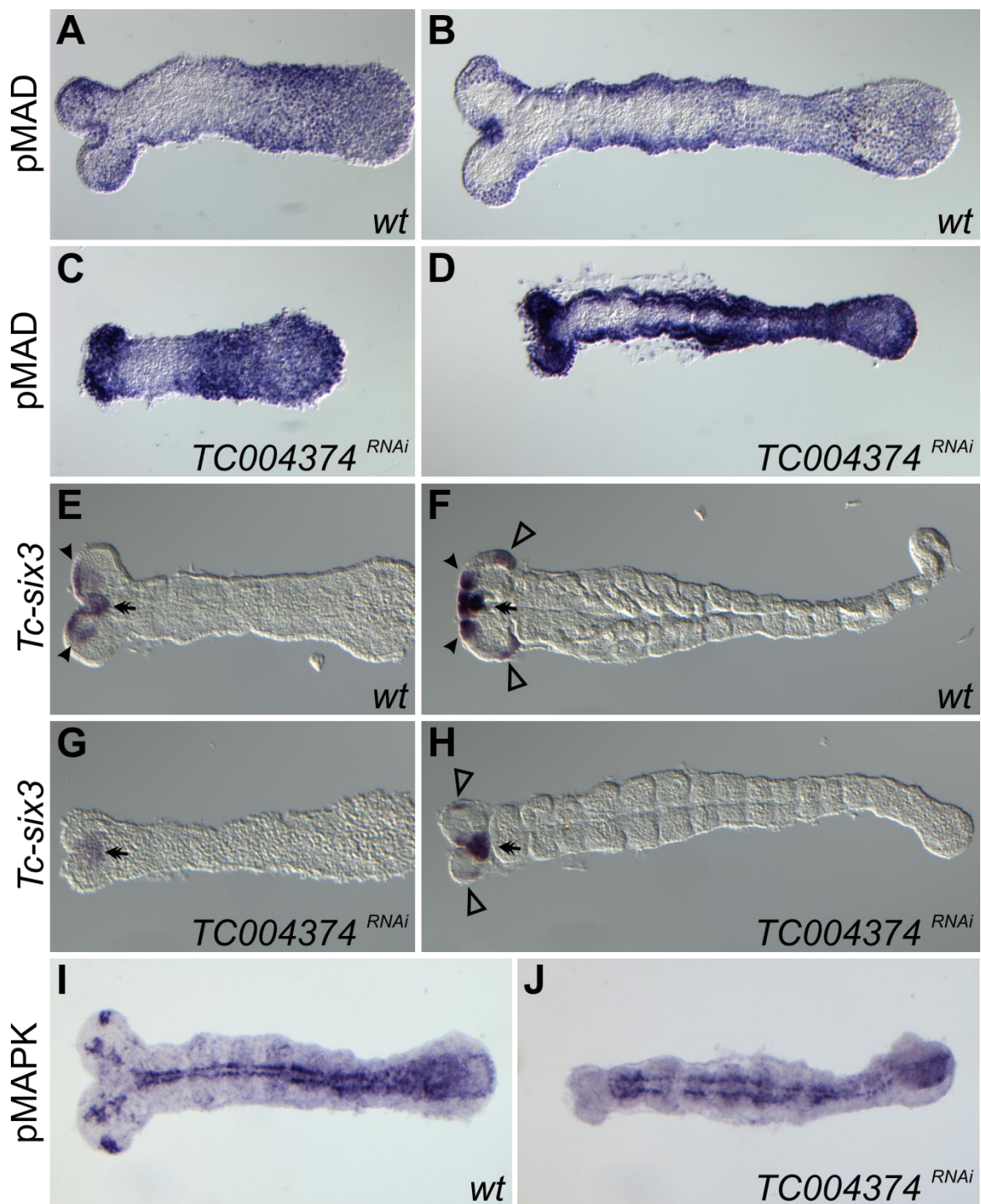


Figure 4-30 Expression of *Tc-six3* and localization of pMAD and pMAPK in *TC004374* RNAi embryos during germ band stages

Anterior to the left in all pictures. (A) In wild type embryos, pMAD was present in the posterior and anterior amnion, the dorsal margin and during later stages also in the developing labrum anlage (anterior centric spot in B). (C+D) pMAD was also detected in the amnion and dorsal margin in *TC004374* RNAi embryos. In contrast to the wild type, high levels of pMAD were present in the reduced headlobes. (E) During early germ band stages, *Tc-six3* expression was detected in a central (arrow) and two lateral, prospective neurogenic domains (arrowheads). These domains persisted during germ band elongation (F) and two lateral, ocular domains occurred *de novo* (open arrowheads in F). (G) In *TC004374* RNAi embryos the anterior lateral *Tc-six3* expression domains were not present during early germ band stages. Only a single circular domain was present in

the anterior center of the head (arrow). (H) During later germ band stages this domain persisted (arrow) and ocular domains (albeit smaller than in wild type) arose *de novo* (open arrowheads). (I) During early elongating germ band stages, activated MAP kinase was found in two columnar stripes next to the ventral midline and in a prominent Y-shaped pattern in the headlobes. Two spots of pMAPK occurred in the ocular margin of every headlobe during germ band elongation. (J) In *TC004374* RNAi embryos, columnar germ band location of pMAPK was detected but activated MAPK was completely absent anterior to the mandibular segment.

4.4.3 TUNEL assay in *TC004374* RNAi embryos

To check whether the reduced head seen in *TC004374* RNAi embryos was due to an increase in anterior cell death during development, a TUNEL assay was performed on *TC004374* RNAi embryos aged 0–48 h at 31°C. In contrast to the phenotype seen for *Tc-smurf* RNAi embryos, no consistent massive increase in cell death in the anterior tissue of germ band stage embryos was detected (Figure 4-31). A few *TC004374* RNAi embryos showed a high level of TUNEL marked cells in the anterior, but also along the complete anterior-posterior axis, indicating severe cell death all over the embryo (not shown). In wild type embryos usually no apoptotic cells were observed in gastrulating embryos and at early germ band stages (Figure 4-32, A and B) (see also Kittelmann, 2012). In contrast, cell death especially in young stages was noticeably increased in *TC004374* RNAi embryos. A very prominent observation made after knock down of *TC004374* was a high level of cell death in extraembryonic tissue, in most cases in the direct vicinity of the embryo. This was never seen in the wild type and also not in *Tc-smurf* RNAi embryos (Figure 4-32, for *Tc-smurf* TUNEL see 4.3.2). It could not be clearly ascertained whether these areas of dying cells overlapped with the embryonic tissue. Dark staining after TUNEL and altered morphology often hampered a decision if the cells were of serosal, amniotic, or embryo proper origin. The embryonic rim of *TC004374* RNAi embryos looked usually a lot less defined compared to the very clearly defined border between embryo proper and extraembryonic tissue in the wild type embryos (Figure 4-32, compare B' with C' and D'). Individuals or clusters of dying cells could also occasionally be detected in the region of the embryo proper. Although at least some of these cells were probably located within or directly above the embryonic tissue, it could not absolutely be excluded that these cells originated from the overlaying extraembryonic cell layers and were excluded from the united cell structure.



Figure 4-31 TUNEL assay in wild type and *TC004374* RNAi embryos during germ band stages

Anterior to the left in all pictures. TUNEL-stained cells marked in dark. (A) Wild type embryo during early germ band stage. (B) Wild type embryo, fully elongated. Levels of cell death were low in wild type embryos. (C) *TC004374* RNAi embryo, early germ band stage, head lobes are almost completely absent. (D) Older *TC004374* RNAi embryo, head lobes are decreased in size. Cell death was usually not noticeably increased in the embryonic tissue of *TC004374* RNAi embryos during germ band stages (C+D). However, some individual embryos showed high levels of cell death all over the embryo (not shown).

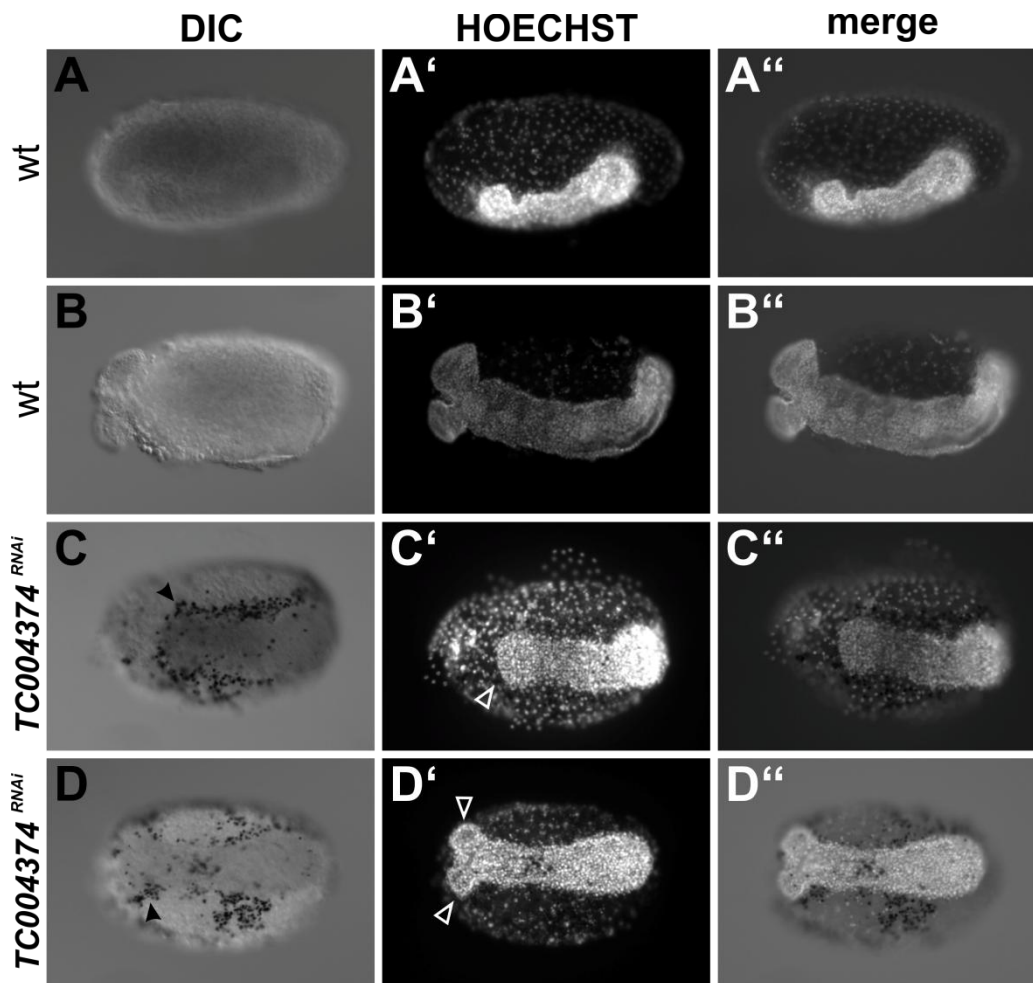


Figure 4-32 TUNEL assay in wild type and *TC004374* RNAi embryos in germ rudiments and during early germ band stages

Anterior to the left in all pictures. TUNEL-stained cells marked in black. Every row shows the same embryo. First column DIC filter, second column nuclei stained with Hoechst 33342, third column show a merge of both modes. Anterior to the left in all pictures, dorsal side up in A–A'', B–B'' ventrolateral view, C–C'' and D–D'' ventral views. (A–A'') Early germ band stage wild type embryo, no cell death was detected. (B–B'') wild type embryo later in development, no TUNEL positive cells were present. (C–C'') *TC004374* RNAi embryo early in development. The headlobes were almost completely missing (open arrowhead in C'). many TUNEL marked cells were detected at the direct border of the embryo proper (black arrowhead in C). (D–D'') substantial cell death in the vicinity of *TC004374* RNAi embryos could also be observed during later germ band stages (black arrowhead in D, open arrowheads in D' point to the headlobes). Note the distinct border between embryo proper and extraembryonic tissue in B' and the less defined borders in C' and D'.

4.4.4 Live Imaging of *TC004374* RNAi

To further clarify the embryonic phenotype after *TC004374* RNAi, live imaging experiments were performed using a transgenic line that expresses nuclear localized GFP in all embryonic cells (Sarrazaïn et al., 2012). Experimental setup,

controls and scoring of embryos were identical to the experiments performed for *Tc-smurf* RNAi 4.3.5.

TC004374 RNAi embryos exhibited several defects during development. The first defect observable for *TC004374* RNAi embryos was a remarkable delay in forming the amniotic fold. Formation of the amniotic fold and gastrulation is a process that happens smoothly and very quickly in wild type embryos. Figure 4-33 shows selected frames of a control embryo undergoing gastrulation. Time points indicated in the given frames are referred to the time after flattening of the posterior pole became firstly visible (*Tc-smurf* live imaging chapter 4.3.5). Pictures were taken every 10 minutes. During each time interval a morphological advancement in development could clearly be identified for the control embryo. The amniotic fold formed about 30 minutes after formation of the differentiated blastoderm stage (Figure 4-33, 150 minutes frame) and within the next 30 minutes, it reached the ventral side of the embryo. 240–280 minutes after posterior flattening the embryo was completely covered with serosa and amnion. In control embryos the amniotic fold reached between 30 and 50 % of the anterior to posterior distance on the ventral side (Figure 4-33 frame 180 min) within 190 minutes after posterior flattening. This was the case in 32 out of 35 embryos (mean time 177 minutes).

The *TC004374* RNAi embryo appeared to be stuck at the differentiated blastoderm stage (Figure 4-34). After formation of the differentiated blastoderm only very low developmental progress was observed for almost 60 minutes. The embryonic cells moved slowly towards posterior and about 180 minutes after posterior flattening an indentation on the posterior dorsal side occurred. In the control the amniotic fold had already reached the ventral side of the amnion at this timepoint. Suddenly, between 210 and 220 minutes after posterior flattening the amniotic fold moved over the posterior pole and the embryo was covered by the extraembryonic membranes. A delay in the progress of the amniotic fold could be seen in a high number of *TC004374* RNAi embryos: 10 out of 22 embryos needed over 210 minutes before the amniotic fold reached between 30 and 50 % of the anterior to posterior distance on the ventral side (mean time 215 minutes). Two other phenotypic aspects after *TC004374* RNAi were observed during live imaging. 6 out of 20 *TC004374* RNAi embryos scorable for the head showed clearly identifiable smaller heads (1 out of 49 in control embryos). 9 out of 26 embryos showed decaying tissue (control 1 out of 46), either in the anterior or laterally at

the border between embryonic and extraembryonic tissue. Cell death was identifiable by loss of fluorescence in the embryo proper. In *TC004374* RNAi embryos the embryonic rim often appeared to be less strictly defined than in the control. Although this observation would fit to the results for the TUNEL assay, this was difficult to score with the given optical resolution. Figure 4-35 shows selected frames for the development of a *TC004374* RNAi embryo displaying all phenotypic features mentioned. All movies are included on the DVD (folder *Movies/TC004374RNAi*).

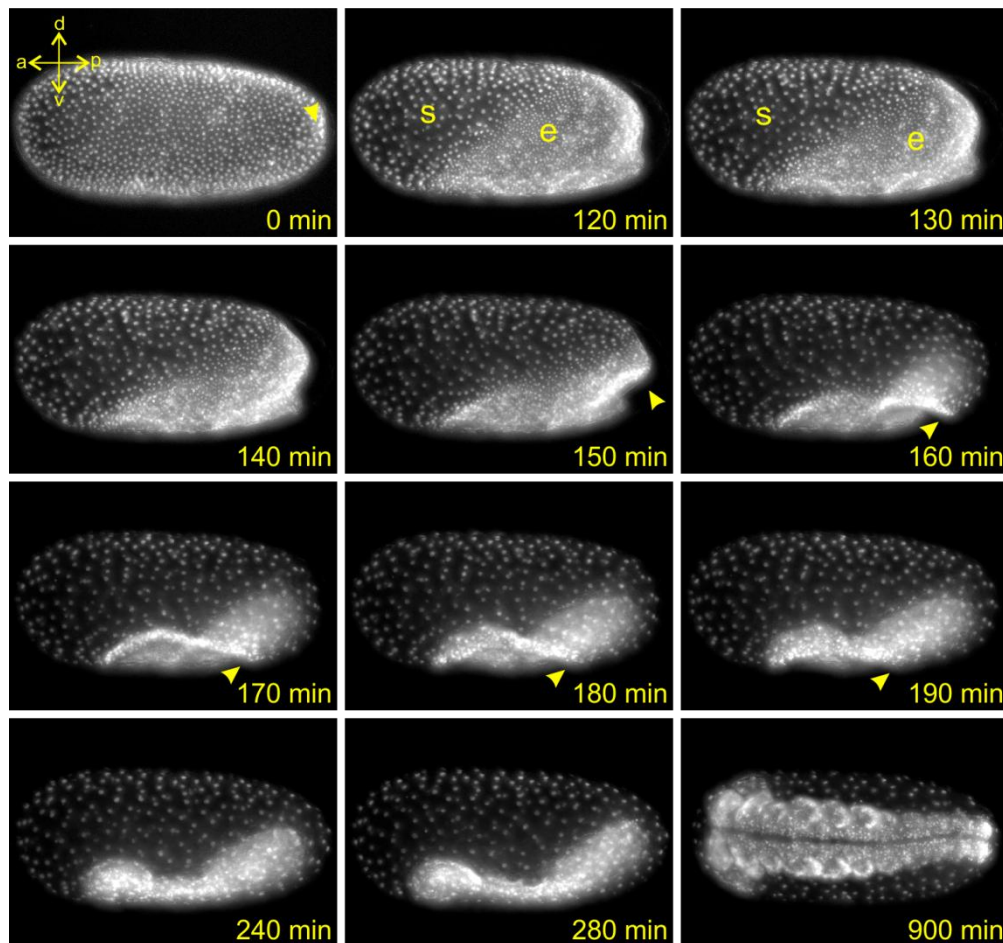


Figure 4-33 Time-lapse of control embryo undergoing gastrulation

0–280 minutes frames: lateral view. 900 minutes frame: ventral view. Given are 10 minutes time lapse frames of a control embryo with focus on the period of amniotic fold formation and embryo enveloping. Reference timepoint is posterior flattening (yellow arrowhead in 0 min frame) of the embryo before posterior pit formation. 120 minutes frame shows the differentiated blastoderm with clearly identifiable embryonic (e) and serosal (s) nuclei. Shortly later the dorsal edge of the embryonic tissue moved over the posterior of the embryo and formed the amniotic fold (arrowhead in 150–190 min frames). 190 min after posterior flattening over 30 % of the posterior embryo was covered with the extraembryonic membranes.

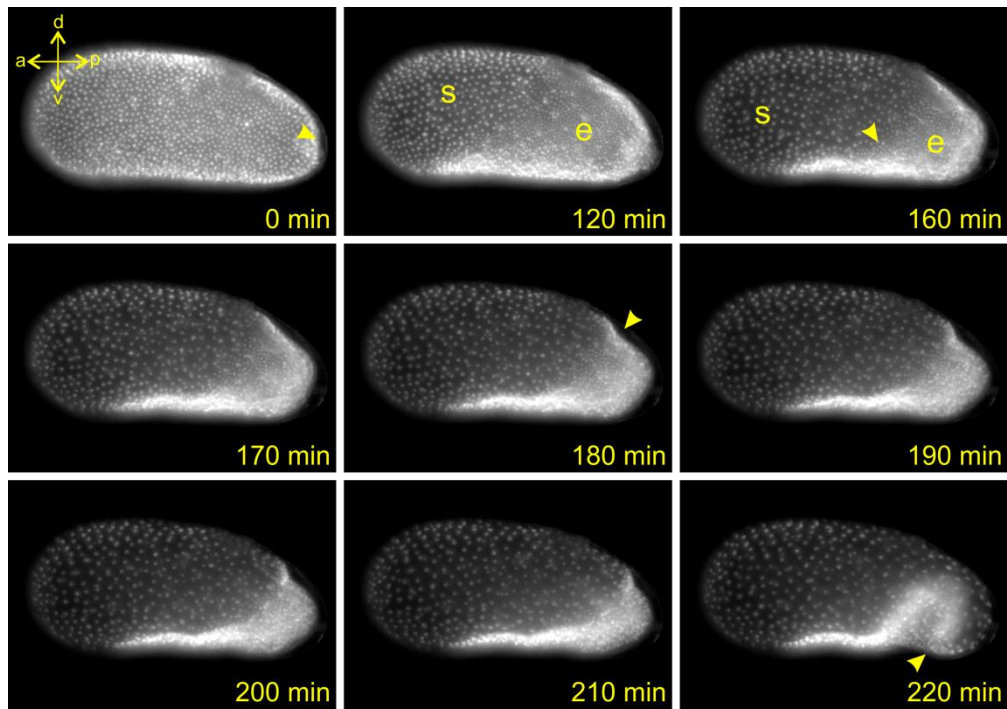


Figure 4-34 Amniotic fold delay in *TC004374* RNAi embryo

Reference timepoint is posterior flattening (yellow arrowhead in 0 min frame) of the embryo before posterior pit formation. Lateral view, anterior to the left, dorsal side up. 120 minutes frame shows the differentiated blastoderm with distinguishable embryonic (e) and serosal (s) nuclei. Cells condensed at the anterior ventrally and in the posterior along the entire dorsal-ventral axis. The posterior cells moved slowly further posteriorly. A bend became apparent at the germ serosa border (arrowhead in 160 min frame). After 180 min an indentation was visible at the dorsal posterior end of the embryo. Only very little developmental progress could be seen until 210 min after posterior flattening. Then, suddenly, the amniotic fold (arrowhead in 220 min frame) quickly moved over the posterior pole and the embryo was covered with the extrembryonic membranes.

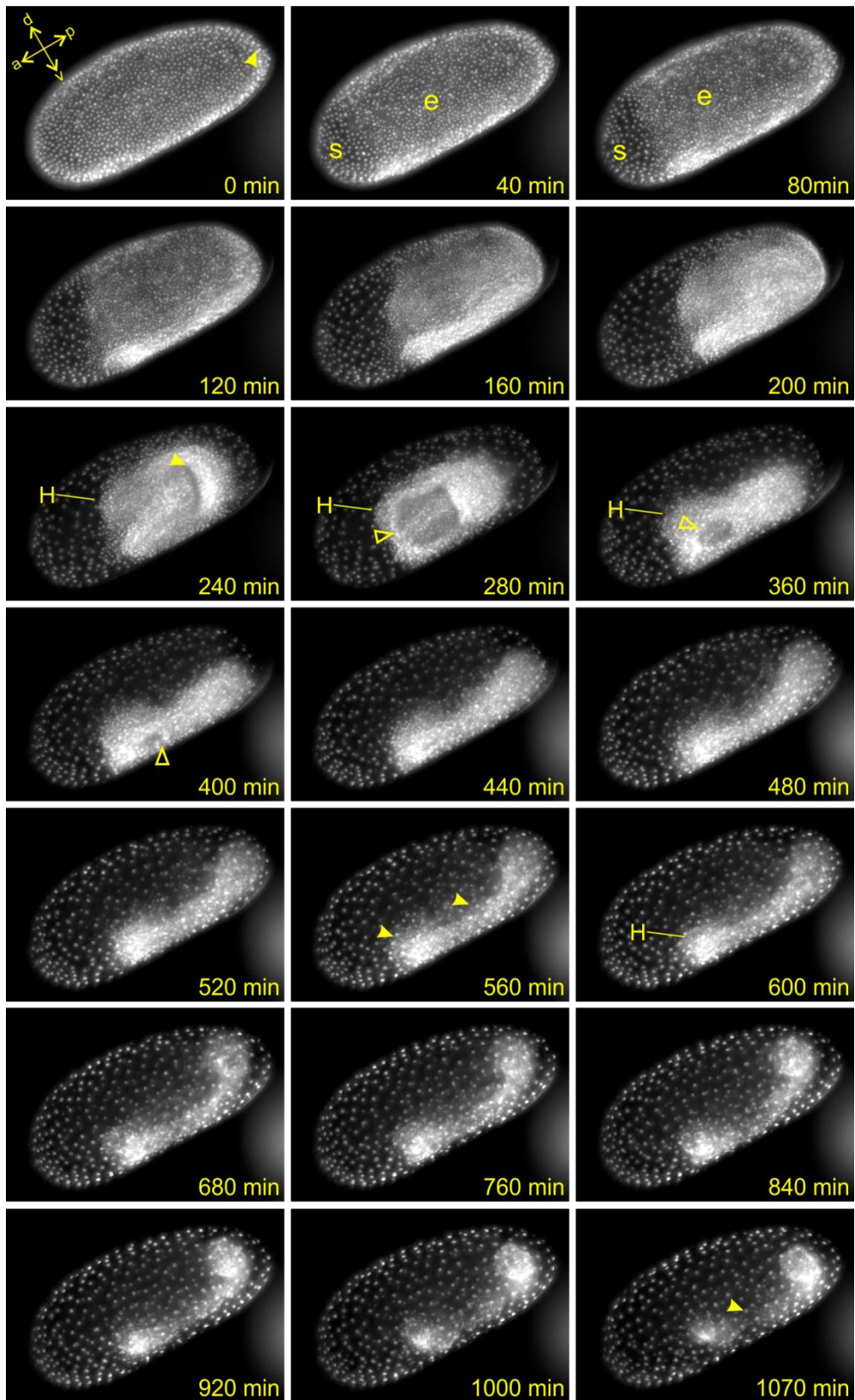


Figure 4-35 Selected frames of the development of a *TC004374* RNAi embryo

Before turning of the embryo (about 360 min time frame) pictures show a slightly tilted ventral view. Afterwards: lateral view. Reference timepoint is posterior flattening (yellow arrowhead in 0 min frame) of the embryo before posterior pit formation. 40 min after posterior flattening, embryonic (e) and serosal (s) nuclei could

be distinguished and a clear differentiated blastoderm had formed after 120 min. The amniotic fold (arrowhead in 240 min frame) started covering the germ rudiment about 240 minutes after posterior flattening, and the serosal window (open arrowheads in 280–360 min time frames) started to close. Headlobes (H in 240–360 min frames and in 600 min frame) were detectable but especially later (600 min) they were clearly reduced in size (compare to control embryo in Figure 4-21 *In vivo* imaging of *Tc-DsRed* RNAi embryo (negative control)). The borders of the embryo appeared abnormally indistinct (arrowheads in 560 min frame) and the head never moved to the anterior as observed in the control. Later, fluorescence in the embryonic tissue vanished from the anterior germ band region, indicating potential cell death (arrowhead in 1070 min frame).

4.5 Isolation and characterization of *Tribolium mothers against dpp*

The presence of a *mothers against dpp* (*mad*) gene in *Tribolium* has previously been determined by antibody staining against the phosphorylated (activated) form of MAD using a crossreactive antibody (van der Zee et al., 2006). In an approach to identify components of the TGF- β pathway in the *Tribolium* genome the gene *TC014924* was later identified to be the ortholog to *Drosophila mad* (Van der Zee et al., 2008). In the following the gene *TC014924* will be referred to as *Tc-mad*. However, *Tc-mad* had not been cloned, limiting sequence information to bioinformatic genome annotation. To be able to reliably identify binding sites for *Tc-smurf* as well as mitogen-activated protein kinase (MAPK) and glycogen synthase kinase 3 (GSK3) phosphorylation sites, the putatively full coding sequence (CDS) of *Tc-mad* was isolated using gene specific primers (JSP204 and JSP205). Several transcripts were isolated and sequenced and the clone JS_M292 was chosen as consensus sequence (all sequences on DVD, folder *Genes_Sequences/Tc_Mad*). The CDS of *Tc-mad* has a length of 1365 bp, encoding a 454 AA protein (Figure 4-36). MH1 and MH2 domains of Tc-MAD were identified using PROSITE (Swiss Institute of Bioinformatics). All other motifs were identified by hand with the help of the Geneious 7.0 software (Biomatters). Receptor regulated Smads (R-Smads) contain a C-terminal SXS motif. Both serines in this motif can be phosphorylated by activated type I Dpp/BMP receptors (Feng and Derynck, 2005). This motif was identified in Tc-MAD (Figure 4-36, see also Van der Zee et al., 2008). One PPxY binding motif for Smurf could be identified to be located at AA positions 225–228 in the linker region between the MH1 and MH2 domain, similar to a location previously described for a PPxY motif in *Drosophila* MAD (Eivers et al., 2008, see introduction). It has been reported, that MAPK phosphorylates MAD/Smad1/5/8 proteins on serines in canonical phosphorylation

sites (PxSP) (Eivers et al., 2008; Kretzschmar et al., 1997; Sapkota et al., 2007). Two PxSP motifs were detected in the amino acid (AA) sequence of Tc-MAD. Both are located in aminoterminal direction to the Smurf binding site. Eight amino acids separate the Smurf binding site and the closest MAPK motif, which is identical to the situation in the *Drosophila* MAD protein (Eivers et al., 2008, see also Figure 2-5). The second MAPK phosphorylation motif is located at AA positions 195–198 and does not have a counterpart in *Drosophila* (Eivers et al., 2008). Many substrates of GSK3 need to be pre-phosphorylated on a serine or a threonine four AA carboxyterminal from a serine or threonine that can then be targeted by GSK3 (S/TXXXS/T) (Cohen and Frame, 2001). Although the linker region of Tc-MAD is rich in serines, and many serines exhibit the proper distance of four AA to the next serine, a consensus sequence was not identified to be located directly at the MAPK phosphorylation sites. Compared to *Drosophila*, *Tribolium* MAD exhibits one additional asparagine between the second MAPK phosphorylation site and the next serine in aminoterminal direction (Figure 4-36 compare also to Figure 2-5).

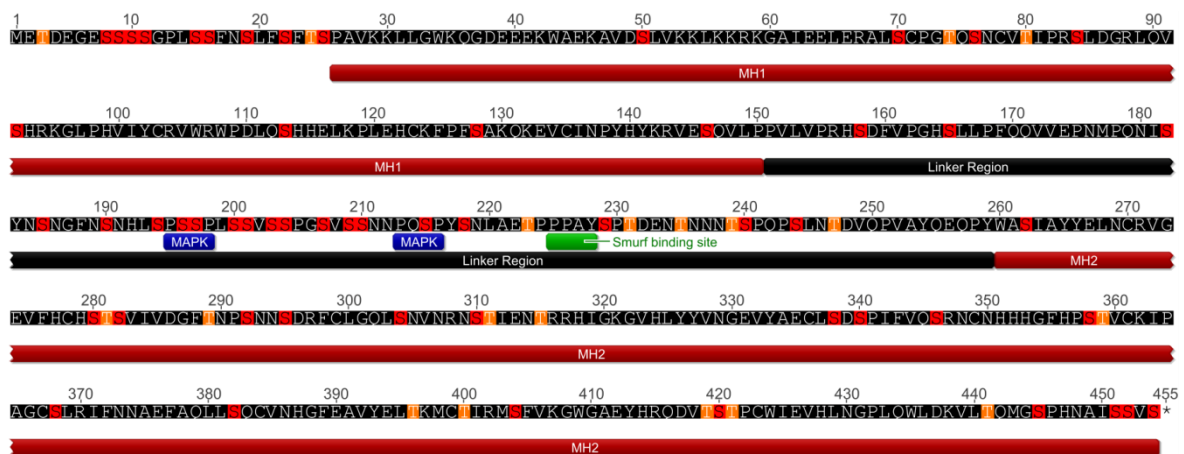


Figure 4-36 Tc-MAD protein sequence, domains and motifs

Serines are highlighted in red, threonines highlighted in orange. The Tc-MAD protein consists of a C-terminal MH1 and an N-terminal MH2 domain, divided by a linker region. The serines in the C-terminal SXS motif (in this case SVS) are phosphorylated via Dpp type I receptors. Green box (PPAY) marks the Smurf binding site. Blue boxes (PxSP) mark canonical phosphorylation sites for MAPK. Typical phosphorylation motifs for GSK3 (S/TXXXS/T) were not identified in aminoterminal direction to the MAPK phosphorylation sites. Image created with Geneious version 7.0 (Biomatters).

5 Discussion

5.1 iBeetle screen and candidate gene selection

The aim of the first part of this project was the identification and characterization of previously unknown factors required for head development and anterior patterning. The approach to achieve this aim was a wide-ranging reverse genetic RNAi screen followed by a stepwise selection of candidate genes. In the next chapters I will evaluate the screening approach by focusing on two aspects:

- Detection of candidate genes for anterior patterning processes in the iBeetle screen.
- Filtering the most promising candidate genes from the iBeetle dataset.

5.1.1 The iBeetle screen is an efficient approach to detect genes involved in head development and anterior patterning

The identification of anterior patterning phenotypes during the screen depended on a sufficient knock down of the respective genes, resulting in defects of the L1 larval cuticle, and the subsequent identification by the screeners. RNAi in *Tribolium* usually causes a robust phenotype (Brown et al., 1999a; Bucher et al., 2002; Cerny et al., 2005) and the results of the positive control injections also indicate that sufficient gene knock down was usually achieved during the iBeetle screen.

Controls were continuously included during the screen in order to monitor the rate of identified phenotypes. The results of the positive control injections demonstrated a correct annotation rate between 90–95 % for the pupal injection screen which suggests that potentially 5–10% of the phenotypes were missed. The analysis of genes with known phenotypes confirmed a high rate of identified phenotypes. Hence, it can be expected that most head or anterior patterning defects that affected the L1 larval cuticle were identified and correctly annotated during the iBeetle screen. This is also confirmed by the results for selected positive control injections for *Tc-six3* and *Tc-empty-spiracles* (*Tc-ems*). Both gene knock downs lead to head defects in *Tribolium*, and the phenotype for *Tc-ems* is also quite subtle (Posnien et al., 2011, Schinko et al., 2008). After RNAi against *Tc-six3* and *Tc-*

ems the phenotypes were correctly annotated for 100 % and 86 % of the injections, respectively (n=8 for *Tc-six3*, n=7 for *Tc-ems*) (Schmitt-Engel et al., in preparation). Thus, highly specific and highly penetrant phenotypes are very unlikely to be missing in the database. The iBeetle screen was designed as a first pass screen and the screeners were instructed to rather annotate a potentially unspecific phenotype than to risk missing an interesting gene. This is represented by my results, since for almost 10 % (305 out of about 3500) of the datasets head phenotypes were annotated. In many cases these head phenotypes were part of a complex and pleiotropic phenotype and not further analysed. Genes required for head development or anterior patterning which might have not been detected during the iBeetle screening process most likely belong to one of the following three categories:

- **Splice variant specific gene functions or different transcripts**

It cannot be completely excluded that certain splice variants of particular genes were missed or that some genes coded for several different transcripts which were not all covered by the dsRNA sequences used during the iBeetle screen. Splice specific knock down in *Tribolium* has been reported previously (Arakane et al., 2005) and differential expression of isoforms is known for *Tribolium* as well (Kittelmann, 2012). The sequence specific RNAi effect seen for *TC004374* demonstrated different functions for different transcripts of the same gene during development. If the *iBeetle fragment 2* for *TC004374* had been used during the screening procedure this gene would not have been detected as potential head patterning gene. Estimating the number of potentially missed genes due to splice specific or transcript specific knock down is to date not possible, as the incidence of these phenomena in *Tribolium* is unknown.

- **Functional redundancies**

dsRNAs targeting single genes were injected during the iBeetle screen, resulting in single gene knock down. For this reason, genes required for anterior patterning could not be identified with the applied approach, if a loss of function phenotype was rescued by the action of another gene. The only possibility to reduce this drawback to a certain extent would be the simultaneous knock down of highly related genes which is not feasible in a large scale screen with respect to time effort and costs. Analysis of redundancies

is done in more focused experiments, dealing with specific gene families. This has for instance been done for the *knirps* gene family in *Drosophila* (Chen et al., 1998; González-Gaitán et al., 1994).

- **Pleiotropic effects**

The first two categories are related to aspects that hamper the detection of a phenotype although a gene is actually involved in a certain process. However, genes with the highest probability to be missed as potential candidate genes for head development and anterior patterning were probably genes, which were involved in more than one process. This includes genes causing lethality during the screen and making downstream analysis of the progeny impossible. But also functions in ovario- or oogenesis mask potential functions during embryonic development, since dsRNA injected females do not produce eggs. Effects like this have been described for RNAi against *Tc-dpp* (van der Zee et al., 2006) and *Tc-axin* (Fu et al., 2012). Pleiotropic effects can also occur during embryogenesis and hamper the identification of phenotypes. Injection of the *iB_05754* dsRNA resulted in rather broad defects of the L1 larval cuticle, indicating a more general defect during development. Still, analysis of the RNAi embryos and concomitant staining against the segment polarity gene *Tc-wingless* (*Tc-wg*) showed a specific shift of the ocular *Tc-wg* domain towards anterior (Figure 4-7 K–K’). This can be an indication for a specific function during head patterning processes, in spite of other defects which occurred simultaneously in other regions of the embryo. To reduce the risk of missing important candidate genes due to pleiotropic effects on the level of the L1 cuticle, non-restrictive database search terms during first candidate selection and careful cuticle analysis are necessary.

The number of false positive annotations was very low for the negative control injections during the screen. During the re-injection experiments also most phenotypes were at least partially confirmed (40 out of 47). However, after injection of non-overlapping fragments for 25 genes in a different strain, 12 of them did not result in the cuticle phenotype observed during the screening process. The cause for this effect has not yet been analyzed in detail. It cannot be excluded that for some of the phenotypes, transcript or splice specific knock down was the reason for missing reproducibility. But also strain specific effects can account for some of the not reproduced phenotypes (Kitzmann et al., 2013). Furthermore, it seems that

head defects are a common aspect of pleiotropic effects in *Tribolium* since about 10 % of all dsRNA injections resulted in some kind of head defects in the L1 larval cuticle. Hence, for a number of the not-reproduced phenotypes, the observed effect after injection of a non overlapping fragment in a different strain might display a stronger knock down phenotype or affect broader regions of the L1 larval cuticle. In summary, the iBeetle screen proved to be an efficient approach to identify head and anterior patterning phenotypes in *Tribolium* and provided a large number of datasets for potential candidates.

5.1.2 New anterior patterning genes for *Tribolium* are identified through the iBeetle screen

Depending on the respective gene model, the *Tribolium* genome consists of between 13.000 (AUGUSTUS predictions) and 16.600 (official gene set, GLEAN) genes (Kim et al., 2010; Park et al., 2008; Richards et al., 2008). Since the dsRNAs for the iBeetle screen were designed according to the AUGUSTUS predictions, all genes identified by this prediction were screened or will be screened in the future according to the iBeetle concept. This in turn means that every potential head or anterior patterning gene represented by the AUGUSTUS gene models will be subjected to the screening process. My results allow a careful estimation of how many new head patterning genes we can expect to identify with the help of the iBeetle screen.

The candidates in this project were selected from datasets for the injection of 3500 dsRNAs, each targeting a single annotated gene. Extrapolated to an estimated set of 14.000 genes (Gregor Bucher, personal communication, Mario Stanke unpublished results) the datasets represented the results for about 25 % of the *Tribolium* genome. Two candidates were finally chosen for deeper analysis. At least two other candidate genes out of the list might be specifically involved in anterior patterning. L1 larval cuticles derived from knock down of the gene *TC006853* (*iB_01098*) showed absence of bristles from the dorsal ridge row (Schinko et al., 2008). *TC015120* (*iB_05754*) RNAi resulted in an anterior shift of the ocular *Tc-wg* domain (Figure 4-7). This argues for a specific function during the development of the anterior head in spite of more diverse cuticle defects observed in the L1 larva after gene knock down. Together with the identification of *Tc-smurf* and *TC004374* this makes 4 identified anterior patterning genes based on a dataset for 3500 in-

jected dsRNAs. These numbers lead to an estimated number of 16 new anterior patterning genes that might be identified in the AUGUSTUS gene set. However, this number probably underscores the real potential. One has to consider, that some candidates were excluded from analysis because they were studied by other members of the iBeetle consortium. Some of those genes are potentially involved in development of the anterior body region of *Tribolium* and might be interesting for upcoming projects. In addition, the criteria of the candidate selection process presented here were rather strict to select the most promising candidates. One can assume, that some of the genes not chosen due to pleiotropy or phenotypic variability, would indeed turn out to be involved in head patterning after a detailed analysis.

5.1.3 Candidate selection from the database

Candidates were selected from the database using the search term “pupal day15/larval head”. I stepwise selected the candidates by analyzing all iBeetle datasets with annotations for the tagma “head”. Although this approach was probably the best way to minimize the risk of missing a potentially specific head or anterior patterning phenotype, it could have been advantageous to be more restrictive by setting a cutoff penetrance value. My results showed that all annotations with a penetrance of under 30 % were eventually sorted out from analysis. Restricting the search to phenotypes with a penetrance of over 30 % or even over 50 % could have led to a quicker finding of final candidates, saving time and work without missing important candidates. The two finally selected candidates for this project were both annotated with a penetrance of over 50 % during the iBeetle screen.

5.1.4 From primary candidates to final candidates

For a project like the one presented in this thesis, it is crucial to identify as quickly as possible the final genes of interest from all screened candidates while at the same time taking due care in this process to not exclude important candidate genes. The experimental steps that led to the eventual selection of *Tc-smurf* and *TC004374* out of a group of 47 genes involved a good part of laboratory and analysis work and although all experiments were of considerable importance, some

steps of the strategy can probably be improved when similar projects are to be planned again.

The re-injection experiment as the first step in the selection process proved to be of major importance and allowed to sort out a large number of genes that were most likely not specifically involved in anterior patterning. As the iBeetle screen involved several different screeners, the use of the controlled vocabulary and the criteria for annotating a phenotypic aspect differed slightly. Additionally, every iBeetle dsRNA was injected only once, no experimental replicates were available, increasing the chance for the annotation of unspecific, naturally occurring aberrations of development. Reproduction of the iBeetle experiment before any subsequent step of analysis turned out to be essential for the identification of potential anterior patterning genes. If time and workload were compared to the gain of knowledge the cost-benefit ratio of this selection step was very effective and reduced the number of candidate genes for the next experiments from 47 to 25.

Chronologically, the next step of analysis was the determination of the expression patterns for the candidate genes. Many genes are locally expressed and have functions in regions which correspond to their expression patterns during development. During *Tribolium* head development this is for instance the case for *Tc-otd1*, *Tc-cap'n'collar*, *Tc-labial*, and *Tc-six3* (Kittelman et al., 2013; Posnien and Bucher, 2010; Posnien et al., 2011; Schinko et al., 2008). However, there are also many cases where a localized loss of function defect does not need the localized expression of the gene, the expression of the Torso receptor in *Tribolium* and *Drosophila* to give an example (Casanova and Struhl, 1989; Klingler et al., 1988; Schoppmeier and Schröder, 2005; Stevens et al., 1990). The expression analysis involved cloning of the gene fragments, probe synthesis and *in situ* hybridization stainings. Only three of the candidates showed localized expression domains, but these three genes were sorted out during later selection steps. Hence determination of the expression patterns did not have an influence on the selection process of the final candidate genes and did not lead to a reduction of the number of genes that had to be analyzed.

Compared to the gene expression screen the analysis of RNAi embryos of the candidate genes with concomitant staining for the expression of the segment polarity gene *Tc-wingless* (*Tc-wg*) served a lot more fruitful. This step was time and labor intensive but provided a very good insight in the embryonic phenotype

caused by knock down of the candidate genes and had a big impact on the selection of the final candidates.

In summary, the approach used in this project to identify head and anterior patterning genes proved to be effective and led to the identification of two promising final candidate genes. However, although the determination of the expression pattern is of undoubted importance for the characterization of a gene, in this project it would have saved much cloning, staining, and analysis time, if the gene expression screen had taken place after the analysis of the RNAi embryos.

5.2 *Tc-smurf*

One of the identified final candidate genes was *Tc-smurf*. *Tc-smurf* RNAi phenotypes were characterized by severe head defects and anterior deletions on the level of the L1 body cuticle. Germ band stage embryos for *Tc-smurf* knock down showed reduced headlobes or absence of anterior body regions. Hence the cuticle as well as the embryonic RNAi phenotype made *Tc-smurf* an excellent anterior patterning gene candidate.

5.2.1 *Tc-smurf* regulates phosphorylated MAD during *Tribolium* embryogenesis

RNAi mediated knock down of *Tc-smurf* stabilized carboxyterminal phosphorylated Mothers against dpp (pMAD) in *Tribolium* embryos as indicated by a noticeably stronger staining in immunohistochemistry. It also resulted in ectopic domains of pMAD during germ band stages. This indicated an important function of *Tc-smurf* on Decapentaplegic (Dpp)-signaling during *Tribolium* embryogenesis. This function consists probably in signal termination through Smurf mediated degradation of pMAD. This function is a common feature of DSmurf in *Drosophila* and Smurf proteins in vertebrates and is probably a conserved function of Smurf proteins at least in the bilaterians. It might even be the original function of these molecules (Liang et al., 2003; Lin et al., 2000, 2; Podos et al., 2001; Zhang et al., 2001; Zhu et al., 1999). However, also other mechanisms for Smurf mediated regulation of Dpp signaling have been described and can play a role in this regulative process. In the *Drosophila* ovary DSmurf has been described to regulate ubiquitination and proteolysis of the Dpp type I receptor Thickveins, working in

concert with the Fused serine/threonine kinase (Xia et al., 2010). Type I receptor ubiquitination mediated degradation through Smurf proteins has also been described in vertebrates but needs the binding of an inhibitory Smad (I-Smad) as adaptor (Ebisawa et al., 2001; Inoue and Imamura, 2008; Kavsak et al., 2000; Murakami et al., 2003). Mainly via biochemical approaches on Smurf proteins in vertebrates it was shown that Smurf proteins can ubiquitinate Smads at various levels of the TGF- β and BMP signaling cascades (reviewed in Cao and Zhang, 2012). It remains to be ascertained whether other ubiquitination mediated degradation processes besides MAD degradation play relevant roles in the function of Tc-Smurf during embryogenesis. Comparing my results to data from *Drosophila* it is most likely that Tc-Smurf acts directly through the degradation of pMAD, since it was described that DSmurf selectively inhibited Dpp signaling in the fly by targeting Dpp-activated MAD but not Medea, Daughters against Dpp (DAD), or dSmad2 for proteasomal degradation (Liang et al., 2003). Nevertheless, a stabilization of Dpp receptors due to *Tc-smurf* knock down could also lead to a Dpp dependent increase in cellular pMAD concentrations and the source of this increase (pMAD stabilization or receptor stabilization) cannot be distinguished with the approaches used in this study. Deeper biochemical analyses using protein interaction assays and analyzing ubiquitination states of Tc-MAD proteins and Tc-Tkv receptors would serve useful to test whether Tc-Smurf solely acts through degradation of Tc-MAD.

5.2.2 Loss of *Tc-smurf* function can lead to pre-blastodermal lethality

Tc-smurf knock down with the *JS_M115* and *Exon 5+6* dsRNA fragments led to a high number of embryos that died before cuticle secretion, resulting in empty egg (EE) phenotypes in cuticle preparations. Analysis of fuchsine stained embryos showed that many *Tc-smurf* RNAi embryos nevertheless developed to germ band stages indicating that probably not all EE phenotypes observed in cuticle preparations were due to undeveloped embryos (Figure 4-12). TUNEL assay and live imaging experiments suggest that at least a fraction of the eggs without any identifiable embryonic tissue observed after RNAi with the *JS_115 fragment* or *Exon 5+6 fragment* dsRNA resulted from embryos that had completely undergone cell death prior to fixation of the embryos. However, the live imaging experiments also showed that indeed many *Tc-smurf* RNAi embryos do not even form a properly

organized blastoderm stage, indicating that *Tc-smurf* has a function during very early developmental processes or even already during oocyte maturation. The data presented in this study cannot decipher how *Tc-smurf* acts exactly prior to blastoderm formation. *Tc-dpp* is already expressed during very early blastoderm stages (Sanchez-Salazar et al., 1996; Sharma et al., 2013; van der Zee et al., 2006) and too high levels of Dpp-signaling might interfere with overall blastoderm integrity. However, the pre-blastodermal *Tc-smurf* function could also be completely independent of Dpp. The Mothers against Dpp (MAD) protein was described to be involved in canonical Wg signaling in *Drosophila* by interacting with the Pangolin-Armadillo complex (Eivers et al., 2011). It is therefore possible that *Tc-smurf* is already necessary to keep Tc-MAD levels low before *Tc-dpp* is expressed in *Tribolium*. *Tc-axin*, which encodes for a component of the β -Catenin destruction complex is maternally provided in *Tribolium* and anteriorly localized (Fu et al., 2012). It could be that early Wg signals play an important role already during early nuclear division cycles in *Tribolium*, making use of Tc-MAD. More experiments are necessary in order to completely understand the functions of Tc-Smurf during pre-blastoderm stages in *Tribolium*. It might also be that the early effects are due to a germ line function of *Tc-smurf*. Smurf function in the regulation of Dpp signaling in the germ line has been described for *Drosophila* (Casanueva and Ferguson, 2004; Chang et al., 2013; Xia et al., 2010). Additionally, knock down of *Tc-dpp* in pupal stages causes female sterility (van der Zee et al., 2006 and data not shown) suggesting an important function of Dpp-signaling in the *Tribolium* germ line. The early defects seen before blastoderm formation might therefore be due to a general loss of egg integrity and not a result of loss of Tc-Smurf function after egg deposition. Pupal and adult injections were performed in this study in order to knock down the function of *Tc-smurf*. Embryonic dsRNA injections could serve useful to elucidate whether the pre-blastodermal defects seen in some *Tc-smurf* RNAi embryos are due to a very early Tc-Smurf function during development.

5.2.3 *Tc-smurf* is involved in patterning the blastodermal fate map in *Tribolium*

Knock down of *Tc-smurf* changed the blastoderm fate map of *Tribolium* embryos. Staining for marker genes and live imaging experiments showed that the fraction of cells specified to form head tissue was clearly reduced upon *Tc-smurf*

knock down. This resulted in a bend in the germ serosa boundary during the differentiated blastoderm stage and eventually in headlobes that were strikingly reduced in size during the germ rudiment stage. Interestingly, the dorsal anterior tissue (in the lateral midline) of the germ anlage in the blastoderm was stronger affected than the most anterior ventral or dorsalmost tissue. This resulted in the obvious bend in the germ serosa border and was most likely due to *Tc-sog* activity on the ventral most side of the embryo which inhibited Dpp-signaling in this region (van der Zee et al., 2006). It has previously been shown that loss of *Tc-sog* leads to a complete loss of the head anlage in the *Tribolium* blastoderm with parts of the labial segment being the only head part remaining, as demonstrated by staining for Hox gene expression in germ band stage embryos (van der Zee et al., 2006). If compared to the severe *Tc-sog* RNAi phenotype, *Tc-smurf* knock down has a relatively small impact on the overall fate map of the *Tribolium* differentiated blastoderm and it seems that Tc-Smurf has rather a function in fine tuning Dpp-signaling during these stages. Weak cuticle phenotypes suggest that the first regions to be affected by loss of *Tc-smurf* function are located between the clypeolabral region (CLR) and the gnathal segments. Figure 4-10 C shows a larva with missing head cuticle between the labrum and the mandibles. The labrum anlage is located anteriorly and medial to the procephalic ocular and antennal region (Kittelman, 2012; Posnien et al., 2010) which is missing in this larva. The loss of the ocular *Tc-wg* domain seen in many *Tc-smurf* RNAi embryos also indicates loss of at least parts of the ocular region (Figure 4-19). While *Tc-sog* is important to form a head per se, *Tc-smurf* is necessary to establish the more posterior procephalic head parts in concert with *Tc-sog*. This indicates a function of Tc-Dpp signaling in patterning the *Tribolium* head along the anterior-posterior axis. This process is most likely performed by a very tightly regulated crossplay between Tc-Sog, Tc-Tolloid (Tc-Tld) and Tc-Smurf. It has formerly been shown that Tc-Tld has an important pro-Dpp function in *Tribolium* (Nunes da Fonseca et al., 2010). This function is probably mediated by the cleavage of Tc-Sog molecules and concomitant release of bound Tc-Dpp that can then bind to its receptors as it has been described for *Drosophila* (Marqués et al., 1997; Srinivasan et al., 2002). My results suggest that Tc-Smurf has an essential function in fine-tuning the crossplay between Tc-Tld and Tc-Sog. During differentiated blastoderm stages, *Tc-dpp* is expressed in a fine stripe in the anterior of the germ anlage, interestingly with highest

expression levels on the ventral side. Dpp signaling is involved in defining the border between embryonic cells and serosa, since interfering with this signaling pathway through *Tc-sog* or *Tc-dpp* RNAi, respectively, changes the position of the germ-serosa boundary (van der Zee et al., 2006). *Tc-sog* is expressed at the ventral most side of the blastoderm stage embryo and is necessary to transport Dpp ligands to the dorsal side of the embryo (van der Zee et al., 2006). *Tc-tld* is expressed broadly during undifferentiated blastoderm stages, excluded only from the egg poles. During the differentiated blastoderm stage *Tc-tld* is expressed in a broad anterior domain within the prospective germ rudiment, uniformly along the DV-axis (Nunes da Fonseca et al., 2010). Tc-Tld is hence present in all regions of *Tc-dpp* expression during this stage. Tc-Smurf is expressed in all cells and is probably necessary to set a threshold level that needs to be reached before activated BMP receptors result in nuclear localization of pMAD and subsequent gene regulation. According to my results, *Tc-smurf* prevents low level Dpp-signals which happen due to Tc-Tld mediated Tc-Sog cleavage on the ventral and lateral side of the prospective embryonic tissue. It might even shut down Dpp signals that occur due to secreted Dpp ligands which directly bind to membrane receptors before they are bound to Tc-Sog molecules. I propose a model in which Tc-Sog, Tc-Tld and Tc-Smurf act in a concerted manner to define a line that separates extraembryonic and embryonic tissue during the differentiated blastoderm stage (Figure 5-1). According to this model, *Tribolium* makes use of at least four systems to define this line and control Dpp-signaling during blastoderm stages:

- Localized expression of the diffusible signaling molecule Tc-Dpp in a dorsal-ventral stripe-like domain along the region of the prospective germ serosa border. After differentiated blastoderm formation, *Tc-dpp* expression is restricted to a thin stripe of expression along the germ serosa border, only a few cells wide.
- Localized expression of the diffusible, extracellular Tc-Dpp antagonist Tc-Sog on the ventral side of the embryo which leads to the ventral inhibition of signaling and at the same time to an amplification of the signal on the dorsal side through a shuttling function of Tc-Sog.

- Broad expression of the extracellular Tc-Sog antagonist Tc-Tld in the presumptive embryonic tissue, which is necessary to reactivate Sog-bound Tc-Dpp molecules and thereby activate signaling.
- Ubiquitous expression of the intracellular Tc-Dpp signaling antagonist Tc-Smurf. Smurf is necessary to cut off ‘leaking’ Dpp-signaling due to diffusing Dpp molecules and untimely cleaved Sog molecules. The crossplay of all regulators results in a clear and localized border between germ and serosa tissue. In *Tc-sog*, *Tc-dpp*, and *Tc-tld* RNAi embryos the germ serosa border is shifted but still clearly defined (Nunes da Fonseca et al., 2010; van der Zee et al., 2006). This clear definition is often lost in *Tc-smurf* RNAi embryos. *Tc-smurf* is also essential to locate the germ serosa border, since *Tc-smurf* RNAi leads to a posterior shift especially of the lateral regions of this border. One more function of Tc-Smurf is the restriction of peak levels of pMAD to the dorsal most region, which defines the amnion. In *Tc-smurf* RNAi embryos an increase of this peak level area can be detected and the amnion in many embryos is enlarged as seen in the embryo in Figure 4-23.

The extracellular Dpp agonist Tc-Twisted-gastrulation (Tc-Tsg), does not seem to play a role in defining these early Dpp-signaling regions. RNAi against *Tc-tsg* leads to a complete loss of Tc-Dpp function and completely ventralized embryos, identical to the phenotype observed after *Tc-dpp* RNAi. *Tc-tsg* rather seems to be necessary for *Tc-dpp* function per se (Nunes da Fonseca et al., 2010).

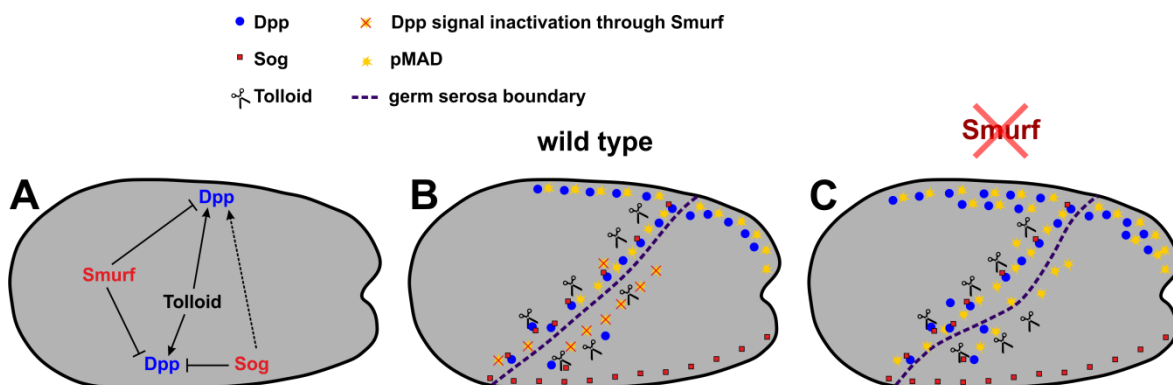


Figure 5-1 Model of *Tc-smurf* function during blastoderm stages of the *Tribolium* embryo

Shown are schematic drawings of a *Tribolium* embryo during the differentiated blastoderm stage. (A) Simplified scheme of the regulation of Dpp during late blastoderm stages in *Tribolium*. (B) Wild type situation, modified after Nunes da Fonseca et al., (2010). (A+B) Tc-Sog binds Dpp molecules on the ventral side, resulting in a block of Dpp signaling. At the same time Sog-Dpp complexes diffuse to the dorsal side of the embryo.

Tolloid cleaves Sog. The dorsal diffusion of Sog-Dpp complexes leads to an increase of free Dpp molecules dorsally after Tolloid induced cleavage of Sog. Sog therefore indirectly enhances Dpp signaling dorsally. This allows Dpp signaling to reach peak levels in the dorsal posterior region of the embryo. Smurf inhibits Dpp signaling in all cells through targeting pMAD for degradation and sets a threshold level that needs to be reached before activated BMP receptors result in nuclear localization of pMAD. Dpp signal is blocked in the neuroectoderm, low in dorsal ectoderm and high in the prospective amnion. **(C)** Loss of Smurf function stabilizes pMAD in more ventral and posterior cells in the embryo. In the ventral most region Sog blocks Dpp signaling. More dorsally, Tld mediated cleavage of Sog allows Dpp ligands to bind to their receptors. Due to lack of Smurf threshold limits are reached more ventrally and posteriorly. Therefore more cells gain serosal fate and parts of the prospective head are lost. The germ serosa boundary is less defined. The scheme integrates results obtained during this work with previously published results (Nunes da Fonseca et al., 2010; van der Zee et al., 2006)

5.2.4 A model for *Tc-smurf* function during germ band stages

The observation that *Tc-smurf* knock down results in broad deletions of anterior body regions in *Tribolium* was a surprising finding. *Drosophila* DSmurf is a negative regulator of Dpp signaling (Chang et al., 2013; Liang et al., 2003; Podos et al., 2001) and molecular characterization of Tc-Smurf strongly suggests the same biochemical functions for Smurf proteins in *Tribolium* and in *Drosophila*. It has previously been described that the dorsal-ventral and anterior-posterior patterning systems in *Tribolium* are connected. Interfering with components of dorsal-ventral patterning processes causes enlargement or loss of prospective head regions on the blastodermal fate map (Kotkamp et al., 2010; Nunes da Fonseca et al., 2010; van der Zee et al., 2006). However, analysis of L1 cuticles showed that often only a few growth zone derived body segments remained after *Tc-smurf* RNAi. In combination with the high amount of cell death detected in TUNEL stainings as well as the data obtained during live imaging experiments, this indicated that missing segments were initially established and lost during further development. The number of remaining segments in *Tc-smurf* RNAi cuticles can differ strongly between different *Tc-smurf* RNAi cuticles and depends probably on the strength of the gene knock down. The severe and variable loss of anterior body regions in combination with the presence of posterior segments showing a normal DV-polarity is highly different from the *Tc-sog* RNAi phenotype which results in loss of all head parts anterior to the labial segment while more posterior segments are present, although completely dorsalized. The missing head regions seen in the *Tc-sog* RNAi phenotype are explained by a shift in the fate map of the differentiated blastoderm stage embryo (van der Zee et al., 2006, also seen in this study).

Loss of *Tc-smurf* function also leads to changes in the blastodermal fate map but to a different and smaller extent (Figure 5-1, Figure 4-19). Furthermore, the *Tc-smurf* RNAi phenotype is highly different from the *Tc-sog* RNAi phenotype in the way that remaining body segments still show dorsal-ventral polarity. This indicates that *Tc-smurf* has a minor or no function for the establishment of dorsal-ventral fate during germ band elongation. Rather, *Tc-smurf* seems to be essential for the maintenance of already established embryonic body segments.

The differences in the loss of function phenotypes seen between the two Tc-Dpp regulators Tc-Sog and Tc-Smurf can probably be explained by the different ways in which the two types of molecules act on the Dpp-pathway. In this section, I will postulate a model that explains these differences and can also explain some observations that have been made in other studies. The model is depicted in Figure 5-2 and will be explained in the following chapters.

5.2.4.1 Dpp displays a positive feedback loop during germ band stages in the *Tribolium* embryo

The suggestion that an inherent positive feedback mechanism might maintain Dpp signaling at the dorsal ectodermal margin during *Tribolium* germ band stages has been suggested before (Nunes da Fonseca et al., 2008; van der Zee et al., 2006). This concept is mainly based on two observations made for the phenotype of *Tc-sog* RNAi embryos. In the wild type germ band stage embryo, *Tc-dpp* is expressed in two stripes in the growth zone which abut the expression domain of *Tc-sog* (van der Zee et al., 2006). Outside of the growth zone, in the established segments, these stripes are not present. Instead, *Tc-dpp* expression can be detected at the dorsal ectodermal margin. *Tc-sog* RNAi embryos display ectopic expression of *Tc-dpp* in two stripes in the ventral midline, continuous with the growth zone expression domain. Additionally, in the wild type germ band, pMAD can be detected in all areas that show *Tc-dpp* expression, except for the *Tc-dpp* expressing stripes in the growth zone, indicating that in this region Dpp-signaling is blocked. However, this is not true for *Tc-sog* RNAi embryos, where pMAD is detected in ectopic ventral stripes in the germ band as well as in the stripe-like *Tc-dpp* expression domains in the growth zone. This indicates that at least one factor that inhibits Dpp-signaling in the growth zone is *Tc-sog* (van der Zee et al., 2006 and this study) and that pMAD in the growth zone might induce the expression of

Tc-dpp in the ventral ectodermal stripes. This suggests that Dpp signaling initiated in the growth zone expression domain initiates and maintains its own activity in ventral domains in the germ band when Tc-Sog is absent. Additionally, the *Tc-dpp* expression in the dorsal margin appears to be weaker in *Tc-sog* RNAi embryos. In some embryos dorsal margin expression has been reported to be even lost (van der Zee et al., 2006, and this study). It might be that missing transport of Tc-Dpp ligands to the embryonic margin in *Tc-sog* RNAi embryos leads to a reduction of *Tc-dpp* expression in the dorsal ectoderm. This indicates requirement of Tc-Dpp signaling for the activation of *Tc-dpp* expression in the dorsal ectoderm. This study gives one more indication for a positive feedback mechanism for *Tc-dpp* signaling during germ band stages.

Tc-smurf RNAi embryos show ectopic *Tc-dpp* expression domains. Some of these domains are quite broad in the anterior body region of germ band stage embryos. In the wild type this region is free of Tc-Dpp signaling except for the dorsal margin expression (Figure 4-15, Figure 4-16). During germ rudiment stages, *Tc-dpp* expression and pMAD are only detected in the amnion, the headlobes and the anterior germ band are free from Tc-Dpp signaling. *Tc-smurf* RNAi embryos show high levels of pMAD in the anterior, even more, many embryos of this stage do not show ectopic pMAD in the posterior (compare G and I in Figure 4-16). Additionally, strong ectopic expression of *Tc-dpp* in the head lobes and in ectopic ventral stripes was detected in germ rudiments and early germ band stage *Tc-smurf* RNAi embryos. The high ectopic abundance of pMAD in this region suggests that pMAD might have initiated these expression domains, which indicates an autoactivation of Dpp signaling in this region.

Based on the molecular function described for homologs in *Drosophila* and vertebrates, Tc-Smurf is able to terminate Tc-Dpp signaling. This raises the question of the initial Dpp source which results in ectopic pMAD in the anterior region of *Tc-smurf* RNAi embryos. The answer can probably be given through the reported expression profiles for *Tc-dpp* and *Tc-tld* (Nunes da Fonseca et al., 2010; van der Zee et al., 2006). *Tc-tld* is expressed in a broad anterior domain during the differentiated blastoderm stage. Later the germ rudiment condenses on the ventral side and *Tc-tld* is broadly expressed in the headlobes and all ectodermal and neuroectodermal tissue of the anterior embryo, restricted only from the mesoderm (Nunes da Fonseca et al., 2010). The expression of a pro-Dpp regulator in this ar-

ea seems strange, since the neuroectoderm in the wild type is completely free of Tc-Dpp signaling and does not show any detectable pMAD (Figure 4-16 G). According to my results, the restriction of Tc-Dpp signaling from the anterior embryonic tissue is achieved by Tc-Smurf function. *Tc-dpp* is expressed in an anterior stripe at the border between serosa and embryonic tissue during differentiated blastoderm stages, hence very near to the developing embryonic head. *Tc-smurf* knock down results in an ectopic anterior Dpp signaling domain, initialized probably due to *Tc-tld* activity, which allows Tc-Dpp ligands to bind to their receptors despite the closely localized expression of *Tc-sog*. In the here proposed model, *Tc-smurf* is necessary to terminate *Tc-tld*-mediated Tc-Dpp signaling in the head and the anterior embryo. An indication for this model is the overlap of pMAD in germ rudiment stage embryos after *Tc-smurf* RNAi with the expression domain of *Tc-tld* seen in wild type embryos during these stages. According to this model, lack of *Tc-smurf* function leads to the formation of an anterior, ectopic, autoactivating Tc-Dpp signaling center. To summarize this briefly, the signaling center forms due to the following reasons:

- *Tc-dpp* expression in the anterior of the embryo, as a source for Tc-Dpp ligands.
- Tc-Sog on the ventral side of the embryo binds Tc-Dpp and transports Dpp ligands away from its expression domain.
- Expression of *Tc-tld* in the anterior embryo leads to cleavage of Tc-Sog and releases Tc-Dpp which in turn activates its receptor and leads to MAD phosphorylation.
- Lack of Tc-Smurf hampers a direct cutoff of this Tc-Dpp signal. MAD phosphorylation therefore results in target gene regulation.
- pMAD activates *Tc-dpp* expression, which generates a positive feedback mechanism of Tc-Dpp signaling.

The formation of a signaling center alone does not explain why *Tc-dpp* expression and pMAD can be found in broad anterior regions of *Tc-smurf* RNAi embryos during later germ band stages. Especially, since the posterior embryo often looks wild type in both aspects. This can however be explained by the hypothesis that anterior *Tc-dpp* expression sends the signal forward posteriorly due to secretion and diffusion of Tc-Dpp ligands. This would result in a signaling wave from an-

terior to posterior which is not terminated due to the absence of Tc-Smurf. In this manner the signal can also reach segments which were initially not established and have just subsequently been added during growth zone elongation. My results suggest that this wave of Tc-Dpp signal can ultimately result in death of all embryonic cells. Autoactivation of Tc-Dpp has been described in several other contexts. In *sog* mutant flies Dpp diffuses in the neuroectodermal region and turns on its own transcription (Biehs et al., 1996) suggesting a conserved mode of regulation between beetle and fly. In *Xenopus leavis* the homeobox gene *Vox* turns on the expression of *BMP-4*. *BMP-4* in turn induces expression of *Vox* (Bier, 1997; Schmidt et al., 1996). Thus the use of positive feedback mechanisms on the Dpp/BMP-pathway to induce and maintain ectodermal fate and discriminate this fate from neuroectodermal tissue might be a conserved feature.

Ectopic expression of *Tc-dpp* in *Tc-smurf* RNAi embryos is only found in a subset of cells in the headlobes and in two ventral ectodermal columns, despite the broad region of Tc-Dpp signaling indicated by pMAD (Figure 4-15 and Figure 4-16). This can probably be explained with the competence of the signal-receiving cells to react to the Tc-Dpp signal. At least mesodermal cells are probably already specified during the germ rudiment stage indicated by the expression of *Tc-twist* (Chen et al., 2000; Handel et al., 2005; Sommer and Tautz, 1994). It appears that only a subset of cells can react to the Tc-Dpp signal by in turn activating the expression of *Tc-dpp*.

5.2.4.2 Tc-Dpp signaling inhibits *Tc-sog* expression

Tc-Sog is a potent inhibitor of Dpp and pMAD can not be found in cells expressing *Tc-sog* in *Tribolium* (van der Zee et al., 2006). This raised the question how the strong Dpp activity seen in *Tc-smurf* RNAi embryos can be accomplished. During early germ band stages, *Tc-sog* is expressed in the midline of the embryo. During further germ band elongation, expression is seen in two stripes directly at the midline that extend into the headlobes where they form prominent expression domains. Except for the growth zone, the mesoderm is free of *Tc-sog* expression during germ band stages (see also van der Zee et al., 2006). In *Tc-smurf* RNAi embryos, *Tc-sog* expression in the head lobes and the anterior germ band was reduced or gone while in the growth zone it could still be detected (Figure 4-18). This indicates that Dpp-signaling in the anterior embryo inhibited *Tc-sog* expres-

sion. The detailed mechanism, how Tc-Dpp inhibits *Tc-sog* expression is still unclear. It is possible that pMAD in concert with Medea and other regulators acts directly as a repressing transcription factor, but it is just as well possible that Tc-Dpp signaling leads to the expression of target genes which in turn repress the expression of *Tc-sog*. One more indication that Dpp signaling inhibits the expression of *Tc-sog* is given by the expression of both genes during differentiated blastoderm stages. *Tc-sog* is expressed intensely on the ventral side of the *Tribolium* embryo. Only a thin stripe, a few cells wide, is free of *Tc-sog* expression. These cells are located at the border between the prospective germ rudiment and the serosa and display the *Tc-dpp* expressing cells during this stage (van der Zee et al., 2006). Hence it might well be that *Tc-dpp* expression already inhibits the expression of *Tc-sog* during these stages of development.

5.2.4.3 An anterior Tc-Dpp signaling center results in severe cell death

The ectopic Tc-Dpp signal in *Tc-smurf* RNAi embryos leads to severe apoptosis in the anterior embryo during germ band stages which explains the missing anterior body regions. This effect of the ectopic Tc-Dpp signal might be explained by the assumption that the cells in this region are already specified to mesodermal, neuroectodermal, and ectodermal fate. This is indicated by the expression of markers like *Tc-twist*, *Tc-achaete-scute*, *Tc-dpp* or *Tc-pannier* in very clearly defined cell populations in germ band stage embryos (Chen et al., 2000; Sommer and Tautz, 1994; van der Zee et al., 2006; Wheeler et al., 2005). If cells specified to mesodermal or neuroectodermal fate receive a Tc-Dpp signal they are suddenly located in a wrong signaling environment which then probably results in an apoptosis response. This would explain why apoptosis in *Tc-smurf* RNAi embryos was not seen before gastrulation. However, during live imaging a high number of embryos did not develop to the differentiated blastoderm stage. Hence it can not be excluded that unusually high cellular levels of pMAD can already be sufficient to induce apoptosis.

The proposed model explains the anterior deletion phenotypes observed after *Tc-smurf* RNAi. The embryo shows an anterior region, with ubiquitous Tc-Dpp-signaling which maintains its own activity and at the same time transduces its signal to neighboring cells. This signal inhibits the expression of the inhibitor Tc-Sog. In the posterior, the embryo develops in a wild type manner and expresses Tc-

Sog, which is necessary to establish proper dorsal-ventral polarity. Tc-Smurf is probably not essential to pattern the growth zone derived segments of the embryo in presence of sufficient levels of Tc-Sog. According to the proposed model there are two possibilities for what can happen in individual embryos. Either the wave of Tc-Dpp signal is transduced in anterior-posterior direction through the entire embryo, resulting in the death of all embryonic cells and in an empty egg phenotype in cuticle preparations. Or the combined action of Tc-Dpp inhibitors, most of all probably Tc-Sog, is strong enough to stop the Dpp signal at a certain point. This would cut off the ectopic signaling wave, resulting in proper development of the posterior segments as seen in many *Tc-smurf* RNAi cuticle phenotypes. It might also be that the anterior *Tc-dpp* expressing cells sometimes die before the Dpp signal can be transduced to the more posterior cells. In this explanation the wave of cell death would overrun the Tc-Dpp signaling wave and would also result in properly established posterior segments. The germ band stage embryos shown in Figure 4-16 argue more for the first explanation, but also both ways might be present. Figure 5-2 summarizes the proposed model.

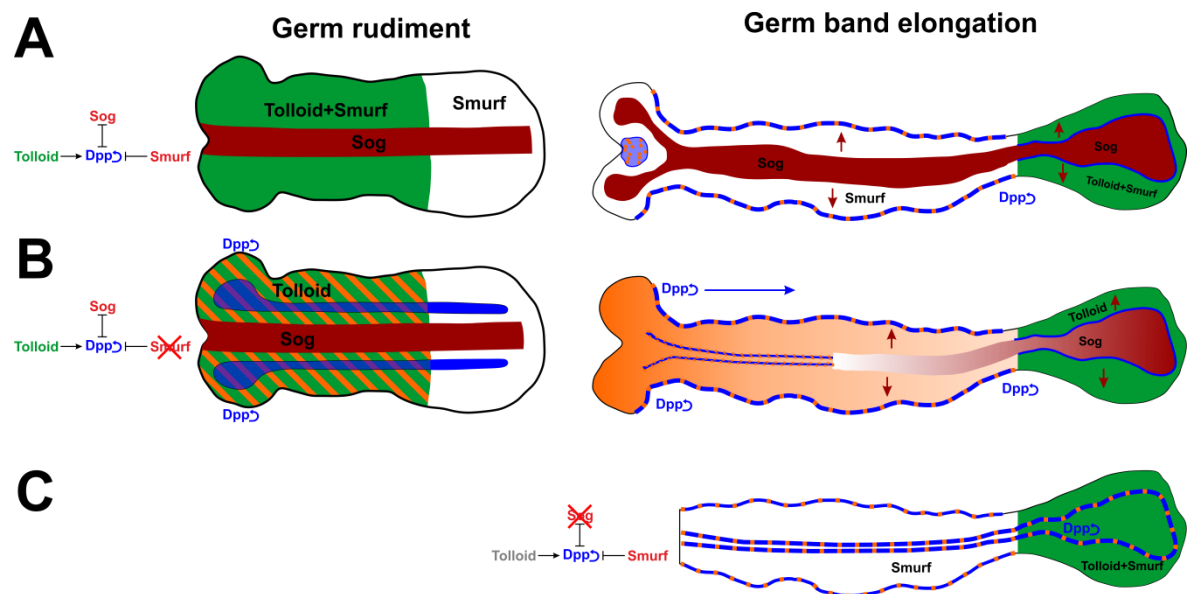


Figure 5-2 Model for the action of Dpp regulators during germ band stages in *Tribolium*

Given are simplified schematics for germ rudiment stages and germ band elongation stages with the regions of expression for *Tc-dpp* (solid blue), *Tc-sog* (red), and *Tc-tld* (green). Dpp signaling detected by pMAD (orange) often corresponds to *Tc-dpp* expression and is in those cases indicated by blue and orange lines or areas. In addition to the growth zone expression, *Tc-tld* is also expressed in the stomodeum during germ band elongation in the wild type (not indicated). Anterior to the left. (A) Wild type situation. *Tc-smurf* is expressed in all cells, *Tc-sog* is expressed in a ventral stripe in the germ rudiment. *Tc-tld* is expressed in two broad anterior domains (green), restricted only from the mesoderm (*Tc-sog* expressing cells). *Tc-smurf* and *Tc-sog* inhibit Tc-

Dpp signaling within inner regions of the germ rudiment. During germ band elongation, Tc-Sog and Tc-Tld restrict Tc-Dpp signaling to the dorsal margin where it autoactivates its own expression. Tc-Smurf and Tc-Sog inhibit Tc-Dpp signaling outside the dorsal ectoderm. TcDpp signaling is restricted also from the growth zone (no pMAD is present). **(B)** After loss of Tc-Smurf function, Tc-Tld induces Tc-Dpp-signaling in the anterior of the germ rudiment (green and orange area). Tc-Sog activity is not sufficient to inhibit Tc-Dpp. Tc-Dpp autoactivates its own expression, causing ectopic *Tc-dpp* expression domains (blue). This results in an anterior signaling center of Tc-Dpp. Tc-Dpp signaling at the same time inhibits expression of *Tc-sog*, leading to loss of anterior *Tc-sog* expression during germ band elongation. During germ band elongation segments are added from the posterior growth zone. Action of Tc-Sog and Tc-Tld is sufficient for the establishment of proper dorsal-ventral polarity in these segments. In the anterior region, Tc-Dpp transduces its own signal towards posterior. The signaling wave either moves through the entire embryo, giving eventually rise to death of all embryonic cells. Or action of Tc-Sog (and potential other inhibitors) blocks the Tc-Dpp-signal at a certain point, resulting in proper development of the more posterior segments. **(C)** Loss of Tc-Sog function results in ectopic expression of *Tc-dpp* in ventral ectodermal stripes where Tc-Dpp activates its own expression. Lack of Tc-Dpp transport due to missing Tc-Sog results in reduced or lost Tc-Dpp expression in the dorsal margin. Tc-Smurf inhibits spreading of the Tc-Dpp signal from the ventral ectodermal domains. Most of the head is never established in *Tc-sog* RNAi embryos. This model integrates results from this study with previously published results (Nunes da Fonseca et al., 2010; van der Zee et al., 2006).

5.2.5 Outlook and conclusions for the function of *Tc-smurf* during embryogenesis

The proposed model for Tc-Smurf function in *Tribolium* can explain all observed phenotypes. However, to proof all assumptions some more experiments need to be done. First of all the expression of *Tc-tld* in *Tc-smurf* RNAi background needs to be determined to verify that *Tc-tld* is actually active during the differentiated blastoderm and germ rudiment stage in these embryos. For the exact expression domains of some of the mentioned genes a few more *in situ* and double *in situ* hybridization stainings are necessary and will be done in the near future. It is possible that also other factors are involved in regulating Dpp signaling during *Tribolium* development and might play a role in the observed phenotypes. One candidate that would be worth studying is the gene *Tc-bambi*, which encodes a pseudoreceptor and is expressed at the dorsal margin during germ band stages (Nunes da Fonseca et al., 2008). It is not yet clear whether the pre-blastodermal defects seen in a subset of embryos after *Tc-smurf* RNAi are directly due to overactive Tc-Dpp signaling. This question could possibly be ruled out by double RNAi experiments against *Tc-dpp* and *Tc-smurf*. Since other pathways have been described to act on MAD/Smad1/5/8 (see Introduction, 2.6.1.2) an effect of *Tc-smurf* on other pathways is not unlikely. Double RNAi experiments can also be beneficial

to learn more about the interactions of the different signaling modulators. Knock down of the function of both *Tc-smurf* and *Tc-sog* might lead to synergistic effects with high levels of pMAD all over the embryo. Double RNAi against *Tc-tld* and *Tc-smurf* can identify whether *Tc-smurf* function is solely necessary to counteract the function of *Tc-tld*.

5.2.6 Smurf is more important for embryonic patterning in *Tribolium* than in *Drosophila*

The *Tc-smurf* RNAi phenotype is much more severe than the phenotype described for loss of *DSmurf* function in *Drosophila*. Loss of function mutations for *DSmurf* result in cuticle phenotypes which show a posterior hole, subtle head defects, and sometimes a dorsal closure defect. The most prominent effect of loss of *DSmurf* function is a defect in hindgut organogenesis (Podos et al., 2001). *DSmurf* is thus of minor importance for embryonic patterning in *Drosophila*. The differences seen between the fly and the beetle are probably due to the different modes of development and differences in the establishment of the dorsal-ventral (DV) axis between *Tribolium* and *Drosophila*. As mentioned in the introduction section (2.5), *Drosophila* makes use of a very defined patterning system along the DV-axis with spatial expression of activators and repressors, resulting in an embryo with horizontal ‘stripes’ of different dorsal-ventral cell fate, perpendicular to the anterior-posterior axis. Thus in the fly a coordinate system is established, and cell fate borders are to a high degree defined by spatial regulation of gene expression (see introduction and Lynch and Roth, 2011). Establishment of such a system appears to be a useful mode, since all body segments are established at the same time during blastoderm stages and can hence also already be patterned with respect to their dorsal-ventral fate directly by maternal informational input. *DSmurf* as an ubiquitously expressed intracellular regulator does not have an important function during this patterning process, although loss of *DSmurf* function leads to spatial expansion of Dpp signaling on the dorsal side (Podos et al., 2001).

Tribolium development involves a high degree of cell movements already before gastrulation (Benton et al., 2013; Handel et al., 2000) and the transcriptional interaction in the dorsal-ventral patterning network appears to involve much less components, is probably also less complex than in *Drosophila*, and is more dependent on zygotic gene regulation than maternal information (Lynch and Roth,

2011). However, Tc-Dpp signaling in *Tribolium* is of high importance for embryonic patterning during blastoderm stages as well as during germ band elongation. Tc-Dpp signaling is involved in setting the border between embryonic and extraembryonic tissue during the differentiated blastoderm stage and *Tc-smurf* has an important function in this process. Aberrations in Tc-Dpp signaling levels cause defects in head formation. My results suggest that the switch from the differentiated blastoderm stage to germ rudiment and germ band elongation is a critical step during *Tribolium* development. If at this step Tc-Dpp signaling in the anterior embryonic tissue is not terminated by Tc-Smurf, an ectopic Tc-Dpp signaling center is established that can eventually result in death of all embryonic cells. Hence one of the main functions of *Tc-smurf* during development seems to be the setting of strict borders between cells that respond to Tc-Dpp ligands and cells where the Tc-Dpp signal is terminated. It might be that the much higher importance of Smurf in *Tribolium* compared to *Drosophila* is due to the very dynamic way of *Tribolium* development in terms of cell movements during early patterning processes.

During germ band elongation, Tc-Dpp signaling is necessary to specify the dorsal ectoderm of the *Tribolium* embryo. According to my model, *Tc-smurf* function does not seem to be essential during the segment addition process since the posterior region still shows dorsal-ventral polarity in those animals that succeed to secrete a cuticle. Marker gene expression for mesodermal and neuroectodermal fate also suggest that the segments are properly established (Figure 4-20). It would be interesting to see whether in other arthropods Smurf proteins are of higher importance also during this process.

5.2.7 Smurf proteins as ancestral regulators of TGF- β signaling

Smurf proteins are conserved within the metazoans. The first member, Smurf1, has been detected in the late 1990s in an approach to identify new members of the SMAD pathway in *Xenopus*, closely followed by the identification of the second member, Smurf2 (Lin et al., 2000; Zhang et al., 2001; Zhu et al., 1999). Despite having been identified as proteins that regulate the degradation of receptor regulated Smads (R-Smads), more and more targets for these E3 ubiquitin ligases have been identified during the last years including many components of the TGF- β pathway (Ebisawa et al., 2001; Kavsak et al., 2000; Murakami et al., 2003; reviewed in Inoue and Imamura, 2008 and Cao and Zhang, 2012). Hence the sum

of substrates of these enzymes remains to be determined. My results suggest that the *Smurf* genes have duplicated somewhere in the deuterostome lineage, since I could neither detect a second *Smurf* gene within the protostomes that I used for phylogenetic analysis nor in the Ctenophore *Mnemiopsis leidyi* or the placozoan *Trichoplax adhaerens*.

The finding of a *smurf* homolog in an approach to identify members of the TGF- β signaling pathway in *Mnemiopsis leidyi* (Pang et al., 2011) has been an interesting finding. Recent phylogenetic analysis using amino acid positions and gene content tends to group the Ctenophora as a sister group of all metazoans (Ryan et al., 2013). The TGF- β pathway is believed to have established early in metazoan evolution and many components of this pathway, including *smurf* genes, could be identified in *M. leidyi* as well as in the placozoan *Trichoplax adhaerens* and in Cnidarians (Huminiacki et al., 2009; Pang et al., 2011; Richards and Degnan, 2009). According to these observations it might be that a functional Smurf E3 ubiquitin ligase already belonged to the initial set of TGF- β signaling components. Functional analysis of *smurf* genes in basic metazoan species could give interesting information about the initial regulation of TGF- β signaling during evolution.

5.3 *TC004374*

TC004374 was mainly analyzed in parallel to *Tc-smurf*, but much remains open for this gene. Due to lack of time, many results are still in a preliminary state and experiments have to be repeated or expanded in order to analyze for instance some embryonic stages in more detail or to confirm certain findings.

5.3.1 *TC004374* encodes a molecule of unknown function

Only RNAi against a 3' region of the annotated gene model for *TC004374* resulted in an anterior patterning phenotype. Although the observed phenotype is very consistent, the mechanism underlying the anterior patterning defect is still entirely enigmatic. Based on transcriptome data, the *Tribolium* gene browser suggests a small transcript for *TC004374* which codes for a 82 AA polypeptide with no conserved domain (based on results using PROSITE, Swiss Institute for Bioinformatics). The enzymatic NUDIX domain is encoded in the exons 1 and 2 and is

thus not present in the part of the sequence that is necessary for proper anterior patterning. Hence the molecular function of *TC004374* for anterior patterning does not depend on the hydrolase activity. One possibility is that the small transcript encodes for a regulatory small peptide. Small peptides have come more into focus of research during the last years and are involved in development both of plants and animals (Hashimoto et al., 2008; Murphy et al., 2012; Savard et al., 2006).

Searching transcriptome data on the *Tribolium* gene browser (<http://bioinf.uni-greifswald.de/gb2/gbrowse/tribolium/>) for reads that expand 5' to exon 3 but do not belong to exon 2 did not result in an unambiguous identification of the g488.t3 transcript. However, this does not exclude the possibility that this transcript exists since small reads are often excluded from transcriptome analysis. The small transcript could so far also not be confirmed with 5'RACE PCR. Although I have selected for small PCR fragments when I chose DNA fragments for subcloning after RACE PCR it might still be that a potential small transcript corresponding to the g488.t3 AUGUSTUS annotation was present but heavily outnumbered by other transcripts. The first strand RACE cDNA pool used consisted of an embryo collection from 0-72 h of age and thus represented transcripts of almost all embryonic stages. If the small transcript was only present during very early stages of development it might be that the longer transcript, coding for the entire nudix hydrolase, was present in far excess compared to the small version which therefore made an isolation via RACE PCR difficult. To clarify whether the annotated transcript is present, RACE PCR experiments on a cDNA pool from 0–12 hours of development could serve useful. Based on the observed phenotype the transcript is present during this time period and it might be that the long *TC004374* transcript is not or less strongly expressed early in embryonic development. Due to the shortage of time these experiments have not yet been done and it remains open how *TC004374* acts on a molecular level. In the next sections I will discuss how this gene might function during early developmental processes based on the available experimental results. Owing to the lack of molecular information for *TC004374* the model is still hypothetical.

5.3.2 Potential function of *TC004374* in MAD regulation

The observed phenotypes for *TC004374* RNAi embryos were highly similar to the phenotypes observed after *Tc-smurf* knock down. Differences in both gene

knock downs affected in particular the strength and the penetrance of the phenotypes: with knock down of *Tc-smurf* resulting generally in stronger phenotypes and higher penetrance. Determination of *Tc-six3* expression in *TC004374* RNAi embryos showed that the expression domains marking neuronal precursors were most prone to loss of *TC004374* function while the central domain which later marks clypeus, labrum and stomodeum reacted less sensitively (Figure 4-30; Kittelmann, 2012; Posnien et al., 2011 for *Tc-six3* expression). This is an indication that *TC004374* is necessary for anterior neuroectoderm formation. Knock down of *TC004374* led to an accumulation of pMAD in the headlobes, which is an interesting similarity to the *Tc-smurf* RNAi phenotype. According to the aforementioned model for *Tc-smurf* function the ectopic pMAD domain is likely to be the reason for the missing head tissue and anterior body regions seen in *TC004374* RNAi embryos. Preliminary results also show *Tc-dpp* expression in headlobes of *TC004374* RNAi embryos, supporting the model shown in Figure 5-2. However, it is not clear how the ectopic pMAD domain arises. There is not many information available for Nudix hydrolases and substrate specificity is known for less than 1 % of all members of the Nudix family (Xu et al., 2013). Interestingly, one *Nudix* member in *Xenopus*, *NUDT22* (also called *P17F11*) was detected in a screening approach to identify head organizer specific genes in the frog and might play a role in neural induction during development (McLennan, 2005; Shibata et al., 2001). Another function of a Nudix hydrolase that is interesting in the context of the here described results has been reported for murine *NUDT3* which is involved in MAP kinase signaling. It was shown that overexpression of *NUDT3* negatively regulated MAPK signaling in the mouse, suggesting that *NUDT3* has an inhibitory function in this process (Chu et al., 2004). In my experiments activated MAPK (pMAPK) was lost in the head lobes of *TC004374* RNAi embryos. This suggests that function of *TC004374* in MAPK regulation is contrary to the function of murine *NUDT3* since the one molecule activates and the other one inhibits the activation of MAPK. This is not too surprising as the transcript that causes the phenotype in *Tribolium* does probably not contain an enzymatic domain, which means that it probably has a different biochemical function. However, this function so far remains elusive. Still, a function of *TC004374* to activate MAPK signaling would make sense with respect to the observed increase of pMAD.

During the last years it has become more and more obvious that the MAPK (ERK1/2), BMP/Dpp and Wnt signaling pathways can be integrated via specific phosphorylation sites on the MAD/Smad1/5/8 protein (Eivers et al., 2008; Eivers et al., 2009b, see introduction). MAPK and Glycogen Synthase Kinase-3 (GSK3) can phosphorylate vertebrate and *Drosophila* MAD/Smad1/5/8 in the linker region. This linker phosphorylation leads to Smurf mediated ubiquitination and degradation of MAD/Smad1/5/8 (Eivers et al., 2008; Fuentealba et al., 2007; Kretzschmar et al., 1997; Sapkota et al., 2007). GSK3 usually needs a priming phosphorylation at a serine or threonine residue four amino acids carboxyterminal to a serine that can in turn be phosphorylated by GSK3 (S/T XXX S/T) (Cohen and Frame, 2001). In *Drosophila*, the serine within the canonical MAPK phosphorylation site was identified to potentially serve for a priming phosphorylation (Eivers et al., 2008; Eivers et al., 2009a). According to the proposed model it is possible that in a so far not known way *TC004374* is necessary for the activation of MAPK in the anterior germ rudiment and the headlobes of germ band stage embryos. Failure in this function would lead to missing pMAPK mediated linker phosphorylation. This again could result in an accumulation of Dpp-activated pMAD in the anterior of the embryo as seen in *TC004374* RNAi embryos (Figure 4-30). In Tc-MAD an additional asparagine was identified in the amino acids aminoterminal to the canonical MAPK phosphorylation site which leads to loss of the consensus motif for GSK3 phosphorylation (Figure 5-3 D). Without biochemical analysis, it cannot be said if this inhibits GSK3 phosphorylation of Tc-MAD. The linker region of Tc-MAD is rich in serines, presenting many potential sites for phosphorylation. Additionally, it might be that CDK8/9 mediated phosphorylation is also involved in priming Tc-MAD for GSK3 phosphorylation. CDK8/9 phosphorylation has been reported to be involved in regulation of Smad molecules in vertebrates and phosphorylation sites for these enzymes have also been described for *Drosophila* MAD (Alarcon et al., 2009; Aragón et al., 2011; Eivers et al., 2011). Detailed biochemical approaches would be necessary to ascertain which factors are involved in MAD phosphorylation in *Tribolium* and how they act on MAD regulation.

Previous studies have shown that active MAPK is present in the region of the germ serosa boundary (prospective anterior amnion) of differentiated blastoderm stage embryos (Schoppmeier and Schröder, 2005 and Figure 5-3 A+B). Since this stage is very short, I could not yet analyze enough *TC004374* RNAi embryos to

reliably say whether this pMAPK domain is lost after *TC004374* RNAi. Analyzing this specific stage in detail for MAPK activity would be necessary to clearly determine *TC004374* function during the differentiated blastoderm stage. Nevertheless, pMAPK is missing in the headlobes of phenotypic germ band stage *TC004374* RNAi embryos. This can be a secondary effect due to missing tissue, but also a primary effect due to missing MAPK activation through *TC004374*. A function of *TC004374* in specifically activating MAPK in the embryonic head lobes would explain why anterior patterning phenotypes for *TC004374* RNAi are usually weaker than *Tc-smurf* RNAi phenotypes. Since Tc-Sog and Tc-Smurf are probably still active in the germ band of *TC004374* RNAi embryos these two inhibitors are probably able to stop an anterior located, ectopic Dpp signaling center caused by *TC004374* knock down. This would also explain why only few *TC004374* RNAi embryos showed excessive apoptosis in the anterior germ band. No localized expression could be detected for *TC004374* which makes a localized upstream or downstream factor likely to restrict *TC004374* action to the anterior. Much remains to be done to understand the function of this gene. The first step would be to clarify the transcript targeted by the knock down of the 3' region of *TC004374* and to identify the molecular identity of the encoded gene product.

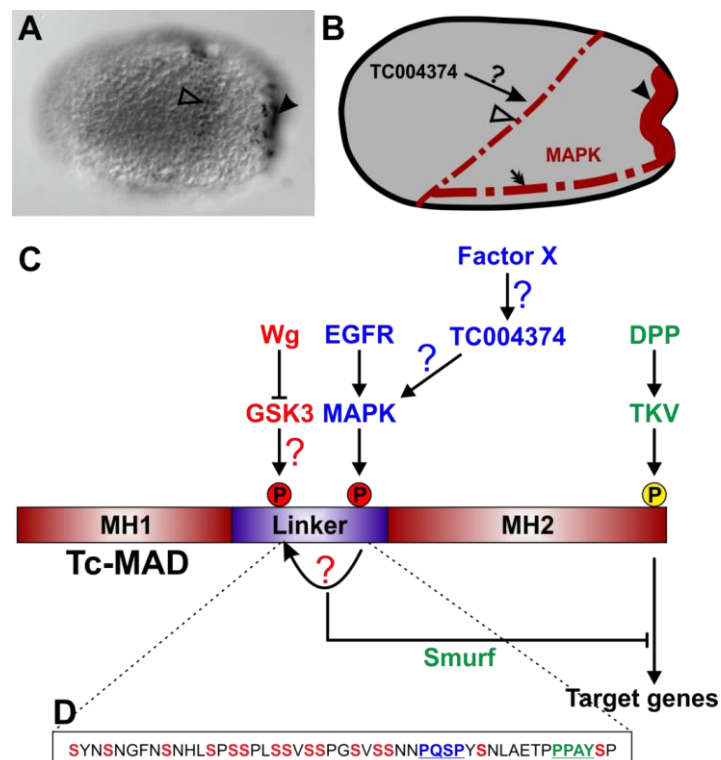


Figure 5-3 Potential function of TC004374 on MAD regulation

Anterior to the left in A and B. Dorsal side up in A, lateral view in B. B shows a schematic drawing of the regions with active MAPK during the differentiated blastoderm stage based on my results and Schoppmeier and Schröder, (2005). **(A+B)** During differentiated blastoderm stages pMAPK can be detected at the germ serosa boundary (open arrowhead), in the posterior pit (black arrowhead), and at the mesodermal margin (small arrow in B). My results suggest that TC004374 might be involved in activating MAPK in the region of the germ serosa boundary. **(C)** Model of different pathways interacting on Tc-MAD, modified after Eivers et al., (2008). Dpp signaling via Thickveins phosphorylates Tc-MAD at the C-terminal site, resulting in target gene regulation. Phosphorylations of MAD in the linker region result in proteosomal degradation by Tc-Smurf, thereby terminating the signal. TC004374 might act via an unknown localized factor to activate MAPK in the anterior of the germ rudiment. Alternatively, a localized factor X activates TC004374 which might then directly activate MAPK. **D** shows a selected amino acid sequence of the linker region of Tc-MAD. PPAY (green) indicates the binding motif for Smurf, PQSP (blue) is the recognition sequence for MAPK. All other serine residues are marked in red.

5.3.3 TC004374 is necessary for proper amnion development

RNAi against *TC004374* led to increased cell death in germ band stage embryos. However, excessive apoptosis in the anterior embryo was found in far less embryos than observed after knock down of *Tc-smurf*. Additionally, the head lobes of *TC004374* RNAi embryos were often already smaller in very early germ band stage embryos, indicating that head patterning was affected before the germ rudiment condensed on the ventral side of the embryo. A likely explanation for the reduced headlobes is impaired amnion development. In the Dipteran *Megaselia*, RNAi against genes of the *u-shaped* group causes loss of the amnion, resulting in head as well as dorsal closure defects, which suggests that the amnion is directly necessary for head formation (Rafiqi et al., 2010). This assumption was strengthened by the finding that the extraembryonic membrane-expressed *u-shaped* group gene *Tc-tailup* is necessary for labrum development in *Tribolium* (Kittelmann, 2012). *TC004374* RNAi embryos show a delay in the formation of the amniotic fold and severe cell death at the embryonic margin, in the region where the embryo proper is connected to the extraembryonic membranes. As already mentioned, MAPK is active in the region of the germ serosa border in a domain which is independent from the terminal system (Schoppmeier et al., 2009 and Figure 5-3 A+B). This region forms the prospective amnion as shown for instance by expression of the amnion marker *Tc-iroquois* (Kotkamp et al., 2010; Nunes da Fonseca et al., 2008; Sharma et al., 2013; Tomoyasu et al., 2005; van der Zee et al., 2006). A necessity of *TC004374* for MAPK activation in the prospective amnion and in turn

requirement of pMAPK for the formation of functional amniotic tissue might explain the defects seen during amniotic fold formation as well as the excessive cell death during germ band stages. However, even if *TC004374* is not directly involved in MAPK activation, it is most likely necessary for proper amnion formation. The amnion is an extraembryonic membrane attached to the embryo and the serosa. Beginning with germ rudiment condensations on the ventral side of the embryo till closure of the serosa window, a membrane thickening and a higher level of F-actin is present at the amnion serosa boundary in *Tribolium* (Benton et al., 2013). Actomyosin cables have been described to be responsible for contractile forces in several different organisms and are probably also responsible for the amniotic fold formation and embryo enveloping in *Tribolium* (Behrndt et al., 2012; Benton et al., 2013; Kiehart et al., 2000; Martin and Lewis, 1992). The defects seen in *TC004374* RNAi embryos suggest defects in the anterior embryonic region and in the formation and regulation of this contractile force. The phenotype seen in the embryo with the strong delay in amniotic fold formation suggests an increased tension, starting at the differentiated blastoderm stage. This is indicated by the indentation seen at the dorsal posterior side of the embryo before amniotic fold formation and the eventual abrupt movement of the amniotic fold over the posterior pole seen in Figure 4-34. This phenotype is potentially induced by shortening of the actomyosin cables due for instance to missing or defect amniotic cells. Therefore the delay in amniotic fold formation and also the bend in the germ serosa boundary might be caused by mechanical defects. A second indication that *TC004374* is necessary for proper development of the amnion is the massive cell death seen at the direct margin of *TC004374* RNAi embryos. This cell death might be induced by impaired amnion differentiation or maintenance. A possible approach to visualize the effect of *TC004374* on amnion formation would be to perform live imaging experiments using embryonic RNAi against *TC004374* simultaneously with transient expression of a membrane marker like GAP43-GFP. This technique has been used successfully before (Benton et al., 2013) and could help to shed some light on the function of this gene. Another approach would be to determine very carefully the expression of the anterior amnion marker *Tc-iroquois* in *TC004374* RNAi embryos (Nunes da Fonseca et al., 2008; Nunes da Fonseca et al., 2010; Sharma et al., 2013).

5.4 General conclusions

The aim of this study was to use the approach of a reverse genetic screen to identify new genes required for anterior patterning by overcoming the candidate gene approach. Hence, a conclusive question is whether the candidates identified during this study would have been identified without the iBeetle screen.

A good collection of functional and biochemical data was available for Smurf proteins in vertebrates and there were also some studies available from *Drosophila* (see introduction 2.6.1.1). However, functional data outside the vertebrates and *Drosophila* was not present. There are two good reasons to assume that *Tc-smurf* would not have been chosen for functional analysis in a candidate gene approach in near future. First, the loss of function phenotype for *DSmurf* in *Drosophila* is weak, suggesting a minor function in embryonic patterning processes for this gene. Second, Smurf proteins are reported regulators of the Dpp/BMP pathway. In a candidate gene approach, *Tc-smurf* would probably not have been selected as a candidate which is required for anterior patterning processes. However, *Tc-smurf* might have been selected one day for analysis of dorsal-ventral patterning processes and the regulation of Dpp-signaling in *Tribolium*.

While there was a chance that *Tc-smurf* would have been selected for a candidate gene approach sometime in the future, this would most likely not have happened for *TC004374*. There was no data for this gene available that would have given reason to analyze its function in early patterning processes. For the identification of candidates like *TC004374* comprehensive and unbiased approaches are necessary. But also for the identification of unexpected functions for already described factors an approach like the iBeetle screen can serve useful.

Altogether it is interesting that the approach to identify anterior patterning genes in a short germ developing insect led to the identification of two genes which are both in some way involved in the regulation of Tc-MAD during early development. There were a number of other dsRNAs that gave rise to anterior patterning phenotypes during the screen and more are like to be detected during the ongoing screening process. It will be exiting to see whether some of them are also involved in fine tuning the activity of Tc-MAD during early *Tribolium* development.

6 References

- Akiyama-Oda, Y. and Oda, H.** (2006). Axis specification in the spider embryo: *dpp* is required for radial-to-axial symmetry transformation and *sog* for ventral patterning. *Development* **133**, 2347–2357.
- Alarcon, C., Zaromytidou, A.-I., Xi, Q., Gao, S., Yu, J., Fujisawa, S., Barlas, A., Miller, A. N., Manova-Todorova, K., Macias, M. J., et al.** (2009). CDK8/9 drive Smad transcriptional action, turnover and YAP interactions in BMP and TGF β pathways. *Cell* **139**, 757–769.
- Alexandrova, E. M. and Thomsen, G. H.** (2006). Smurf1 regulates neural patterning and folding in *Xenopus* embryos by antagonizing the BMP/Smad1 pathway. *Dev. Biol.* **299**, 398–410.
- Altschul, S. F., Gish, W., Miller, W., Myers, E. W. and Lipman, D. J.** (1990). Basic local alignment search tool. *J. Mol. Biol.* **215**, 403–410.
- Ambegaonkar, A. A., Pan, G., Mani, M., Feng, Y. and Irvine, K. D.** (2012). Propagation of Dachsous-Fat Planar Cell Polarity. *Curr. Biol.* **22**, 1302–1308.
- Aragón, E., Goerner, N., Zaromytidou, A.-I., Xi, Q., Escobedo, A., Massagué, J. and Macias, M. J.** (2011). A Smad action turnover switch operated by WW domain readers of a phosphoserine code. *Genes Dev.* **25**, 1275–1288.
- Arakane, Y., Muthukrishnan, S., Kramer, K. J., Specht, C. A., Tomoyasu, Y., Lorenzen, M. D., Kanost, M. and Beeman, R. W.** (2005). The *Tribolium* chitin synthase genes *TcCHS1* and *TcCHS2* are specialized for synthesis of epidermal cuticle and midgut peritrophic matrix. *Insect Mol. Biol.* **14**, 453–463.
- Attisano, L. and Tuen Lee-Hoeflich, S.** (2001). The Smads. *Genome Biol.* **2**, reviews3010.1–reviews3010.8.
- Bai, S., Shi, X., Yang, X. and Cao, X.** (2000). Smad6 as a Transcriptional Corepressor. *J. Biol. Chem.* **275**, 8267–8270.
- Baker, N. E.** (1988). Localization of transcripts from the wingless gene in whole *Drosophila* embryos. *Development* **103**, 289–298.
- Balemans, W. and Van Hul, W.** (2002). Extracellular Regulation of BMP Signaling in Vertebrates: A Cocktail of Modulators. *Dev. Biol.* **250**, 231–250.
- Barker, D. D., Wang, C., Moore, J., Dickinson, L. K. and Lehmann, R.** (1992). *Pumilio* is essential for function but not for distribution of the *Drosophila* abdominal determinant *Nanos*. *Genes Dev.* **6**, 2312–2326.
- Behrndt, M., Salbreux, G., Campinho, P., Hauschild, R., Oswald, F., Roensch, J., Grill, S. W. and Heisenberg, C.-P.** (2012). Forces driving epithelial spreading in zebrafish gastrulation. *Science* **338**, 257–260.
- Benton, M. A. and Pavlopoulos, A.** (2014). *Tribolium* embryo morphogenesis: May the force be with you. *BioArchitecture* **4**, 0–1.
- Benton, M. A., Akam, M. and Pavlopoulos, A.** (2013). Cell and tissue dynamics during *Tribolium* embryogenesis revealed by versatile fluorescence labeling approaches. *Development* **140**, 3210–3220.

- Berghammer, A., Bucher, G., Maderspacher, F. and Klingler, M.** (1999a). A system to efficiently maintain embryonic lethal mutations in the flour beetle *Tribolium castaneum*. *Dev. Genes Evol.* **209**, 382–389.
- Berghammer, A. J., Klingler, M. and Wimmer, E. A.** (1999b). A universal marker for transgenic insects. *Nature* **402**, 370–371.
- Bessman, M. J., Frick, D. N. and O’Handley, S. F.** (1996). The MutT Proteins or “Nudix” Hydrolases, a Family of Versatile, Widely Distributed, “Housecleaning” Enzymes. *J. Biol. Chem.* **271**, 25059–25062.
- Biehs, B., François, V. and Bier, E.** (1996). The *Drosophila* short gastrulation gene prevents Dpp from autoactivating and suppressing neurogenesis in the neuroectoderm. *Genes Dev.* **10**, 2922–2934.
- Biemar, F., Nix, D. A., Piel, J., Peterson, B., Ronshaugen, M., Sementchenko, V., Bell, I., Manak, J. R. and Levine, M. S.** (2006). Comprehensive identification of *Drosophila* dorsal–ventral patterning genes using a whole-genome tiling array. *Proc. Natl. Acad. Sci.* **103**, 12763–12768.
- Bier, E.** (1997). Anti-neural-inhibition: a conserved mechanism for neural induction. *Cell* **89**, 681–684.
- Bilic, J., Huang, Y.-L., Davidson, G., Zimmermann, T., Cruciat, C.-M., Bienz, M. and Niehrs, C.** (2007). Wnt induces LRP6 signalosomes and promotes dishevelled-dependent LRP6 phosphorylation. *Science* **316**, 1619–1622.
- Bonds, M., Sands, J., Poulson, W., Harvey, C. and Von Ohlen, T.** (2007). Genetic screen for regulators of ind expression identifies shrew as encoding a novel twisted gastrulation-like protein involved in Dpp signaling. *Dev. Dyn.* **236**, 3524–3531.
- Brönner, G. and Jäckle, H.** (1991). Control and function of terminal gap gene activity in the posterior pole region of the *Drosophila* embryo. *Mech. Dev.* **35**, 205–211.
- Brown, S. J. and Denell, R. E.** (1996). Segmentation and dorsoventral patterning in *Tribolium*. *Semin. Cell Dev. Biol.* **7**, 553–560.
- Brown, S. J., Patel, N. H. and Denell, R. E.** (1994). Embryonic expression of the single *Tribolium* engrailed homolog. *Dev. Genet.* **15**, 7–18.
- Brown, S. J., Mahaffey, J. P., Lorenzen, M. D., Denell, R. E. and Mahaffey, J. W.** (1999a). Using RNAi to investigate orthologous homeotic gene function during development of distantly related insects. *Evol. Dev.* **1**, 11–15.
- Brown, S., Holtzman, S., Kaufman, T. and Denell, R.** (1999b). Characterization of the *Tribolium* Deformed ortholog and its ability to directly regulate Deformed target genes in the rescue of a *Drosophila* Deformed null mutant. *Dev. Genes Evol.* **209**, 389–398.
- Brown, S., Fellers, J., Shippy, T., Denell, R., Stauber, M. and Schmidt-Ott, U.** (2001). A strategy for mapping bicoid on the phylogenetic tree. *Curr. Biol. CB* **11**, R43–44.
- Brown, S. J., Shippy, T. D., Miller, S., Bolognesi, R., Beeman, R. W., Lorenzen, M. D., Bucher, G., Wimmer, E. A. and Klingler, M.** (2009). The Red

Flour Beetle, *Tribolium castaneum* (Coleoptera): A Model for Studies of Development and Pest Biology. *Cold Spring Harb. Protoc.* **2009**, pdb.emo126–pdb.emo126.

Bucher, G. and Klingler, M. (2004). Divergent segmentation mechanism in the short germ insect *Tribolium* revealed by giant expression and function. *Development* **131**, 1729–1740.

Bucher, G. and Wimmer, E. A. (2005). Beetle a-head. *BIF FUTURA* **20**, 164–169.

Bucher, G., Scholten, J. and Klingler, M. (2002). Parental RNAi in *Tribolium* (Coleoptera). *Curr. Biol.* **12**, R85–R86.

Cao, Y. and Zhang, L. (2012). A Smurf1 tale: function and regulation of an ubiquitin ligase in multiple cellular networks. *Cell. Mol. Life Sci. CMLS.*

Carroll, S. B., Laughon, A. and Thalley, B. S. (1988). Expression, function, and regulation of the hairy segmentation protein in the *Drosophila* embryo. *Genes Dev.* **2**, 883–890.

Casanova, J. and Struhl, G. (1989). Localized surface activity of torso, a receptor tyrosine kinase, specifies terminal body pattern in *Drosophila*. *Genes Dev.* **3**, 2025–2038.

Casanueva, M. O. and Ferguson, E. L. (2004). Germline stem cell number in the *Drosophila* ovary is regulated by redundant mechanisms that control Dpp signaling. *Development* **131**, 1881–1890.

Casares, F. and Sanchez-Herrero, E. (1995). Regulation of the infraabdominal regions of the bithorax complex of *Drosophila* by gap genes. *Development* **121**, 1855–1866.

Cerny, A. C., Bucher, G., Schröder, R. and Klingler, M. (2005). Breakdown of abdominal patterning in the *Tribolium* Krüppel mutant jaws. *Development* **132**, 5353–5363.

Cerny, A. C., Grossmann, D., Bucher, G. and Klingler, M. (2008). The *Tribolium* ortholog of knirps and knirps-related is crucial for head segmentation but plays a minor role during abdominal patterning. *Dev. Biol.* **321**, 284–294.

Chang, Y.-J., Pi, H., Hsieh, C.-C. and Fuller, M. T. (2013). Smurf-mediated differential proteolysis generates dynamic BMP signaling in germline stem cells during *Drosophila* testis development. *Dev. Biol.*

Chen, C. K., Kuhnlein, R. P., Eulenberg, K. G., Vincent, S., Affolter, M. and Schuh, R. (1998). The transcription factors KNIRPS and KNIRPS RELATED control cell migration and branch morphogenesis during *Drosophila* tracheal. *Development* **125**, 4959–4968.

Chen, G., Handel, K. and Roth, S. (2000). The maternal NF-kappaB/dorsal gradient of *Tribolium castaneum*: dynamics of early dorsoventral patterning in a short-germ beetle. *Dev. Camb. Engl.* **127**, 5145–5156.

Chu, C., Alapat, D., Wen, X., Timo, K., Burstein, D., Lisanti, M., Shears, S. and Kohtz, D. S. (2004). Ectopic expression of murine diphosphoinositol polyphos-

- phate phosphohydrolase 1 attenuates signaling through the ERK1/2 pathway. *Cell Signal*. **16**, 1045–1059.
- Cohen, P. and Frame, S.** (2001). The renaissance of GSK3. *Nat. Rev. Mol. Cell Biol.* **2**, 769–776.
- Cohen, S. M. and Jürgens, G.** (1990). Mediation of *Drosophila* head development by gap-like segmentation genes. *Nature* **346**, 482–485.
- Copf, T., Schröder, R. and Averof, M.** (2004). Ancestral role of caudal genes in axis elongation and segmentation. *Proc. Natl. Acad. Sci. U. S. A.* **101**, 17711–17715.
- Curtis, C. D., Brisson, J. A., DeCamillis, M. A., Shippy, T. D., Brown, S. J. and Denell, R. E.** (2001). Molecular characterization of *Cephalothorax*, the *Tribolium* ortholog of *Sex combs reduced*. *genesis* **30**, 12–20.
- Das, S. and Chang, C.** (2012). Regulation of early *xenopus* embryogenesis by Smad ubiquitination regulatory factor 2. *Dev. Dyn. Off. Publ. Am. Assoc. Anat.* **241**, 1260–1273.
- Davis, G. K. and Patel, N. H.** (2002). Short, long, and beyond: molecular and embryological approaches to insect segmentation. *Annu. Rev. Entomol.* **47**, 669–699.
- De Robertis, E. M.** (2006). Spemann's organizer and self-regulation in amphibian embryos. *Nat. Rev. Mol. Cell Biol.* **7**, 296–302.
- De Robertis, E. M.** (2008). Evo-Devo: Variations on Ancestral Themes. *Cell* **132**, 185–195.
- De Robertis, E. M. and Kuroda, H.** (2004). Dorsal-Ventral Patterning and Neural Induction in *Xenopus* Embryos. *Annu. Rev. Cell Dev. Biol.* **20**, 285–308.
- De Robertis, E. M. and Sasai, Y.** (1996). A common plan for dorsoventral patterning in Bilateria. *Nature* **380**, 37–40.
- Denell, R.** (2008). Establishment of *Tribolium* as a Genetic Model System and Its Early Contributions to Evo-Devo. *Genetics* **180**, 1779–1786.
- Derynck, R. and Zhang, Y. E.** (2003). Smad-dependent and Smad-independent pathways in TGF-beta family signalling. *Nature* **425**, 577–584.
- DiNardo, S. and O'Farrell, P. H.** (1987). Establishment and refinement of segmental pattern in the *Drosophila* embryo: spatial control of engrailed expression by pair-rule genes. *Genes Dev.* **1**, 1212–1225.
- DiNardo, S., Kuner, J. M., Theis, J. and O'Farrell, P. H.** (1985). Development of embryonic pattern in *D. melanogaster* as revealed by accumulation of the nuclear engrailed protein. *Cell* **43**, 59–69.
- Dorfman, R. and Shilo, B. Z.** (2001). Biphasic activation of the BMP pathway patterns the *Drosophila* embryonic dorsal region. *Development* **128**, 965–972.
- Driever, W. and Nüsslein-Volhard, C.** (1988). The bicoid protein determines position in the *Drosophila* embryo in a concentration-dependent manner. *Cell* **54**, 95–104.

- Driever, W. and Nüsslein-Volhard, C.** (1989). The bicoid protein is a positive regulator of hunchback transcription in the early *Drosophila* embryo. *Nature* **337**, 138–143.
- Dubnau, J. and Struhl, G.** (1996). RNA recognition and translational regulation by a homeodomain protein. *Nature* **379**, 694–699.
- Ebisawa, T., Fukuchi, M., Murakami, G., Chiba, T., Tanaka, K., Imamura, T. and Miyazono, K.** (2001). Smurf1 Interacts with Transforming Growth Factor- β Type I Receptor through Smad7 and Induces Receptor Degradation. *J. Biol. Chem.* **276**, 12477–12480.
- Eivers, E., Fuentealba, L. C. and De Robertis, E. M.** (2008). Integrating positional information at the level of Smad1/5/8. *Curr. Opin. Genet. Dev.* **18**, 304–310.
- Eivers, E., Fuentealba, L. C., Sander, V., Clemens, J. C., Hartnett, L. and De Robertis, E. M.** (2009a). Mad is required for wingless signaling in wing development and segment patterning in *Drosophila*. *PLoS One* **4**, e6543.
- Eivers, E., Demagny, H. and De Robertis, E. M.** (2009b). Integration of BMP and Wnt signaling via vertebrate Smad1/5/8 and *Drosophila* Mad. *Cytokine Growth Factor Rev.* **20**, 357–365.
- Eivers, E., Demagny, H., Choi, R. H. and De Robertis, E. M.** (2011). Phosphorylation of Mad Controls Competition Between Wingless and BMP Signaling. *Sci. Signal.* **4**,.
- Eldar, A., Dorfman, R., Weiss, D., Ashe, H., Shilo, B.-Z. and Barkai, N.** (2002). Robustness of the BMP morphogen gradient in *Drosophila* embryonic patterning. *Nature* **419**, 304–308.
- Ephrussi, A., Dickinson, L. K. and Lehmann, R.** (1991). Oskar organizes the germ plasm and directs localization of the posterior determinant nanos. *Cell* **66**, 37–50.
- Falciani, F., Hausdorf, B., Schröder, R., Akam, M., Tautz, D., Denell, R. and Brown, S.** (1996). Class 3 Hox genes in insects and the origin of zen. *Proc. Natl. Acad. Sci.* **93**, 8479–8484.
- Felsenstein, J.** (1985). Confidence Limits on Phylogenies: An Approach Using the Bootstrap. *Evolution* **39**, 783.
- Feng, X.-H. and Derynck, R.** (2005). Specificity and versatility in tgf-beta signaling through Smads. *Annu. Rev. Cell Dev. Biol.* **21**, 659–693.
- Ferguson, E. L. and Anderson, K. V.** (1992). Localized enhancement and repression of the activity of the TGF-beta family member, decapentaplegic, is necessary for dorsal-ventral pattern formation in the *Drosophila* embryo. *Development* **114**, 583–597.
- Francois, V., Solloway, M., O'Neill, J. W., Emery, J. and Bier, E.** (1994). Dorsal-ventral patterning of the *Drosophila* embryo depends on a putative negative growth factor encoded by the short gastrulation gene. *Genes Dev.* **8**, 2602–2616.
- Frasch, M., Hoey, T., Rushlow, C., Doyle, H. and Levine, M.** (1987). Characterization and localization of the even-skipped protein of *Drosophila*. *EMBO J.* **6**, 749–759.

- Fu, J., Posnien, N., Bolognesi, R., Fischer, T. D., Rayl, P., Oberhofer, G., Kitzmann, P., Brown, S. J. and Bucher, G.** (2012). Asymmetrically expressed axin required for anterior development in *Tribolium*. *Proc. Natl. Acad. Sci. U. S. A.* **109**, 7782–7786.
- Fuentealba, L. C., Eivers, E., Ikeda, A., Hurtado, C., Kuroda, H., Pera, E. M. and De Robertis, E. M.** (2007). Integrating Patterning Signals: Wnt/GSK3 Regulates the Duration of the BMP/Smad1 Signal. *Cell* **131**, 980–993.
- Fujioka, M., Emi-Sarker, Y., Yusibova, G. L., Goto, T. and Jaynes, J. B.** (1999). Analysis of an even-skipped rescue transgene reveals both composite and discrete neuronal and early blastoderm enhancers, and multi-stripe positioning by gap gene repressor gradients. *Development* **126**, 2527–2538.
- Furriols, M. and Casanova, J.** (2003). In and out of Torso RTK signalling. *EMBO J.* **22**, 1947–1952.
- Gallitano-Mendel, A. and Finkelstein, R.** (1997). Novel Segment Polarity Gene Interactions during Embryonic Head Development in *Drosophila*. *Dev. Biol.* **192**, 599–613.
- Garcia-Fernández, J.** (2005). The genesis and evolution of homeobox gene clusters. *Nat. Rev. Genet.* **6**, 881–892.
- Gavrieli, Y., Sherman, Y. and Ben-Sasson, S. A.** (1992). Identification of programmed cell death in situ via specific labeling of nuclear DNA fragmentation. *J. Cell Biol.* **119**, 493–501.
- Gergen, J. P. and Butler, B. A.** (1988). Isolation of the *Drosophila* segmentation gene *runt* and analysis of its expression during embryogenesis. *Genes Dev.* **2**, 1179–1193.
- Gilbert, S. F.** (2003). *Developmental Biology, Seventh Edition*. Sutherland, Massachusetts: Sinauer Associates Inc.
- González-Gaitán, M., Rothe, M., Wimmer, E. A., Taubert, H. and Jäckle, H.** (1994). Redundant functions of the genes *knirps* and *knirps-related* for the establishment of anterior *Drosophila* head structures. *Proc. Natl. Acad. Sci.* **91**, 8567–8571.
- González-Reyes, A., Elliott, H. and St Johnston, D.** (1995). Polarization of both major body axes in *Drosophila* by *gurken-torpedo* signalling. *Nature* **375**, 654–658.
- Gurley, K. A., Rink, J. C. and Sánchez Alvarado, A.** (2008). Beta-catenin defines head versus tail identity during planarian regeneration and homeostasis. *Science* **319**, 323–327.
- Handel, K., Grünfelder, C. G., Roth, S. and Sander, K.** (2000). *Tribolium* embryogenesis: a SEM study of cell shapes and movements from blastoderm to serosal closure. *Dev. Genes Evol.* **210**, 167–179.
- Handel, K., Basal, A., Fan, X. and Roth, S.** (2005). *Tribolium castaneum* twist: gastrulation and mesoderm formation in a short-germ beetle. *Dev. Genes Evol.* **215**, 13–31.

- Harding, K. and Levine, M.** (1988). Gap genes define the limits of antennapedia and bithorax gene expression during early development in *Drosophila*. *EMBO J.* **7**, 205–214.
- Harding, K., Rushlow, C., Doyle, H. J., Hoey, T. and Levine, M.** (1986). Cross-regulatory interactions among pair-rule genes in *Drosophila*. *Science* **233**, 953–959.
- Harland, R. and Gerhart, J.** (1997). Formation and function of Spemann's organizer. *Annu. Rev. Cell Dev. Biol.* **13**, 611–667.
- Hartenstein, V.** (1993). *Atlas of Drosophila development. In: The development of Drosophila melanogaster.* Cold Spring Harbor, NY: Cold Spring Harbor Laboratory Press.
- Hartmann, C., Taubert, H., Jäckle, H. and Pankratz, M. J.** (1994). A two-step mode of stripe formation in the *Drosophila* blastoderm requires interactions among primary pair rule genes. *Mech. Dev.* **45**, 3–13.
- Hashimoto, C., Kim, D. R., Weiss, L. A., Miller, J. W. and Morisato, D.** (2003). Spatial regulation of developmental signaling by a serpin. *Dev. Cell* **5**, 945–950.
- Hashimoto, Y., Kondo, T. and Kageyama, Y.** (2008). Lilliputians get into the limelight: Novel class of small peptide genes in morphogenesis. *Dev. Growth Differ.* **50**, S269–S276.
- Hata, A., Lagna, G., Massagué, J. and Hemmati-Brivanlou, A.** (1998). Smad6 inhibits BMP/Smad1 signaling by specifically competing with the Smad4 tumor suppressor. *Genes Dev.* **12**, 186–197.
- Hayashi, H., Abdollah, S., Qiu, Y., Cai, J., Xu, Y.-Y., Grinnell, B. W., Richardson, M. A., Topper, J. N., Gimbrone, M. A., Wrana, J. L., et al.** (1997). The MAD-Related Protein Smad7 Associates with the TGF β Receptor and Functions as an Antagonist of TGF β Signaling. *Cell* **89**, 1165–1173.
- Hicke, L. and Dunn, R.** (2003). Regulation of membrane protein transport by ubiquitin and ubiquitin-binding proteins. *Annu. Rev. Cell Dev. Biol.* **19**, 141–172.
- Horn, T. and Boutros, M.** (2010). E-RNAi: a web application for the multi-species design of RNAi reagents—2010 update. *Nucleic Acids Res.* **38**, W332–W339.
- Horn, C. and Wimmer, E. A.** (2000). A versatile vector set for animal transgenesis. *Dev. Genes Evol.* **210**, 630–637.
- Huang, L., Kinnucan, E., Wang, G., Beaudenon, S., Howley, P. M., Huibregtse, J. M. and Pavletich, N. P.** (1999). Structure of an E6AP-UbcH7 complex: insights into ubiquitination by the E2-E3 enzyme cascade. *Science* **286**, 1321–1326.
- Hülkamp, M., Schröder, C., Pfeifle, C., Jäckle, H. and Tautz, D.** (1989). Posterior segmentation of the *Drosophila* embryo in the absence of a maternal posterior organizer gene. *Nature* **338**, 629–632.
- Hülkamp, M., Pfeifle, C. and Tautz, D.** (1990). A morphogenetic gradient of hunchback protein organizes the expression of the gap genes Krüppel and knirps in the early *Drosophila* embryo. *Nature* **346**, 577–580.

- Huminiacki, L., Goldovsky, L., Freilich, S., Moustakas, A., Ouzounis, C. and Heldin, C.-H.** (2009). Emergence, development and diversification of the TGF- β signalling pathway within the animal kingdom. *BMC Evol. Biol.* **9**, 28.
- Hynes, R. O. and Zhao, Q.** (2000). The Evolution of Cell Adhesion. *J. Cell Biol.* **150**, F89–F96.
- Ingham, P. W., Baker, N. E. and Martinez-Arias, A.** (1988). Regulation of segment polarity genes in the *Drosophila* blastoderm by *fushi tarazu* and *even-skipped*. *Nature* **331**, 73–75.
- Inoue, Y. and Imamura, T.** (2008). Regulation of TGF-beta family signaling by E3 ubiquitin ligases. *Cancer Sci.* **99**, 2107–2112.
- Irish, V., Lehmann, R. and Akam, M.** (1989a). The *Drosophila* posterior-group gene *nanos* functions by repressing *hunchback* activity. *Nature* **338**, 646–648.
- Irish, V. F., Martinez-Arias, A. and Akam, M.** (1989b). Spatial regulation of the *Antennapedia* and *Ultrabithorax* homeotic genes during *Drosophila* early development. *EMBO J.* **8**, 1527–1537.
- Itoh, S. and ten Dijke, P.** (2007). Negative regulation of TGF- β receptor/Smad signal transduction. *Curr. Opin. Cell Biol.* **19**, 176–184.
- Jack, T. and McGinnis, W.** (1990). Establishment of the *Deformed* expression stripe requires the combinatorial action of coordinate, gap and pair-rule proteins. *EMBO J.* **9**, 1187–1198.
- Jazwinska, A., Rushlow, C. and Roth, S.** (1999). The role of *brinker* in mediating the graded response to *Dpp* in early *Drosophila* embryos. *Development* **126**, 3323–3334.
- Johnston, D. S. and Nüsslein-Volhard, C.** (1992). The origin of pattern and polarity in the *Drosophila* embryo. *Cell* **68**, 201–219.
- Kavsak, P., Rasmussen, R. K., Causing, C. G., Bonni, S., Zhu, H., Thomsen, G. H. and Wrana, J. L.** (2000). Smad7 binds to Smurf2 to form an E3 ubiquitin ligase that targets the TGF beta receptor for degradation. *Mol. Cell* **6**, 1365–1375.
- Kiecker, C. and Niehrs, C.** (2001). A morphogen gradient of Wnt/ β -catenin signalling regulates anteroposterior neural patterning in *Xenopus*. *Development* **128**, 4189–4201.
- Kiehart, D. P., Galbraith, C. G., Edwards, K. A., Rickoll, W. L. and Montague, R. A.** (2000). Multiple Forces Contribute to Cell Sheet Morphogenesis for Dorsal Closure in *Drosophila*. *J. Cell Biol.* **149**, 471–490.
- Kim, H. S., Murphy, T., Xia, J., Caragea, D., Park, Y., Beeman, R. W., Lorenzen, M. D., Butcher, S., Manak, J. R. and Brown, S. J.** (2010). BeetleBase in 2010: revisions to provide comprehensive genomic information for *Tribolium castaneum*. *Nucleic Acids Res.* **38**, D437–D442.
- Kingsley, D. M.** (1994). The TGF-beta superfamily: new members, new receptors, and new genetic tests of function in different organisms. *Genes Dev.* **8**, 133–146.
- Kirov, N., Childs, S., O'Connor, M. and Rushlow, C.** (1994). The *Drosophila* dorsal morphogen represses the *tolloid* gene by interacting with a silencer element. *Mol. Cell. Biol.* **14**, 713–722.

- Kitisin, K., Saha, T., Blake, T., Golestaneh, N., Deng, M., Kim, C., Tang, Y., Shetty, K., Mishra, B. and Mishra, L.** (2007). Tgf-Beta signaling in development. *Sci. STKE Signal Transduct. Knowl. Environ.* **2007**, cm1.
- Kittelmann, S.** (2012). Formation of the Clypeolabral Region During Embryonic Head Development of the Red Flour Beetle *Tribolium castaneum*. Dissertation, Georg August Universität Göttingen.
- Kittelmann, S., Ulrich, J., Posnien, N. and Bucher, G.** (2013). Changes in anterior head patterning underlie the evolution of long germ embryogenesis. *Dev. Biol.* **374**, 174–184.
- Kitzmann, P., Schwirz, J., Schmitt-Engel, C. and Bucher, G.** (2013). RNAi phenotypes are influenced by the genetic background of the injected strain. *BMC Genomics* **14**, 5.
- Klingler, M. and Gergen, J. P.** (1993). Regulation of runt transcription by *Drosophila* segmentation genes. *Mech. Dev.* **43**, 3–19.
- Klingler, M. and Tautz, D.** (1999). Formation of Embryonic Axes and Blastoderm Pattern in *Drosophila*. In *Development* (ed. Russo, P. D. V. E. A., Cove, P. D. D. J., Edgar, P. D. L. G., Jaenisch, P. D. R., and Salamini, P. D. F.), pp. 311–330. Springer Berlin Heidelberg.
- Klingler, M., Erdélyi, M., Szabad, J. and Nüsslein-Volhard, C.** (1988). Function of torso in determining the terminal Anlagen of the *Drosophila* embryo. *Nature* **335**, 275–277.
- Kotkamp, K., Klingler, M. and Schoppmeier, M.** (2010). Apparent role of *Tribolium* orthodenticle in anteroposterior blastoderm patterning largely reflects novel functions in dorsoventral axis formation and cell survival. *Dev. Camb. Engl.* **137**, 1853–1862.
- Kraut, R. and Levine, M.** (1991a). Spatial regulation of the gap gene giant during *Drosophila*. *Development* **111**, 601–609.
- Kraut, R. and Levine, M.** (1991b). Mutually repressive interactions between the gap genes giant and Kruppel define middle body regions of the *Drosophila* embryo. *Development* **111**, 611–621.
- Kretzschmar, M., Doody, J. and Massagué, J.** (1997). Opposing BMP and EGF signalling pathways converge on the TGF-beta family mediator Smad1. *Nature* **389**, 618–622.
- Langeland, J. A., Attai, S. F., Vorwerk, K. and Carroll, S. B.** (1994). Positioning adjacent pair-rule stripes in the posterior *Drosophila* embryo. *Development* **120**, 2945–2955.
- Lawrence, P. A. and Struhl, G.** (1996). Morphogens, compartments, and pattern: lessons from *Drosophila*? *Cell* **85**, 951–961.
- Lawrence, P. A., Johnston, P., Macdonald, P. and Struhl, G.** (1987). Borders of parasegments in *Drosophila* embryos are delimited by the fushi tarazu and even-skipped genes. *Nature* **328**, 440–442.
- Lewis, E. B.** (1978). A gene complex controlling segmentation in *Drosophila*. *Nature* **276**, 565–570.

- Li, Y., Brown, S. J., Hausdorf, B., Tautz, D., Denell, R. E. and Finkelstein, R.** (1996). Two orthodenticle-related genes in the short-germ beetle *Tribolium castaneum*. *Dev. Genes Evol.* **206**, 35–45.
- Li, W., Bengtson, M. H., Ulbrich, A., Matsuda, A., Reddy, V. A., Orth, A., Chanda, S. K., Batalov, S. and Joazeiro, C. A. P.** (2008). Genome-wide and functional annotation of human E3 ubiquitin ligases identifies MULAN, a mitochondrial E3 that regulates the organelle's dynamics and signaling. *PLoS One* **3**, e1487.
- Liang, Y.-Y., Lin, X., Liang, M., Brunicardi, F. C., ten Dijke, P., Chen, Z., Choi, K.-W. and Feng, X.-H.** (2003). dSmurf selectively degrades decapentaplegic-activated MAD, and its overexpression disrupts imaginal disc development. *J. Biol. Chem.* **278**, 26307–26310.
- Liang, H.-L., Xu, M., Chuang, Y.-C. and Rushlow, C.** (2012). Response to the BMP gradient requires highly combinatorial inputs from multiple patterning systems in the *Drosophila* embryo. *Development* **139**, 1956–1964.
- Ligoxygakis, P., Roth, S. and Reichhart, J.-M.** (2003). A serpin regulates dorsal-ventral axis formation in the *Drosophila* embryo. *Curr. Biol. CB* **13**, 2097–2102.
- Lin, X., Liang, M. and Feng, X.-H.** (2000). Smurf2 Is a Ubiquitin E3 Ligase Mediating Proteasome-dependent Degradation of Smad2 in Transforming Growth Factor- β Signaling. *J. Biol. Chem.* **275**, 36818–36822.
- Lin, X., Liang, Y.-Y., Sun, B., Liang, M., Shi, Y., Brunicardi, F. C., Shi, Y. and Feng, X.-H.** (2003). Smad6 Recruits Transcription Corepressor CtBP To Repress Bone Morphogenetic Protein-Induced Transcription. *Mol. Cell. Biol.* **23**, 9081–9093.
- Little, S. C. and Mullins, M. C.** (2006). Extracellular modulation of BMP activity in patterning the dorsoventral axis. *Birth Defects Res. Part C Embryo Today Rev.* **78**, 224–242.
- Liu, X., Sun, Y., Weinberg, R. A. and Lodish, H. F.** (2001). Ski/Sno and TGF- β signaling. *Cytokine Growth Factor Rev.* **12**, 1–8.
- Liu, S.-Y., Selck, C., Friedrich, B., Lutz, R., Vila-Farré, M., Dahl, A., Brandl, H., Lakshmanaperumal, N., Henry, I. and Rink, J. C.** (2013). Reactivating head re-growth in a regeneration-deficient planarian species. *Nature*.
- Logan, C. Y. and Nusse, R.** (2004). The Wnt signaling pathway in development and disease. *Annu. Rev. Cell Dev. Biol.* **20**, 781–810.
- Lönn, P., Morén, A., Raja, E., Dahl, M. and Moustakas, A.** (2009). Regulating the stability of TGF β receptors and Smads. *Cell Res.* **19**, 21–35.
- Lorenzen, M. D., Berghammer, A. J., Brown, S. J., Denell, R. E., Klingler, M. and Beeman, R. W.** (2003). piggyBac-mediated germline transformation in the beetle *Tribolium castaneum*. *Insect Mol. Biol.* **12**, 433–440.
- Lynch, J. A. and Roth, S.** (2011). The evolution of dorsal–ventral patterning mechanisms in insects. *Genes Dev.* **25**, 107–118.
- Macias, M. J., Wiesner, S. and Sudol, M.** (2002). WW and SH3 domains, two different scaffolds to recognize proline-rich ligands. *FEBS Lett.* **513**, 30–37.

- Manoukian, A. S. and Krause, H. M.** (1992). Concentration-dependent activities of the even-skipped protein in *Drosophila* embryos. *Genes Dev.* **6**, 1740–1751.
- Marqués, G., Musacchio, M., Shimell, M. J., Wünnenberg-Stapleton, K., Cho, K. W. Y. and O'Connor, M. B.** (1997). Production of a DPP Activity Gradient in the Early *Drosophila* Embryo through the Opposing Actions of the SOG and TLD Proteins. *Cell* **91**, 417–426.
- Marques-Souza, H., Aranda, M. and Tautz, D.** (2008). Delimiting the conserved features of hunchback function for the trunk organization of insects. *Development* **135**, 881–888.
- Martin, P. and Lewis, J.** (1992). Actin cables and epidermal movement in embryonic wound healing. *Nature* **360**, 179–183.
- Martinez-Arias, A. and Lawrence, P. A.** (1985). Parasegments and compartments in the *Drosophila* embryo. *Nature* **313**, 639–642.
- Massagué, J.** (1998). TGF-beta signal transduction. *Annu. Rev. Biochem.* **67**, 753–791.
- Matakatsu, H. and Blair, S. S.** (2004). Interactions between Fat and Dachshous and the regulation of planar cell polarity in the *Drosophila* wing. *Development* **131**, 3785–3794.
- Maxton-Küchenmeister, J., Handel, K., Schmidt-Ott, U., Roth, S. and Jäckle, H.** (1999). Toll homolog expression in the beetle *Tribolium* suggests a different mode of dorsoventral patterning than in *Drosophila* embryos. *Mech. Dev.* **83**, 107–114.
- McLennan, A. G.** (2005). The Nudix hydrolase superfamily. *Cell. Mol. Life Sci.* **63**, 123–143.
- Mizutani, C. M., Nie, Q., Wan, F. Y. M., Zhang, Y.-T., Vilmos, P., Sousa-Neves, R., Bier, E., Marsh, J. L. and Lander, A. D.** (2005). Formation of the BMP Activity Gradient in the *Drosophila* Embryo. *Dev. Cell* **8**, 915–924.
- Mizutani, C. M., Meyer, N., Roelink, H. and Bier, E.** (2006). Threshold-Dependent BMP-Mediated Repression: A Model for a Conserved Mechanism That Patterns the Neuroectoderm. *PLoS Biol* **4**, e313.
- Moses, H. L. and Serra, R.** (1996). Regulation of differentiation by TGF-beta. *Curr. Opin. Genet. Dev.* **6**, 581–586.
- Moussian, B. and Roth, S.** (2005). Dorsoventral Axis Formation in the *Drosophila* Embryo—Shaping and Transducing a Morphogen Gradient. *Curr. Biol.* **15**, R887–R899.
- Murakami, G., Watabe, T., Takaoka, K., Miyazono, K. and Imamura, T.** (2003). Cooperative Inhibition of Bone Morphogenetic Protein Signaling by Smurf1 and Inhibitory Smads. *Mol. Biol. Cell* **14**, 2809–2817.
- Murphy, E., Smith, S. and Smet, I. D.** (2012). Small Signaling Peptides in Arabidopsis Development: How Cells Communicate Over a Short Distance. *Plant Cell Online* **24**, 3198–3217.
- Nagy, L. M. and Carroll, S.** (1994). Conservation of wingless patterning functions in the short-germ embryos of *Tribolium castaneum*. *Nature* **367**, 460–463.

- Narimatsu, M., Bose, R., Pye, M., Zhang, L., Miller, B., Ching, P., Sakuma, R., Luga, V., Roncari, L., Attisano, L., et al.** (2009). Regulation of Planar Cell Polarity by Smurf Ubiquitin Ligases. *Cell* **137**, 295–307.
- Nie, W., Stronach, B., Panganiban, G., Shippy, T., Brown, S. and Denell, R.** (2001). Molecular characterization of Tc labial and the 3' end of the Tribolium homeotic complex. *Dev. Genes Evol.* **211**, 244–251.
- Niehrs, C.** (2004). Regionally specific induction by the Spemann-Mangold organizer. *Nat. Rev. Genet.* **5**, 425–434.
- Nunes da Fonseca, R. N. da, Levetzow, C. von, Kalscheuer, P., Basal, A., Zee, M. van der and Roth, S.** (2008). Self-Regulatory Circuits in Dorsoventral Axis Formation of the Short-Germ Beetle *Tribolium castaneum*. *Dev. Cell* **14**, 605–615.
- Nunes da Fonseca, R., van der Zee, M. and Roth, S.** (2010). Evolution of extracellular Dpp modulators in insects: The roles of tolloid and twisted-gastrulation in dorsoventral patterning of the *Tribolium* embryo. *Dev. Biol.* **345**, 80–93.
- O'Connor, M. B., Umulis, D., Othmer, H. G. and Blair, S. S.** (2006). Shaping BMP morphogen gradients in the *Drosophila* embryo and pupal wing. *Development* **133**, 183–193.
- Oda, H. and Akiyama-Oda, Y.** (2008). Differing strategies for forming the arthropod body plan: Lessons from Dpp, Sog and Delta in the fly *Drosophila* and spider *Achaearanea*. *Dev. Growth Differ.* **50**, 203–214.
- Onichtchouk, D., Chen, Y. G., Dosch, R., Gawantka, V., Delius, H., Massagué, J. and Niehrs, C.** (1999). Silencing of TGF-beta signalling by the pseudoreceptor BAMBI. *Nature* **401**, 480–485.
- Pang, K., Ryan, J. F., Baxevanis, A. D. and Martindale, M. Q.** (2011). Evolution of the TGF- β Signaling Pathway and Its Potential Role in the Ctenophore, *Mnemiopsis leidyi*. *PLoS ONE* **6**, e24152.
- Pankratz, M. J. and Jäckle, H.** (1990). Making stripes in the *Drosophila* embryo. *Trends Genet. TIG* **6**, 287–292.
- Park, Y., Aikins, J., Wang, L. J., Beeman, R. W., Oppert, B., Lord, J. C., Brown, S. J., Lorenzen, M. D., Richards, S., Weinstock, G. M., et al.** (2008). Analysis of transcriptome data in the red flour beetle, *Tribolium castaneum*. *Insect Biochem. Mol. Biol.* **38**, 380–386.
- Patel, N. H., Condron, B. G. and Zinn, K.** (1994). Pair-rule expression patterns of even-skipped are found in both short- and long-germ beetles. *Nature* **367**, 429–434.
- Pavlopoulos, A., Berghammer, A. J., Averof, M. and Klingler, M.** (2004). Efficient Transformation of the Beetle *Tribolium castaneum* Using the Minos Transposable Element Quantitative and Qualitative Analysis of Genomic Integration Events. *Genetics* **167**, 737–746.
- Peel, A. D., Chipman, A. D. and Akam, M.** (2005). Arthropod Segmentation: beyond the *Drosophila* paradigm. *Nat. Rev. Genet.* **6**, 905–916.
- Persson, U., Izumi, H., Souchelnytskyi, S., Itoh, S., Grimsby, S., Engström, U., Heldin, C. H., Funahashi, K. and ten Dijke, P.** (1998). The L45 loop in type I recep-

tors for TGF-beta family members is a critical determinant in specifying Smad isoform activation. *FEBS Lett.* **434**, 83–87.

Petersen, C. P. and Reddien, P. W. (2008). Smed-betacatenin-1 is required for anteroposterior blastema polarity in planarian regeneration. *Science* **319**, 327–330.

Pickart, C. M. (2001). Mechanisms Underlying Ubiquitination. *Annu. Rev. Biochem.* **70**, 503–533.

Podos, S. D., Hanson, K. K., Wang, Y. C. and Ferguson, E. L. (2001). The DSmurf ubiquitin-protein ligase restricts BMP signaling spatially and temporally during *Drosophila* embryogenesis. *Dev. Cell* **1**, 567–578.

Pollock, D. D. and Larkin, J. C. (2004). Estimating the Degree of Saturation in Mutant Screens. *Genetics* **168**, 489–502.

Posnien, N. and Bucher, G. (2010). Formation of the insect head involves lateral contribution of the intercalary segment, which depends on Tc-labial function. *Dev. Biol.* **338**, 107–116.

Posnien, N., Schinko, J., Grossmann, D., Shippy, T. D., Konopova, B. and Bucher, G. (2009a). RNAi in the red flour beetle (*Tribolium*). *Cold Spring Harb. Protoc.* **2009**, pdb.prot5256.

Posnien, N., Bashasab, F. and Bucher, G. (2009b). The insect upper lip (labrum) is a nonsegmental appendage-like structure. *Evol. Dev.* **11**, 480–488.

Posnien, N., Schinko, J. B., Kittelmann, S. and Bucher, G. (2010). Genetics, development and composition of the insect head – A beetle's view. *Arthropod Struct. Dev.* **39**, 399–410.

Posnien, N., Koniszewski, N. D. B., Hein, H. J. and Bucher, G. (2011). Candidate gene screen in the red flour beetle *Tribolium* reveals six3 as ancient regulator of anterior median head and central complex development. *PLoS Genet.* **7**, e1002416.

Prpic, N.-M. and Damen, W. G. M. (2005). Cell death during germ band inversion, dorsal closure, and nervous system development in the spider *Cupiennius salei*. *Dev. Dyn.* **234**, 222–228.

Rafiqi, A. M., Lemke, S. and Schmidt-Ott, U. (2010). Postgastrular zen expression is required to develop distinct amniotic and serosal epithelia in the scuttle fly *Megaselia*. *Dev. Biol.* **341**, 282–290.

Reinitz, J. and Sharp, D. H. (1995). Mechanism of eve stripe formation. *Mech. Dev.* **49**, 133–158.

Richards, G. S. and Degnan, B. M. (2009). The Dawn of Developmental Signaling in the Metazoa. *Cold Spring Harb. Symp. Quant. Biol.* **74**, 81–90.

Richards, S., Gibbs, R. A., Weinstock, G. M., Brown, S. J., Denell, R., Beeman, R. W., Gibbs, R., Beeman, R. W., Brown, S. J., Bucher, G., et al. (2008). The genome of the model beetle and pest *Tribolium castaneum*. *Nature* **452**, 949–955.

Riechmann, V. and Ephrussi, A. (2001). Axis formation during *Drosophila* oogenesis. *Curr. Opin. Genet. Dev.* **11**, 374–383.

- Rivera-Pomar, R. and Jäckle, H.** (1996). From gradients to stripes in *Drosophila* embryogenesis: filling in the gaps. *Trends Genet. TIG* **12**, 478–483.
- Rivera-Pomar, R., Niessing, D., Schmidt-Ott, U., Gehring, W. J. and Jäckle, H.** (1996). RNA binding and translational suppression by bicoid. *Nature* **379**, 746–749.
- Roth, S. and Lynch, J. A.** (2009). Symmetry Breaking During *Drosophila* Oogenesis. *Cold Spring Harb. Perspect. Biol.* **1**, a001891.
- Roth, S., Stein, D. and Nüsslein-Volhard, C.** (1989). A gradient of nuclear localization of the dorsal protein determines dorsoventral pattern in the *Drosophila* embryo. *Cell* **59**, 1189–1202.
- Rotin, D. and Kumar, S.** (2009). Physiological functions of the HECT family of ubiquitin ligases. *Nat. Rev. Mol. Cell Biol.* **10**, 398–409.
- Ryan, J. F., Pang, K., Schnitzler, C. E., Nguyen, A.-D., Moreland, R. T., Simmons, D. K., Koch, B. J., Francis, W. R., Havlak, P., Smith, S. A., et al.** (2013). The Genome of the Ctenophore *Mnemiopsis leidyi* and Its Implications for Cell Type Evolution. *Science* **342**, 1242592.
- Saitou, N. and Nei, M.** (1987). The neighbor-joining method: a new method for reconstructing phylogenetic trees. *Mol. Biol. Evol.* **4**, 406–425.
- Sambrook, J. and Russell, D. W.** (2001). *Molecular Cloning: A Laboratory Manual (Third Edition)*. New York: Cold Spring Harbor Laboratory.
- Sanchez-Salazar, J., Pletcher, M. T., Bennett, R. L., Brown, S. J., Dandamudi, T. J., Denell, R. E. and Doctor, J. S.** (1996). The *Tribolium* decapentaplegic gene is similar in sequence, structure, and expression to the *Drosophila* dpp gene. *Dev. Genes Evol.* **206**, 237–246.
- Sanson, B.** (2001). Generating patterns from fields of cells. *EMBO Rep.* **2**, 1083–1088.
- Sapkota, G., Alarcón, C., Spagnoli, F. M., Brivanlou, A. H. and Massagué, J.** (2007). Balancing BMP signaling through integrated inputs into the Smad1 linker. *Mol. Cell* **25**, 441–454.
- Sarrazin, A. F., Peel, A. D. and Averof, M.** (2012). A segmentation clock with two-segment periodicity in insects. *Science* **336**, 338–341.
- Savard, J., Marques-Souza, H., Aranda, M. and Tautz, D.** (2006). A segmentation gene in *tribolium* produces a polycistronic mRNA that codes for multiple conserved peptides. *Cell* **126**, 559–569.
- Schinko, J. B., Kreuzer, N., Offen, N., Posnien, N., Wimmer, E. A. and Bucher, G.** (2008). Divergent functions of orthodenticle, empty spiracles and buttonhead in early head patterning of the beetle *Tribolium castaneum* (Coleoptera). *Dev. Biol.* **317**, 600–613.
- Schinko, J., Posnien, N., Kittelmann, S., Koniszewski, N. and Bucher, G.** (2009). Single and Double Whole-Mount In Situ Hybridization in Red Flour Beetle (*Tribolium*) Embryos. *Cold Spring Harb. Protoc.* **2009**, pdb.prot5258–pdb.prot5258.

- Schmidt, J. E., Dassow, G. von and Kimelman, D.** (1996). Regulation of dorsal-ventral patterning: the ventralizing effects of the novel *Xenopus* homeobox gene *Vox*. *Development* **122**, 1711–1721.
- Schmitt-Engel, C.** (2010). Die Funktion von Genen der posterioren Gruppe und die Etablierung eines genomweiten RNAi-Screens in *Tribolium castaneum*. Dissertation, Friedrich-Alexander-Universität Erlangen-Nürnberg.
- Schmitt-Engel, C., iBeetle Consortium (includes Schwirz, J.) and Bucher, G.** iBeetle: RNAi-screening for insect development. in preparation.
- Schoppmeier, M. and Schröder, R.** (2005). Maternal Torso Signaling Controls Body Axis Elongation in a Short Germ Insect. *Curr. Biol.* **15**, 2131–2136.
- Schoppmeier, M., Fischer, S., Schmitt-Engel, C., Löhr, U. and Klingler, M.** (2009). An ancient anterior patterning system promotes caudal repression and head formation in ecdysozoa. *Curr. Biol. CB* **19**, 1811–1815.
- Schröder, R.** (2003). The genes *orthodenticle* and *hunchback* substitute for *bicoid* in the beetle *Tribolium*. *Nature* **422**, 621–625.
- Schröder, R., Beermann, A., Wittkopp, N. and Lutz, R.** (2008). From development to biodiversity—*Tribolium castaneum*, an insect model organism for short germband development. *Dev. Genes Evol.* **218**, 119–126.
- Schulz, C. and Tautz, D.** (1994). Autonomous concentration-dependent activation and repression of *Kruppel* by *hunchback* in the *Drosophila* embryo. *Development* **120**, 3043–3049.
- Schulz, C. and Tautz, D.** (1995). Zygotic caudal regulation by *hunchback* and its role in abdominal segment formation of the *Drosophila* embryo. *Development* **121**, 1023–1028.
- Schulz, C., Schröder, R., Hausdorf, B., Wolff, C. and Tautz, D.** (1998). A caudal homologue in the short germ band beetle *Tribolium* shows similarities to both, the *Drosophila* and the vertebrate caudal expression patterns. *Dev. Genes Evol.* **208**, 283–289.
- Serpe, M., Ralston, A., Blair, S. S. and O'Connor, M. B.** (2005). Matching catalytic activity to developmental function: Toll-like related processes *Sog* in order to help specify the posterior crossvein in the *Drosophila* wing. *Development* **132**, 2645–2656.
- Sharma, R., Beermann, A. and Schröder, R.** (2013). The dynamic expression of extraembryonic marker genes in the beetle *Tribolium castaneum* reveals the complexity of serosa and amnion formation in a short germ insect. *Gene Expr. Patterns* **13**, 362–371.
- Shi, Y. and Massagué, J.** (2003). Mechanisms of TGF-beta signaling from cell membrane to the nucleus. *Cell* **113**, 685–700.
- Shibata, M., Itoh, M., Ohmori, S., Shinga, J. and Taira, M.** (2001). Systematic Screening and Expression Analysis of the Head Organizer Genes in *Xenopus* Embryos. *Dev. Biol.* **239**, 241–256.

- Shimell, M. J., Ferguson, E. L., Childs, S. R. and O'Connor, M. B.** (1991). The *Drosophila* dorsal-ventral patterning gene *tolloid* is related to human bone morphogenetic protein 1. *Cell* **67**, 469–481.
- Shimmi, O., Umulis, D., Othmer, H. and O'Connor, M. B.** (2005a). Facilitated Transport of a Dpp/Scw Heterodimer by Sog/Tsg Leads to Robust Patterning of the *Drosophila* Blastoderm Embryo. *Cell* **120**, 873–886.
- Shimmi, O., Ralston, A., Blair, S. S. and O'Connor, M. B.** (2005b). The *crossveinless* gene encodes a new member of the Twisted gastrulation family of BMP-binding proteins which, with Short gastrulation, promotes BMP signaling in the crossveins of the *Drosophila* wing. *Dev. Biol.* **282**, 70–83.
- Shippy, T. D., Brown, S. J. and Denell, R. E.** (1998). Molecular characterization of the *Tribolium* abdominal-A ortholog and implications for the products of the *Drosophila* gene. *Dev. Genes Evol.* **207**, 446–452.
- Shippy, T. D., Guo, J., Brown, S. J., Beeman, R. W. and Denell, R. E.** (2000). Analysis of maxillopedia Expression Pattern and Larval Cuticular Phenotype in Wild-Type and Mutant *Tribolium*. *Genetics* **155**, 721–731.
- Simpson-Brose, M., Treisman, J. and Desplan, C.** (1994). Synergy between the hunchback and bicoid morphogens is required for anterior patterning in *Drosophila*. *Cell* **78**, 855–865.
- Sokoloff, A.** (1972). *The Biology of Tribolium: with special emphasis on genetic aspects I-III*. Oxford: Clarendon Press.
- Sokoloff, A., Slatis, H. M. and Stanley, J.** (1960). The Black Mutation in *Tribolium Castaneum*. *J. Hered.* **51**, 131–135.
- Sommer, R. J. and Tautz, D.** (1993). Involvement of an orthologue of the *Drosophila* pair-rule gene *hairy* in segment formation of the short germ-band embryo of *Tribolium* (Coleoptera). *Nature* **361**, 448–450.
- Sommer, R. J. and Tautz, D.** (1994). Expression patterns of twist and snail in *Tribolium* (Coleoptera) suggest a homologous formation of mesoderm in long and short germ band insects. *Dev. Genet.* **15**, 32–37.
- Sprenger, F., Stevens, L. M. and Nüsslein-Volhard, C.** (1989). The *Drosophila* gene *torso* encodes a putative receptor tyrosine kinase. *Nature* **338**, 478–483.
- Srinivasan, S., Rashka, K. E. and Bier, E.** (2002). Creation of a Sog Morphogen Gradient in the *Drosophila* Embryo. *Dev. Cell* **2**, 91–101.
- St Johnston, D.** (2002). The art and design of genetic screens: *Drosophila melanogaster*. *Nat. Rev. Genet.* **3**, 176–188.
- Stathopoulos, A. and Levine, M.** (2002). Dorsal Gradient Networks in the *Drosophila* Embryo. *Dev. Biol.* **246**, 57–67.
- Stathopoulos, A. and Levine, M.** (2005). Genomic Regulatory Networks and Animal Development. *Dev. Cell* **9**, 449–462.
- Stathopoulos, A., Van Drenth, M., Erives, A., Markstein, M. and Levine, M.** (2002). Whole-genome analysis of dorsal-ventral patterning in the *Drosophila* embryo. *Cell* **111**, 687–701.

- Stauber, M., Jäckle, H. and Schmidt-Ott, U.** (1999). The anterior determinant bicoid of *Drosophila* is a derived Hox class 3 gene. *Proc. Natl. Acad. Sci.* **96**, 3786–3789.
- Stevens, L. M., Frohnhofer, H. G., Klingler, M. and Nüsslein-Volhard, C.** (1990). Localized requirement for torso-like expression in follicle cells for development of terminal anlagen of the *Drosophila* embryo. *Nature* **346**, 660–663.
- Struhl, G., Struhl, K. and Macdonald, P. M.** (1989). The gradient morphogen bicoid is a concentration-dependent transcriptional activator. *Cell* **57**, 1259–1273.
- Sutherland, D. J., Li, M., Liu, X., Stefancsik, R. and Raftery, L. A.** (2003). Stepwise formation of a SMAD activity gradient during dorsal-ventral patterning of the *Drosophila* embryo. *Development* **130**, 5705–5716.
- Tang, L.-Y., Yamashita, M., Coussens, N. P., Tang, Y., Wang, X., Li, C., Deng, C.-X., Cheng, S. Y. and Zhang, Y. E.** (2011). Ablation of Smurf2 reveals an inhibition in TGF- β signalling through multiple mono-ubiquitination of Smad3. *EMBO J.* **30**, 4777–4789.
- Tanimoto, H., Itoh, S., ten Dijke, P. and Tabata, T.** (2000). Hedgehog creates a gradient of DPP activity in *Drosophila* wing imaginal discs. *Mol. Cell* **5**, 59–71.
- Taru, H., Iijima, K., Hase, M., Kirino, Y., Yagi, Y. and Suzuki, T.** (2002). Interaction of Alzheimer's β -Amyloid Precursor Family Proteins with Scaffold Proteins of the JNK Signaling Cascade. *J. Biol. Chem.* **277**, 20070–20078.
- Tautz, D.** (1988). Regulation of the *Drosophila* segmentation gene hunchback by two maternal morphogenetic centres. *Nature* **332**, 281–284.
- Tian, M., Bai, C., Lin, Q., Lin, H., Liu, M., Ding, F. and Wang, H.-R.** (2011). Binding of RhoA by the C2 domain of E3 ligase Smurf1 is essential for Smurf1-regulated RhoA ubiquitination and cell protrusive activity. *FEBS Lett.* **585**, 2199–2204.
- Tomoyasu, Y., Wheeler, S. R. and Denell, R. E.** (2005). Ultrabithorax is required for membranous wing identity in the beetle *Tribolium castaneum*. *Nature* **433**, 643–647.
- Trauner, J., Schinko, J., Lorenzen, M. D., Shippy, T. D., Wimmer, E. A., Beeman, R. W., Klingler, M., Bucher, G. and Brown, S. J.** (2009). Large-scale insertional mutagenesis of a coleopteran stored grain pest, the red flour beetle *Tribolium castaneum*, identifies embryonic lethal mutations and enhancer traps. *BMC Biol.* **7**, 73.
- Umesono, Y., Tasaki, J., Nishimura, Y., Hrouda, M., Kawaguchi, E., Yazawa, S., Nishimura, O., Hosoda, K., Inoue, T. and Agata, K.** (2013). The molecular logic for planarian regeneration along the anterior-posterior axis. *Nature*.
- Van der Zee, M., Berns, N. and Roth, S.** (2005). Distinct functions of the *Tribolium* zerknüllt genes in serosa specification and dorsal closure. *Curr. Biol. CB* **15**, 624–636.
- Van der Zee, M., Stockhammer, O., von Levetzow, C., Nunes da Fonseca, R. and Roth, S.** (2006). Sog/Chordin is required for ventral-to-dorsal Dpp/BMP transport and head formation in a short germ insect. *Proc. Natl. Acad. Sci. U. S. A.* **103**, 16307–16312.

- Van der Zee, M., da Fonseca, R. N. and Roth, S.** (2008). TGFbeta signaling in Tribolium: vertebrate-like components in a beetle. *Dev. Genes Evol.* **218**, 203–213.
- Vilmos, P., Sousa-Neves, R., Lukacsovich, T. and Lawrence Marsh, J.** (2005). crossveinless defines a new family of Twisted-gastrulation-like modulators of bone morphogenetic protein signalling. *EMBO Rep.* **6**, 262–267.
- Wang, Y.-C. and Ferguson, E. L.** (2005). Spatial bistability of Dpp–receptor interactions during Drosophila dorsal–ventral patterning. *Nature* **434**, 229–234.
- Wang, C. and Lehmann, R.** (1991). Nanos is the localized posterior determinant in Drosophila. *Cell* **66**, 637–647.
- Weigel, D., Jürgens, G., Klingler, M. and Jäckle, H.** (1990). Two gap genes mediate maternal terminal pattern information in Drosophila. *Science* **248**, 495–498.
- Weil, T. T., Forrest, K. M. and Gavis, E. R.** (2006). Localization of bicoid mRNA in Late Oocytes Is Maintained by Continual Active Transport. *Dev. Cell* **11**, 251–262.
- Wheeler, S. R., Carrico, M. L., Wilson, B. A., Brown, S. J. and Skeath, J. B.** (2003). The expression and function of the achaete-scute genes in Tribolium castaneum reveals conservation and variation in neural pattern formation and cell fate specification. *Development* **130**, 4373–4381.
- Wheeler, S. R., Carrico, M. L., Wilson, B. A. and Skeath, J. B.** (2005). The Tribolium columnar genes reveal conservation and plasticity in neural precursor patterning along the embryonic dorsal–ventral axis. *Dev. Biol.* **279**, 491–500.
- Wolff, C., Sommer, R., Schroder, R., Glaser, G. and Tautz, D.** (1995). Conserved and divergent expression aspects of the Drosophila segmentation gene hunchback in the short germ band embryo of the flour beetle Tribolium. *Development* **121**, 4227–4236.
- Xia, L., Jia, S., Huang, S., Wang, H., Zhu, Y., Mu, Y., Kan, L., Zheng, W., Wu, D., Li, X., et al.** (2010). The Fused/Smurf complex controls the fate of Drosophila germline stem cells by generating a gradient BMP response. *Cell* **143**, 978–990.
- Xu, A., Desai, A. M., Brenner, S. E. and Kirsch, J. F.** (2013). A continuous fluorescence assay for the characterization of Nudix hydrolases. *Anal. Biochem.* **437**, 178–184.
- Yamaguchi, K., Ohara, O., Ando, A. and Nagase, T.** (2008). Smurf1 directly targets hPEM-2, a GEF for Cdc42, via a novel combination of protein interaction modules in the ubiquitin-proteasome pathway. *Biol. Chem.* **389**,.
- Yamashita, M., Ying, S.-X., Zhang, G., Li, C., Cheng, S. Y., Deng, C. and Zhang, Y. E.** (2005). Ubiquitin Ligase Smurf1 Controls Osteoblast Activity and Bone Homeostasis by Targeting MEKK2 for Degradation. *Cell* **121**, 101–113.
- Yan, X., Liu, Z. and Chen, Y.** (2009). Regulation of TGF- β signaling by Smad7. *Acta Biochim. Biophys. Sin.* **41**, 263–272.
- Zeitlinger, J., Zinzen, R. P., Stark, A., Kellis, M., Zhang, H., Young, R. A. and Levine, M.** (2007). Whole-genome ChIP–chip analysis of Dorsal, Twist, and Snail

suggests integration of diverse patterning processes in the *Drosophila* embryo. *Genes Dev.* **21**, 385–390.

Zhang, Y., Chang, C., Gehling, D. J., Hemmati-Brivanlou, A. and Derynck, R. (2001). Regulation of Smad degradation and activity by Smurf2, an E3 ubiquitin ligase. *Proc. Natl. Acad. Sci.* **98**, 974–979.

Zhang, S., Fei, T., Zhang, L., Zhang, R., Chen, F., Ning, Y., Han, Y., Feng, X.-H., Meng, A. and Chen, Y.-G. (2007). Smad7 Antagonizes Transforming Growth Factor β Signaling in the Nucleus by Interfering with Functional Smad-DNA Complex Formation. *Mol. Cell. Biol.* **27**, 4488–4499.

Zhu, H., Kavsak, P., Abdollah, S., Wrana, J. L. and Thomsen, G. H. (1999). A SMAD ubiquitin ligase targets the BMP pathway and affects embryonic pattern formation. *Nature* **400**, 687–693.

7 Appendix

7.1 DVD content

Content	Folder
Digital Copy of this Thesis	no subfolder
Candidate List (Excel Sheet)	<i>Candidates_List</i>
Gene sequences	<i>Genes_Sequences</i>
Subfolder for every gene, including all isolated sequences in FASTA and GenBank Flat file Format (folder <i>Isolated_Sequences</i>) and AUGUSTUS gene predictions (folder <i>GeneModel_AUGUSTUS</i>)	
Movies (can be opened with ImageJ)	<i>Movies</i>
Control embryo (Figure 4-21): <i>wt_131204a02_07_R3D.dv.tif</i>	<i>Movies/Control</i>
Early lethal smurf RNAi embryo (embryo from Figure 4-22): <i>smurf_early_lethal_131204a02_23_R3D.dv.tif</i>	<i>Movies/smurfRNAi</i>
smurfRNAi embryo (embryo from Figure 4-23): <i>smurf_301113a04_11_R3D.dv.tif</i>	<i>Movies/smurfRNAi</i>
sogRNAi embryo (embryo from Figure 4-24): <i>sog_031213a02_51.tif</i>	<i>Movies/sogRNAi</i>
TC004374RNAi embryo (embryo from Figure 4-34): <i>TC_004374_131128a02_32_R3D.dv.tif</i>	<i>Movies/TC004374RNAi</i>
TC004374RNAi embryo (embryo from Figure 4-35): <i>TC_004374_301113a04_46_R3D.dv.tif</i>	<i>Movies/TC004374RNAi</i>
Phylogeny for Smurf	<i>Smurf_Phylogeny</i>
Contains a file linking species names to the gene product names (<i>ID_GeneName_Smurf_Phylogeny.txt</i>), all AA sequences as FASTA files, and the alignments as FASTA files (subfolder <i>Alignments</i>)	
Phylogeny for TC004374	<i>TC004374_Phylogeny</i>
Contains a file linking Gene product names in the tree to the protein identifiers (<i>AAA_SummaryID_Name_Nudix_Phylogeny</i>), all AA sequences as FASTA files (named with the protein identifiers), and the alignment as FASTA file (subfolder <i>Alignments</i>)	
Primers (Excel sheet)	<i>Primers</i>

7.2 Abbreviations

AA	amino acid
bp	base pair
cDNA	complementary DNA
CDS	coding sequence
CNS	central nervous system
dai	days after injection
dsRNA	double stranded RNA
EE	empty egg', egg without cuticle in cuticle preparation
GFP	green fluorescent protein
mRNA	messenger RNA
NCBI	National Center for Biotechnology Information
NOF	non-overlapping fragment
PCR	polymerase chain reaction
RACE	rapid amplification of cDNA ends
RNAi	RNA interference
<i>SB</i>	<i>San Bernardino</i> ; a <i>Tribolium</i> wild type strain
<i>Tc</i>	<i>Tribolium castaneum</i>
TUNEL	terminal deoxynucleotidyl transferase dUTP nick end labeling
wt	wild type
AP	anterior-posterior
DV	dorsal-ventral
T1, T2, T3	Thoracic segment 1, 2, 3
A1, A2, ...	Abdominal segment 1, 2, ...
la	labrum
lb	labium
an	antenna
mx	maxilla
md	mandible
ug	urogomphi
pg	pygopodia

Genes and proteins

Tc-	prefix for <i>Tribolium</i> genes and proteins
<i>ash</i>	<i>achaete-scute</i>
<i>dad</i>	<i>daughters against Dpp</i>
<i>dpp</i>	<i>decapentaplegic</i>
<i>hb</i>	<i>hunchback</i>
<i>mlpt</i>	<i>mille-pattes</i>
<i>otd1</i>	<i>orthodenticle1</i>
<i>pnr</i>	<i>pannier</i>
<i>smurf</i>	<i>Smad ubiquitin regulatory factor</i>
<i>sog</i>	<i>short-gastrulation</i>
<i>tkv</i>	<i>thickveins</i>
<i>tld</i>	<i>tolloid</i>
<i>tsg</i>	<i>twisted-gastrulation</i>
<i>wg</i>	<i>wingless</i>
<i>zen1/2</i>	<i>zerknüllt1/2</i>
MAD	mothers against Dpp protein
pMAD	mothers against Dpp protein, activated via the Dpp signaling pathway
MAPK	mitogen activated protein kinase
pMAPK	phosphorylated (activated) form of mitogen activated protein kinase
GSK3	glycogen synthase kinase 3
TGF	Transforming growth factor
BMP	Bone morphogenetic protein

7.3 Primer list

Name	Name as ordered	Primer Sequence (5' to 3')	Application
JSP36	T7	GAATTGTAATACGACTCACTATAGG	dsRNA Template synthesis
JSP37	SP6-T7	TAATACGACTCACTATAGGATTTAGGTGACACTATAGA	dsRNA Template synthesis
JSP38	T3-T7	TAATACGACTCACTATAGG ATTAAACCTCACTAAAGGGA	dsRNA Template synthesis
JSP39	pCRII_M13rev	GCGGATAACAATTTACACAGGAAACAGCTATGAC	Probe Template synthesis
JSP40	pCRII_M13fw20	CCCAGTCACGACGTTGTAAAACGACGGCCAG	Probe Template synthesis
JSP61	UPM_short_T3	ATTAAACCTCACTAAAGGGA	RACE
JSP62	UPM_long_T3	ATTAAACCTCACTAAAGGGA AAGCAGTGGTATCAACGCAGAGT	RACE
JSP47	00388_3RACE	CATCGCACACCAAAAATTCAGCACCA	gene cloning
JSP48	00388_5RACE	AAGGCGATATGCCCATGATGGGCG	gene cloning
JSP101	iB5324cDNA5'	ATGGCAGATTTCGAAGCGCAAACG	gene cloning
JSP102	iB5324cDNA3'	TCAATTGAGAATTTTGGAGCGCCTGTAA	gene cloning
JSP103	iB5326cDNA5'	ATGATCATTTTTTAAGTGGGTTAATACAAGCTGG	gene cloning
JSP104	iB5326cDNA3'	TTATTGTTCTGTATTTTATGGAACATGATGGATAAAG	gene cloning

Name	Name as ordered	Primer Sequence (5' to 3')	Application
JSP105	iB5394cDNA5'	ATGTGCGAGGGCGGCTTCAGTG	gene cloning
JSP106	iB5394cDNA3'	TTACATACAATTACGTCTATGGTTGCCTTTGC	gene cloning
JSP107	5324_3'RACE	GTTGAAAGTGTGCGGGATGGGCAGAAAAT	RACE
JSP108	5324_5'RACE	TGACGTGGATCAAACCGTTAATCCGACTCC	RACE
JSP109	5326_3'RACE	GCGGCCAAGTTTATGTTTTTATGCCAATGGC	RACE
JSP110	5326_5'RACE	CGATTTGCTGGGTGTTAATGGACGGTTG	RACE
JSP111	5394_3'RACE	GTCCTCAAGGTCTGCAAAACCCGCAAG	RACE
JSP112	5394_5'RACE	GTCCATCGAACTCACCACCTGAGCGGGT	RACE
JSP114	iB_01217_ORF_rev	TCAATAACAATAATAATCTTGGTATCTTTTGGGTCTTC	gene cloning
JSP115	iB_01556_ORF_fw	ATGAGTGATTATTACGCGGTAGCGC	gene cloning
JSP116	iB_01556_ORF_rev	ACTTACACGTAGAGTCTTAGTTGTCCGAG	gene cloning
JSP117	iB_01574_ORF_for	ATGGACAACGTGCTGCCCAACTG	gene cloning
JSP118	iB_01574_ORF_rev	CTACCCTACGTCCGAAATGGTATTCAAATCC	gene cloning
JSP119	iB_01766_ORF_for	ATGATCAAATACAGTGTGTGATTTAATAGTGTGG	gene cloning
JSP120	iB_01766_ORF_rev	GGAGTTAACTTACAAATACACTGAATTGGACTTTG	gene cloning
JSP121	iB_02262_ORF_for	ATGGCCGAATCTGGTATTGATTTAGGTTAC	gene cloning
JSP122	iB_02262_ORF_rev	TCATGCAATCATGTCAATATCGAGGGTG	gene cloning
JSP123	iB_02476_ORF_for	AAGAGTCCAATGGCGAGTGGCGG	gene cloning
JSP124	iB_02476_ORF_rev	TTATCTCACTTGCTGATTTCCGGTATGGGC	gene cloning
JSP125	iB_00009_3for	ACATCGCCACGAGCTGGCCGTC	gene cloning
JSP126	iB_00009_ORFfor	ATGAGTTGTGCGCGTTTCATTATATGG	gene cloning
JSP127	iB_00009_3rev	AGTCCCTTTGCTTTGAGAGATCACGCATG	gene cloning
JSP128	iB_00067_Ex5for	GGTTGGGGCGTGCGCACGAAAC	gene cloning
JSP129	iB_00067_Ex5rev	CAAAGCGTTGCCAGTCTTGGAACTTTCC	gene cloning
JSP130	iB_00388_for1	TGGTGTAACACGAGCTCGAAATGCTGG	gene cloning
JSP131	iB_00992_ORF_for	CAACCTAACCTCACTCCACAATGGGCATAG	gene cloning
JSP132	iB_00992_5_rev	GAATGGTGGGATGAGGATGACCGGAG	gene cloning
JSP133	iB_00992_3_RACE	CTCCGGTCATCCTCATCCCCACCATTTCCC	RACE
JSP134	iB_01098_for	GAACAGGCCGATATGGAGAAGATGAAGATG	gene cloning
JSP135	iB_01098_rev	GACTAGTGTGCCGAAATGAACGTCAGG	gene cloning
JSP136	iB_01217_ORF_fw1	GAATTCCACTCCCATGATGGATGTAG	gene cloning
JSP137	iB_01556_Ex8_rev	AACCTGCATGGCGTTTTGTGTGTGGG	gene cloning
JSP138	iB_01702_for	TCCAATTCTGTAAGAACTCTTGTGATAG	gene cloning
JSP139	iB_01702_rev	GTTTAGCTCAGAATTGAAGACTTTCAAAGATC	gene cloning
JSP140	iB_02587_for	ATTGGTGTGCCTATCGACGATTTCTGC	gene cloning
JSP141	iB_02587_rev2	CTGACCAAGTCCGTCTCGTAGTCGATC	gene cloning
JSP142	iB_02587_rev1	TTACTACCAAACCTGGGCGTAAGGG	gene cloning
JSP143	iB_02881_ORF_for	ATGTCCAACGCCCCACGAGTCG	gene cloning
JSP144	iB_02881_3RACE_for	GAACAACAGTTTCGGAATCGTAAAAGTGCACG	RACE
JSP145	iB_02881_ORF_rev	TTATCACTCCACGGCAAACCCGCACG	gene cloning
JSP146	iB_03525_for1	ATGGCCAGAAGTACCTCCTTGTGTTTTG	gene cloning
JSP147	iB_03525_rev1	TCCAACGCCCTCTCCACACCTC	gene cloning
JSP148	iB_03735_ORF_for	ATGCCGACTCTGTGGAAGTGGCG	gene cloning

Appendix

Name	Name as ordered	Primer Sequence (5' to 3')	Application
JSP149	iB_03735_ORF_rev	CCTTAACAAATGACATGGATCGGAATGGTGG	gene cloning
JSP150	iB_03951_for1	GTTTTGTGTTCCGGTGGTTCAAATGTTGG	gene cloning
JSP151	iB_03951_rev1	CTACTTCCAGATTCTTTTCTCTCCTCTTCTCG	gene cloning
JSP152	iB_04050_for	TGAGGGCAAACACGTGTCCCAATC	gene cloning
JSP153	iB_04050_rev	TTATGGCCTCCAACCCATGATTACTTTCTTAAACG	gene cloning
JSP154	iB_04130_for1	GGTGCAATACTTGTACAAGACTCTAGACTGAG	gene cloning
JSP155	iB_04130_rev1	ACCGGGATGGTGGTAACACTGTCC	gene cloning
JSP156	iB_05324_for1	AAGCGCAAACGGAAGCTTGAAGATGCC	gene cloning
JSP157	iB_05324_rev1	GGCAGCGCGAAGCCGTGTTCAAG	gene cloning
JSP158	iB_05326_for1	AAGCAATGGTACTAAAAGCCGAAAAAGAAGCC	gene cloning
JSP159	iB_05326_rev1	CACTGCACTGCACTTATTGTTCTGTATTTATGG	gene cloning
JSP160	iB_05394_for1	GCCATGAAGTACTCCATGGAAGCGGAC	gene cloning
JSP161	iB_05394_rev1	CAGTGAGGGGTCTCCGGAACCTCCTC	gene cloning
JSP162	iB_05573_for1	TGACGCAGACAGATGCTCCAAACTCGG	gene cloning
JSP163	iB_05573_rev1	TAGTTGTAAACGTCTTGTGTTGATTTGTCCGTGG	gene cloning
JSP164	iB_05636_3RACE	TTCCGTGATTTCTCCGGAGTGTTCGCGTG	RACE
JSP165	iB_05636_5RACE	TCGGTATCCACAGAGACAAGATCGAGAACGTGCTC	RACE
JSP166	iB_05754_for1	TGCGCAAGTCAACGTCAACAAACCTC	gene cloning
JSP167	iB_05754_rev1	GCGTGCTGGCACTGGAGAACGAC	gene cloning
JSP168	iB_06031_for1	TCAGGGACCGGATTCGACTAACGC	gene cloning
JSP169	iB_06031_rev1	TCATCTGGCAGCATCGTGTCTCCTC	gene cloning
JSP170	iB_04393_ORF_for	ATGCGGCTCACTTCTGCTTTCTGG	gene cloning
JSP171	iB_04393_rev1	AACCTCGACTTCGTACGTCTCGACC	gene cloning
JSP172	iB_04437_ORF_for	ATGTTAGGCTTTGCTGAAACCGCCC	gene cloning
JSP173	iB_04437_rev1	TCATCGGTTGGTAAGTTTCAATGACGTTTG	gene cloning
JSP174	iB_04484_ORF_for	AGTATTTAAGTACGACCATGCAGAATCACACG	gene cloning
JSP175	iB_04484_ORF_rev	TTAAGGCCCTCGTCTGGTGGTATCAC	gene cloning
JSP176	iB_04484_for2	TTACACGGTCTTGCTGGCACTGCC	gene cloning
JSP177	iB_04484_rev2	TCATCGGATCTTTGGTAATAATTGTAAGGAATGG	gene cloning
JSP178	iB_04393_rev2	TCGTCAACTGTGCAACATGGCATTGAAG	gene cloning
JSP179	iB_05636_for1	GACAAGGGAACAAATGATCCTCTGGC	gene cloning
JSP180	iB_04484_Ex5_rev3	TTCACACTGTGAAGCTCCAAAAGCACG	gene cloning
JSP181	iB_04484_seq1_for	ATCAACAACACCAACTCCGACCGG	Sequencing
JSP182	iB_02881_seq1_for	ATCGCCGACTTCGACGCTGTATTCC	Sequencing
JSP183	iB_01098_seq1_for	TCTGATCTCATTGTACCGCAGCGACAAG	Sequencing
JSP184	iB_04439_ORF_for	ATGTCTGCGGAAGCTGTCGATCGATC	gene cloning
JSP185	iB_04439_ORF_rev	TTAGCCATGAGAAACCATTTTACAGAAGGCTG	gene cloning
JSP187	iB_04439_5RACE_n1	TGAGGTGATTTCTGGATAACTCAAATAGCCGTCTTTG	RACE
JSP188	iB_04439_ORF_for1	ATGACCCTCCCTGGGGGTACCG	gene cloning
JSP189	iB_04439_3RACE	TCGGGATTTTTTCTGATCATGGTTTTGATACAAGC	RACE
JSP190	iB_04439_3RACE_n	ACATCACCCGAGAGGAGGCGGTC	RACE
JSP191	iB_05636_3RACE_n	GTGGAGAACTATAACTTTGGGTTTTACGTTATCGAGTTC	RACE
JSP192	iB_05636_5RACE_n	GAACTCGATAACGTAAAACCCAAAGTTATAGTCTCCAC	RACE

Name	Name as ordered	Primer Sequence (5' to 3')	Application
JSP193	iB_03735_embr_for	TAACAACGCGTTTAAAAATCCTCCCTGTATTC	gene cloning
JSP194	iB_03735_Exon3_for	ACCAAACCTGGCACAAGACCAACTTC	gene cloning
JSP195	iB_03735_5RACE_nest ed	CAGACACACTTGCCGATGATGGGACCTCCTC	RACE
JSP198	CyclinJ_ORF_fw	ATGGACCAACACCACATAATCCCCGAAAAAC	gene cloning
JSP199	CyclinJ_ORF_rv	TCACACATACCCTAGCAAATTTTGTACGATTTCC	gene cloning
JSP204	Tc-Mad_for	TCGTCCGTTTATTAACTCCGATAGCATGG	gene cloning
JSP205	Tc-Mad_rev	ACTCATAACGTCCTGTTATTACCGATTACG	gene cloning
JSP212	Tc-Mad_fw_T7	TAATACGACTCACTATAGGGAGAAGTGTTCGTGCAATAATCCGCAGAG	dsRNA Template synthesis
JSP213	Tc-Mad_rv_T7	TAATACGACTCACTATAGGGAGAACTAGACACACTCGACAGTGGCGAAC	dsRNA Template synthesis
JSP214	03735_rv_T7	TAATACGACTCACTATAGGGAGATCTGTTAATCAAATCCATGATATCGGT GG	dsRNA Template synthesis
JSP219	03735_Ex3u4_forT7	TAATACGACTCACTATAGGGAGAAAGGCCACATGGGTTGCTTTC	dsRNA Template synthesis
JSP220	03735_Ex3u4_revT7	TAATACGACTCACTATAGGGAGACGAACAAATCCACCATAAAGC	dsRNA Template synthesis
JSP221	iB_02881_fw_T7	TAATACGACTCACTATAGGGAGACGCAAAAGACTGATGGTGAAG	dsRNA Template synthesis
JSP222	iB_02881_rv_T7	TAATACGACTCACTATAGGGAGATTGTTCTCCACCGAGAAGGTG	dsRNA Template synthesis
JSP223	smurf_NOF_fwT7	TAATACGACTCACTATAGGGAGAACAGGAAATTTCTGAATAATAACACG	dsRNA Template synthesis
JSP224	smurf_NOF_rvT7	TAATACGACTCACTATAGGGAGATCGTCCTGTTGTTGTGATCAAC	dsRNA Template synthesis

7.4 Table for *DsRed* control movies

	Apoptosis			AF formation and embryo enveloping			Embryonic head			Death before BD	Not developed at all
	Apoptosis	No clear Apoptosis	Apoptosis not Scorable	delayed or altered	not noticeably altered	Not scorable	Head clearly too small	Head size not altered	Head not scorable		
131125a02_03		1				1		1			
131125a02_04		1				1		1			
131125a02_05			1			1		1			
131125a02_06		1				1		1			
131125a02_07		1			1			1			
131125a02_08		1			1			1			
131126a01_01		1			1			1			
131126a01_02		1			1			1			
131126a01_03		1				1		1			
131126a01_04		1			1			1			
131126a01_05		1			1			1			
131126a01_06		1			1			1			
131126a01_07		1			1			1			
131126a01_08		1				1		1			
131126a01_09		1			1			1			
131126a01_10		1			1			1			
131126a01_11			1			1			1		
131126a01_12		1			1			1			
131126a01_13		1			1			1			
131127a02_01			1			1			1		
131127a02_03			1			1			1		
131127a02_09			1			1			1		
131127a02_10			1			1			1		
131127a02_11			1			1			1		
131127a02_12		1			1			1			
131128a02_01			1			1			1		
131128a02_02		1			1			1			
131128a02_03			1		1				1		
131128a02_04		1			1			1			
131128a02_05			1			1			1		
131128a02_06		1			1			1			
131128a02_07		1				1		1			
131128a02_08			1			1			1		
301113a04_01		1			1			1			
301113a04_02		1		1					1		

301113a04_03		1			1			1	1		
301113a04_04	1			1			1				
301113a04_05		1			1		1				
301113a04_07		1			1			1			
131202a02_01	1				1		1				
131202a02_02	1				1		1				
131202a02_03	1			1			1				
131202a02_04	1				1		1				
131202a02_05	1			1			1				
131202a02_06	1			1			1				
131202a02_07		1			1			1	1		
131202a02_08	1			1			1				
131202a02_09	1			1			1				
031213a02_01		1	1				1				
031213a02_02	1			1			1				
031213a02_03	1			1			1				
031213a02_04	1			1		1					
031213a02_05	1			1			1				
031213a02_06		1	1					1			
031213a02_07		1	1				1				
031213a02_08	1			1			1				
031213a02_09	1			1			1				
131204a02_01	1			1			1				
131204a02_02	1			1			1				
131204a02_03	1			1			1				
131204a02_04	1			1			1				
131204a02_05		1			1			1			
131204a02_06	1			1			1				
131204a02_07	1			1			1				
131204a02_08	1			1			1				
131204a02_09		1			1			1			
Summary	0	46	20	4	37	25	1	48	17	2	0
Total Movies	66										

7.5 Table for *Tc-smurf* RNAi movies

Movie ID	Apoptosis			AF formation and embryo enveloping			Embryonic head			Death before BD	Not developed at all
	Apoptosis	No clear Apoptosis	Apoptosis not Scorable	delayed or altered	not noticeably altered	Not scorable	Head clearly too small	Head size not altered	Head not scorable		
131125a02_09		1			1				1		
131125a02_10			1			1			1		1
131127a02_13	1			1			1				
131127a02_14			1	1					1		
131127a02_15		1			1			1			
131127a02_16			1			1			1		1
131127a02_17			1			1			1	1	
131127a02_18			1			1			1	1	
131127a02_19	1					1	1				
131127a02_20	1				1		1				
131127a02_21			1			1			1		
131127a02_22			1	1			1				
131127a02_23	1			1			1				
131127a02_24	1					1	1				
131127a02_25			1			1			1		1
131127a02_26			1			1			1		1
131127a02_27			1			1			1	1	
131128a02_10	1					1	1				
131128a02_11			1			1			1	1	
131128a02_12			1	1					1		
131128a02_13			1	1					1		
131128a02_14	1			1			1				
131128a02_15			1			1			1		
131128a02_16			1			1			1		
131128a02_17			1			1			1		
131128a02_18			1			1			1		
131128a02_19	1				1		1				
131128a02_20			1			1			1		
131128a02_21			1	1					1		
131128a02_22	1			1			1				
131128a02_23			1			1			1	1	
131128a02_24			1			1			1	1	
131128a02_25	1			1			1				
131128a02_26			1			1			1	1	
301113a04_09			1			1			1		1
301113a04_10			1			1			1	1	

301113a04_11	1			1			1				
301113a04_12			1				1			1	
301113a04_13			1				1			1	
301113a04_14			1				1			1	
301113a04_15			1				1			1	
301113a04_16			1				1			1	
301113a04_17			1				1			1	
301113a04_18			1				1			1	
301113a04_19	1						1			1	
301113a04_20			1				1			1	
131204a02_10			1				1			1	
131204a02_11		1				1			1		
131204a02_12			1				1			1	
131204a02_13			1				1			1	
131204a02_14	1					1				1	
131204a02_15			1				1			1	
131204a02_16			1				1			1	
131204a02_17			1				1			1	
131204a02_18			1				1			1	
131204a02_20			1				1			1	
131204a02_21	1					1				1	
131204a02_22			1				1			1	
131204a02_23			1				1			1	
131204a02_24			1				1			1	
131204a02_25			1				1			1	
131204a02_26			1				1			1	
131204a02_27			1				1			1	
131204a02_29			1				1			1	
131204a02_30			1				1			1	
131204a02_31			1				1			1	
131204a02_32			1				1			1	
131204a02_33			1				1			1	
131204a02_34			1				1			1	
131204a02_35			1				1			1	
131204a02_36		1					1			1	
131204a02_37			1				1			1	
131204a02_38			1				1			1	
131204a02_39			1				1			1	
131204a02_40			1				1			1	
131204a02_41			1				1			1	
131204a02_42	1						1			1	
131204a02_43			1				1			1	
131204a02_44			1				1			1	
131204a02_45			1				1			1	
131204a02_46			1				1			1	1

Appendix

131204a02_47			1			1			1	1	
131204a02_48			1			1			1		
131204a02_49			1			1			1	1	
131204a02_50			1			1			1	1	
131204a02_51		1			1			1			
131204a02_52			1			1			1	1	
131204a02_53			1			1			1	1	
131204a02_54			1	1					1		
Summary	15	5	69	16	7	66	15	4	70	43	6
Total Movies (w/o not de- veloped)	83										

7.6 Tables for *TC004374* RNAi movies

Movie number	Apoptosis		AF formation and embryo enveloping			Embryonic head			
	Apoptosis	No clear Apoptosis	Apoptosis not Scorable	Delayed or altered	Not noticeably altered	Not scorable	Head clearly too small	Head size not altered	Head not scorable
131127a02_29			1			1			1
131127a02_30		1			1			1	
131127a02_31	1					1	1		
131127a02_32			1			1			1
131127a02_33			1			1			1
131127a02_34		1			1			1	
131127a02_35		1			1			1	
131127a02_36		1			1			1	
131127a02_37		1			1			1	
131127a02_38		1			1			1	
131127a02_39	1					1			1
131128a02_27	1			1					1
131128a02_28	1					1	1		
131128a02_29		1			1				1
131128a02_30			1			1			1
131128a02_31		1			1		1		
131128a02_32			1	1					1
131128a02_33			1			1			1
131128a02_34			1			1			1
131128a02_35		1			1				1
131128a02_36		1			1				1
131128a02_37		1			1			1	
131128a02_38		1			1			1	
131128a02_39			1		1				1
131128a02_40	1				1				1
301113a04_37			1			1			1
301113a04_38			1		1			1	
301113a04_39		1			1			1	
301113a04_40		1			1			1	
301113a04_41		1			1			1	
301113a04_42		1			1			1	
301113a04_43			1			1			1
301113a04_44			1			1			1
301113a04_45			1			1			1
301113a04_46	1			1			1		

Appendix

301113a04_47	1			1					1
301113a04_48	1				1				1
301113a04_49	1			1			1		
301113a04_50			1			1	1		
301113a04_51		1			1			1	
Sum	9	17	14	5	21	14	6	14	20
Total Movies	40								

dsRed control		
DsRed Movie ID	Imaging Intervals (min)	30-50% ventral amniotic fold
131125a02_02	5	180
131125a02_04	5	180
131125a02_08	5	150
131126a01_01	10	180
131126a01_02	10	160
131126a01_04	10	190
131126a01_06	10	160
131126a01_07	10	170
131126a01_09	10	180
131126a01_10	10	170
131126a01_12	10	160
131126a01_13	10	170
131127a02_12	10	170
131128a02_02	10	170
131128a02_04	10	170
131128a02_06	10	180
301113a04_01	10	180
301113a04_02	10	240
301113a04_04	10	160
131202a02_03	10	160
131202a02_05	10	170
131202a02_06	10	200
131202a02_08	10	180
131202a02_09	10	170
031213a02_02	10	170
031213a02_04	10	260
031213a02_06	10	180
031213a02_08	10	180
031213a02_09	10	180
131204a02_01	10	170
131204a02_02	10	170
131204a02_03	10	170
131204a02_04	10	170
131204a02_06	10	160

131204a02_07	10	180
	Mean	176,8571429
	Standard deviation	20,8314565

TC004374		
TC004374 Movie ID	Imaging Intervals	30-50% ventral amniotic fold
131127a02_30	10	180
131127a02_34	10	180
131127a02_35	10	200
131127a02_36	10	170
131127a02_38	10	170
131128a02_28	10	240
131128a02_29	10	200
131128a02_31	10	230
131128a02_32	10	240
131128a02_35	10	170
131128a02_36	10	250
131128a02_38	10	220
301113a04_38	10	210
301113a04_39	10	180
301113a04_40	10	190
301113a04_41	10	220
301113a04_42	10	250
301113a04_45	10	220
301113a04_46	10	230
301113a04_47	10	210
301113a04_48	10	200
301113a04_49	10	380
	Mean	215,4545455
	Standard deviation	45,01082121

